UNIVERSITÉ DU QUÉBEC À CHICOUTIMI

MÉMOIRE PRÉSENTÉ À

L'UNIVERSITÉ DU QUÉBEC À CHICOUTIMI

COMME EXIGENCE PARTIELLE

DE LA MAÎTRISE EN INGÉNIERIE

PAR

LI LIU

ÉVALUATION DE LA PROPRETÉ DES ALLIAGES D'ALUMINIUM DE FONDERIE A356.2 ET C357 À L'AIDE DE LA TECHNIQUE PoDFA

DECEMBRE 1997

Bibliothèque
Paul-Émile-Boulet

UQAC
Université du Québec
à Chicoutimi

Mise en garde/Advice

Afin de rendre accessible au plus grand nombre le résultat des travaux de recherche menés par ses étudiants gradués et dans l'esprit des règles qui régissent le dépôt et la diffusion des mémoires et thèses produits dans cette Institution, **l'Université du Québec à Chicoutimi (UQAC)** est fière de rendre accessible une version complète et gratuite de cette œuvre.

Motivated by a desire to make the results of its graduate students' research accessible to all, and in accordance with the rules governing the acceptation and diffusion of dissertations and theses in this Institution, the **Université du Québec à Chicoutimi (UQAC)** is proud to make a complete version of this work available at no cost to the reader.

L'auteur conserve néanmoins la propriété du droit d'auteur qui protège ce mémoire ou cette thèse. Ni le mémoire ou la thèse ni des extraits substantiels de ceux-ci ne peuvent être imprimés ou autrement reproduits sans son autorisation.

The author retains ownership of the copyright of this dissertation or thesis. Neither the dissertation or thesis, nor substantial extracts from it, may be printed or otherwise reproduced without the author's permission.

RÉSUMÉ

Le présent tavail a été entrepris afin d'étudier le rôle des paramètres d'opérations communément appliqués dans les fonderies d'aluminium ainsi que l'effet des éléments d'alliages mineurs sur la formation d'inclusions dans l'alliages Al-Si le plus largement utilisé, i.e., l'alliage primaire A356.2 et C357, à l'aide de la technique PoDFA (Porous Disc Filtration Apparatus). Une série de vingt neuf expériences a été réalisée (chacune utilisant un mélange de 25 Kg d'alliage). Dans chaque cas, 4 à 6 essais PoDFA successifs ont été exécutés. Les échantillons PoDFA contenant la partie non filtrée du métal en contact avec le filtre PoDFA (~5 mm d'épaisseur) ont été polis en vue d'un examen métallographique. La classification et le dénombrement des inclusions a été réalisée en utilisant la méthode de la grille.

Les résultats obtenus sur les types et les concentrations d'inclusions non métalliques ainsi que sur les films d'oxyde d'aluminium se produisant dans cet alliage avant la coulée, ont été analysés en terme de leur effet sur le temps de filtration et sur la fluidité (mesurée par la longueur du métal solidifié dans des tubes en quartz à l'aide d'un appareil de mesure de la fluidité Ragone). La scorie, i.e., la couche d'oxyde qui se forme sur la surface du métal en fusion a été soigneusement recueillie, pesée et examinée par microscopie électronique à balayage équipée d'un système EDX. Les résultats ont montré que les inclusions ne sont pas les seuls paramètres à être considérés. Les oxydes Al_2O_3 (films et particules) sont les plus importants et constituent le facteur déterminant. On trouve cependant qu'il est assez difficile de séparer le rôle individuel de chaque paramètre en utilisant la technique PoDFA, i.e., l'échantillonnage sans perturber le métal en fusion. Ce procédé introduirait certainement des oxydes indésirables dans le creuset PoDFA, résultant en une augmentation artificielle de la quantité de scories. Dans tous les cas, la scorie était liquide, i.e., contenant une quantité appréciable de métal en fusion. Les principaux types d'oxydes dans la scorie étaient MgO, $MgAl_2O_4$, Al_4C_3 et Al_2O_3.

Deux types de matériau initial de A356.2 et C357ont été utilisés, i.e., frais et recyclé. Un total de treize opérations, représentant celles normalement appliquées dans les fonderies d'aluminium ont été simulées sous atmosphère sec (humidité ~12-15%). Le métal fondu a été moulé dans des éprouvettes qui ont ensuite été thermiquement traitées selon T6 avant les essais de traction. Les résultats ont montré que le maintien du métal liquide à 735°C durant un long temps i.e. 72 h conduit à la sédimentation de la plupart des inclusions vers le fond du creuset. Cependant, une variation de l'humidité environnante peut provoquer l'absorption d'hydrogène et ainsi une grande quantité de porosités. Le

dégazage à l'aide d'argon sec injecté dans le métal liquide par l'intermédiaire d'un agitateur rotatif (vitesse ~160 rpm) semble être la meilleure technique pour éliminer les inclusions. L'efficacité de ce procédé est grandement améliorée lorsque celui-ci est couplé avec la filtration utilisant des filtres à écume en céramique (10 et 20 ppi). Une relation linéaire entre la ductilité de l'alliage et le logarithme du pourcentage d'inclusion au d'oxide films a été établi. A cause de la décohésion entre l'inclusion/film d'oxyde et la matrice environnante, des fissures sont facilement initialisées à leur interface, conduisant à des défauts imprévus.

ABSTRACT

The present work was undertaken to study the role of the major operating parameters commonly applied in aluminum foundries, as well as the effect of minor alloying elements on inclusion formation in two of the most widely used Al-Si alloys, i.e., A356.2 and C357 primary alloys, using the PoDFA (Porous Disc Filtration Apparatus) technique. A set of twenty nine experiments was conducted (each using a melt of 25 kg of fresh alloy material). In each case, four to six successive PoDFA trials were executed. PoDFA samples containing the unfiltered part of the metal (~5 mm in thickness) in contact with the PoDFA filter were polished for metallographic examination. Inclusion classification and counting was done using the grid method. The types and concentrations of nonmetallic inclusions as well as aluminum oxides films that can occur in this alloy prior to casting will be summarized.

The data obtained on inclusion types and concentration has been analyzed in term of their effect on filtration time and fluidity (measured by the length of solidified metal in the quartz tube of a Ragone fluidity tester). The dross, i.e., the oxide layer that formed on the surface of the molten metal was carefully collected, weighed and examined under a scanning electron microscope equipped with an EDX system. The results show that inclusions are not the only parameter to be considered. More importantly, it is the Al_2O_3 oxides (films or particles), which seem to be the deciding facor. It is found, however, that it is quite difficult to separate the individual role of each parameter using the PoDFA technique, i.e., sampling without disturbing the molten metal. This process would certainly introduce undesirable oxides into the PoDFA crucible, resulting in an artificial increase in the filtration time. Increasing the holding periods of the molten metal increase the quantity of dross, In all cases, the dross was wet i.e., containing an appreciable amount of molten metal. The main inclusion/oxide types observed in the dross are MgO, $MgAl_2O_4$, Al_4C_3 and Al_2O_3.

Two types of initial materials of A356.2 and C357 were used, i.e., fresh and recycled. A sum of thirteen operations representing those normally applied in aluminum foundries were simulated under dry atmospheric conditions (humidity ~ 12-15%). The molten metal was cast into test bars which were T6 tempered prior to tensile testing. The results show that holding the liquid metal for a long time i.e. 72 h at 735°C leads to sedimentation of most inclusions towards the bottom of the melting crucible. However, a change in the surrounding humidity may cause absorption of hydrogen and, hence, a large amount of porosity. Degassing using dry argon injected into the liquid metal through a

rotary impeller (speed ~160 rpm) appears to be the best technique for inclusion removal. The efficiency of this process is significantly improved when it is coupled with filtration using ceramic foam filters (10 and 20 ppi). A linear relationship between alloy ductility and logarithm of the percentage of inclusion/oxide films has been established. Due to decohesion between the inclusion/oxide films and the surrounding matrix, cracks are easily initiated at their interfaces, leading to unpredicted failure.

REMERCIEMENTS

En premier lieu, je me dois de remercier mon directeur de thèse, le professeur F.H.Samuel, qui par ses conseils et sa disponibilité m'a permis de réaliser ce travail.

Je désire également remercier Mme Agnès Samuel pour son aide et ses précieux conseils, messieurs Régis Boucher et André Bouchard pour leurs conseils techniques et leurs supports.

Je souhaite exprimer toute ma reconnaissance aux organisations et aux fonderies de R&D (au Canada, aux États-Unis et au Mexique) qui ont contribué à ce projet de recherche: Bomem, Inc. (Québec-Canada), Cercast Group (Montreal-Canada), la Société d'Électrolyse et de Chimie Alcan (Jonquière, Qc., Canada), Grenville Castings Limited (Ontario-Canada), General Motors Powertrain Group (Saginaw-États-Unis), Corporation Nemak (Monterrey-Mexique), KB Alloys, Inc. (Robards-États-Unis), Hi-Tech Ceramics (NewYork-États-Unis). Je tiens tout particulièrement à remercier la Fondation de l'Université du Québec à Chicoutimi, le Centre Québécois de recherche et de développement de l'aluminium, et le Conseil de Recherche en Sciences Naturelles et en Génie du Canada.

Mes remerciements s'adressent également à mon mari et mes collègues de travail pour avoir créé une atmosphère de travail des plus agréable.

TABLE OF CONTENTS

RÉSUMÉ III

ABSTRACT V

REMERCIEMENTS I

TABLE OF CONTENTS I

LIST OF FIGURES I

LIST OF TABLES I

CHAPTER 1

DEFINITION OF THE PROBLEM 1

1.1 INTRODUCTION 2
1.2 OBJECTIVES 4

CHAPTER 2

BACKGROUND 5

2.1 INTRODUCTION 6
2.2 ALUMINUM CASTING ALLOYS 7
2.3 TYPES AND SOURCES OF INCLUSIONS IN ALUMINUM CASTING ALLOYS 9
2.3.1 Deleteriousness of Inclusions 9
2.3.2 Types and Sources of Inclusions 12
2.4 INCLUSION ASSESSMENT 17
2.4.1 Ultrasonic Technique 17
2.4.2 On-Line Melt Cleanliness Determination-LiMCA 18
2.4.3 Vacuum-Filtration Technique 20
2.4.4 Fracture -Test Technique 22
2.4.5 Qualiflash Technique 23

2.5 TENSILE PROPERTIES 28
2.5.1 Tensile Property Parameters 28
2.5.2 Factors Affecting Tensile Properties 30
2.5.2.1 Effect of alloy composition 31
2.5.2.2 Effect of degassing 32
2.5.2.3 Effect of grain refinement 33
2.5.2.4 Effect of modification 34
2.5.2.5 Effect of heat treatment 35
2.5.2.6 Effect of inclusion removal 37
2.6 FATIGUE PROPERTIES 41
2.6.1 Parameters and Tests for Measuring Fatigue 42
2.6.2 Effect of Non-Metallic Inclusions 45

CHAPTER 3

INCLUSION MEASUREMENT 48

3.1 INTRODUCTION 49
3.2 EXPERIMENTAL PROCEDURE 50
3.2.1 Melt Preparation 50
3.2.2 Inclusion Measurements 53
3.3 RESULTS AND DISCUSSION 54
3.3.1 Inclusion Type and Concentration 54
3.3.1.1 Foundry parameters 54
3.3.1.2 Minor alloying elements 57

CHAPTER 4

INCLUSION ANALYSIS 119

4.1 INTRODUCTION 120
4.2 RESULTS AND DISCUSSION 123
4.2.1 Dross Formation 123
4.2.2.1 Cold chamber 139
4.2.2.2 Hot chamber 140
4.2.2.2.1 effect of foundry parameters 140
4.2.2.2.2 effect of minor additions 144
4.2.3 Inclusion - Fluidity Relationship 146
4.2.4 Examples of Inclusion Concentrations 151

CHAPTER 5

EFFECT OF INCLUSIONS ON MECHANICAL PROPERTIES 161

5.1 INTRODUCTION 162
5.2 EXPERIMENTAL PROCEDURE 165
5.3 RESULTS AND DISCUSSION 166
5.3.1 Fresh Alloy 166
5.3.2 Recycled (Scrap) Alloy 181
5.3.3 Ductility - Percentage Inclusion Relationship 188

CHAPTER 6

CONCLUSIONS 203

REFERENCES 208

LIST OF FIGUES

Figure 1 Variation in tensile properties with filtration for an Al-4.5%Cu-1.5%Mg alloy [1]..... 9

Figure 2 The effect of filtration on metal fluidity [2]..... 10

Figure 3 Photomicrographs showing : a) gamma alumina (Al_2O_3), b) magnesia (MgO), c) dispersoid spinel cluster ($MgAl_2O_4$)..... 15

Figure 4 Schematic diagram of an ultrasonic apparatus [10]..... 18

Figure 5 Schematic diagram of the LiMCA technique [12]..... 19

Figure 6 Schematic diagram of the vacuum-filtration technique [13]..... 21

Figure 7 Schematic diagram of K-Mold fracture plates [10]..... 22

Figure 8 The Qualiflash apparatus [14]..... 23

Figure 9 Principle of the PoDFA method of measuring metal cleanliness [15]..... 25

Figure 10 An engineering stress-strain curve [18]..... 28

Figure 11 Effect of hydrogen porosity on the tensile and yield strengths of sand cast 356-T6 aluminum castings [21]..... 32

Figure 12 Variation in quality index (Q) with Sr content for three different cooling rates. Melts degassed with N_2-CCl_2F_2: Band 1 cooling rate 1.5°C/s; Band 2 cooling rate 0.5°C/s ; Band 3 cooling rate 0.08°C/s [23]..... 34

Figure 13 Variation in (a) UTS, YS, (b) elongation percent, and (c) quality index as a function of oxide-inclusion content [32]..... 39

Figure 14 Nomenclature to describe test parameters involved in cyclic stress testing..... 43

Figure 15 Typical S-N curves for constant amplitude and sinusoidal loading..... 44

Figure 16 Typical plot of strain range versus cycles-to-failure for low-cycle fatigue. 45

Figure 17 Stress concentration effects arising from elastic modulus mismatch [38]. 46

Figure 18 (a) Principle of the PoDFA apparatus, and (b) pore size distribution of the PoDFA filter. 52

Figure 19 Example of graphite particles. 86

Figure 20 Examples of fine Al_4C_3 ($\leq 3\mu m$) particles observed on: a) a freshly prepared sample, b) after almost a week. 87

Figure 21 Examples of coarse Al_4C_3 ($> 3\mu m$) particles observed on: a) a freshly prepared sample, b) after almost a week. 88

Figure 22 Examples of MgO particles: a) regular fragment, b) pale-colored pieces c) MgO (marked 1) Mg cuboides (marked 2) - Note the presence of both types of magnesium oxide in the same regions. 89

Figure 23 Example of spinel inclusions. The long platelets are undissolved pieces of Al-Ti-B master alloy. 91

Figure 24 Examples of potential chloride particles (arrowed): a) bright field, b) dark field images. The short arrows in (a) point to SrO particles..... 92

Figure 25 Examples of TiB_2 particles: a) bright field, b) dark field images. 93

Figure 26 Examples of oxide films: a) thin films, b) thick films. 95

Figure 27 Experimental conditions that maximize the concentration of graphite inclusions. 96

Figure 28 Experimental conditions that maximize the concentration of potential chloride inclusions: a) fine particles, b) coarse particles. 97

Figure 29 Experimental conditions that maximize the concentration of fine Al_4C_3 ($\leq 3\mu m$) inclusions: a) effect of mechanical stirring, b) effect of filtration without and with degassing, c) effect of the type of initial charge. 98

Figure 30 Experimental conditions that maximize the concentration of coarse Al_4C_3 ($> 3\mu m$) inclusions. 100

Figure 31 Experimental conditions that maximize the concentration of MgO inclusions in A356.2 alloy: a) effect of mechanical stirring and settling time, b) effect of prolonged holding time (72 h), c) effect of the type of initial charge (scrap). 102

Figure 32 Experimental conditions that maximize the concentration of MgO inclusions in C357 alloy: a) effect of settling time, b) effect of mechanical stirring. 103

Figure 33 Experimental conditions that maximize the concentration of MgO cuboide inclusions in A356.2 alloy : a) effect of type of initial charge, b) effect of prolonged holding time (72 h). 105

Figure 34 Experimental conditions that maximize the concentration of MgO cuboides inclusions in C357 alloy: a) effect of settling time, b) effect of mechanical stirring. 106

Figure 35 Experimental conditions that maximize the concentration of $MgAl_2O_4$ inclusions in A356.2 alloy: a) effect of type of initial charge, b) effect of filtration conditions, c) effect of prolonged holding time (72 h). 108

Figure 36 Experimental conditions that maximize the concentration of $MgAl_2O_4$ inclusions in C357 alloy: a) effect of settling time, b) effect of mechanical stirring. 110

Figure 37 Experimental conditions that maximize the concentration of TiB_2 inclusions in A356.2 alloy. 112

Figure 38 Pouring cups mounted with: a) 10 ppi, b) 20 ppi ceramic foam filters. 112

Figure 39 Effect of Sr and TiB_2 additions on the weight of filtered metal. 113

Figure 40 Effect of TiB_2 additions on the weight of filtered metal obtained in: a) Experiment 22A, b) Experiment 22E. Compare the droplet-like surface in 22E with the smooth surface in 22A. 114

Figure 41 Effect of TiB_2 additions on: a) filtration time, b) total inclusions, c) weight of filtered metal 115

Figure 42 Effect of grain refining agent type on the number of inclusion particles: a) Al_3Ti, b) TiB_2 116

Figure 43 Experimental conditions that maximize the concentration of SrO inclusions in A356.2 alloy (Experiment 22H- degassing applied). 118

Figure 44 Morphology of the dross collected from A356.2 alloy: a) air-exposed surface, b) melt-exposed surface. Note the roughness of the surface when holding time is increased to 72 h. 125

Figure 45 Morphology of the dross collected from C357 alloy: a) Experiment 24A - air-exposed surface, b) Experiment 25A - air-exposed surface, c) Experiment 25A - melt-exposed surface. 126

Figure 46 SEM micrographs of dross specimens collected from A356.2 alloy: a) Experiment 18A - air-exposed surface, b) Experiment 20A - air-exposed surface, c) Experiment 20A - melt-exposed surface. 129

Figure 47 EDX spectrums corresponding to the dross specimens of A356.2 alloys shown in Figure 46: a) Experiment 18A - air-exposed surface, b) Experiment 20A - air-exposed surface, c) Experiment 20A - melt-exposed surface 131

Figure 48 SEM micrographs of dross collected from C357 alloys: a) Experiment 24A - air-exposed surface, b) Experiment 25A - air-exposed surface, c) Experiment 25A - air-exposed surface, d) Experiment 25C - air-exposed surface. 134

Figure 49 EDX spectrums corresponding to dross specimens of C357 alloy: a) Experiment 24A - air-exposed surface, b) Experiment 25A - air-exposed surface, c) Experiment 25A - air-exposed surface, d) Experiment 25A - melt-exposed surface, e) Experiment 25C - air-exposed surface. 137

Figure 50 Dependence of filtration time on inclusion concentrations and oxide films for hot chamber: a) total inclusions, b) total harmful inclusions, c) oxide film rating. 141

Figure 51 Dependence of filtration time on inclusions caused by minor element additions: a) total inclusions, b) total harmful inclusions, c) oxide film rating. 145

Figure 52 Dependence of the length of solidified metal obtained in the Ragone fluidity test on inclusions caused by variations in the foundry parameters: a) total inclusions, b) total harmful inclusions, c) oxide film rating. 147

Figure 53 Dependence of the length of solidified metal obtained in the Ragone fluidity test on minor element additions: a) total inclusions, b) total harmful inclusions, c) oxide film rating. 149

Figure 54 Microstructure of base alloy away from the inclusion cake. 152

Figure 55 Examples of inclusion concentrations: a) very light - Experiment 4A, b) light - Experiment 1D, c) moderate-Experiment 15E, d) heavy - Experiment 12C, e) excessive - Experiment 29H, f) excessive - Experiment 29I. 155

Figure 56 Examples of Al_2O_3 oxide films/particles: a) none-Experiment 3E, b) thin/light - Experiment 1D, c) thin/moderate - Experiment 1A, d) thin/heavy - Experiment 1B, e) thick/light - Experiment 15E, f) thick/moderate - Experiment 14E, g) thick/heavy - Experiment 7E. 159

Figure 57 Effect of Al_2O_3 oxide density on filtration time : a) Experiment 2E - 3 min, b) Experiment 7A - 5 min..... 160

Figure 58 Schematic diagram showing the motion of inclusions under different conditions. 172

Figure 59 Schematic diagram showing the effectiveness of degassing with respect to amount of liquid metal. 177

Figure 60 Optical macrographs showing the size and distribution of non-metallic inclusions/oxide films in tensile-tested bars obtained from fresh alloy, and corresponding to elongations of: a) 19%, b) 16%, c) 10%, d) 8%, e) 5%, f) 3.5%, g) 1.5%. 192

Figure 61 Optical macrographs showing the size and distribution of non-metallic inclusions/oxide films in tensile-tested bars obtained from recycled (scrap) alloy, and corresponding to elongations of a) 7.5%, b) 5%, c) 3.5%..... 193

Figure 62 Percentage Elongation-log Percentage Inclusions/Oxide Films relationship. 194

Figure 63 Fracture surface of a tensile tested bar obtained from an alloy melt held for 72 h at 735°C, showing: a) fragmentation of oxides particles (corresponding to Fig. 60(g)), b) presence of liquid aluminum entrapped within oxide film particles..... 197

Figure 64 The energy dispersive X-ray (EDX) spectrum corresponding to the arrowed particle in Fig. 63(c), showing strong reflections due to O, Mg and Al. 199

Figure 65 Fracture surface of a tensile-tested bar obtained from recycled alloy, showing a crumpled mass of oxide films: a) near the edge, and b) close to the centre of the test bar.....200

Figure 66 Typical energy dispersive X-ray (EDX) spectrum corresponding to the Al_2O_3 oxide films shown in Fig.65(a). Note the very weak Mg reflection.....201

Figure 67 Fracture surfaces showing crack paths located at oxide/matrix interfaces in the samples corresponding to those shown in a) Fig.61(a), and b) Fig.61(c).....202

LIST OF TABLES

Table 1 Compositions of some common aluminum-silicon casting alloys [1]. 8

Table 2 Chemical compositions (wt%) of the as-received A356.2 and C357 alloys..... 51

Table 3 Foundry parameters for experiments conducted with A356.2 alloy..... 56

Table 4 Foundry parameters for experiments conducted with C357 alloy..... 57

Table 5 Minor additions and other parameters for experiments conducted with A356.2 alloy. 58

Table 6 Minor additions and other parameters for experiments conducted with C357 alloy. 59

Table 7 Chemical compositions of A356.2 alloy under different melt treatment conditions. 62

Table 8 Concentrations of additives in A356.2 alloy. 63

Table 9 Explanation of alloy codes used in the Tables 7 and 8..... 64

Table 10 Effect of foundry parameters on the filtration and fluidity data obtained for A356.2 alloy..... 66

Table 11 Effect of minor additions on the filtration and fluidity data obtained for A356.2 alloy. 69

Table 12 Effect of foundry parameters on the total and harmful inclusion concentrations (mm^2/kg) obtained in A356.2 alloy. 70

Table 13 Effect of minor additions on the total and harmful inclusion concentrations (mm^2/kg) obtained in A356.2 alloy. 72

Table 14 Effect of foundry parameters on the concentrations of major inclusions (mm^2/kg) obtained in A356.2 alloy. 73

Table 15 Effect of minor additions on the concentrations of major inclusions (mm^2/kg) obtained in A356.2 alloy. 75

Table 16 Effect of foundry parameters on the concentration of Al_2O_3 oxide films obtained in A356.2 alloy and their classification. 76

Table 17 Effect of minor additions on the concentration of Al_2O_3 oxide films obtained in A356.2 alloy and their classification. 78

Table 18 Chemical compositions of C357 alloy under different melt treatment conditions. 79

Table 19 Concentrations of additives in C357 alloy. 80

Table 20 Explanation of alloy codes used in Tables 18 and 19 81

Table 21 Effect of foundry parameters and minor additions on the filtration and fluidity data obtained for C357 alloy 82

Table 22 Effect of foundry parameters and minor additions on the total and harmful inclusion concentrations (mm^2/kg) obtained in C357 alloy. 83

Table 23 Effect of foundry parameters and minor additions on the concentrations of major inclusions (mm^2/kg) obtained in C357 alloy 84

Table 24 effect of foundry parameters and minor additions on the concentration of Al_2O_3 oxide films obtained in C357 alloy and their classification. 85

Table 25 Weight of dross 124

Table 26 EDX analysis (at %) of dross samples obtained from various alloy melts. 132

Table 27 Arbitrary codes used for inclusion classification 138

Table 28 Codes used for oxide film classification (Alcan's procedure). 138

Table 29 Chemical composition (wt%) of A356.2 alloy. 165

Table 30 Melt conditions for preparation of tensile test bars. 167

Table 31 Tensile test results of Experiment #3 (fresh alloy). 168

Table 32 Tensile test results of Experiment #4 (fresh alloy). 169

Table 33 Tensile test results of Experiment #5 (fresh alloy). 170

Table 34 Tensile test results of Experiment #15 (fresh alloy). 171

Table 35 Tensile test results of Experiment #6 (fresh alloy). 174

Table 36 Tensile test results of Experiment #9 (fresh alloy). 176

Table 37 Tensile test results of Experiment #7 (fresh alloy). 179

Table 38 Tensile test results of Experiment #8 (fresh alloy). 180

Table 39 Tensile test results of Experiment #11 (scrap alloy). 182

Table 40 Tensile test results of Experiment #10 (scrap alloy). 183

Table 41 Tensile test results of Experiment #12 (scrap alloy). 184

Table 42 Tensile test results of Experiment #14 (scrap alloy). 185

Table 43 Tensile test results of Experiment #13 (scrap alloy). 186

Table 44 Average tensile properties of A356.2 alloy (fresh alloy). 187

Table 45 Average tensile properties of A356.2 alloy (scrap alloy). 187

Table 46 Inclusion/oxide - tensile properties relationships for A356.2 alloy 196

CHAPTER 1

DEFINITION OF THE PROBLEM

CHAPTER 1

DEFINITION OF THE PROBLEM

1.1 INTRODUCTION

Aluminum casting alloys are characterized by their low specific gravity, low melting point, negligible gas solubility with the exception of hydrogen, excellent castability, good machinability, and good corrosion resistance. So, they are often used in the aeronautics and automotive industries. Premium quality castings are an essential requisite for the critical structural components used in these applications. The production of such castings requires that porosity and inclusions be minimized (or even eliminated) to negate their harmful influence on the mechanical properties, so that these properties are then mainly controlled by the microstructure of the castings.

Among the more widely used aluminum casting alloys in such applications are the A201, A206, C355, A356, A357 and A319 alloys. The more recently developed alloys like A201, A206 have provided tensile properties much higher than those of any previous aluminum casting alloys, and are being used to cast premium quality aerospace parts. Among the most popular of Al-Si alloys hardened by magnesium silicide precipitation is A356 alloy. The Al-Si-Mg family of alloys, to which A356 belongs, have excellent casting characteristics and are heat treatable to provide various combinations of tensile and physical

properties that are attractive for many applications. Alloy A357 is similar to A356 but has a higher magnesium content (0.5%) and can be heat treated to a higher strength level. The alloy also contains a small amount of beryllium. Both alloys are capable of much higher ductilities than their lower purity counterparts, 356 and 357, and are among the premium quality casting alloys specified for military and aircraft applications. C355 is another premium quality casting alloy, and is used for products such as tank engine cooling fans and higher speed rotating parts and impellers.

Detrimental effects of the presence of porosity and inclusions in aluminum are well documented. Although a substantial number of methods are used to remove the inclusions either prior to or during casting, the problem of measuring metal cleanliness through a sensitive, quantitative method still exists. The difficulty is further compounded by the fact that the inclusions to be measured are usually very small, about 10-20 μm.

The PoDFA (Porous Disc Filtration Apparatus) technique introduced by Alcan has been used for assessing metal cleanliness for many years. It can provide both qualitative information on the nature of inclusions and quantitative information on the inclusion concentration. This technique can also distinguish inclusion types and differentiate, for instance, between the level of borides, carbides and spinels present within an individual sample. It has proved invaluable in establishing the cause of the problem in unsatisfactory metal.

1.2 OBJECTIVES

The present research work was undertaken to study the assessment of melt cleanliness in A356.2 and C357 aluminum casting alloys using the PoDFA technique.

The work was divided into three parts to cover the following aspects:

(i) Study the effect of different foundry parameters on inclusion formation in A356.2 and C357 alloys;

(ii) Evaluate the reliability of the PoDFA technique in assessing melt cleanliness (inclusion identification and measurement) in these alloys for the above foundry conditions; and

(iii) Correlate the tensile properties with the inclusion/oxide film content.

CHAPTER 2

BACKGROUND

CHAPTER 2

BACKGROUND

2.1 Introduction

Aluminum alloys are popularly used in a large number of applications such as automotive-, domestic food-, and pump castings or castings exposed to marine atmospheres. It is also well established that a large variety of inclusions are present in commercial aluminum alloys. Their presence can lead to a reduction in mechanical properties of the casting, poor surface quality, increased gas porosity, poor machinability, high wear, etc. These are the main factors that will cause the rejection of final products by the customers. Thus, the need for precise analysis of inclusions is important.

The assessment of melt cleanliness is an important step in the chain of events constituting molten metal processing. Without a reliable assessment technique one cannot properly evaluate the "goodness" of an inclusion removal treatment. From a generic point of view, there are essentially six fundamental methods of measuring metal cleanliness: ultrasonic, LiMCA, vacuum filtration, pressure filtration, fracture test, and Qualiflash techniques.

2.2 Aluminum Casting Alloys

Aluminum casting became affordable only after the invention of the Hall-Heroult process for aluminum refining. In the early days, decorative trims, airplanes and cooking utensils were the only applications of aluminum casting. After World War II, the aluminum casting industry developed rapidly. Many new aluminum alloys were made, and casting processes were undertaken with the request of engineering specifications. The use of cast aluminum further increased since the energy crisis of the 1970s. Many metals can be added to aluminum, according to the product demand. Silicon, magnesium, copper, iron, lithium, zinc, nickel, silver, tin and titanium are among the most commonly used alloying elements. Different alloying elements have different functions because of their different solid solubilities.

Aluminum-copper alloys containing less than 5.7% copper are typical solid solution alloys. After heat treatment, $CuAl_2$ particles are precipitated from the quenched alloy. These alloys have a great tendency to hot tearing and microshrinkage formation. They are used in premium-quality aerospace castings due to their excellent tensile strength. Now, the aluminum-silicon alloys have replaced the aluminum-copper alloys because of their better casting properties.

Aluminum-silicon alloy castings make up to 85% - 90% of the total aluminum cast parts. The major alloying element, i.e., silicon, imparts high fluidity and low shrinkage which result in good castability and weldability. The most common aluminum-silicon casting alloys are listed in Table 1 [1].

Table 1 Compositions of some common aluminum-silicon casting alloys [1].

Alloy	Casting Method	Element(wt %)					
		Si	Cu	Mg	Fe	Zn	Others
319.0	S,P	6.0	3.5	<0.10	<1.0	<1.0	
332.0	P	9.5	3.0	1.0	1.2	1.0	
355.0	S,P	5.0	1.25	0.5	<0.06	<0.35	
A356.0	S,P	7.0	<0.20	0.35	<0.2	<0.1	
A357.0	S,P	7.0	<0.20	0.55	<0.2	<0.1	0.05 Be
380.0	D	8.5	3.5	<0.1	<1.3	<3.0	
383.0	D	10.0	2.5	0.10	1.3	3.0	0.15 Sn
384.0	D	11.0	2.0	<0.3	<1.3	<3.0	0.35 Sn
390.0	D	17.0	4.5	0.55	<1.3	<0.1	<0.1 Mn
413.0	D	12.0	<0.1	<0.10	<2.0	-	
443.0	S,P	5.25	<0.3	<0.05	<0.8	<0.5	

Note : S: Sand Casting; P: Permanent Mold Casting;
D: High Pressure Die Casting.

The 319.0 alloy produced from recycled material is used in cylinder heads and intake manifolds. A356.0 and A357.0 alloys have provided much higher tensile properties and are used to cast premium quality aerospace parts. A356 is hardened by magnesium silicide precipitation. A357 is similar to A356 but has a higher magnesium content and can be heat-treated to a higher strength level. Premium quality A356.0 and A357.0 alloys are particularly used for military and aircraft applications. High purity C355.0 alloys are cast to produce tank engines, pump parts, high speed rotating parts and impellers. The 332.0 alloy can be used for automobile gas and diesel pistons. When nickel is added to this alloy, the elevated temperature properties are improved, through the formation of stable intermetallics. The hypereutectic 390.0 alloy was first high pressure die cast for

engine blocks without iron liners. The 380.0 alloy is also widely used for engine casting, transmission parts and various other automotive parts in the United States and Canada.

2.3 Types and Sources of Inclusions in Aluminum Casting Alloys

2.3.1 Deleteriousness of Inclusions

The presence of inclusions in molten metal leads to several problems which include the following:

(1) Reduction in mechanical properties of the casting

Both tensile strength and elongation are reduced drastically with the increase in inclusion content. Clean metal, in general, is characterized by high tensile properties (yield strength, ultimate tensile strength, percent elongation). Figure 1 shows the results of filtering an Al-4.5%Cu-1.5%Mg alloy through a bed filter. As can be seen, the deeper the filter bed, the cleaner the metal, and the higher the tensile strength and elongation.

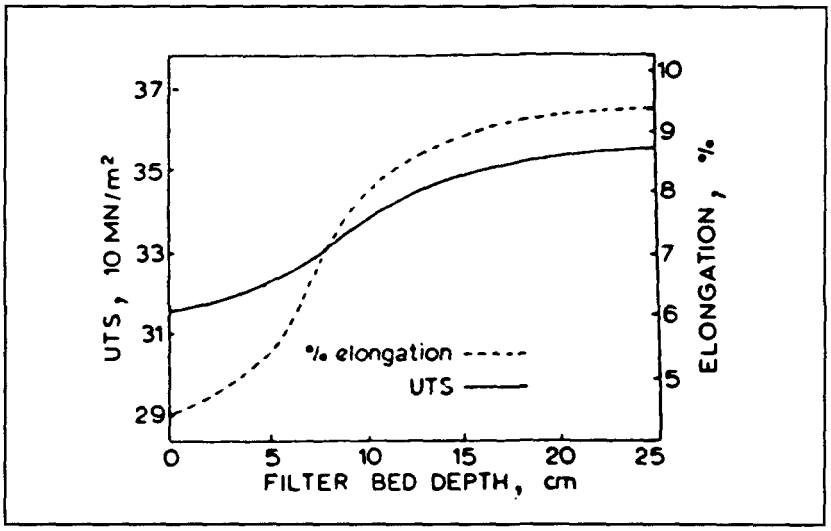

Figure 1 Variation in tensile properties with filtration for an Al-4.5%Cu-1.5%Mg alloy [1].

(2) Poor machinability and high tool wear

Some of the inclusions that may often be present in the casting are ceramic particles. They are brittle and extremely hard. The hardness of some inclusions has been measured to be about 9.5 on Moh's scale as compared to 10 for diamond. Small amounts of these inclusions in the casting can lead to extensive tool wear during machining. When an alloy melt is cleaned by filtration before casting, machinability improves quite significantly [1].

(3) Loss of fluidity and feeding properties

Oxides, other nonmetallics, and intermetallic compounds in molten metal produce a decrease in fluidity. Producing clean molten metal through filtration can increase the fluidity substantially - by as much as 30% at normal operating temperatures [2]. The effect of filtration on metal fluidity is demonstrated in Figure 2.

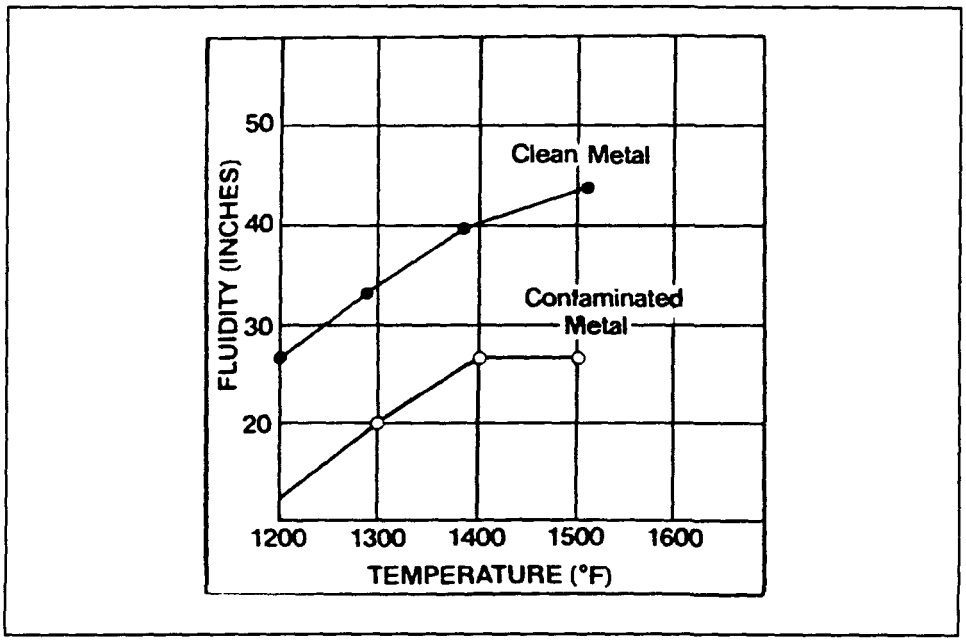

Figure 2 The effect of filtration on metal fluidity [2].

(4) Increased gas porosity

It is well known that the dissolved hydrogen level in aluminum alloy melts is the main factor responsible for gas porosity formation during solidification. The solubility limit of hydrogen in molten aluminum is significant, but reduces considerably when the metal is solidified, leading to gas porosity formation. Simple experiments on A356 and 319 alloys made by Laslaz and Laty [3] confirm that the gas porosity after solidification depends not only on the hydrogen content in the molten metal, but also on metal cleanliness. Oxides act as pore nucleation sites, and hydrides decompose upon cooling to produce dissolved hydrogen.

(5) Poor surface quality and lack of pressure tightness

Defects in aluminum-silicon products such as pinholes in thin foils and razor streaks in lithographic plates are commonly caused by inclusions [4]. Inclusions, in size range of 10-20 μm effective diameter can, at a concentration of a few parts per million, be harmful in rolled aluminum products.

However, there is no general agreement on the question of what size and which types of non-metallic inclusions are the most harmful, and which inclusions are tolerable in aluminum alloys.

2.3.2 Types and Sources of Inclusions

According to Gruzleski and Closset [1], there are two general types of inclusions : exogenous inclusions and indigenous inclusions. Exogenous inclusions come from outside the melt itself and can include refractory particles resulting from the erosion of the crucible material. Their size is random. They may include dross, salts, furnace oxides, unmelted elements, corrundum or sludge. Indigenous inclusions appear as a result of chemical treatments, such as fluxing or grain refinement, applied to the melt. It is inevitable that these inclusion particles will appear in the molten metal during the various stages of processing and from the charge material before casting.

According to Apelian and Shivkumar [5], inclusion particles can be further classified as:

Solid inclusions: isolated, rigid particles or masses of different phases, textures and shapes which may be brought into the molten metal from outside (e.g., refractory brick material, melt treatment additives), or during processing.

Liquid inclusions: particles which are deformable and may coalesce into large globules.

Fluxes and salts: suspended in the melt as a result of prior melt treatment processing.

Solid inclusions are metallic or non-metallic and are formed at various stages. Oxides, nitrides, carbides and borides are the common types. Oxides are very easily formed, as molten aluminum reacts readily with oxygen. Also, as aluminum alloys contain Fe, Si, Mg, etc., various kinds of oxides will form, viz., Al_2O_3, SiO_2, MgO, Al_2MgO_4, FeO or Fe_3O_4. The most common type of oxide in aluminum alloys is Al_2O_3.

Lewis [6] found that aluminum oxides appeared in the molten metal bath and became entrained in the solidified metal. X-ray diffraction analysis of isolated particles on filters showed that the oxides were heavy alpha aluminum oxide (corundum), α-Al_2O_3, and light gamma oxide, γ-Al_2O_3, which adhere to the liquid metal bath. Dispersed γ-Al_2O_3 oxide is related to the purity of the initial charge, i.e., fresh or scrap. When the scrap is cut into small pieces, there is significant increase in the total surface of charge. Therefore, more Al_2O_3 oxide is expected to occur. There are at least 15 forms of aluminum oxides. With time, temperature, and pressure, they all transform to the corundum form that settles at the bottom of the reverberatory furnace. These oxides are very harmful and cause machining difficulties.

Lewis [6] has explained clearly how these oxides come into the melt. All aluminum solids have an oxide coating or oxide skins. When these pieces are melted, the oxide coatings remain in the melt. As more scrap is put into the furnace, a skim layer or barrier, which is formed by oxides develops on the surface of bath. Most of these oxides remain on the top of the bath by the surface tension of the molten melt. Those oxides suspended below the metal line will be trapped also by surface tension. The furnace side wall is the main site where the light oxides will form. Once trapped in the melt bath, the oxide will continue to increase in weight, dropping gradually to the bottom of the bath until it becomes corundum at the bottom of the bath. Another source of oxide formation is the addition of oxygen or moisture to a furnace hearth at elevated temperature. When air enters the hearth through any undesirable openings in the furnace, it will introduce these oxide-forming ingredients. Combustion will produce moisture (especially in the

reverberatory furnace), then oxides will generate around these openings. In an electric glow-bar type reverberatory furnace, oxide products are less than in the reverberatory furnace, because these furnaces do not have the voluminous products of combustion associated with natural gas burners. Once the oxygen-rich air goes into the furnace, it will react with the newly exposed aluminum-silicon liquid alloy. The furnace-generated aluminum oxide needs time and temperature to be developed. When the melt temperature is above 787 C, the rate of oxide formation increases.

Lessiter [7] reported that in addition to Al_2O_3, magnesium oxide (MgO) and magnesium aluminate spinel ($MgAl_2O_4$) are the most common oxides observed. These inclusions are black or brown, thick films or elongated lumps (consisting of loosely adherent particles). These broken films appear in dross, an area deserving careful attention in the quest for clean aluminum.

Eckert [8] observed that magnesia (MgO) inclusions appear in aluminum-silicon alloys containing magnesium in the form of 1-5 micron dispersoids, films and clusters. Dispersoid magnesia mainly results from oxidation of original concentrations of magnesium that form during poor alloying. Oxide films and clusters are formed by direct melt oxidation.

The spinel ($MgAl_2O_4$) is formed by melt oxidation and occurs in the form of a thick film or cluster. Spinel formation is accelerated if there exist magnesia (MgO) inclusions, and is reduced by adding up to 0.1% beryllium to the melt [7]. Figure 3 shows typical examples of these oxide inclusions.

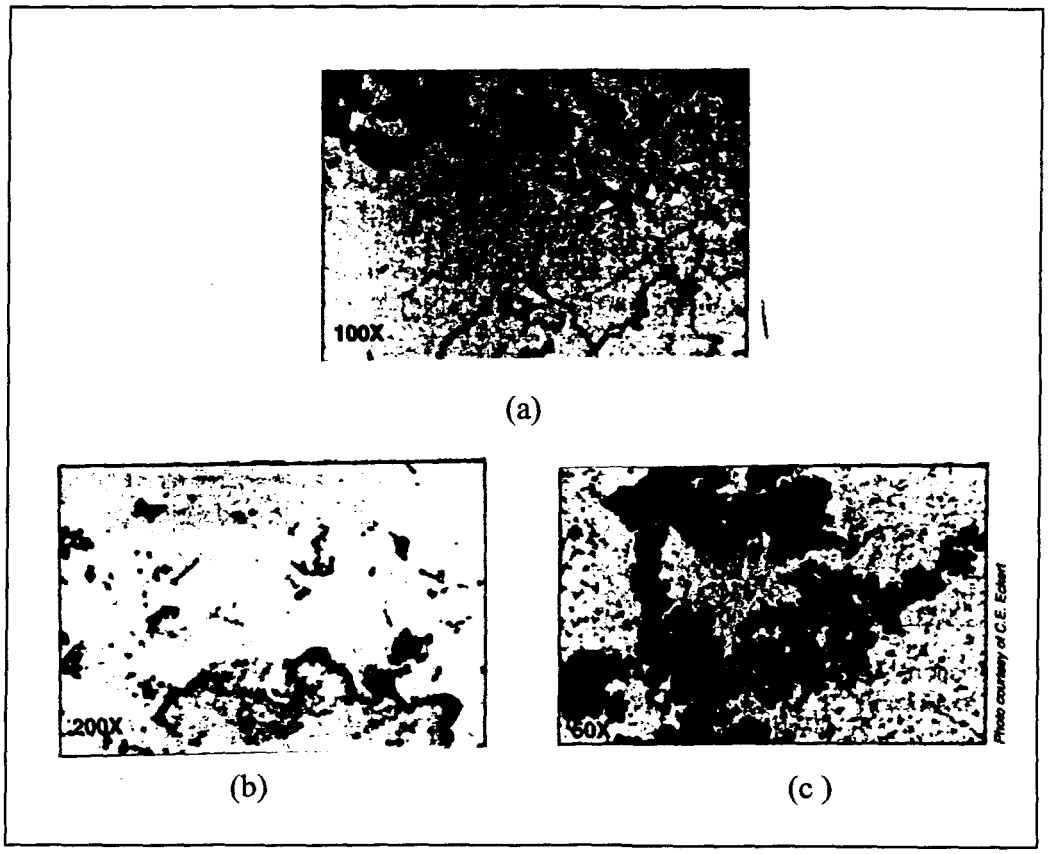

Figure 3 Photomicrographs showing : a) gamma alumina (Al_2O_3), b) magnesia (MgO), c) dispersoid spinel cluster ($MgAl_2O_4$) [7].

Normally, there are three sources of carbides: 1) reaction between air and melt, 2) bricking lines in the furnace, etc., and 3) charge and tools. The dominant type of carbides is Al_4C_3. These carbides appear as hexagonal or rectangular disks in clusters, isolated or together with oxides and borides. In the present work, coarse Al_4C_3 inclusion particles could have formed : i) during degassing of the molten metal using a graphite impeller for long times at temperatures as high as 735°C, ii) due to reaction between the molten metal and the surface of the silicon carbide crucible used for melting, iii) due to reaction between the molten metal and air, or iv) have been already present in the commercially pure aluminum used to produce the alloy.

Nitrides in the aluminum-silicon alloys have been identified by electron diffraction patterns to be AlN and possibly oxynitrate. They may be formed also by the reaction between air and molten metal. Nitrides are commonly found in association with oxides [5].

The chemical equations below show how the molten metal reacts with air at the melt temperature.

$$2Al + N_2 \rightarrow 2AlN$$

$$6Al + 3CO \rightarrow Al_4C_3 + Al_2O_3$$

$$8Al + 3CO_2 \rightarrow Al_4C_3 + 2Al_2O_3$$

$$\frac{4}{3}mAl + C_mH_n \rightarrow \frac{m}{3}Al_4C_3 + nH$$

At high temperature, the nitride and carbide can also react with oxygen.

$$4AlN + 3H_2O \xrightarrow{>900^\circ C} 2N_2 + 2Al_2O_3$$

$$Al_4C_3 + 6CO_2 \xrightarrow{>500^\circ C} 2Al_2O_3 + 3CO_2$$

The most common borides are TiB_2 and VB_2. An aluminum-silicon melt contains about 1 ppm borides. When the melt is grain refined, it can contain up to 100 ppm borides [5]. Liquid inclusions also contain chlorides and flourides, when chlorine gas or chloride flux is used for degassing the melt. The chloride inclusions may form, especially in Mg-containing alloys [9]. Usually, there are less than 1 ppm fluoride-cryolite inclusions in aluminum-silicon alloys, appearing in the form of medium grey

spherical particles. Cryolite particles are inhomogeneous and contain smaller particles of Al_2O_3 and CaF_2, and traces of MgO. The source of cryolite particles is the aluminum electrolyte. The higher the temperature, the quicker the speed of aluminum oxidation. If the flux materials which are used to help remove dross are not taken away at the proper temperature, these particles will be present in the final product.

2.4 Inclusion Assessment

The control of metal cleanliness in molten aluminum alloys is an integral part of meeting quality control requirements in the modern aluminum cast shop, in particular for high-quality thin gauge or surface critical applications (can body and can end stock, foil, anodizing or lithographic sheet material) [10].

There are several techniques for measuring the inclusions in aluminum castings, including ultrasonic, LiMCA, vacuum filtration, pressure filtration (e.g., PoDFA), fracture test, and Qualiflash techniques.

2.4.1 Ultrasonic Technique

This is a non-destructive technique since it allows detection of inclusions via wave analysis, and is based on the principle of energy dissipation of a sound pulse. To measure inclusions using this technique, a signal from a piezoelectric crystal is sent through the metal by a transmitter (Figure 4). When the signal passes through the melt, some amount of its energy is reflected at inclusions. The reflection results in the reduction of the signal

energy. The reduced energy signals are collected by a receiver and displayed on an oscilloscope. These signals give an indication of the content and size of inclusions and a counter records the data.

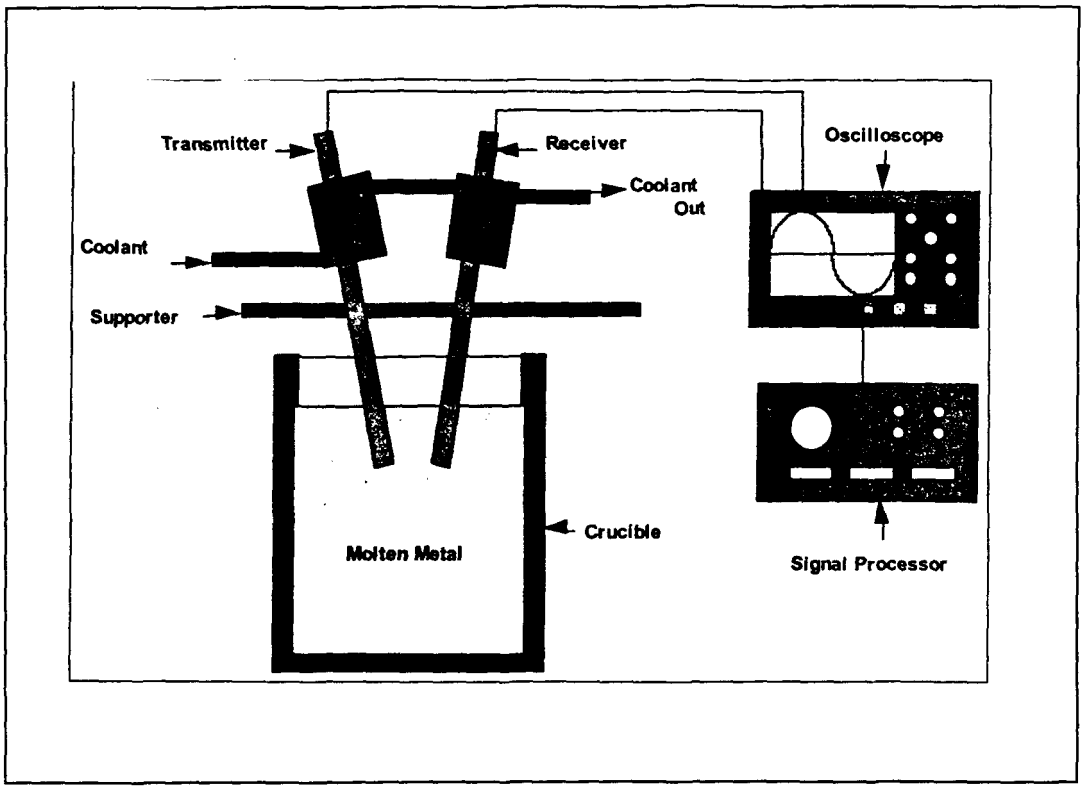

Figure 4 Schematic diagram of an ultrasonic apparatus [10].

With the ultrasonic technique, both nonmetallic and metallic inclusions can be detected [11]. The disadvantage of this technique is that it can only detect inclusions greater than 100 μm.

2.4.2 On-Line Melt Cleanliness Determination-LiMCA

The LiMCA (liquid metal cleanliness analyser) technique is based on the electric sensing zone (ESZ) principle [12] and is shown in Figure 5.

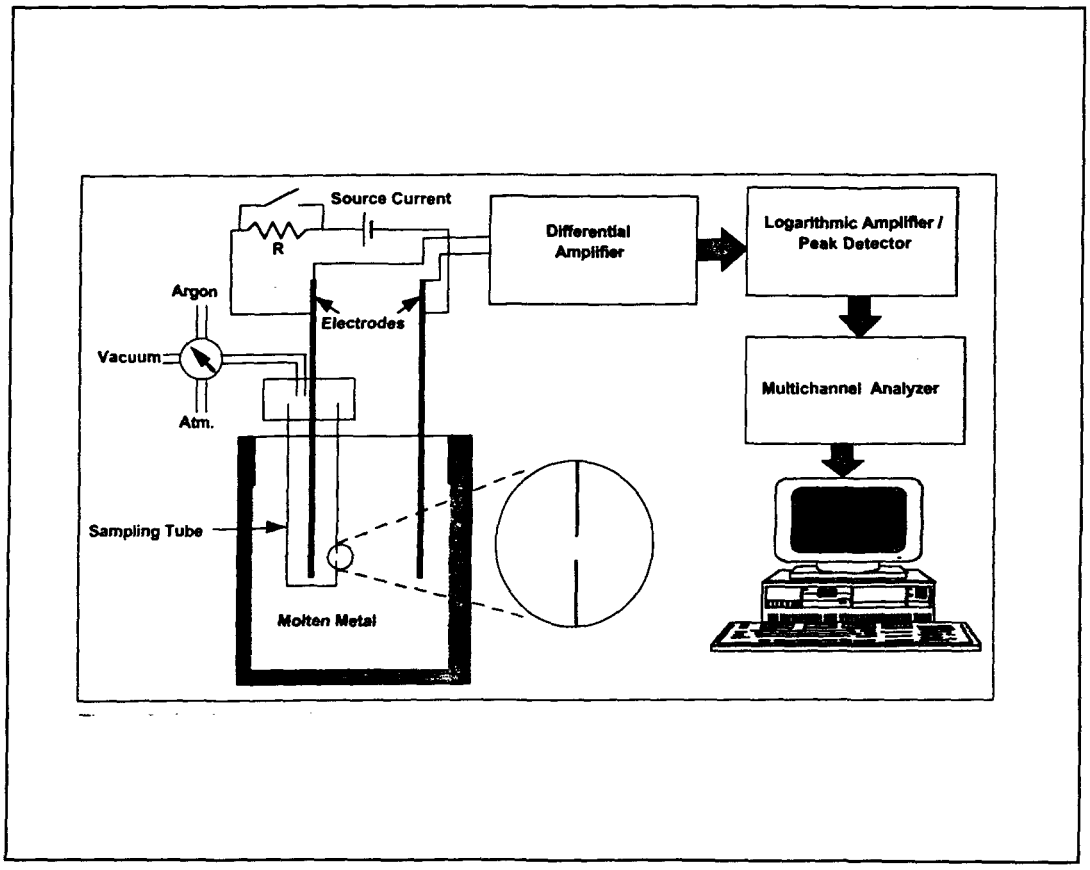

Figure 5 Schematic diagram of the LiMCA technique [12].

The LIMCA unit consists of a probe, a current source, and a signal processing system. The probe consists of two electrodes and a sampling tube made of non-conducting material (e.g., glass), and having a small orifice (~ 300 μm) through its surface. The tube is immersed in liquid metal, generally in a trough carrying molten aluminum. A negative pressure is applied inside the tube to force the metal to flow into it via the orifice. A constant electric current is applied between the two electrodes located inside and outside the probe. This current must circulate through the orifice where it is carried by the incoming liquid metal, as it is the only electrically conducting path between the electrodes. The voltage drop across the orifice is monitored. For pure metal/alloy, the drop remains

constant, but when non-electrically conducting inclusions pass through the orifice, a slight increase in voltage drop is observed. The signal processing system translates the voltage fluctuation and the distribution of their amplitudes to particle densities, and volume distributions are expressed as histograms, showing the particle density per particle size interval.

The advantage of this technique is that the measurement can be made available on-line very quickly at time intervals on the order of one minute. This enables the LiMCA to monitor quasicontinuously and in real time the evolution of cleanliness along a cast, either as a function of process parameters or only as a function of time. Using this technique, we can detect inclusions as small as 20 μm.

The disadvantage of this technique is that it cannot detect conductive inclusions such as intermetallic inclusions effectively, and the orifice is very easily blocked by large-sized inclusions. It cannot provide information on the chemistry, shape, or the physical state of inclusions. The cost of the apparatus, as well, is very high.

2.4.3 Vacuum-Filtration Technique

This technique is an off-line inclusion measurement type [13]. A typical example of this technique is the Union Carbide-type vacuum-filtering system, shown in Figure 6.

As shown in the figure, the system includes a filter, a filter cup, a tapered plug, and a vacuum container. The test is carried out as follows: Using a tapered plug to protect the filter from contamination, the whole unit is immersed in the molten metal and kept as such for a period of time sufficient to preheat the unit; next, the tapered plug is pulled out, the

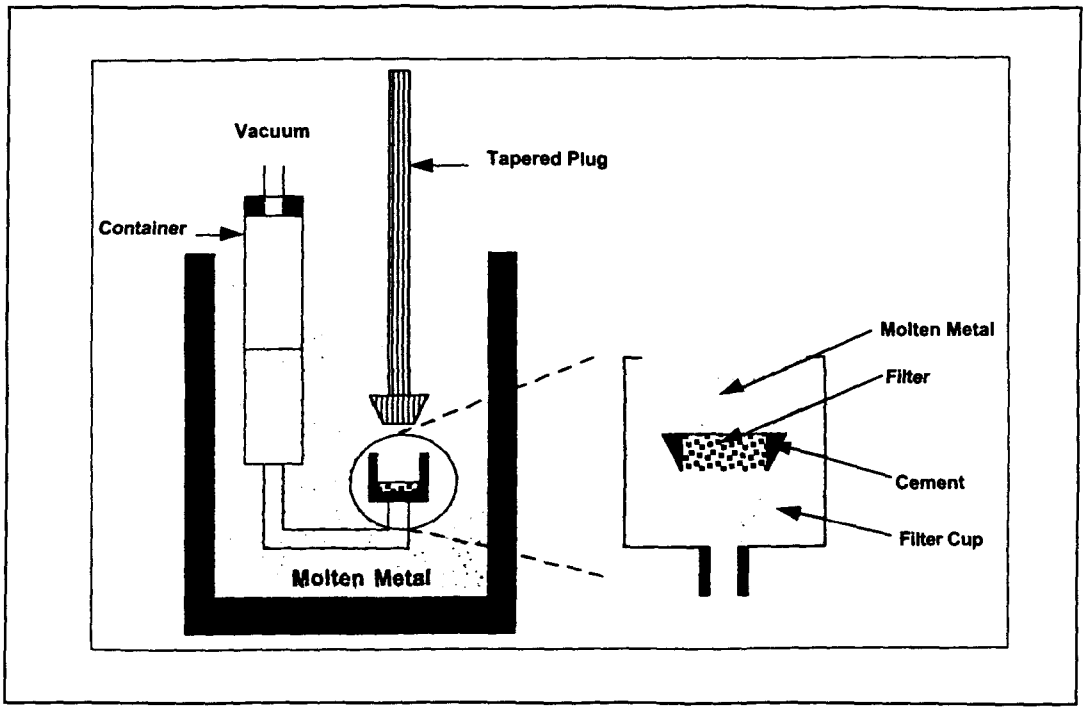

Figure 6 Schematic diagram of the vacuum-filtration technique [13].

vacuum starts to draw the molten metal through the filter. Finally, after a certain amount of the metal has been sampled, the unit is pulled out of the bath for cooling, and upon solidification, the filter is removed and sectioned along the diameter perpendicular to the filter surface. The inclusion concentration is determined in terms of the volume fraction of particles per unit weight of metal drawn through the filter.

The advantage of this technique is that the filtration can be carried out directly in the bulk molten metal at any location, and a large volume of molten metal can be filtered through the filter, improving the accuracy of the inclusion assessment.

The technique has some practical disadvantages. For example, if, on the completion of vacuuming, the metal head is not appropriately balanced in the container by a corresponding vacuum, back flow of molten metal from the container to the filter cup may

take place. Also, if the bottom of the filter cup is not chilled before the unit is lifted out of the molten bath, the inclusions in the filter cup will be drawn through the filter during the solidification period. Moreover, leakage may also occur during sampling if any of the joints are not sealed tightly.

2.4.4 Fracture -Test Technique

Fracture tests have been extensively used to evaluate the characteristics of metals. The K-Mold device is a typical application of this technique.

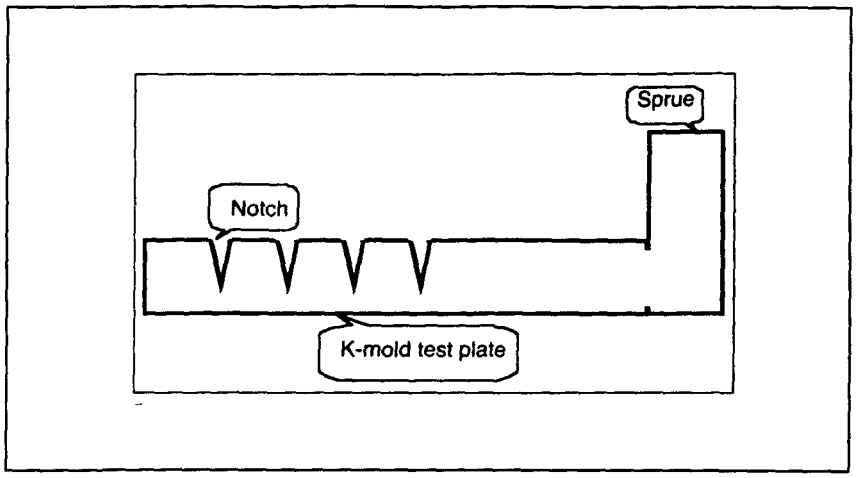

Figure 7 Schematic diagram of K-Mold fracture plates [10].

As shown in Figure 7, a flat plate having four notches is cast. These notches serve as fracture points. The shape of the knife edges improves the efficiency of capturing the inclusions on the fracture faces through the effect of some eddy occurring during mold filling. In one test, a number of sampling plates are cast in preheated molds using the molten metal to be evaluated. Thereafter, the cast plates are fractured immediately. Each fracture face that contains one or more inclusions is considered as one event. Based on this

criterion, four events can possibly occur in each plate. The result is interpreted by means of the ratio of events to the total number of fractures, called the K-Value. The lower the K-Value, the higher the quality of the metal. For quality castings, K should not exceed 0.05.

There are many advantages of this technique. The cost is low, and no large investment in either first cost or continuing examination is needed, for the tooling and other equipment required to cast a test coupon or fracture a notched plate. The results are quickly obtained on the shop floor, and the technique is easy to learn. The disadvantage of this technique is that it cannot provide good quantitative and accurate results compared with other techniques.

2.4.5 Qualiflash Technique

Qualiflash [14] is a shop apparatus that can be used to ensure bath quality before casting. The apparatus is shown in Figure 8.

Measuring the cleanliness of the aluminum melt

Figure 8 The Qualiflash apparatus [14].

The unit is mounted on a trolley. A funnel-shaped shell is used to cast the sample of metal taken. This shell is heated by an electrical resistance furnace and its temperature is regulated. A fresh extruded ceramic filter is used for each measurement. The filter is held against the bottom of the shell by a spring plug. There is an ingot mold under the shell to recover the metal that flows through the filter. The ingot mold has ten steps. The ingot mold and the shell can be moved by hand about a horizontal axis to remove the excess metal left in the shell and the metal that has flowed. A thermocouple is used to measure the temperature of the metal in the spoon before it is poured into the shell. The filter and the thermocouple are the only consumable elements. The measuring principle is simple. It involves the intentional near-complete clogging of the section of the filter by inclusions. The cleanliness of the alloy is estimated immediately (once the metal has stopped flowing through the filter), using a nomograph, specific to each alloy, that indicates the degree of cleanliness according to the quantity of metal that passed through the filter.

The temperature of the shell is controlled between 420 and 430°C, which allows the metal to flow through the filter until it clogs before solidification starts. The pouring temperature is kept at about 720°C. A temperature range appropriate to the alloy to be tested is specified to optimize the sensitivity of the system to differences in oxide levels. The oxide level as measured by image analysis can range from 0 to 50%, and the mass of metal passing through the filter from 2.7 to 0.8 kg. The metal flows through the filter for about 20 seconds at most. The result can therefore be read instantaneously, simply by counting the number of steps covered in the ingot mold.

This device is a very simple and quick way of estimating the quantity of oxides, basically alumina skins, in an aluminum alloy bath, and can be operated even by relatively unskilled personnel.

2.4.6 PoDFA Technique

The PoDFA (Porous Disc Filtration Apparatus) technique comprises direct examination of polished sections that provide information about the type and morphology of inclusions [15]. In order to obtain accurate results, it is necessary that the inclusions be preconcentrated in a small section. Figure 9 shows a schematic diagram of the PoDFA method [15].

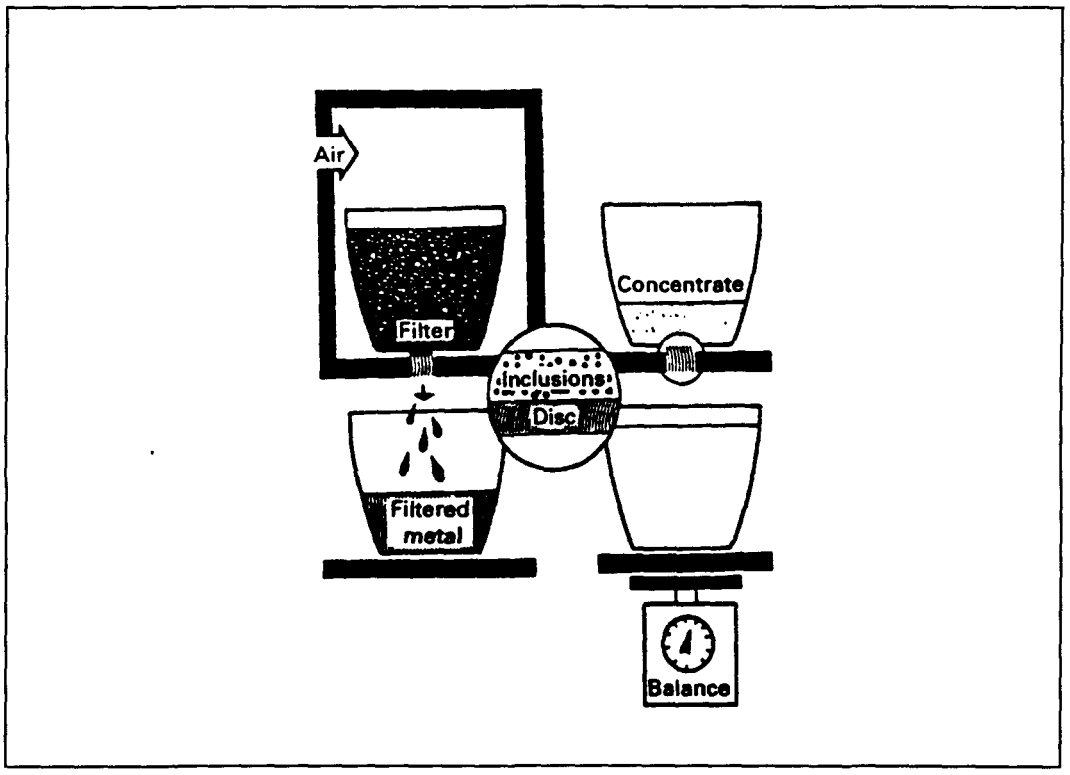

Figure 9 Principle of the PoDFA method of measuring metal cleanliness [15].

The PoDFA technique involves two different operations, the first, preparation and filtering of a molten metal sample carried out at the casting center, the second, the preparation and evaluation of the sample obtained from the solidified metal above the filter disc, performed in a metallography laboratory.

The first operation is carried out as follows : a 2 kg sample of molten metal (at ~735 C) is taken from the melting furnace and poured into a preheated crucible (at ~850 C) which contains a porous alumina refractory disc. The cover of the apparatus is then lowered over the crucible, and the system is pressurized to force metal through the filter disc. When about 1.5 kg of metal has filtered through, the pressure (~10 psi) is relieved, and the weight of filtered metal recorded. After the sample in the crucible has solidified, the disc and overlying unfiltered metal is removed from the crucible, cut to a smaller size and sent to the laboratory for analysis.

The second operation is carried out as follows : After removing excess metal, the sample is sectioned through the central plane perpendicular to the disc, hot mounted in bakelite, and polished on a mechanical polisher, taking care to see that the interface between the disc and metal is uniform. The polished sample is then examined under an optical microscope, and the type and concentration of inclusions determined.

The method of inclusion identification is proprietary to Alcan International Limited. The total inclusion concentration area per kilogram is given by:

Total Inclusion (mm^2/kg) = [{Mean Measured Residue Area (mm^2) × Inclusion Area Fraction}/{Filtrate Metal Weight (kg)}] × [{Nominal Chord length (mm)}/Measured Chord Length (mm)}]

This technique can distinguish inclusion types and differentiate between the levels of boride, carbide and spinel which are present within an individual sample. It is easy to set up and to produce the samples.

Practice for thirty years in more than fifty aluminum cast houses worldwide has shown that this technique is a good tool for process optimization and quality control [16], and is invaluable in establishing the cause of the problem in unsatisfactory metal [17].

2.5 Tensile Properties

2.5.1 Tensile Property Parameters

When we talk about the mechanical properties of aluminum casting alloys, we often mean these parameters : ultimate tensile strength (UTS), yield strength (YS) and percent elongation (%EL). The first two parameters are strength parameters, the last one is a ductility parameter. These parameters provide basic information on the strength of materials for design purposes, and are determined by means of the engineering tension test.

In this test, a specimen (usually a cylindrical bar, 0.505 inch in diameter and 2 inch gauge length) is subjected to a continually increasing unaxial load or force applied coaxially. The elongation of the specimen is noted simultaneously, and an engineering stress-strain curve recorded, as shown in Figure 10.

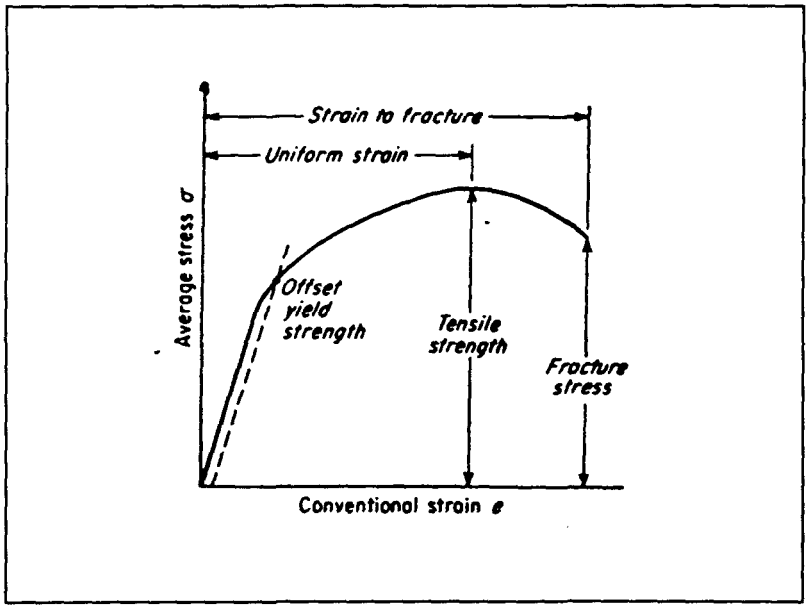

Figure 10 An engineering stress-strain curve [18].

The engineering stress, σ, is defined as the load (force), P, divided by the original area of cross-section of the specimen, A_0:

$$\sigma = \frac{P}{A_0}$$

The strain, e, is the average linear strain, which is the elongation of the gauge length of the specimen, ΔL, divided by its original length, L_0:

$$e = \frac{\Delta L}{L_0} = \frac{L - L_0}{L_0}$$

The shape and magnitude of the stress-strain curve of a metal or alloy depend on the composition, heat treatment, strain rate, temperature, and the type of stress applied during the testing. The parameters used to describe the stress-strain curve are the tensile strength, yield strength and percent elongation, as mentioned above.

The tensile strength or ultimate tensile strength is the maximum load divided by the original cross-section area of the specimen:

$$\sigma = \frac{P_{max}}{A_0}$$

Although the tensile strength is the more frequently quoted property obtained from a tension test, and is a useful design parameter for brittle materials, in the case of ductile materials, however, the yield strength is considered to be more appropriate as it takes into account the plastic deformation or yielding of the material.

The yield strength is the stress required to produce a small specified amount of plastic deformation, and is usually defined as the offset yield strength that is given by the

stress corresponding to the intersection of the stress-strain curve and a line parallel to the elastic part of the curve (straight part) offset by a specified strain, usually 0.2%.

Thus, yield strength is given by:

$$\sigma_0 = \frac{P_{e=0.002}}{A_0}$$

The yield strength is more sensitive than the tensile strength to differences in heat treatment and the method of testing. It gives an indication of the extent to which the material may be deformed before fracture takes place.

The third parameter, percent elongation, gives a measure of the ductility of the metal or alloy. It is expressed by :

$$e_f = \frac{L_f - L_0}{L_0}$$

L_f being the gauge length at fracture.

2.5.2 Factors Affecting Tensile Properties

In order to obtain the best mechanical properties, it is necessary to optimize the metal quality before casting. This includes important molten metal processing steps like degassing of the melt, inclusion removal by floatation and/or filtration, grain refinement, modification of the eutectic silicon, and adjusting the metal composition. By carefully controlling each of these steps, the properties of the casting can be significantly improved.

2.5.2.1 Effect of Alloy Composition

For aluminum alloy castings, Si and Mg are the main alloying elements. In Al-Si alloys, Si appears as hard and discontinuous particles embedded in a ductile matrix. The strength of the Si phase is 1520 MPa, whereas that of the matrix is 546 MPa [19]. Increasing the Si content up to 7% increases the tensile strength and yield strength, but decreases the ductility.

The shape and distribution of the Si particles in the matrix have a strong influence on the mechanical properties of the cast alloy. Good tensile, impact and fatigue properties are achievable if the Si particles are small, spherical, and evenly distributed. This can be achieved through the addition of small amounts of elements like Na or Sr that change the brittle, acicular form of the silicon into a fibrous form. The Na or Sr are said to "modify" the silicon.

In Al-Si-Mg alloys, Mg combines with Si to form the age-hardening compound Mg_2Si. The increase in strength with Mg content becomes evident after heat treatment, and the improvement in strength properties is accompanied by a corresponding reduction in ductility.

DasGupta *et al.* [20] have studied the effect of increasing the magnesium content from ~0.07% to ~0.59% on the mechanical properties of sand-cast 319 aluminum alloy. The authors conclude that increase in magnesium content in this range has a negligible effect on the mechanical properties of the alloy. Furthermore, no significant microstructural changes occur (either in the as-cast or in the T5 condition).

Generally, iron is the main impurity in most Al-Si alloys. Efforts are made to keep it as low as economically possible, because of its deleterious effects on ductility and corrosion resistance. The formation of certain iron intermetallic compounds such as the brittle Al_5FeSi phase can be harmful to the alloy properties.

2.5.2.2 Effect of Degassing

During melting and holding, molten aluminum easily absorbs hydrogen. The solubility of hydrogen in liquid aluminum is an exponential function, increasing rapidly with temperature. During solidification, the hydrogen rejected from the liquid metal forms gas porosity which significantly impairs the alloy mechanical properties. Figure 11

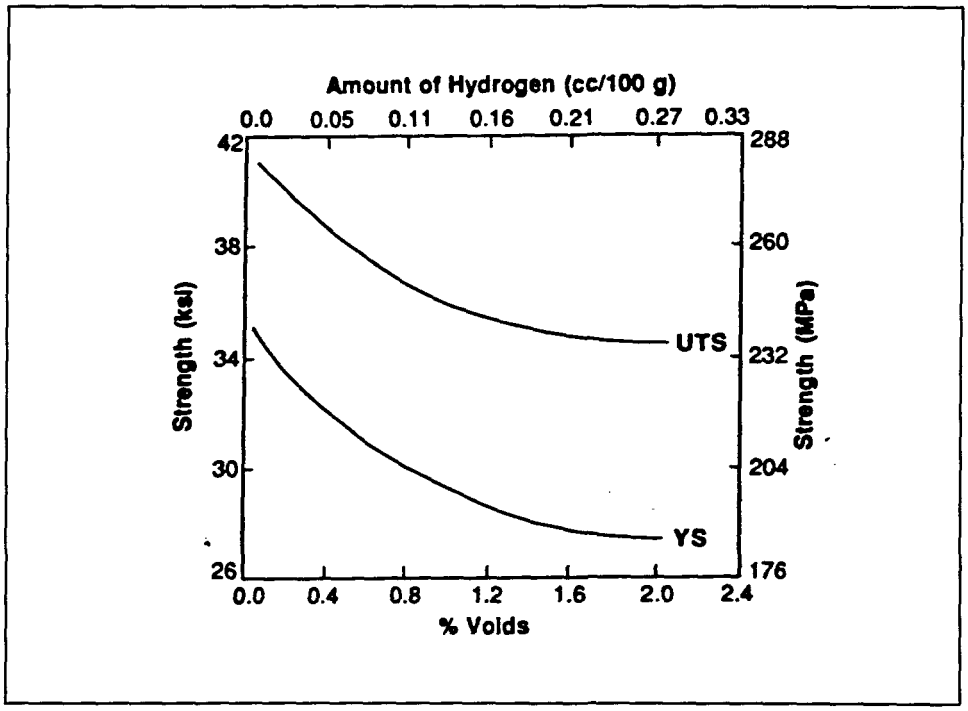

Figure 11 Effect of hydrogen porosity on the tensile and yield strengths of sand cast 356-T6 aluminum castings [21].

depicts the relationship between amount of hydrogen and alloy strength in 356-T6 aluminum alloy sand castings [21].

There are a number of methods to degas molten aluminum. Gas purging is the most popular method. Hydrogen exists in liquid aluminum in atomic form. Effective hydrogen removal requires that the hydrogen atoms combine to form hydrogen gas molecules. When hydrogen-free bubbles of an inert gas are introduced into the melt, hydrogen atoms diffuse into these bubbles. Since the gas phase is already present, there is no need to nucleate separate bubbles of hydrogen. The hydrogen (H_2 gas) can proceed easily with the gas bubble and be lifted out of the melt as the bubble rises to the surface. The most commonly used gases are pure, dry nitrogen or argon. These gases are usually introduced into the melt by means of a porous graphite head.

2.5.2.3 Effect of Grain Refinement

Small amounts of grain refiners are often added to molten metal to control the grain structure in commercial castings. The grain size has an inverse relationship to the number of nuclei present in the liquid. The grain refiner particles provide nucleating sites for the formation of primary α-aluminum dendrites and facilitate the production of a casting with a large number of small, uniform, and equiaxed grains. However, small amounts of finely dispersed porosity in the cast product are associated with grain refining. Vass [22] found grain refining improves the mechanical properties, especially fatigue resistance.

2.5.2.4 Effect of Modification

Mondolfo [19] reported that in the Al-Si system, there are divorced eutectic areas of aluminum with Si in solid solution mixed with discrete particles of silicon and intermetallic compounds (Mg_2Si). In this case, the mechanical properties of the casting are affected appreciably by the morphology of the eutectic Si. Coarse, acicluar plates of silicon in the as-cast structure act as internal stress builders in the microstructure and provide easy paths for fracture. If these silicon particles are transformed or "modified" to a finer, fibrous form, the alloy properties are significantly improved. Na or Sr are customarily used to modify the melt to improve the mechanical properties. Figure 12 shows the variation in quality index Q (Q = UTS + (K) log elongation) with Sr content for three different cooling rates [23].

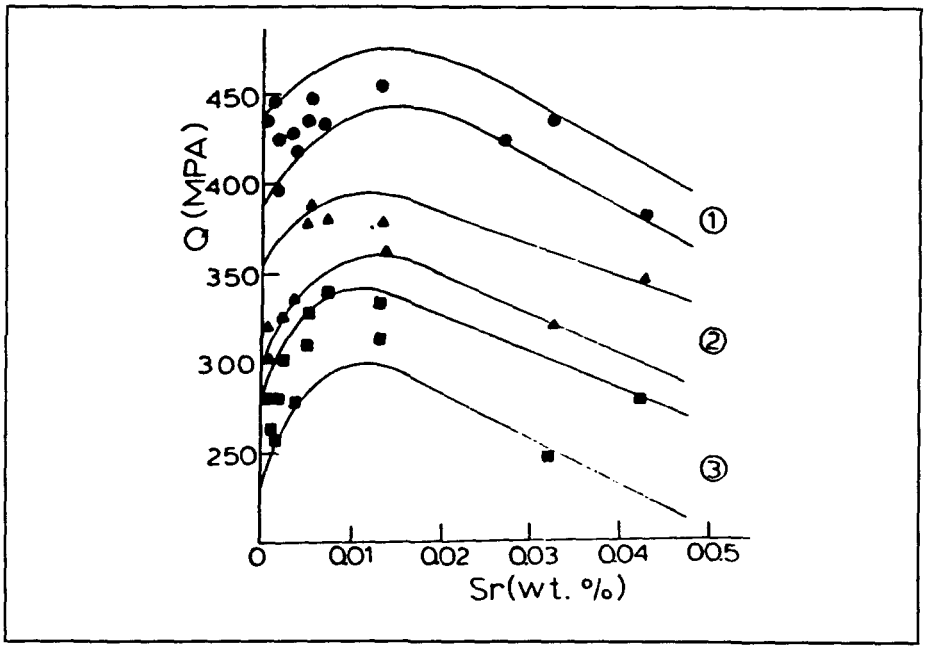

Figure 12 Variation in quality index (Q) with Sr content for three different cooling rates. Melts degassed with N_2-CCl_2F_2: Band 1 cooling rate 1.5°C/s; Band 2 cooling rate 0.5°C/s ; Band 3 cooling rate 0.08°C/s [23].

Fat-Halla [24] investigated the fracture behavior in a modified Al-7%Si-0.3%Mg alloy, and concluded that the fracture takes place in a transgranular fashion, the fracture surface exhibiting a dimple-like pattern characteristic of ductile fracture. Consequently, modified alloys possess higher ductility compared to unmodified alloys.

2.5.2.5 Effect of Heat Treatment

When an Al-Si alloy which contains Mg is heat-treated, the Mg combines with Si to form the age-hardening compound Mg_2Si. This compound, when precipitated from solid solution during heat treatment, is responsible for improvement in mechanical properties. The changes in mechanical properties resulting from heat treatment are due to the fine, coherent precipitation of β - Mg_2Si.

Meyers *et al.* [25] studied the effect of solution heat treatment on ultimate tensile strength and uniform elongation in A357 aluminum alloys. They found that the desirable levels of tensile strength achieved are largely attributed to the formation of the non-equilibrium Mg_2Si precipitation. They also established the relationship between heat treatment time, silicon-rich structure and tensile properties (UTS and EL). A strong influence of the silicon-rich structures in the eutectics of A357 alloys on the tensile strength and uniform elongation was observed.

From their study, they concluded that the combined effect of chemical modification and grain refinement is to change the silicon-rich structure parameter that controls uniform deformation in A357 alloys. In modified and grain refined A357 alloys, the properties are sensitive to the numerical densities of the eutectic silicon-rich structure.

The same properties in the non-grained refined and unmodified alloys are strongly influenced by the Si particle size, rather than the number of these structures.

Shivkumar *et al.* [26] studied the effect of solution treatment parameters on the tensile properties of cast aluminum alloy, using ASTM B 108 test bars cast in permanent mold, and employing metallography and image analysis to examine the microstructural changes occurring during heat treatment. They concluded that the effect of Sr modification is to increase the spheroidization rate and lower the coarsening rate of Si particles. The solution temperature has a strong influence on the Si particle morphology. Extremely high coarsening rates can be obtained at temperatures greater than 560 C. Solution treatment at these temperatures, however, has a detrimental effect on the mechanical properties because of grain boundary melting. The solution times can be reduced significantly in modified samples. Increasing the solution temperature from 540 C to 550 C enhances the strength properties.

Samuel and Samuel [27] have also investigated the effect of heat treatment on the tensile properties of Al-Si-Mg/SiC_p composite castings. They have found that the effect of solution temperature on tensile properties is evident only during the first 4 hours, after which hardly any difference is observed on increasing the solution temperature from 520 C to 550 C. The tensile properties vary significantly with aging time and temperature. Prolonged solution treatment at 550 C for 24 hours results in a slight improvement in the ductility of the aged test bars.

2.5.2.6 Effect of Inclusion Removal

Intermetallic compounds such as oxides, carbides, borides and nitrides are typical of solid-phase inclusions. $MgCl_2$, Na-containing salts and CaF_2 salts are examples of liquid-phase inclusions. Oxides are the most common inclusions found in 356 and 357 alloys. These inclusions may originate from foreign particles that are added to the melt such as grain refiners, or from refractory materials, dross, furnace oxides, and unmelted flux material, or else in the form of films that result from the oxidation of the molten metal surface, and become entrained within the melt during processing. The presence of these inclusions leads to a drastic reduction in the mechanical properties, mainly tensile strength and elongation. The yield strength is relatively unaffected. The oxides also have an undesirable effect on fatigue properties.

Green and Campbell [28] studied the influence of oxide film filling defects on the strength of Al-7Si-Mg alloy castings. Metallographic and fractographic studies of the castings showed tangled networks of oxide films which were actually filling cracks in the casting. The oxide films were frequently observed in the fracture surfaces of the specimen, and often manifested themselves as gross, cliff-like discontinuities. It was found that oxide film filling defects controlled the strength distribution of the resultant castings.

Hedjazi *et al.* [29] analyzed the effect of non-metallic inclusions on the tensile properties of Al-4.5%Cu-1.5%Mg aluminum alloy ingots produced by the semicontinuous casting technique, and containing varying types and volume fractions of non-metallic inclusions. Tensile properties in the longitudinal, long-transverse, and short-transverse

directions obtained on rolled products were seen to decrease with increasing inclusion content in the alloy, the short-transverse test showing the greatest decrease. Changes in properties were related to the percentage area of inclusions in the fracture of the test piece and the results showed that the effects of inclusions on properties are dependent on the total content, size, type, and distribution of inclusions, as well as on the structural condition of the alloy.

Their experimental technique made it possible to obtain specimens containing micro-inclusions only, or those containing both micro- and macro-inclusions. As the film-type inclusions generally occupy ten times as large an area in the fracture as do non-film-type inclusions, it was possible to plot a relationship between tensile properties and film inclusions area. Their results indicated that both film and non-film inclusions lower the ductility, i.e., the percent elongation, to a greater extent than the strength of the alloy.

Arai *et al.* [30] and Kato *et al.* [31] investigated the effects of non-metallic inclusions on strength and ductility of aluminum alloys. Their results show that molten metal filtration increases the alloy strength. The smaller the pore diameter of the filter, the more the non-metallic inclusions removed, and the greater the improvement in mechanical properties. The non-metallic inclusions are seen to act as nucleating sites for dimple cleavage.

Samuel *et al.* [32] have studied the effect of melt cleanliness with respect to the presence of inclusions on the mechanical properties of Al-10% Si metal matrix composite (MMC) reinforced with 10 vol pct SiC particles. The test bars from unfiltered and filtered metal (using filters of 10, 20, 30 ppi size) were T6-tempered and tensile tested at room

temperature. The test bars were examined by X-ray radiography. The results indicated that various factors influence the casting quality and mechanical properties of the cast composite. There are two major kinds of oxides, Al_2O_3 films and $MgAl_2O_4$, (or spinel), which have a strong harmful effect on the mechanical properties. In addition, SiC sedimentation, Al_4C_3 formation, the hydrogen level of the melt, and the starting material used can also influence the mechanical properties. Their fracture studies also revealed that the inclusions and associated microvoids act as the crack initiation sites during composite fracture. The use of 10 ppi filters removed these inclusions, producing the desired properties. Figure 13 shows the variation in the tensile properties with oxide/inclusion content.

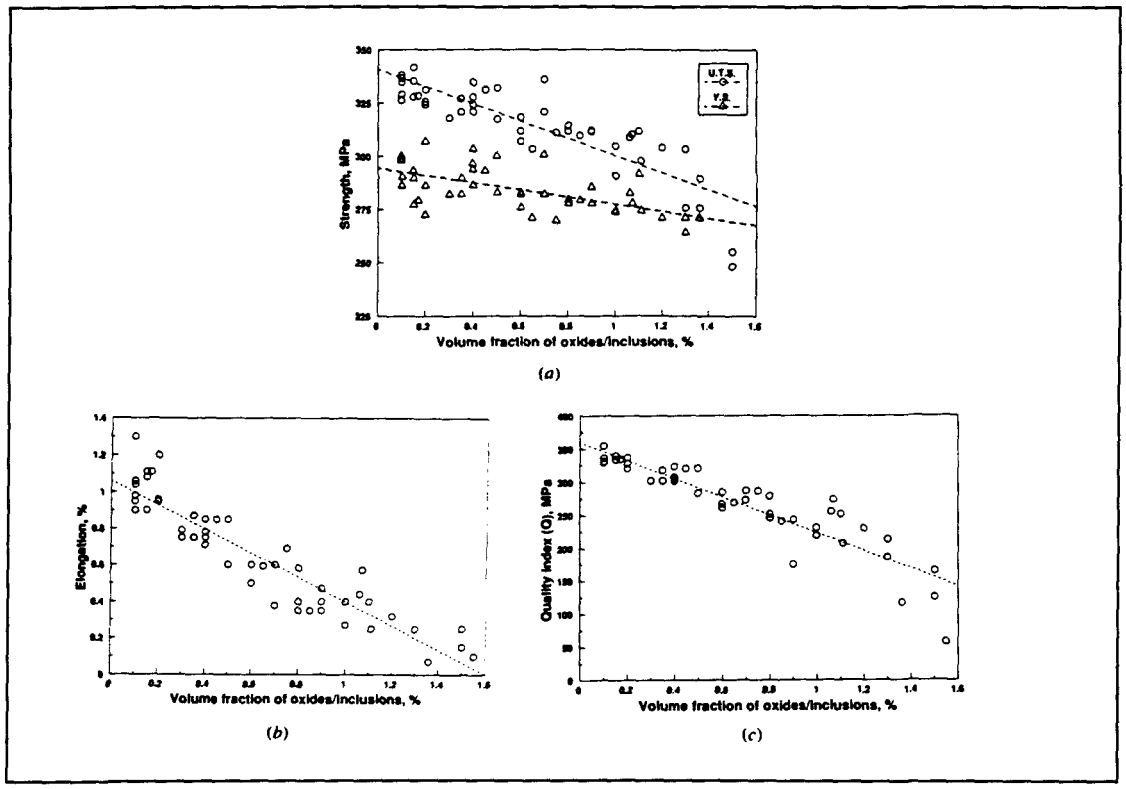

Figure 13 Variation in (a) UTS, YS, (b) elongation percent, and (c) quality index as a function of oxide-inclusion content [32].

In Figure 13, the dashed lines represent linear relations between UTS/YS and oxide-inclusion content. The relationships can be represented by the following equations:

$$UTS = 340.77 - 40.24x$$

$$YS = 294.43 - 16.81x$$

$$EL = 1.06 - 0.66x$$

where x represents the volume fraction of oxide inclusions.

Rios et al. [33] have studied the influence of coarse inclusions on the anisotropy of mechanical properties - strength, ductility and fracture - of hot extruded AA2014 aluminum tubes. Hot-extruded aluminum alloys may exhibit significant anisotropy in their mechanical properties: both the tensile strength and ductility are higher along the extrusion direction. Their results showed that the lower ductility and strength in the transverse direction of hot-extruded aluminum 2014 tubes can be correlated well with the preferential orientation of coarse inclusions. These coarse inclusions fracture early during tensile deformation and the resultant cracks may induce void formation around the small inclusions in the matrix. The coarse inclusions undergo multiple fracture which can be satisfactorily understood in terms of load transfer concepts normally used to analyze fibre fractures in composite materials.

Filtered metal, in general, produces improved tensile properties with slightly increased values of UTS, and with significant improvements in ductility. Increases in percent elongation of 25-100% can be obtained by filtration. Aluminum casting alloys are not, however, ductile materials, and an improvement of say 50% in the tensile ductility may not be large in absolute terms. As shown in Figure 1 previously, for filtration of Al-

4.5%Cu-1.5%Mg alloy through a bed filter, filtration improves with bed depth, as do the tensile properties [1].

2.6 Fatigue Properties

Metal failure under conditions of dynamic loading is called fatigue failure, presumably because it is generally observed that such failures occur only after a considerable period of service. A fatigue failure (or fracture) is particularly harmful, because it occurs without any obvious warning.

Fatigue fractures are caused by the simultaneous action of cyclic stress, tensile stress and plastic strain [34]. The cyclic stress starts the crack, while the tensile stress produces crack propagation.

The fatigue process takes place in three steps: first, there is initial fatigue damage that results in crack nucleation and initiation, followed by progressive cyclic growth or "propagation" of the crack until the uncracked cross-section of the specimen or part becomes too weak to support the applied loads, followed finally by sudden fracture of the remainder of the specimen (or part) cross-section.

Fatigue cracks initiate and propagate in regions which are most severely strained. As defects in materials are regions of stress concentration that intensify strain, most fatigue cracks generally initiate and grow from structural defects. Under the action of cyclic loading, a region of deformation (called the "plastic zone") develops at the tip of the defect. This region becomes an initiation site for a fatigue crack. Under the applied stress, the crack further propagates through the material until complete fracture occurs.

2.6.1 Parameters and tests for measuring fatigue

The *fatigue life* of a specimen is the number of stress (strain) cycles (N) required to cause failure. This number is a function of different factors such as the stress level, the stress state, the cyclic wave form used, the test environment and the metallurgical condition or microstructural characteristics of the specimen material.

Most laboratory fatigue testing is done either with axial loading, or in bending, thus producing only tensile and compressive stresses. The stress is cycled either between a maximum and minimum tensile stress, or between a maximum tensile stress and maximum compressive stress (considered as a negative tensile stress or minimum stress).

The applied stresses are described by these parameters, *mean stress*, *range of stress*, and *stress amplitude.*

The *mean stress,* S_m , is the algebraic average of the maximum and minimum stresses in one cycle ($S_m = \frac{S_{max} + S_{min}}{2}$);

The *range of stress,* S_r, is the algebraic difference between the maximum and minimum stresses in the cycle ($S_r = S_{max} - S_{min}$);

The *stress amplitude,* S_a, is one-half the range of stress ($S_a = \frac{S_r}{2} = \frac{S_{max} - S_{min}}{2}$);

During a fatigue test, the stress cycle is generally kept constant, so that S_m becomes the static or mean stress, and S_a, the alternating stress (equal to half the stress range).

Figure 14 explains the various parameters involved in cyclic stress testing.

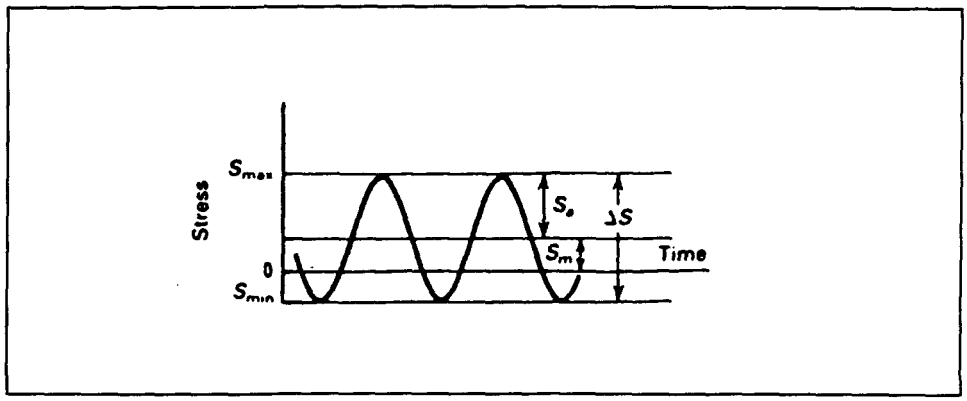

Figure 14 Nomenclature to describe test parameters involved in cyclic stress testing.

Another parameter commonly used is the *stress ratio*, which is the algebraic ratio of two specified stress values in a stress cycle. Two stress ratios commonly used are A and R, where $A = \frac{S_a}{S_m}$, and $R = \frac{S_{\min}}{S_{\max}}$.

Laboratory fatigue tests are classified either as crack initiation or crack propagation tests. In the former type, the specimen or part is subjected to the number of stress cycles required for a fatigue crack to initiate, propagate, and cause failure. In crack propagation testing, fracture mechanic methods are used to determine the crack growth rates of pre-existing cracks under cyclic loading, prior to their reaching a size critical for fracture.

In fatigue crack initiation tests, the data is usually presented in the form of an S-N curve, where the maximum stress, minimum stress, or stress amplitude (S) is plotted against the number of cycles (N) to failure, using a logarithmic scale for N, and either a linear or a logarithmic scale for S. Typical S-N curves are shown in Figure 15.

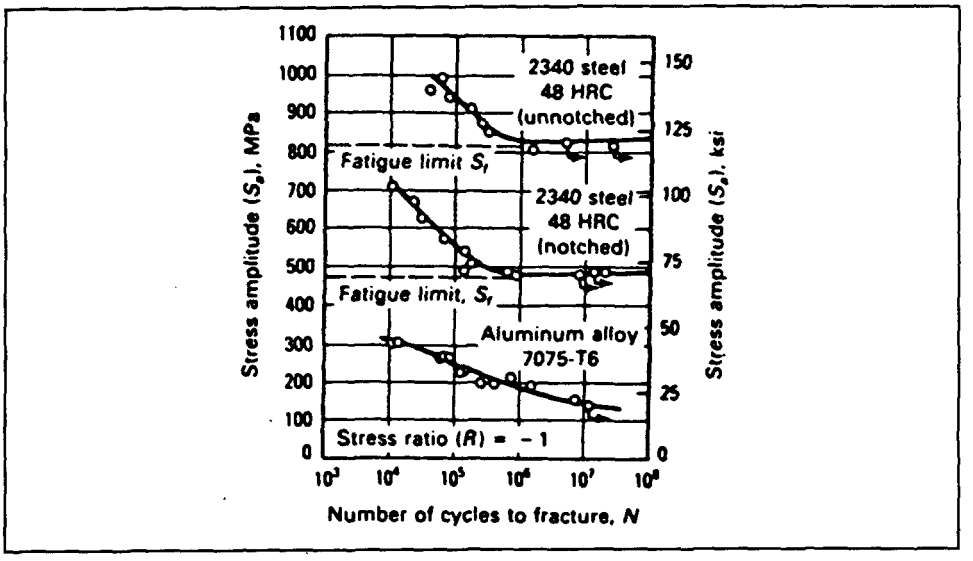

Figure 15 Typical S-N curves for constant amplitude and sinusoidal loading.

The S-N curve becomes horizontal at a certain limiting stress, S_f, called the *fatigue limit* or *endurance limit*, below which the material can endure an infinite number of cycles without failure.

Most non-ferrous metals do not exhibit a fatigue limit, and their S-N curves continue to drop slowly, as shown for the aluminum alloy sample in Figure 16. In such metals, *fatigue strength* rather than *fatigue limit* is reported, which is the stress to which the metal can be subjected for a specified number of cycles.

In the low-cycle fatigue region ($N<10^4$ cycles), the testing is carried out under controlled strain (elastic + plastic) rather than controlled stress cycles, and the fatigue behavior is represented by a log-log plot of the total strain range Δe_t versus the number of cycles to failure (Figure 16).

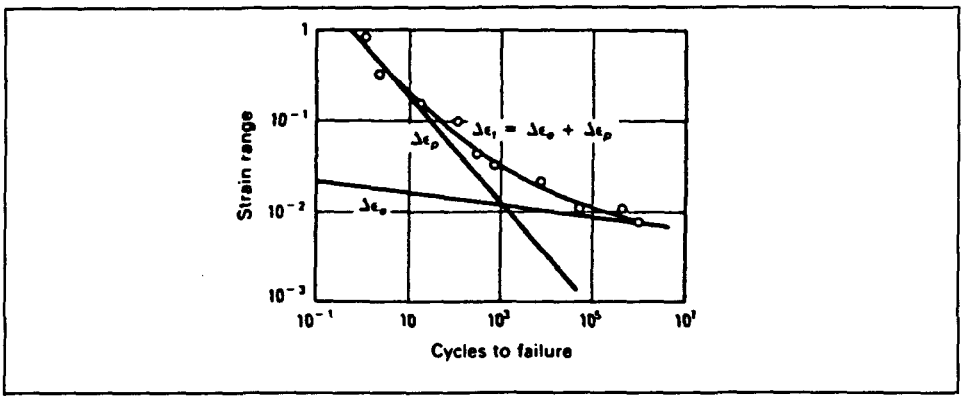

Figure 16 Typical plot of strain range versus cycles-to-failure for low-cycle fatigue.

2.6.2 Effect of non-metallic inclusions

The fatigue process is generally separated into a crack initiation phase and a crack propagation phase [35].

Tanaka and Mura [36] have studied fatigue crack initiation at inclusions in high strength aluminum alloys. They conclude that fatigue crack initiation in such alloys can be classified into three types, based on the inclusion strength relative to the alloy matrix: (i) the slip-band crack emanating from a debonded inclusion, (ii) inclusion cracking by impinging slip bands, and (iii) the slip-band crack emanating from an uncracked inclusion. The last two types are responsible for fatigue in these alloys.

Knott and King [37] have investigated the effects of non-metallic particles on fatigue performance, in particular, their influence on fatigue crack propagation. The non-metallic particles are defined as those ceramic, glassy or intermetallic particles that are not present as strengthening precipitates. Such particles are generally > 0.5 μm in diameter, and include oxides, silicates, MnS, AlFeSi intermetallics and sulphides.

The properties mismatch of such properties as elastic modulus E, coefficient of thermal expansion, toughness (or fracture toughess) between the non-metallic particles and the metallic matrices also have an important effect on the alloy properties. For example, for the case of elastic modulus, particles can be divided into two groups according to their modulus. Those where E is greater than, and those where E is lower than the modulus of the matrix. When loading, the modulus difference between a particle and the matrix will improve the local elastic stress concentration as shown in Figure 17.

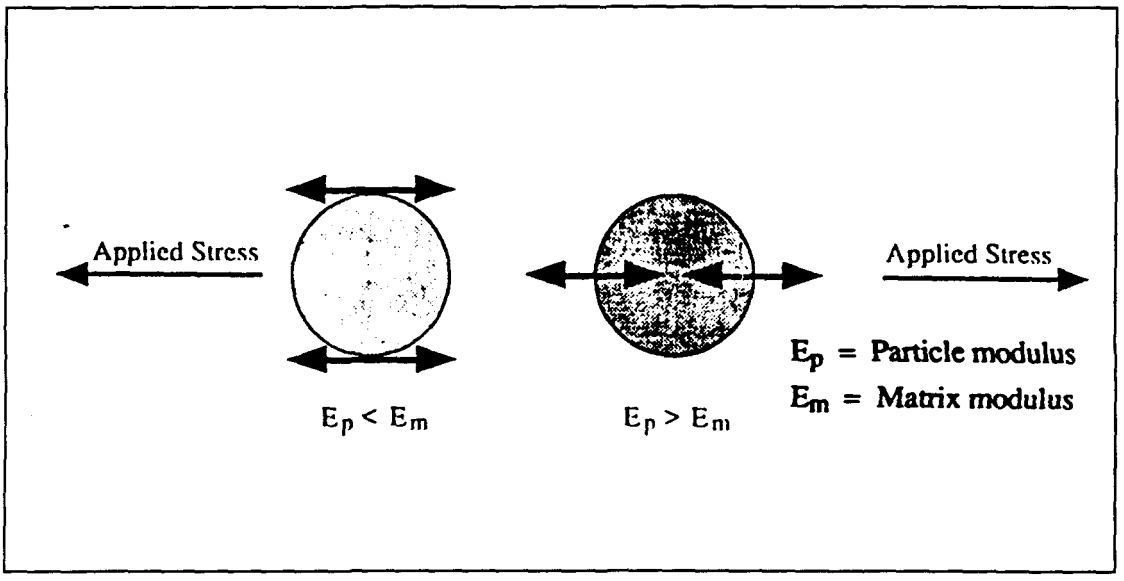

Figure 17 Stress concentration effects arising from elastic modulus mismatch [38].

Baker [38] studied the effect of nonmetallic inclusions and test temperature on the fatigue life of cast aluminum C355, C354 and A206 alloys. Examination of the surface of test bars determined the type of defects that caused fatigue initiation. From the results, most of the test bars showed non-metallic inclusions at the fatigue crack origins and there were no cases in which initiation occurred at porosity defects. The dependence of fatigue life on defect size and test stress were assumed to be as follows:

$$\text{Log}N_f = A + B \log\sigma_{max} + Cd$$

where N_f is the number of cycles to failure, σ_{max} is the maximum stress during cycling in MPa, d is the defect diameter in cm, and A, B, and C are parameters determined by the analysis.

For the three alloys studied, A differed for each combination of temperature and material. B and C, assumed to be the same for all alloys/temperatures, were found to be 6.106 and 7.024, respectively. Thus, the above equation shows how the size of non-metallic defects influences fatigue life.

CHAPTER 3

INCLUSION MEASUREMENT

CHAPTER 3

INCLUSION MEASUREMENT

3.1 INTRODUCTION

An important requirement of structural cast components used in aerospace and automotive applications is that they must be of premium quality. The production of such castings requires that porosity and inclusions be minimized to limit their harmful influence on the mechanical properties, so that these properties are then mainly controlled by the microstructure of the casting. Among the more widely used aluminum casting alloys are A356.2 and C357 alloys. These two alloys represent the most popular of heat-treatable Al-Si alloys that are hardened by magnesium silicide precipitation. Alloy C357 is similar to A356, but has a higher Mg content (~0.5 %) and can be heat treated to a higher strength level [39, 40, 41]. The alloy also contains a small amount of beryllium (Be) to improve the resistance of the liquid melt to oxidation, as well as to improve the morphology of the iron intermetallics [42].

The detrimental effects of the presence of inclusions in aluminum are well documented. Although much work has been reported on the study of inclusions, the problem of measuring metal cleanliness through a sensitive, quantitative method still exists. The difficulty is further compounded by the fact that the inclusions to be measured are

usually very small, about 10-20 mm in diameter, and present in trace amounts (~ 10 ppm). The main inclusions that occur during melting of aluminum alloy or holding periods prior to casting are aluminum oxide (Al_2O_3) as dispersed particles or oxide films, aluminum carbide (Al_3O_4), magnesium oxide (MgO), spinel ($MgAl_2O_4$), titanium diboride (TiB_2), aluminum boride (AlB) and titanium aluminide ($TiAl_3$) [4, 43, 44, 45, 46, 47, 48, 49].

The PoDFA (Porous Disc Filtration Apparatus) technique was introduced as a method of assessing metal cleanliness by Alcan International Limited [20]. Using this method, the factors controlling the precipitation and sedimentation of non-metallic inclusions (with dimensions between 20 and 50 μm) could be evaluated. In the present work, the melt cleanliness of A356.2 premium quality alloy was assessed using the PoDFA technique. This alloy was selected for study due to its popular use in automotive and aerospace applications. The main objective was to study the effect of various foundry parameters and minor alloying elements (i.e., the effects of recycling) on the type and concentration of inclusions and aluminum oxide films that can occur in A356.2 alloy melts prior to casting. In some cases, commercial C357 alloy was used for comparison purposes.

3.2 EXPERIMENTAL PROCEDURE

3.2.1 Melt preparation

Table 2 shows the chemical compositions of the A356.2 and C357 alloys. The alloy was received in the form of 12.5 kg ingots that were cut into two halves. The cut pieces were cleaned with ether, then dried in an electric oven prior to being transferred

into the melting crucible. Melting was done in an electric resistance furnace, using a silicon carbide crucible of 35 kg capacity.

Table 2 Chemical compositions (wt%) of the as-received A356.2 and C357 alloys.

Alloy	Si	Mg	Fe	Mn	Cu	Be	Sr	Al
A356.2	6.78	0.33	0.11	0.04	0.02	—	—	Bal.
C357	7.06	0.56	0.048	0.007	0.012	0.017	0.0015	Bal.

Fluidity of the liquid melts either as a function of foundry parameters or of minor alloying elements was measured using a 4210 Ragone Fluidity Tester, where the length of solidified metal in the quartz tube of the tester (at 200 mm Hg metallostatic pressure) indicated the corresponding fluidity. PoDFA trials were carried out following the instructions established by Alcan International Limited, Arvida R & D Centre, Jonquière, Québec, Canada. The principle of the PoDFA test is outlined schematically in Figure 18(a), while the pore size distribution of the filter is shown in Figure 18(b).

For each experiment, a charge of 25 kg of as-received alloy (or, in some cases scrap) was melted in a 35 kg capacity crucible. The inner walls of the crucible were coated with a thin layer of refractory material to avoid interaction between the liquid metal and the crucible material. When the melt temperature reached 735 ± 5°C , the required melt treatment was given, followed by repeated surface skimming, prior to executing the PoDFA test. In each experiment, four to six successive PoDFA trials were carried out, separated by about 40 minute intervals, the time required to complete one trial and to bring the melt temperature back to 735°C for the next trial. The filtration time was taken as the time needed to filter approximately 1.5 kg of the liquid metal from the PoDFA crucible.

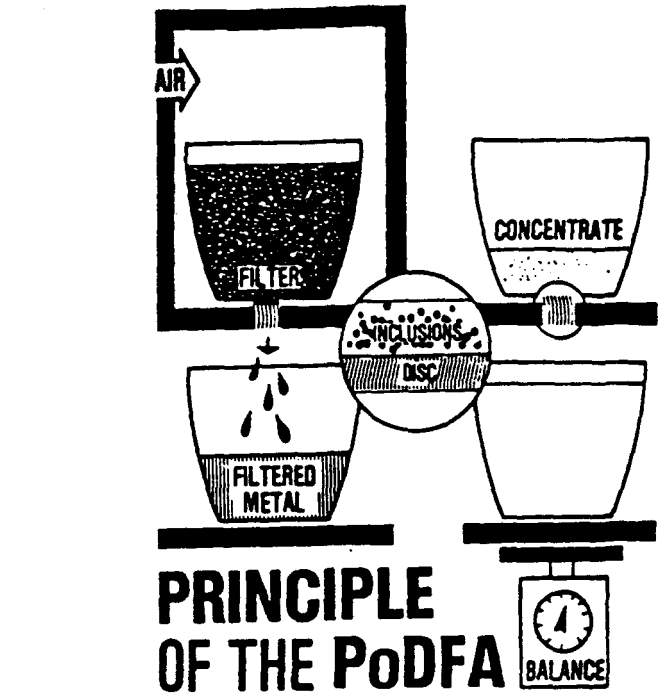

a

(a)

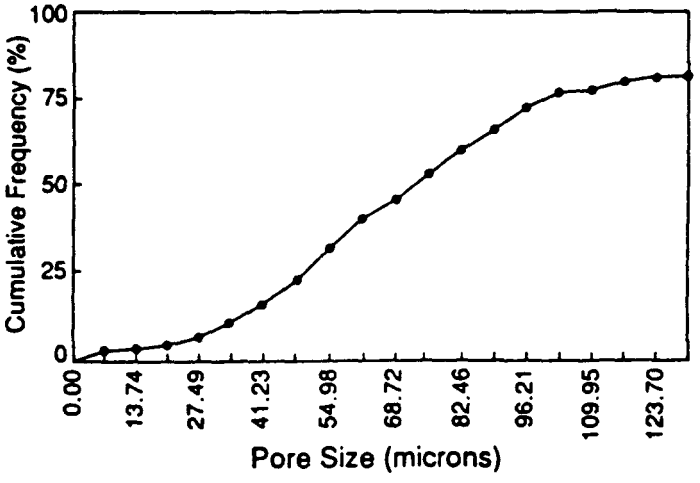

(b)

Figure 18 (a) Principle of the PoDFA apparatus, and (b) pore size distribution of the PoDFA filter.

3.2.2 Inclusion measurements

The PoDFA samples (circled in Figure 18(a)) containing the unfiltered part of the metal (~5 mm) in contact with the filter, were hot mounted in bakelite and polished to a mirror-like finish. Using the grid method, the total inclusion area was obtained. This area was then divided by the weight of the metal that had passed through the filter (~1.5 kg). The method of inclusion identification is proprietary to Alcan International Limited. The total inclusion concentration area per kilogram was calculated using the formula :

Total Inclusion (mm^2/kg) = [{Mean Measured Residue Area (mm^2)
× Inclusion Area Fraction}/{Filtrate Metal Weight(kg)}]
× [{Nominal Chord Length (mm)}/Measured Chord Length(mm)}]

where the inclusions were classified into two categories :

(i) Total inclusions that take into account all types of inclusions existing in the cake above the filter, and

(ii) Harmful inclusions which are the sum of $Al_4C_3 > 3\mu m$, dispersed Al_2O_3, MgO, $MgAl_2O_4$, and potential chlorides. Fine $Al_4C_3 \leq 3\mu m$ and TiB_2 have no harmful effect on the alloy mechanical properties.

3.3 RESULTS AND DISCUSSION

3.3.1 Inclusion Type and Concentration

There are different types of inclusions that occur in Al-Si alloy melts, such as TiB_2, Al_2O_3, Al_4C_3, MgO, etc., some of which can harm the tensile properties seriously. These inclusions can be introduced into the melt through any one of the operations or melt treatments carried out in foundries on a daily basis. An understanding of the type and amount of inclusions that can occur as a result of these operations would, therefore, be of practical importance. This was done for the A356.2 and C357 alloys, as described below.

3.3.1.1 Foundry parameters

The experimental conditions applied in the present work simulated those used in production foundries, and are summarized in Tables 3 and 4 for the two alloys. A set of twenty experiments (each using a melt of 25 kg) was carried out to investigate the following variables.

1. Settling time - during melting, the molten metal surface was isolated from the surrounding atmosphere by covering the top portion of the furnace with a thick plate of refractory material (commercially known as B3). Once the molten temperature reached 735 ± 5°C, the inclusions were allowed to settle to the bottom of the crucible. The settling time was varied between 0 and 72 h. Prior to executing the PoDFA trial, the dross was carefully skimmed, without folding, and weighed.

2. Superheating - the molten metal temperature was allowed to increase to 850°C (about 120°C above the normal working temperature), at which temperature the metal was held for 1 h. Thereafter, it was allowed to cool to 735°C prior to executing the PoDFA trial.

3. Type of initial charge - two types of initial materials were used : fresh ingots and scrap. In both cases, the charge materials were cleaned with ether and dried at 400°C prior to melting.

4. Stirring - once the molten metal temperature reached the required temperature (735 ± 5°C), a preheated graphite impeller was introduced into the melting crucible. The rotation speed selected was 120 - 130 r.p.m, enough to agitate the molten metal but without the introduction of the oxide films formed at the surface of the liquid metal into the melt.

5. Degassing - in this case, a continuous stream of high purity argon was passed into the molten metal through the graphite impeller. Degassing was done for about 40–50 minutes, using the same rotation speed of 120 - 130 r.p.m.

6. Filtration - ceramic foam filter (10, 20, and 30 ppi) discs were placed at the bottom of ceramic pouring cups and fixed in place using refractory cement. The pouring cups were preheated to 800°C, then held above the PoDFA crucible. The molten metal was then poured through these cups into the PoDFA crucible. It is evident that at such a high temperature, the molten metal would be reoxidized on passing from the cup to the PoDFA crucible (the size of the pouring cup being a fraction of that of the PoDFA crucible). Nevertheless, this method would eventually prevent the coarse oxides and dross from entering into the molten metal.

Table 3 Foundry parameters for experiments conducted with A356.2 alloy.

Experiment #	Type of Charge	Charge (kg)	Settling Time (hr)	Stirring Speed (rpm)	Stirring Time (min)	Degassing (Time) (min)	Filter Size (ppi)
1	Fresh	25	0[a]	—	—	—	—
2	Fresh	25	4[a]	—	—	—	—
3	Fresh	25	0[a]	—	—	—	—
4	Fresh	25	0[a]	—	—	—	—
5	Fresh	25	4[a]	—	—	—	—
6	Scrap	25	0[a]	—	—	—	—
7	Scrap	25	4[a]	—	—	—	—
10	Fresh	25	0[b]	125-130	30	—	—
11	Fresh	25	4[b]	125-130	30	—	—
8	Scrap	25	0[b]	125-130	30	—	—
9	Scrap	25	4[b]	125-130	30	—	—
14	Fresh	25	0[b]	125-130	—	45	—
15	Fresh	25	4[b]	125-130	—	45	—
12	Scrap	25	0[b]	125-130	—	45	—
13	Scrap	25	4[b]	125-130	—	45	—
18	Fresh	25	0[a]	—	—	—	10
16	Scrap	25	0[a]	—	—	—	10
17	Scrap	25	0[b]	125-130	—	45	10
19(A,B)	Fresh	25	0[b]	125-130	—	45	10
19(C,D)			0[b]	125-130	—	45	20
19(E)	Fresh	–	0[b]	125-130	—	45	30
20(A,B)	Fresh	25	72[a]	—	—	—	—
20(C,D)			72[a]	—	—	—	10
20(E,F)			72[a]	125-130	—	45	10

Note: - Melt temperature was ~ 735 ± 5°C (expect for experiments 4 & 5 where the melt was superheated to ~850°C).

- PoDFA crucible temperature ~850°C.
- a, settling time before stirring/degassing.
- b, settling time after stirring/degassing.

Table 4 Foundry parameters for experiments conducted with C357 alloy.

Experiment #	Type of Charge	Charge (kg)	Settling Time (hr)	Stirring Speed (rpm)	Stirring Time (min)	Degassing (Time) (min)	Filter Size (ppi)
24 (A)	Fresh	25	0[a]	—	—	—	—
24 (B)			0[a]	—	—	—	10
24 (C)			4[a]	—	—	—	—
24 (D)			4[a]	—	—	—	10
24 (E)			4[a]	—	—	—	20
24 (F)			0[a]	125-130	10	—	—
24 (G)			0[a]	125-130	10	—	10
24 (H)			2[a]	125-130	10	—	10
25 (A)	Fresh	25	72[a]	–	—	—	—
25 (B)				–	—	—	10
25(C)				125-130	—	45	—
25 (D)				125-130	—	45	10
25 (E)				—	—	—	—
25 (F)				—	—	—	10
25 (G)				—	—	—	20

Note: - Melt temperature was ~ 735 ± 5°C (expect for experiments 25(E), 25(F), 25(G) where the melt was superheated to ~850°C).
- PoDFA crucible temperature ~850°C.
- a, settling time before stirring/degassing.

3.3.1.2 Minor alloying elements

Tables 5 and 6 show the experimental conditions simulating some of the important daily foundry operations such as modification, grain refining, and melt chemistry adjustment. These are discussed in detail below.

Table 5 Minor additions and other parameters for experiments conducted with A356.2 alloy.

Experiment #	Additive	Stirring Speed (rpm)	Stirring Time (min)	Settling Time (hr)	Degassing Time (min)	Filter Size (ppi)
21 (A,B)	Sr	125 -130	15	0[b]	—	—
21 (C)				2[b]	—	—
21 (D)				2[b]	—	10
21 (E)	TiB_2	125 -130	15	0[b]	—	—
21 (F,G)	TiB_2	125 -130	15	2[b]	—	10
22 (A,B)	Sr	125 -130	15	0[b]	—	—
22 (C)				2[b]	—	—
22 (D)				2[b]	—	10
22 (E)	TiB_2	125 -130	15	0[b]	—	10
22 (F)				2[b]	—	20
22 (H)				2[b]	15	10
23 (A,B)	Fe,Mn,Cr	125 -130	15	0[b]	—	—
23 (C,D)				2[b]	—	—
23 (E,F)	Be	125 -130	15	0[b]	—	—
23 (G,H)				2[b]	—	—
23 (I)	Sr	125 -130	10	0[b]	—	—
23 (J)				0[b]	—	10

Charge : 25 kg/experiment - fresh ingots.

Table 6 Minor additions and other parameters for experiments conducted with C357 alloy.

Experiment #	Additive	Stirring Speed (rpm)	Stirring Time (min)	Settling Time (hr)	Degassing Time (min)	Filter Size (ppi)
26 (A)	Sr	125 -130	15	0[b]	—	—
26 (B)					—	10
26 (C)					—	20
26 (D)	TiB_2	125 -130	15	0[b]	—	—
26 (E)				0[b]	—	10
26 (F)				0[b]	—	20
26 (G)				0[b]	45	—
26 (H)				0[b]		20
27 (A)	TiB_2	125 -130	10	0[b]	—	—
27 (B)				0[b]	—	10
27 (C)				12[b]	—	—
27 (D)				12[b]	—	10
28 (A)	Ti	125 -130	15	0[b]	—	—
28 (B)				0[b]	—	10
28 (C)				3[b]	—	—
28 (D)				3[b]	—	10
29 (A)	Fe,Mn,Cr	125 -130	15	0	—	—
29 (B)				0	—	20
29 (C)	Be	125 -130	15	0	—	—
29 (D)				0	—	20
29 (E)	Sr	125 -130	15	0	—	—
29 (F)				0	—	20
29 (G)	Ti	125 -130	15	0	—	—
29 (H)				0	—	20
29 (I)	TiB_2	125 -130	15	0	—	10

Charge : 25 kg/experiment - fresh ingots.

1. *Modification* - Strontium (Sr) is the main modifying agent used by most aluminum foundries [50, 51, 52]. The maximum allowable level to achieve a complete modified structure in A356.2 alloy is about 300 ppm. In the present work, Sr was added in the form of Al-10 wt% Sr master alloy (~250 - 300 ppm Sr).
2. *Grain refining* - TiB_2 is found to be the most effective grain refining agent [17-19] in the case of aluminum alloys [53, 54, 55]. It is normally added in the form of an Al-Ti-B master alloy viz., as Al-5 wt% Ti-1 wt% B, Al-5 wt% Ti-5 wt% B, Al-2.5 wt% Ti-2.5 wt% B or Al-10 wt% Ti-1 wt% B. In the present work, Al-5 wt% Ti-1 wt% B was used. The concentration of TiB_2 was calculated on the basis of a 0.02 wt% Ti addition (with respect to the weight of the molten metal that was required to be treated).
3. *Magnesium addition* - Magnesium (Mg) is normally present in C357 in concentrations ranging between 0.45 and 0.7 wt%. It combines with Si to form the age-hardening compound Mg_2Si. Fine, coherent precipitation of Mg_2Si from solid solution during heat treatment is responsible for the improvement in mechanical properties.
4. *Beryllium addition* - Beryllium (Be) is also added to C357 alloy in small quantities, of the order of 0.05 wt%, to improve the precipitation hardening response of the alloy upon artificial aging [56]. It is added in the form of Al-5wt% Be master alloy.
5. *Intermetallics* - Sludge is one of the important intermetallics that may form when the concentrations of Fe, Mn and Cr impurities exceed the allowable limit. Such contamination occurs when steel tools such as skimmers, ladles, and stirrers are used without proper coating. Sludge particles are formed in the liquid state. Due to their higher density, they tend to precipitate to the bottom of the melting crucible. The

formula used to calculate the possibility of sludge formation or the sludge factor, SF, is given by [57] :

$$SF = Fe\% + 2*Mn\% + 3*Cr\%$$

When $SF \geq 1.8$, the possibility of sludge formation is very high, especially when the molten metal is held for a sufficiently long time at temperatures close to that required for sludge formation (~ 680°C). In the present case, Fe, Mn, Cr were introduced into the molten metal in the form of Al-25 wt% Fe, Al-25 wt% Mn, and Al-20 wt% Cr master alloys. The concentrations of these elements were calculated in such a way that the SF was higher than 1.8, in order to study the effect of sludge on inclusion formation and precipitation.

The chemical compositions of the liquid A356.2 alloy melts in the different cases is shown in Table 7, while the concentrations of the various additives are given in Table 8. An explanation of the alloy codes used in Tables 7 and 8 is provided in Table 9.

Table 7 Chemical compositions of A356.2 alloy under different melt treatment conditions.

Alloy Code	Element (wt%)												
	Si	Fe	Cu	Mn	Mg	Cr	Ni	Zn	B	Sn	Sr	V	Ti
A0	7.05	0.108	0.0122	0.0381	0.36	0.00184	0.00642	0.0324	0.00116	<0.00100	0.00023	0.0135	0.08
AS0	7.03	0.107	0.0126	0.0374	0.36	0.00182	<0.00650	0.0339	0.00157	<0.00100	0.0237	0.0134	0.08
AS2	7.04	0.105	0.0121	0.0379	0.353	0.00184	0.00656	0.0326	0.00115	<0.00100	0.0162	0.0134	0.106
AST0	7.04	0.106	0.0122	0.0371	0.341	0.00203	<0.00589	0.0321	0.00348	<0.00100	0.0254	0.0136	0.105
AST2	6.95	0.113	0.0124	0.0363	0.337	0.00175	< 0.00500	0.0309	0.00351	<0.00100	0.0236	0.0135	0.0803
AF0	6.84	0.714	0.0134	0.459	0.337	0.122	<0.00610	0.032	0.00517	<0.00100	0.00034	0.014	0.0754
AF2	6.68	0.711	0.013	0.455	0.33	0.12	< 0.00500	0.0308	0.00488	<0.00100	0.00029	0.0137	0.0731
AFB0	6.66	0.706	0.0131	0.44	0.324	0.117	<0.00500	0.0298	0.00495	<0.00100	0.00056	0.015	0.0729
AFB2	6.59	0.699	0.0129	0.445	0.337	0.119	<0.00570	0.03	0.00531	<0.00100	0.00099	0.0149	0.0734
AFBS0	6.78	0.684	0.0136	0.477	0.33	0.119	<0.00643	0.0308	0.00466	<0.00100	0.031	0.0146	0.0736

(See Table 9 for alloy codes).

Table 8 Concentrations of additives in A356.2 alloy.

Alloy Code	Element (wt%)												
	Si	Fe	Cu	Mn	Mg	Cr	Ni	Zn	B	Sn	Sr	V	Ti
AS0	-0.02	-0.001	0.0004	-0.0007	0	-2E-05	<0.0007	0.0015	0.00041	0	0.02347	-1E-04	0
AS2	-0.01	-0.003	-0.0001	-0.0002	-0.007	0	0.00014	0.0002	-0.00001	0	0.01597	-1E-04	0.026
AST0	-0.01	-0.002	0	-0.001	-0.019	0.00019	<-0.00053	-0.0003	0.00232	0	0.02517	1E-04	0.025
AST2	-0.1	0.005	0.0002	-0.0018	-0.023	-0.00009	<-0.00142	-0.0015	0.00235	0	0.02337	0	0.0003
AF0	-0.21	0.606	0.0012	0.4209	-0.023	0.12016	<-0.00032	-0.0004	0.00401	0	0.00011	0.0005	-0.0046
AF2	-0.37	0.603	0.0008	0.4169	-0.03	0.11816	<-0.00142	-0.0016	0.00372	0	0.00006	0.0002	-0.0069
AFB0	-0.39	0.598	0.0009	0.4019	-0.036	0.11516	<-0.00142	-0.0026	0.00379	0	0.00033	0.0015	-0.0071
AFB2	-0.46	0.591	0.0007	0.4069	-0.023	0.11716	<-0.00072	-0.0024	0.00415	0	0.00076	0.0014	-0.0066
AFBS0	-0.27	0.576	0.0014	0.4389	-0.03	0.11716	<9.99E-06	-0.0016	0.0035	0	0.03077	0.0011	-0.0064

(See Table 9 for alloy codes).

Table 9 Explanation of alloy codes used in the Tables 7 and 8.

A0:	A: A356	0: Settling time is 0 hours			
AS0 :	A: A356	0: settling time is 0 hours	S: Sr		
AS2 :	A: A356	2: settling time is 2 hours	S: Sr		
ASTO:	A: A356	0: settling time is 0 hours	S: Sr	T: TiB_2	
AST2:	A: A356	2: settling time is 2 hours	S: Sr	T: TiB_2	
AF0:	A: A356	0: settling time is 0 hours	F: Fe, Mn, Cr		
AF2:	A: A356	2: settling time is 2 hours	F: Fe, Mn, Cr		
AFB0:	A: A356	0: settling time is 0 hours	F: Fe, Mn, Cr	B: Be	
AFB2:	A: A356	2: settling time is 2 hours	F: Fe, Mn, Cr	B: Be	
AFBS0	A: A356	0: settling time is 0 hours	F: Fe, Mn, Cr	B: Be	S: Sr

In all the above-mentioned cases, the molten metal was mechanically stirred for 10-15 minutes after the addition of each alloying element to ensure its proper dissolution into the liquid metal.

From the above experiments, the data on the following parameters was obtained : i) filtration time (for 1.5 kg of filtered metal), ii) length of solidified metal (Ragone fluidity tests), iii) total inclusions (mm^2/kg), iv) total harmful inclusions (mm^2/kg), v) types and concentrations of inclusions, and vi) oxide films, and is summarized in Tables 10 - 17 for both foundry parameters and minor alloying element additions.

In the present work, the inclusion concentrations were arbitrarily classified into five classes viz., "very light", "light", "moderate", "heavy" and "excessive", according to the total inclusion concentration, viz., 0-0.05, 0.05-0.1, 0.1-0.4, 0.4-1.2 and >1.2 mm^2/kg, respectively. On the basis of the casting quality expected to result from such inclusion concentrations, the corresponding castings were categorized as excellent castings (very light and light), acceptable castings (moderate), acceptable scrap for castings (heavy), and rejected scrap for castings (excessive).

With respect to the oxide film concentrations, however, these were classified according to the procedures followed at Alcan, i.e., the oxide film type/density were classified into seven categories from 0 to 6, corresponding to "none" (no oxide films observed), "thin/slight", "thin/moderate", "thin/heavy", "thick/slight", "thick/moderate", and "thick/heavy", respectively, as shown in Tables 27 and 28 in the next chapter, where the oxide film inclusions are discussed in greater details.

Table 10 Effect of foundry parameters on the filtration and fluidity data obtained for A356.2 alloy.

Experiment #	Weight of Filtered Metal (kg)	Filtration Time (min)	Length of Solidified Metal (cm)
1A*	1.366	10	36.5
1B	1.602	7	37
1C	0.964	6	38.1
1D	1.074	7	37
1E	1.627	7	35.5
2A*	1.418	6	34.7
2B	1.544	5	34.3
2C	1.52	5	34.7
2D	1.399	3	35.5
2E	1.524	3	34.8
3A*	1.258	5	—
3B	1.209	7	—
3C	1.381	8	—
3D	1.518	3	—
3E	1.553	4	—
4A*	1.05	7	34.4
4B	1.291	7	34.5
4C	1.467	4	35.2
4D	1.325	8	35.3
4E	1.495	5	33.5
5A*	1.52	5	34.9
5B	1.505	9	35.7
5C	1.466	4	34
5D	1.536	4	35
5E	1.457	6	34
6A*	1.361	6	35.2
6B	1.498	4	—
6C	1.706	7	—
6D	1.278	9	34.2
6E	1.52	5	36
7A*	1.506	5	35.5
7B	1.557	5	36.8
7D	1.536	5	35.3
7E	1.534	5	34.8
8A*	0.944	7	37
8B	1.505	5	37
8C	1.477	6	36.3
8D	1.448	8	37.5

Note: * : Cold Chamber

Continued...

Table 10 Effect of foundry parameters on the filtration and fluidity data obtained for A356.2 alloy.

Experiment #	Weight of Filtered Metal (kg)	Filtration Time (min)	Length of Solidified Metal (cm)
9A*	1.287	8	36.6
9B	1.454	7	38.5
9C	1.441	5	36.5
9D	1.473	5	37.8
10A	1.494	7	36.5
10B	1.294	6	36.5
10C	1.143	8	37.6
10D	1.31	9	38
10E	1.535	5	35.8
11A	1.509	8	37.4
11B	1.447	10	36.7
11C	1.32	8	37.2
11D	1.488	5	41.2
11E	1.452	8	36.9
12A	1.491	5	36.9
12B	1.414	9	36
12C	1.544	5	36
12D	1.505	7	35.8
13A	1.49	6	36.1
13B	1.494	5	36.8
13C	1.502	5	36.3
13D	1.502	6	35.2
14A	1.454	6	35.8
14B	1.479	8	36.5
14C	1.366	9	35.8
14D	1.456	5	36.9
14E	1.57	4	36.3
15A	1.453	5	32.8
15B	1.454	5	38.1
15C	1.457	7	35.9
15D	1.49	5	36.8
15E	1.48	4	36.7
16A	1.524	5	37.7
16B	1.521	3	36.3
16C	0.736	5	38
16D	1.469	5	37

Continued...

Table 10 Effect of foundry parameters on the filtration and fluidity data obtained for A356.2 alloy.

Experiment #	Weight of Filtered Metal (kg)	Filtration Time (min)	Length of Solidified Metal (cm)
17A	1.481	6	37.6
17B	1.446	5	35.2
17C	1.455	5	35.9
17D	1.495	6	37.3
18A	1.452	6	35.7
18B	1.468	5	36.3
18C	1.65	4	36.9
18D	1.515	7	36.2
19A	1.378	6	34.9
19B	1.498	4	35.5
19C	1.245	5	36
19D	1.268	5	36.4
19E	1.179	6	35.8
20A	1.503	5	36.3
20B	1.476	6	35.5
20C	1.512	4	36.5
20D	1.33	6	37.4
20E	1.174	10	36.1
20F	1.278	8	34.8

Table 11 Effect of minor additions on the filtration and fluidity data obtained for A356.2 alloy.

Experiment #	Weight of Filtered Metal (kg)	Filtration Time (min)	Length of Solidified Metal (cm)
21A	1.435	8	35.3
21B	1.424	11	38.1
21C	1.011	10	36.3
21D	1.48	10	37.1
21E	0.39	10	36.9
21F	0.516	10	36.1
21G	0.494	12	36.8
22A	1.279	7	37.5
22B	1.432	5	37.9
22C	1.442	5	35.6
22D	0.67	5	35
22E	0.252	10	33.7
22F	0.254	8	36.1
22G	0.307	5	38
22H	0.381	11	36.3
23A	1.228	6	37
23B	1.466	6	36.3
23C	1.515	5	—
23D	1.47	6	36.1
23E	1.504	4	36.5
23F	1.471	3	37.2
23G	1.107	4	36.1
23H	1.535	4	36.9
23I	1.462	5	36.3
23J	1.554	5	36.3

Table 12 Effect of foundry parameters on the total and harmful inclusion concentrations (mm^2/kg) obtained in A356.2 alloy.

Experiment #	Total Inclusions (mm^2/kg)	Harmful Inclusions (mm^2/kg)
1A	0.041	0.009
1B	0.041	0.01
1C	0.256	0.049
1D	0.088	0.02
2A	0.034	0.008
2B	0.032	0.007
2C	0.023	0.006
2E	0.015	0.002
3A	0.044	0.008
3B	0.041	0.011
3C	0.043	0.012
3D	0.047	0.015
3E	0.079	0.021
4A	0.041	0.013
4B	0.078	0.032
4C	0.084	0.029
4D	0.063	0.027
4E	0.076	0.034
5A	0.062	0.031
5B	0.05	0.031
5C	0.033	0.018
5D	0.048	0.034
5E	0.054	0.035
6A	0.035	0.016
6B	0.026	0.011
6C	0.013	0.002
6D	0.037	0.009
6E	0.034	0.009
7A	0.061	0.049
7D	0.119	0.08
7E	0.078	0.047
8B	0.035	0.032
8C	0.051	0.027
8D	0.227	0.182
9B	2.628	2.076
9C	0.139	0.115
9D	0.129	0.125

Continued...

Table 12 Effect of foundry parameters on the total and harmful inclusion concentrations (mm^2/kg) obtained in A356.2 alloy.

Experiment #	Total Inclusions (mm^2/kg)	Harmful Inclusions (mm^2/kg)
10A	0.244	0.024
10D	0.678	0.244
10E	0.543	0.19
11A	1.489	0.476
11B	1.172	0.445
11E	1.113	0.579
12A	0.852	0.213
12C	0.93	0.483
12D	0.37	0.222
13A	0.153	0.069
13C	0.18	0.097
13D	0.286	0.194
14A	0.159	0.119
14D	0.181	0.145
14E	0.021	0.019
15A	0.221	0.188
15D	0.03	0.023
15E	0.173	0.138
16A	0.1	0.074
16B	0.034	0.028
16D	0.131	0.118
17A	1.405	1.124
17B	0.239	0.187
17D	0.362	0.286
18A	1.129	0.395
18C	1.252	0.363
18D	0.636	0.35
19B	0.032	0.01
19D	0.151	0.017
19E	0.87	0.07
20A	4.244	3.777
20C	2.151	1.979
20F	1.285	1.105

Table 13 Effect of minor additions on the total and harmful inclusion concentrations (mm^2/kg) obtained in A356.2 alloy.

Experiment #	Total Inclusions (mm^2/kg)	Harmful Inclusions (mm^2/kg)
21B	0.24	0.07
21D	0.139	0.026
21F	6.437	0.515
22B	0.07	0.056
22C	0.092	0.077
22E	1.679	0.084
22F	0.826	0.091
22G	0.277	0.033
22H	1.122	0.123
23B	0.432	0.237
23D	1.01	0.687
23F	0.824	0.511
23H	0.766	0.398
23I	1.05	0.892
23J	0.902	0.793

Table 14 Effect of foundry parameters on the concentrations of major inclusions (mm^2/kg) obtained in A356.2 alloy.

Experiment #	TiB_2/TiC (mm^2/kg)	$Al_4C_3 \leq 3\mu m$ (mm^2/kg)	$Al_4C_3 > 3\mu m$ (mm^2/kg)	MgO (mm^2/kg)	MgO(cuboides) (mm^2/kg)	$MgAl_2O_4$ (mm^2/kg)
1A	0.0061	0.0253	0.0094	—	—	—
1B	0.0062	0.0257	0.0095	—	—	—
1C	0.0332	0.1738	0.0486	—	—	—
1D	0.0097	0.058	0.0202	—	—	—
2A	0.004	0.0219	0.0078	—	—	—
2B	0.0032	0.0221	0.0071	—	—	—
2C	0.0022	0.0146	0.0059	—	—	—
2E	0.003	0.0094	0.0018	0.0003	—	0.0001
3A	0.0065	0.0285	0.0065	0.0008	—	0.0008
3B	0.0057	0.0237	0.0081	0.0012	—	0.0016
3C	0.0043	0.0269	0.0094	—	—	0.0021
3D	0.007	0.0243	0.0117	0.0009	—	0.0028
3E	0.0087	0.0491	0.0214	—	—	—
4A	0.0061	0.0216	0.013	—	—	—
4B	0.0094	0.0361	0.0314	0.0008	—	—
4C	0.0109	0.0438	0.0295	—	—	—
4D	0.0094	0.0264	0.0264	0.0006	—	—
4E	0.0076	0.0332	0.034	—	—	—
5A	0.0094	0.0212	0.0312	—	—	—
5B	0.009	0.01	0.0299	—	—	0.001
5C	0.005	0.01	0.0181	—	—	0.0003
5D	0.0058	0.0087	0.0315	—	—	0.0024
5E	0.0082	0.0109	0.0332	—	—	0.0022
6A	0.0052	0.0138	0.0138	—	—	0.0017
6B	0.0015	0.0129	0.0093	—	—	0.0021
6C	0.0013	0.0096	0.002	—	—	0.0003
6D	0.0026	0.0251	0.0033	0.0007	—	0.0049
6E	0.0041	0.021	0.0034	0.0007	—	0.0052
7A	0.0031	0.0092	0.0354	—	—	0.0012
7D	0.0036	0.0356	0.0463	—	—	0.0036
7E	0.0117	0.0195	0.0117	—	—	0.0078
8B	0.0035	—	0.0053	0.0007	0.0238	0.0018
8C	0.0041	0.0205	0.0128	—	0.0128	0.001
8D	0.0114	0.0341	0.1566	0.0068	0.0182	—
9B	0.1577	0.3941	0.2102	0.1314	1.524	0.2102
9C	0.0097	0.0139	0.0208	0.0069	0.0735	0.0139
9D	0.0039	—	0.0233	0.0763	0.0258	—

Continued...

Table14 Effect of foundry parameters on the concentrations of major inclusions (mm^2/kg) obtained in A356.2 alloy.

Experiment #	TiB_2/TiC (mm^2/kg)	$Al_4C_3 \leq 3\mu m$ (mm^2/kg)	$Al_4C_3 > 3\mu m$ (mm^2/kg)	MgO (mm^2/kg)	MgO(cuboides (mm^2/kg	$MgAl_2O_4$ (mm^2/kg)
10A	0.039	0.1802	0.0195	0.0024	—	0.0024
10D	0.0813	0.3524	0.0678	0.0474	0.1017	0.0203
10E	0.0706	0.2824	0.0543	0.0597	0.0434	0.0272
11A	0.1489	0.8634	0.2977	0.1489	0.0149	0.0149
11B	0.1758	0.5508	0.293	0.1406	—	0.0117
11E	0.167	0.3674	0.3897	0.167	0.0111	0.0111
12A	—	0.6393	0.1705	0.0426	—	—
12C	—	0.4462	0.3718	0.0744	0.0093	0.0279
12D	—	0.148	0.1813	0.037	—	0.0037
13A	0.003	0.0812	0.0459	—	0.0183	0.0045
13C	0.0071	0.0755	0.0539	0.0035	0.0359	0.0035
13D	0.0057	0.0858	0.1429	0.0086	0.0143	0.0286
14A	—	0.0398	0.1114	0.0079	—	—
14D	0.009	0.027	0.1264	0.018	—	—
14E	—	0.0016	0.0139	0.0052	—	—
15A	0.011	0.022	0.1699	0.0176	—	—
15D	0.0006	0.006	0.0199	—	—	0.0036
15E	0.0035	0.0311	0.0104	0.0346	—	—
16A	0.005	0.02	0.055	0.009	0.003	0.007
16B	0.0007	0.0051	0.0027	0.0055	0.0034	0.0164
16D	0.0026	0.0065	0.0196	0.017	0.0118	0.0693
17A	—	0.281	0.5338	0.0281	0.1826	0.3793
17B	—	0.0526	0.0909	0.0024	0.0239	0.067
17D	0.0036	0.0724	0.2101	0.0036	0.0254	0.0471
18A	0.1694	0.5646	0.2145	0.0226	0.0452	0.1129
18C	0.1627	0.7259	0.1627	0.0125	0.0751	0.1126
18D	0.0127	0.2734	0.2544	—	0.0254	0.0636
19B	0.0006	0.0205	0.0019	0.0013	0.0003	0.007
19D	0.0015	0.1331	0.0061	0.003	0.0015	0.0061
19E	0.0087	0.7917	0.0174	0.0087	0.0087	0.0348
20A	0.2546	0.2122	2.0796	0.0849	1.2732	0.3395
20C	0.1076	0.0645	1.1832	0.1721	0.5378	0.0861
20F	0.0129	0.1671	0.0643	0.9512	0.0386	0.0514

Table 15 Effect of minor additions on the concentrations of major inclusions (mm^2/kg) obtained in A356.2 alloy.

Experiment #	TiB_2/TiC (mm^2/kg)	$Al_4C_3 \leq 3\mu m$ (mm^2/kg)	$Al_4C_3 > 3\mu m$ (mm^2/kg)	MgO (mm^2/kg)	MgO(cuboides) (mm^2/kg	$MgAl_2O_4$ (mm^2/kg)	SrO (mm^2/kg)
21B	0.0024	0.1104	0.0096	0.0168	0.0024	0.0192	0.0216
21D	0.0014	0.0806	0.0028	0.0056	0.0014	0.0083	0.0083
21F	5.4069	0.2575	0.1287	0.0644	—	0.0644	0.2575
22B	0.0049	0.0063	0.0035	0.0395	—	0.0021	0.0106
22C	0.0018	0.011	0.0036	0.0679	—	0.0027	0.0027
22E	1.4607	0.1343	0.0167	0.0335	0.0167		0.0167
22F	0.6858	0.0495	0.0165	0.0413	—	0.0082	0.0165
22G	0.2269	0.0166	0.0027	0.0083	0.0027	0.0055	0.011
22H	0.9197	0.0672	0.0112	0.0224	—	0.0112	0.0672
23B	0.1252	0.0604	0.1511	0.0561	0.0043	0.0215	—
23D	0.2221	0.0908	0.3736	0.1514	0.0403	0.111	—
23F	0.1401	0.1565	0.2966	0.0659	0.0082	0.1318	—
23H	0.1762	0.1916	0.2912	0.0383	0.0076	0.0536	—
23I	0.0419	0.1154	0.3149	0.4199	0.0209	0.1259	—
23J	0.0541	0.0541	0.2434	0.3967	0.009	0.1352	—

Table 16 Effect of foundry parameters on the concentration of Al_2O_3 oxide films obtained in A356.2 alloy and their classification.

Experiment #	Thin Film			Thick Film		
	Slight	Moderate	Heavy	Slight	Moderate	Heavy
1A		X				
1B			X			
1C		X				
1D	X					
2A		X				
2B		X				
2C		X				
2E			X			
3A		X				
3B		X		X		
3C		X				
3D			X			
3E	—	—	—	—	—	—
4A	—	—	—	—	—	—
4B		X				
4C		X		X		
4D	X					
4E	X					
5A				X		
5B			X			
5C			X			
5D			X			
5E		X				
6A		X				
6B		X				
6C			X			
6D		X				
6E		X				
7A			X			X
7E			X			X

Continued...

Table 16 Effect of foundry parameters on the concentration of Al_2O_3 oxide films obtained in A356.2 alloy and their classification.

Experiment #	Thin Film			Thick Film		
	Slight	Moderate	Heavy	Slight	Moderate	Heavy
8C		X				X
8D			X			X
9B	X				X	
9D			X			X
10A		X			X	
10D		X			X	
10E		X			X	
11A		X			X	
11B		X			X	
11E		X			X	
12A	X			X		
12C		X			X	
12D	X			X		
13A		X			X	
13C			X			X
13D		X		X		
14D	X			X		
14E		X			X	
15E	X				X	
16A			X			X
16B			X			X
16D			X			X
17A			X		X	
17B			X		X	
17D		X		X		
18A		X			X	
18C		X			X	
18D		X			X	
19B	X			X		

Table 17 Effect of minor additions on the concentration of Al_2O_3 oxide films obtained in A356.2 alloy and their classification.

Experiment	Thin Film			Thick Film		
	Slight	Moderate	Heavy	Slight	Moderate	Heavy
22C		X		X		
22E	X					
22G		X		X		
22H	X			X		
23B			X			X
23D			X			X
23F			X			X
23H			X			X
23I			X			X
23J			X			X

Similar experiments was carried out using C357 alloy. Tables 18 and 19 show the corresponding chemical compositions of the alloy melts and the concentrations of the various additives, respectively. Table 20 gives an explanation of the alloy codes used in these two tables. As in the case of A356.2 alloy, the data obtained from these experiments are listed in Tables 21 through 24, showing the effects of foundry parameters and minor additions on the inclusion and oxide film concentrations obtained for the C357 alloy. The classifications for inclusion and oxide film concentrations are the same as those described earlier.

Table 18 Chemical compositions of C357 alloy under different melt treatment conditions.

Alloy Code	Element wt%												
	Si	Fe	Cu	Mn	Mg	Cr	Ni	Zn	Ti	Sn	Be	Sr	V
C01	7.06	0.0485	0.012	0.007	0.556	< 0.000	0.006	0.001	0.143	< 0.0000	0.0171	0.0015	0.00615
C41	7.06	0.049	0.012	0.008	0.576	< 0.000	0.007	0.002	0.138	< 0.0000	0.0157	0.0013	0.0062
C71	7.16	0.047	0.032	0.005	0.524	< 0.000	0.006	<0.000	0.138	< 0.0000	0.0035	0.0011	0.006
C71H	7.19	0.048	0.032	0.005	0.516	< 0.000	0.007	< 0.000	0.139	< 0.0000	0.005	0.0012	0.0064
CS1	7.17	0.043	0.013	0.005	0.556	< 0.000	0.007	0.001	0.135	< 0.0000	0.0276	0.0238	0.0057
CSTB1	7.2	0.047	0.013	0.005	0.568	<0.000	0.007	0.002	0.162	< 0.0000	0.0272	0.0374	0.0061
CTB1	7.44	0.049	0.012	0.005	0.554	< 0.000	0.007	< 0.000	0.156	< 0.0000	0.0384	0.02	0.006
CT1	7.07	0.049	0.012	0.005	0.564	< 0.000	0.007	0.002	0.171	< 0.0000	0.0363	0.0011	0.0063
CF1	6.9	0.304	0.0125	0.304	0.5615	0.119	0.007	0.002	0.133	< 0.0000	0.0289	0.00105	0.00595
CFB1	6.98	0.632	0.012	0.36	0.546	0.117	0.007	0	0.131	<0.0000	0.0561	0.0011	0.0061
CFBS1	6.83	0.623	0.013	0.358	0.547	0.114	0.007	0.001	0.13	< 0.0000	0.0574	0.0215	0.006
CFBST	6.95	0.627	0.013	0.357	0.545	0.115	0.007	0	0.149	< 0.0000	0.0534	0.0202	0.0058
FBST1	6.92	0.643	0.013	0.365	0.556	0.117	0.007	0.002	0.162	< 0.0000	0.055	0.022	0.006

(See Table 20 for alloy codes).

Table 19 Concentrations of additives in C357 alloy.

Alloy Code	Element wt%												
	Si	Fe	Cu	Mn	Mg	Cr	Ni	Zn	Ti	Sn	Be	Sr	V
C41	0	0.0005	0	0.001	0.02	0	0.001	0.001	-0.005	0	-0.0014	-0.0002	5E-05
C71	0.1	-0.0015	0.02	-0.002	-0.032	0	0	-0.001	-0.005	0	-0.0136	-0.0004	-0.00015
C71H	0.13	-0.0005	0.02	-0.002	-0.04	0	0.001	-0.001	-0.004	0	-0.0121	-0.0003	0.00025
CS1	0.11	-0.0055	0.001	-0.002	0	0	0.001	0	-0.008	0	0.0105	0.0223	-0.00045
CSTB1	0.14	-0.0015	0.001	-0.002	0.012	0	0.001	0.001	0.019	0	0.0101	0.0359	-0.00005
CTB1	0.38	0.0005	0	-0.002	-0.002	0	0.001	-0.001	0.013	0	0.0213	0.0185	-0.00015
CT1	0.01	0.0005	0	-0.002	0.008	0	0.001	0.001	0.028	0	0.0192	-0.0004	0.00015
CF1	-0.16	0.2555	0.0005	0.297	0.0055	0.119	0.001	0.001	-0.01	0	0.0118	-	-0.0002
CFB1	-0.08	0.5835	0	0.353	-0.01	0.117	0.001	-0.001	-0.012	0	0.039	-0.0004	-5E-05
CFBS1	-0.23	0.5745	0.001	0.351	-0.009	0.114	0.001	0	-0.013	0	0.0403	0.02	-0.00015
CFBST1	-0.11	0.5785	0.001	0.35	-0.011	0.115	0.001	-0.001	0.006	0	0.0363	0.0187	-0.00035
FBST1B	-0.14	0.5945	0.001	0.358	0	0.117	0.001	0.001	0.019	0	0.0379	0.0205	-0.00015

(See Table 20 for alloy codes).

Table 20 Explanation of alloy codes used in Tables 18 and 19.

C01:	C: C357	1: 1st sampling			0: settling time is 0 hours			
C41:	C: C357	"			4: settling time is 4 hours			
C71:	C: C357	"			7: settling time is 72 hours			
C71H:	C: C357	"			7: settling time is 72 hours			H: superheat
CS1:	C: C357	"	S: Sr					
CSTB1:	C: C357	"	S: Sr	TB: TiB_2				
CTB1:	C: C357	"	TB: TiB_2					
CT1:	C: C357	"	T: Ti					
CF1:	C: C357	"	F: Fe, Mn, Cr					
CFB1:	C: C357	"	F: Fe, Mn, Cr	B: Be				
CFBS1:	C: C357	"	F: Fe, Mn, Cr	B: Be	S: Sr			
CFBST1:	C: C357	"	F: Fe, Mn, Cr	B: Be	S: Sr	T: Ti		
CFBST1B:	C: C357	"	F: Fe, Mn, Cr	B: Be	S: Sr	T: Ti	B: TiB_2 (corresponding to 2nd B in alloy code)	

Table 21 Effect of foundry parameters and minor additions on the filtration and fluidity data obtained for C357 alloy.

Experiment #	Weight of Filtered Metal (kg)	Filtration Time (min)
24A	1.528	4
24B	1.531	3
24C	1.525	3
24D	1.381	3
24E	1.168	3
24F	1.509	3
24G	1.481	3
24H	1.379	4
25A	1.567	3
25B	1.473	4
25C	1.487	5
25D	1.32	5
25F	1.127	5
25G	1.412	4
25H	0.938	3
26A	1.488	3
26B	1.231	3
26C	0.842	3
26D	0.252	8
26E	0.512	5
26F	0.245	6
26G	0.263	12
26H	0.245	6
27A	0.35	7
27B	0.353	9
27C	0.452	10
27D	0.401	9
28A	1.442	4
28B	1.014	4
28C	1.514	3
28D	1.507	5
29A	1.566	3
29B	1.348	3
29C	1.374	5
29D	1.158	3
29E	1.178	5
29F	1.255	5
29G	1.169	4
29H	1.233	5
29I	0.293	6

Table 22 Effect of foundry parameters and minor additions on the total and harmful inclusion concentrations (mm^2/kg) obtained in C357 alloy.

Experiment #	Total Inclusions (mm^2/kg)	Harmful Inclusions (mm^2/kg)
24B	0.387	0.349
24D	0.452	0.416
24E	0.28	0.252
24H	0.822	0.74
25A	0.446	0.446
25D	0.493	0.395
25E	0.84	0.714
25G	1.292	0.905
26A	0.729	0.729
26C	0.77	0.462
26D	11.564	1.041
26E	4.257	0.255
26H	8.311	0.582
27B	8.618	0.862
27C	11.695	1.754
27D	12.06	1.447
28A	0.948	0.863
28D	2.271	0.954
29A	2.157	1.596
29B	2.314	1.805
29C	2.592	2.048
29D	1.104	0.773
29E	1.488	1.235
29F	1.574	1.102
29H	1.954	1.387
29I	12.766	2.809

Table 23 Effect of foundry parameters and minor additions on the concentrations of major inclusions (mm^2/kg) obtained in C357 alloy.

Experiment #	TiB_2/TiC (mm^2/kg)	$Al_4C_3 \leq 3mm$ (mm^2/kg)	$Al_4C_3 > 3mm$ (mm^2/kg)	MgO (mm^2/kg)	MgO(cuboides) (mm^2/kg	$MgAl_2O_4$ (mm^2/kg)
24D		0.0362	0.0904		0.009	0.3165
24E		0.028	0.0364	0.0028	0.0028	0.2103
24H		0.0822	0.2054			0.5341
25A				0.0668	0.0891	0.2896
25D		0.0987	0.3207	0.0493	0.0099	0.0148
25E		0.126	0.6302	0.0588		0.0252
25G		0.3877	0.7754	0.0646	0.0388	0.0258
26A			0.0364	0.4007		0.2914
26C		0.308	0.077	0.2695		0.1155
26D	10.408	0.1156	0.1156	0.5782		0.3469
26E	3.6608	0.3405	0.0851	0.0851		0.0851
26H	7.6461	0.0831	0.1662	0.2493		0.1662
27B	7.7561		0.1724			0.6894
27C	9.824	0.117	0.3509	0.117	0.2339	1.0526
27D	10.492	0.1206	0.1206	0.1206	0.2412	0.9648
28A	0.0568	0.0284	0.0094	0.0189	0.0948	0.7395
28D	0.1816	1.1354	0.0454	0.0227	0.1589	0.7266
29A	0.0215	0.5392	1.0785		0.1509	0.3451
29B	0.0231	0.4859	1.1338		0.2082	0.4396
29C	0.0259	0.5184	0.8814	0.1036	0.311	0.7258
29D	0.0221	0.3081	0.2208	0.0773	0.1656	0.3091
29E	0.0149	0.238	0.2975	0.1488	0.2231	0.5053
29F	0.015	0.4565	0.2518	0.2991	0.1417	0.4092
29H	0.0195	0.5472	0.254	0.3517	0.1954	0.5862
29I	9.1916	0.766	0.2553	1.2766	0.383	0.766

Table 24 Effect of foundry parameters and minor additions on the concentration of Al_2O_3 oxide films obtained in C357 alloy and their classification.

Experiment	Thin Film			Thick Film		
	Slight	Moderate	Heavy	Slight	Moderate	Heavy
24B			X			X
24D		X			X	
24E			X			X
24H		X			X	
25A	X			X		
25D	X			X		
25E	X			X		
25G	X			X		
26A			X			X
26C	X			X		
26D	X			X		
26E	X			X		
26H	X			X		
27B	X			X		
27C	X			X		
27D	X				X	
29D		X			X	
29E		X			X	
29F		X			X	
29H		X			X	
29I		X			X	

3.3.2 Examples of inclusions

The various types of inclusions present in the PoDFA samples obtained from the PoDFA experiments carried out for A356.2 and C357 alloys were examined using optical microscopy and identified. Optical micrographs showing these different inclusions are presented in this section.

An example of a graphite inclusion is shown in Figure 19. It appears as a long, thin brown layer. The Al_4C_3 particles precipitate in the form of black needles, as shown in Figures 20 and 21. Their contrast changes with exposure to the surrounding humidity. These inclusions may have occurred from stirring/degassing of the molten metal using a graphite impeller for a fairly lengthy period of time (~45 min) at temperatures as high as 735°C. Another possibility for the formation of these inclusions can arise when the molten aluminum reacts with the inner surface of the silicon carbide crucible at places where the coating on the surface has deteriorated. The reaction may be written as :

$$4Al + 3Si \rightarrow 3Si + Al_4C_3$$

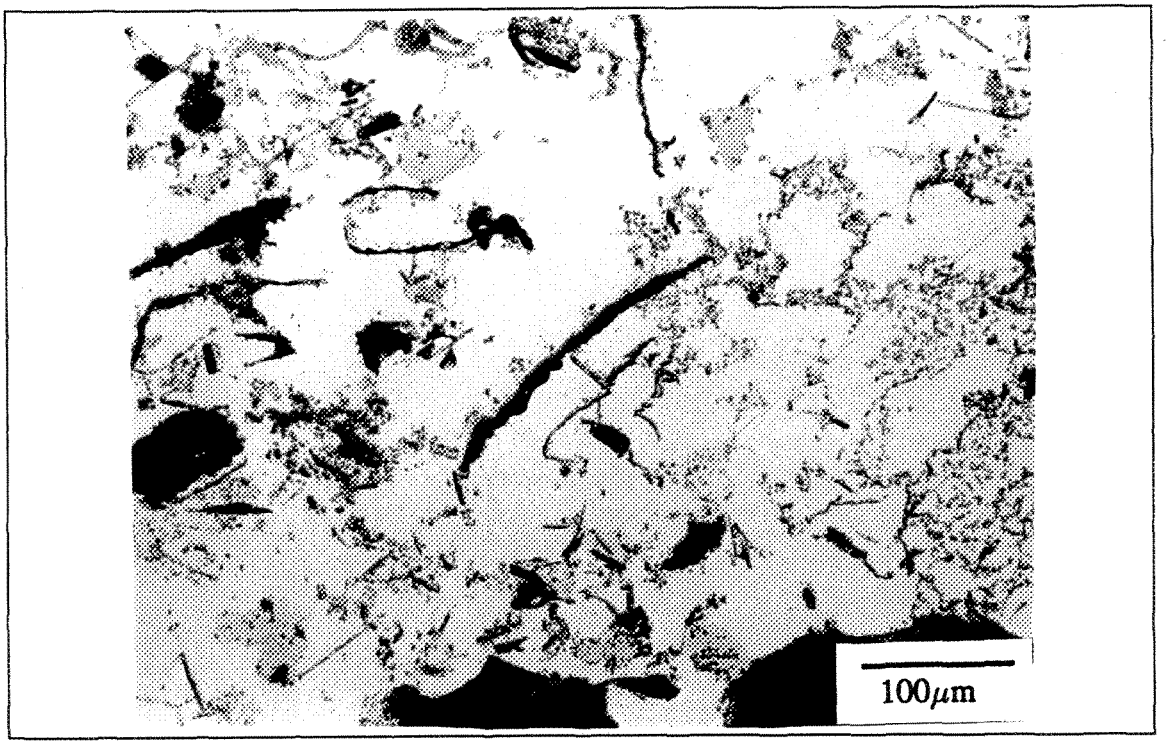

Figure 19 Example of graphite particles.

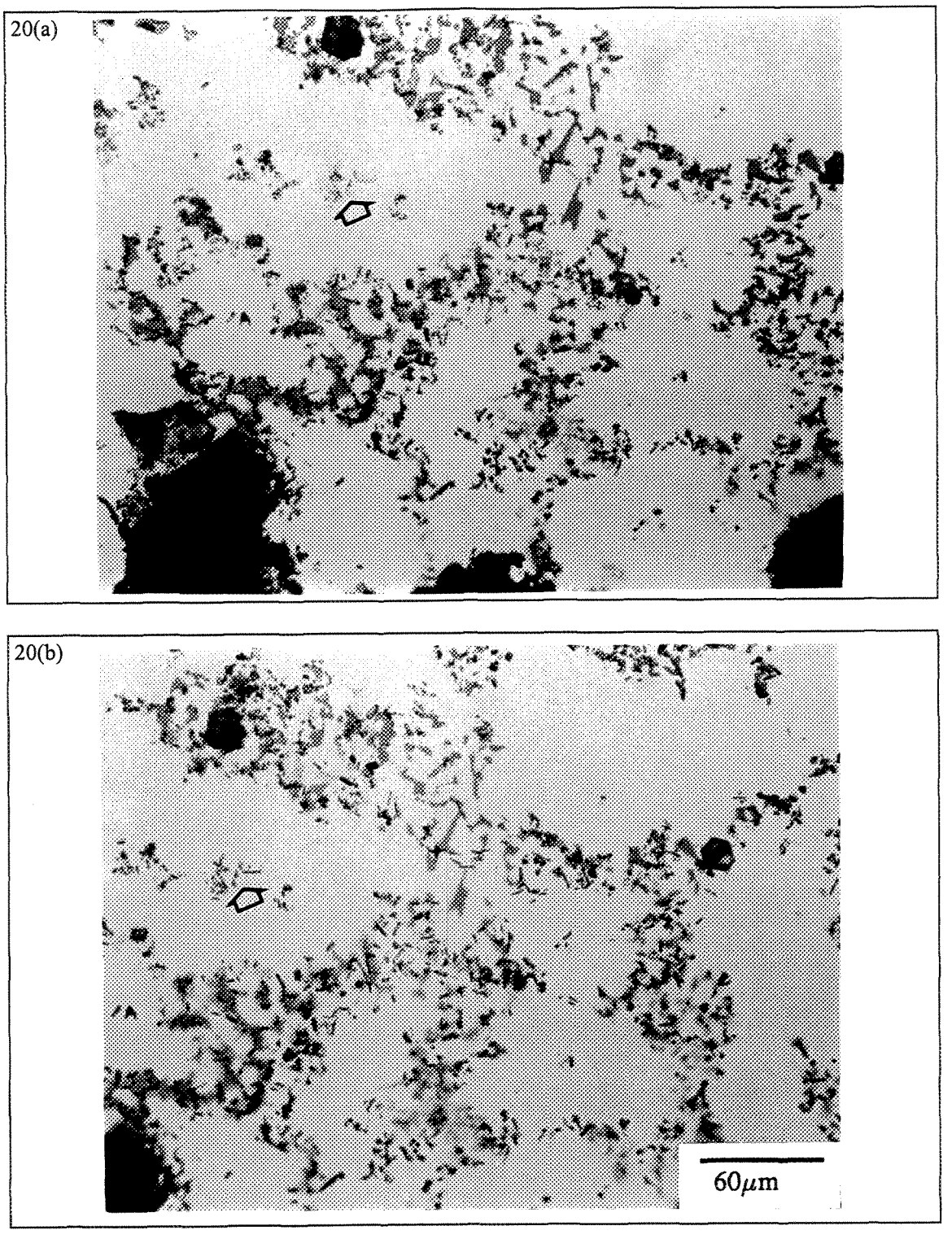

Figure 20 Examples of fine Al_4C_3 ($\leq 3\mu m$) particles observed on: a) a freshly prepared sample, b) after almost a week.

It should be noted that Al_4C_3 particles are already present in the commercially pure aluminum ingots used to produce aluminum alloy.

The MgO inclusions were seen either in the form of patches with a regular shape, Figure 22(a), or fairly pale in color, Figure 22(b). An example of MgO cuboides is shown in Figure 22(c).

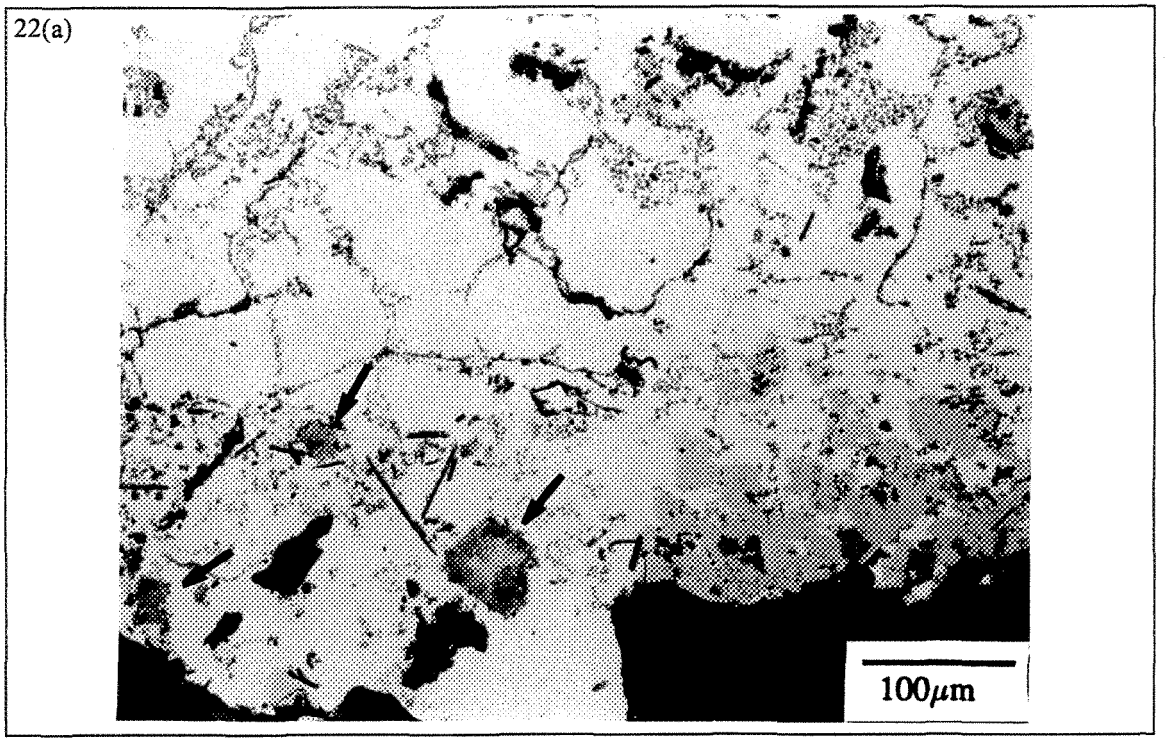

Figure 22 Examples of MgO particles: a) regular fragment, b) pale-colored pieces c) MgO (marked 1) Mg cuboides (marked 2) - Note the presence of both types of magnesium oxide in the same regions.

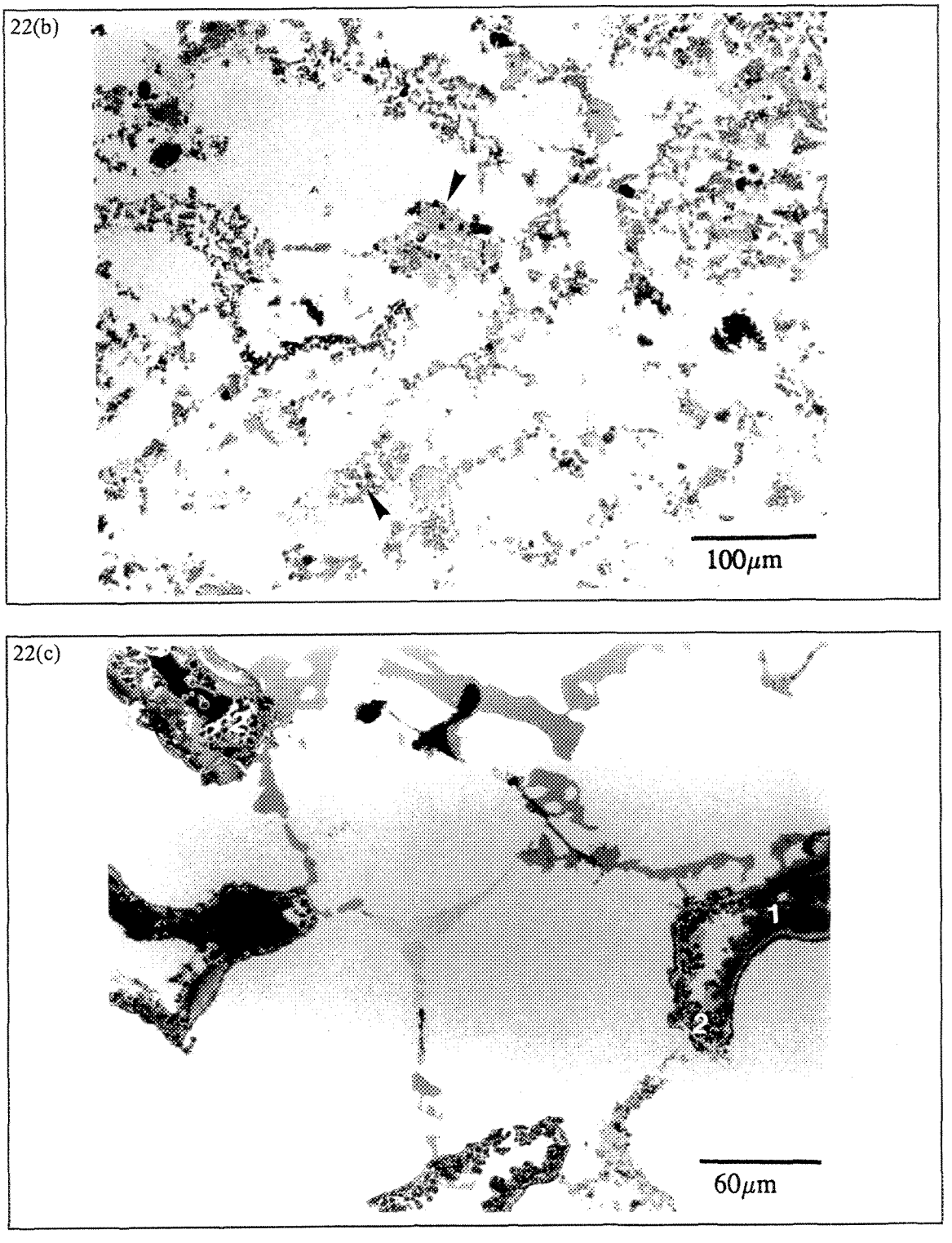

Figure 22 Examples of MgO particles: a) regular fragment, b) pale-colored pieces c) MgO (marked 1) Mg cuboides (marked 2) - Note the presence of both types of magnesium oxide in the same regions.

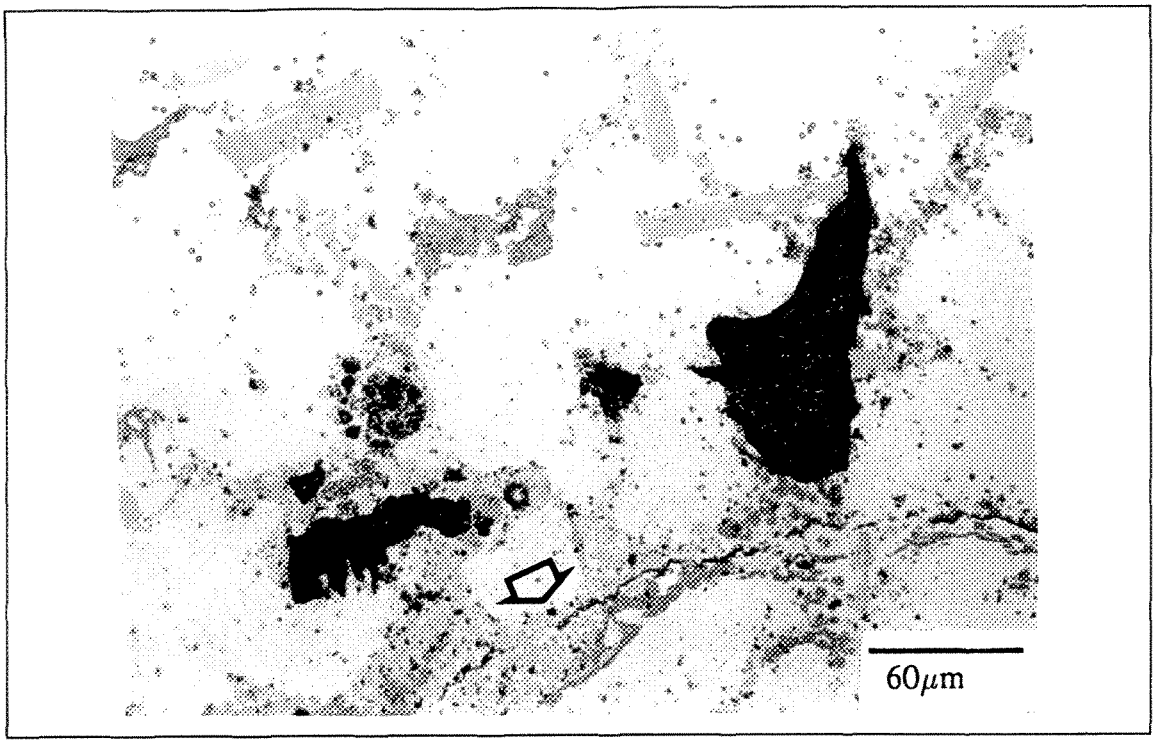

Figure 23 Example of spinel inclusions. The long platelets are undissolved pieces of Al-Ti-B master alloy.

Figure 23 shows a classic example of spinel ($MgAl_2O_4$) particles, very dark (almost black) in color.

Other inclusions that are considered less harmful are potential chlorides and TiB_2. Figures 24(a) and 24(b) are bright and dark field images, respectively, of potential chlorides. They appear as small roundish holes (see long arrows). Usually, the contours of a hole are crusted with small inclusions that have been collected by the liquid salt (during production of the aluminum ingots). The SrO particles appear as tiny black particles dotting the eutectic silicon particles, in some cases clustered together, as shown by the short arrows in Figure 24(a). The presence of these oxide particles may explain the formation of porosity in Sr-modified Al-Si castings [58].

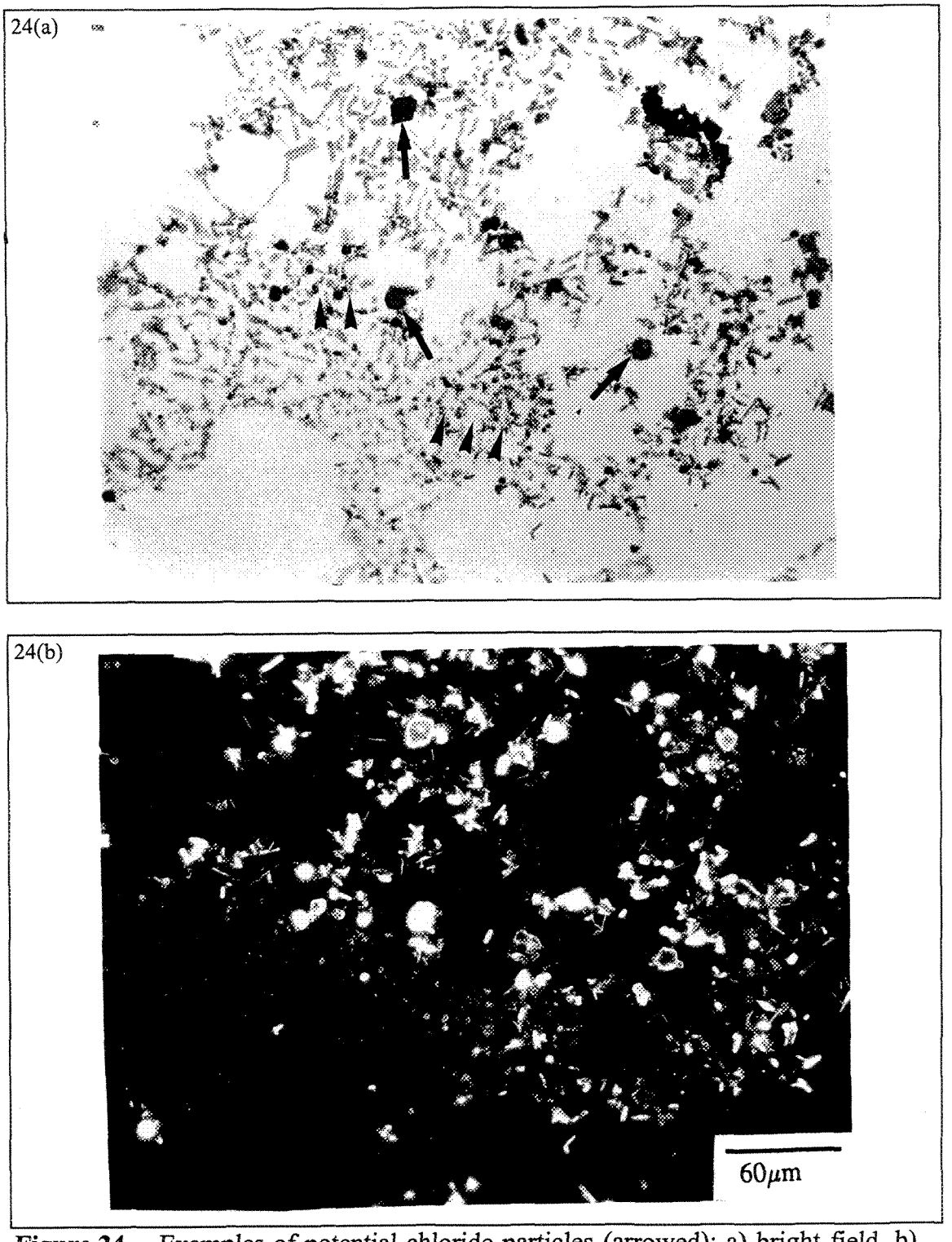

Figure 24 Examples of potential chloride particles (arrowed): a) bright field, b) dark field images. The short arrows in (a) point to SrO particles.

The TiB_2 inclusion particles are normally pushed to the interdendritic cell regions, forming a "cake" that seals the filter pores as shown in Figure 25. This observation may explain the fact that the addition of a small amount of TiB_2 resulted in increasing the filtration time to 15 min in order to collect only 300 g of filtered metal, compared to 3 min for 1.5 kg of filtered metal obtained without TiB_2 addition.

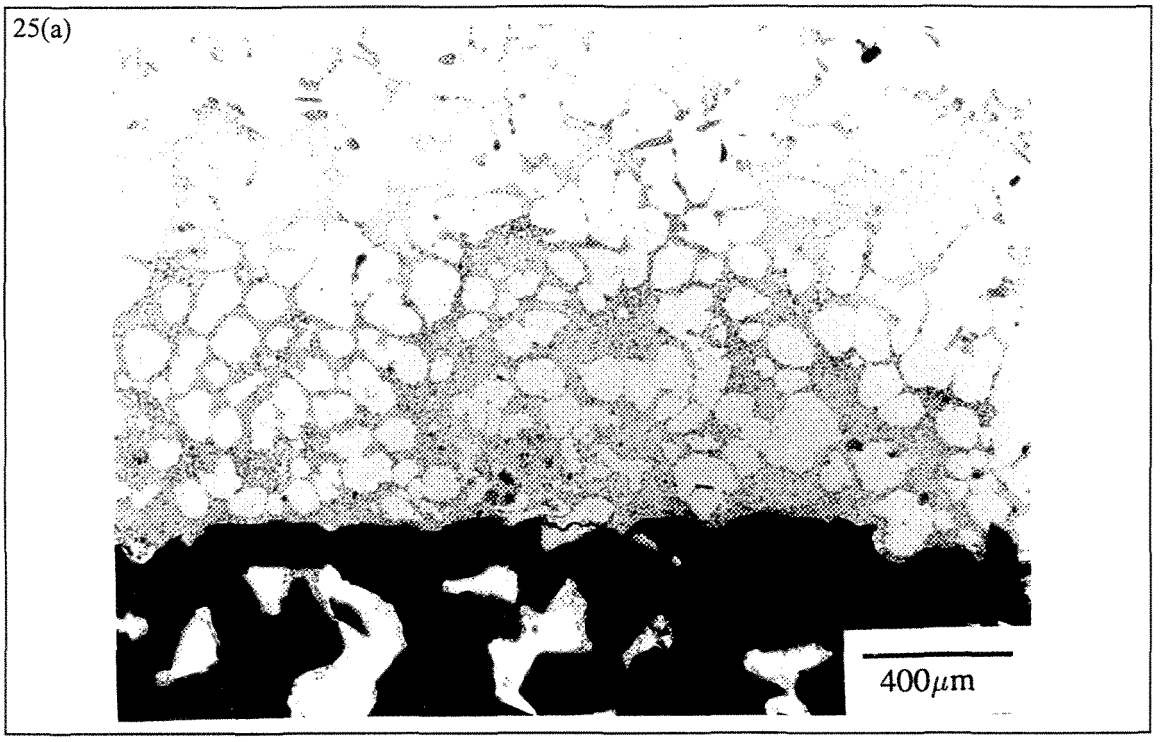

Figure 25 Examples of TiB_2 particles: a) bright field, b) dark field images.

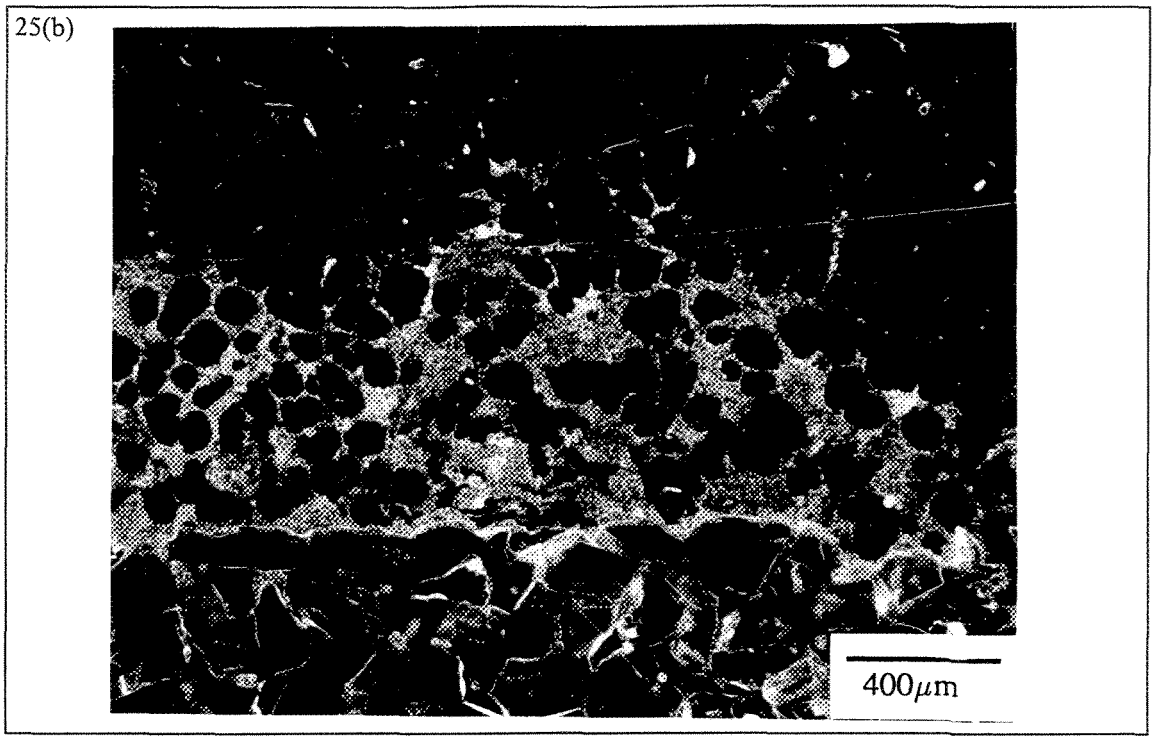

Figure 25 Examples of TiB_2 particles: a) bright field, b) dark field images.

Figure 26(a) illustrates examples of "thin oxide films". They appear as pencil line-like defects, i.e., they show no measurable thickness at the optical level. An example of "thick oxide films" is shown in Figure 26(b). As can be seen, these films have a measurable width compared to the former.

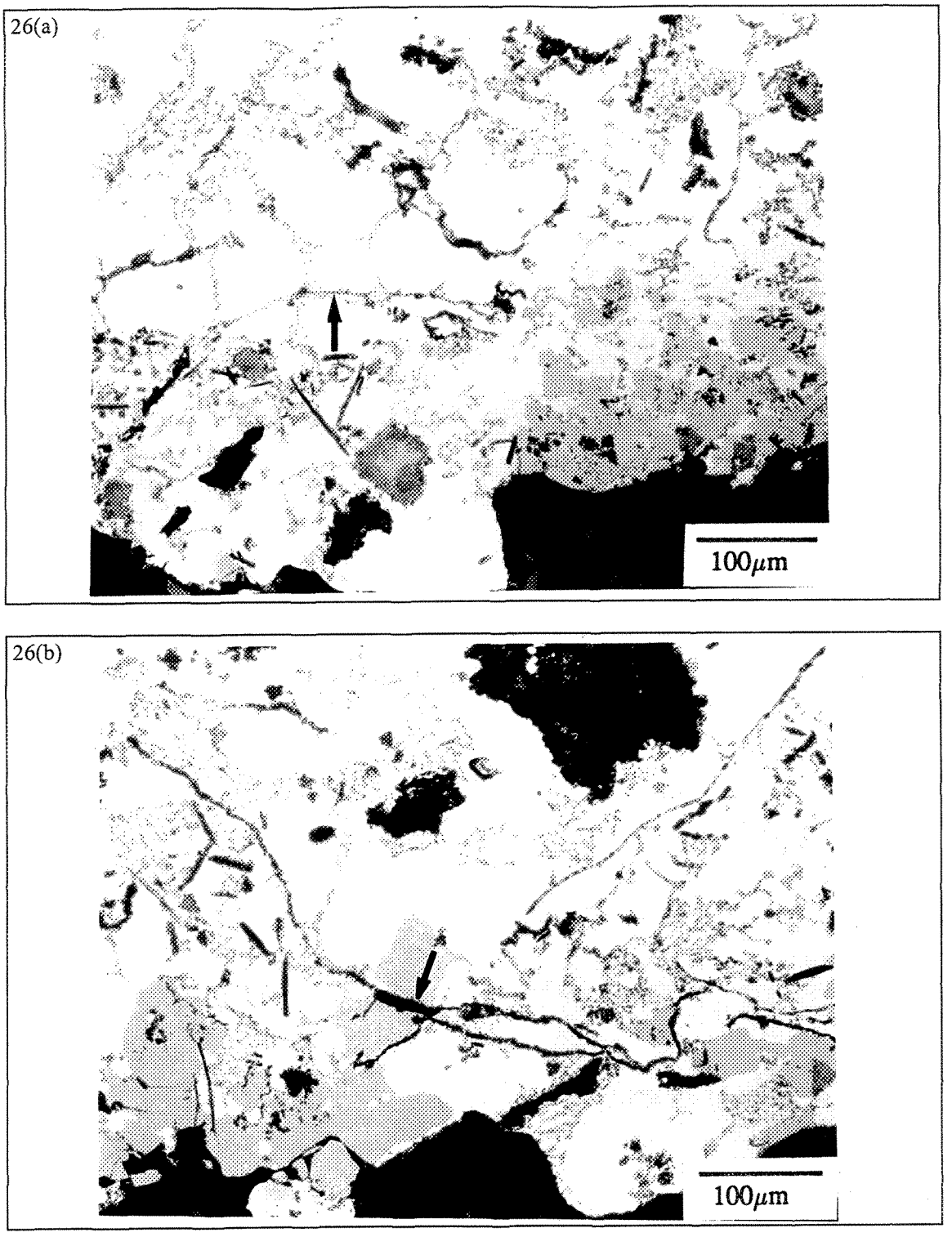

Figure 26 Examples of oxide films: a) thin films, b) thick films.

Figures 27 through 34 indicate the experimental conditions that maximize the concentrations of the different inclusion types observed for the two alloys. Figure 27 shows that graphite mainly occurs when stirring or degassing is done using a graphite impeller. Potential chlorides are found in very small amounts, of the order of 0.0008 mm^2/kg, as shown in Figure 28(a). The maximum attainable quantity (0.0065 mm^2/kg) of these inclusions is shown in Figure 28(b), corresponding to the case when the molten metal was vigorously stirred.

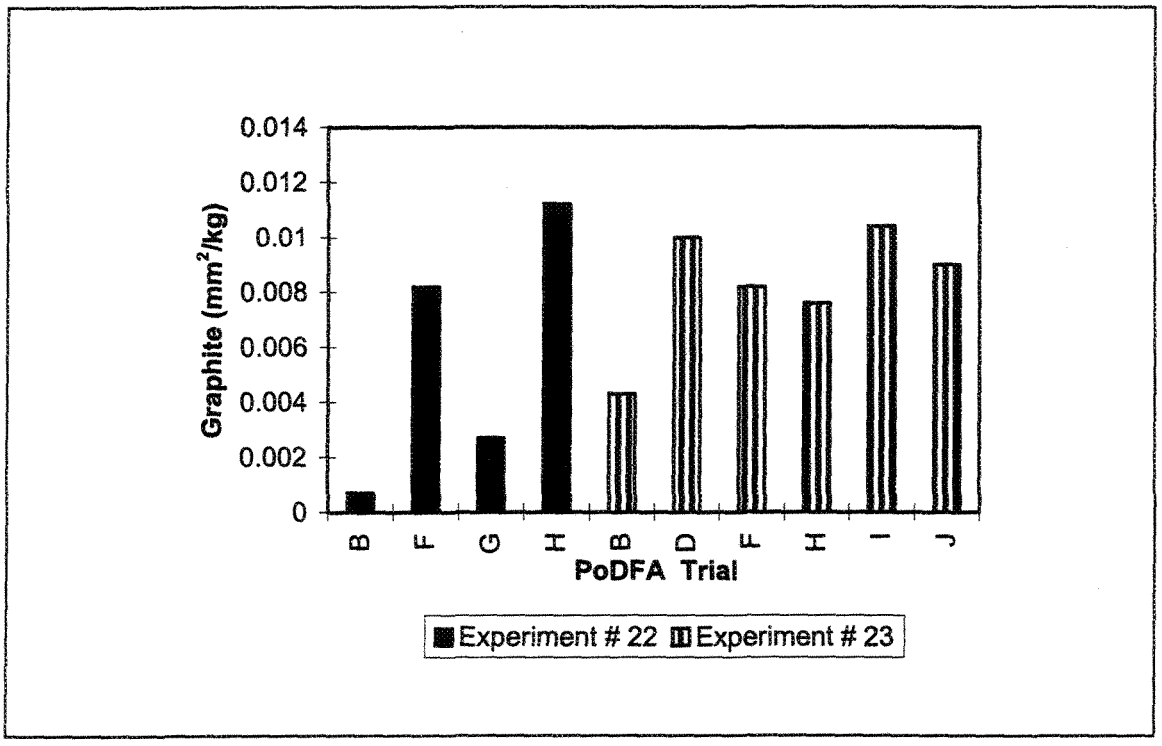

Figure 27 Experimental conditions that maximize the concentration of graphite inclusions.

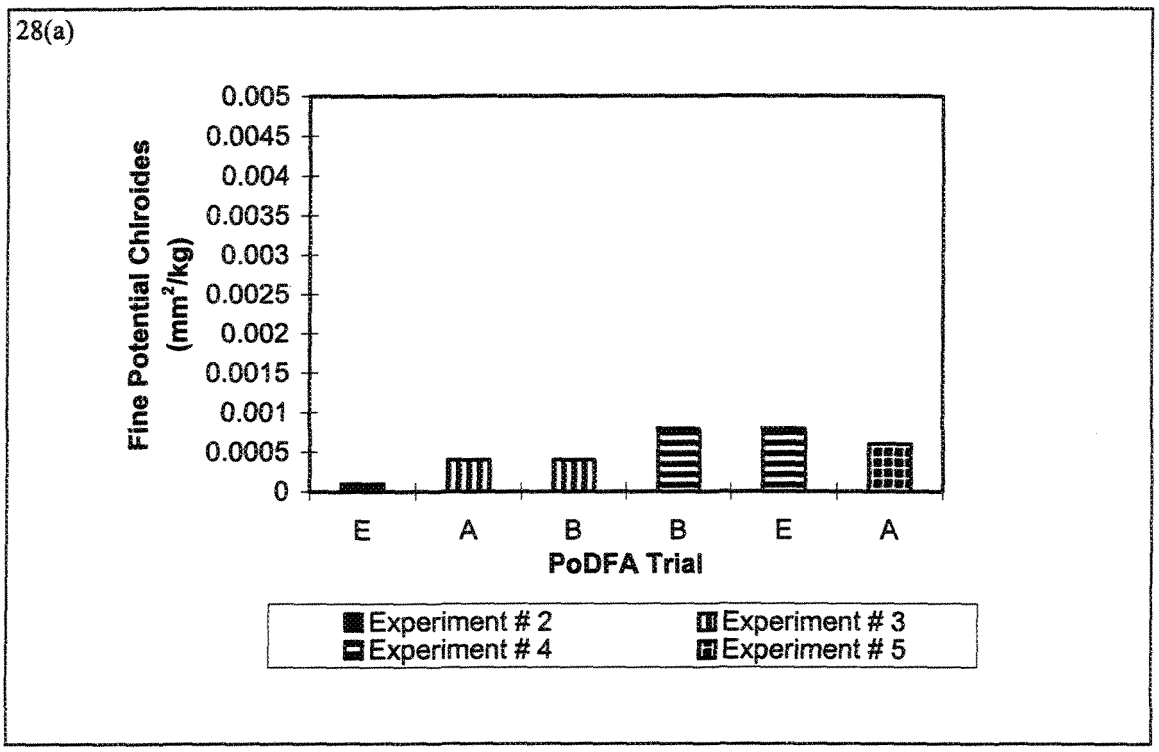

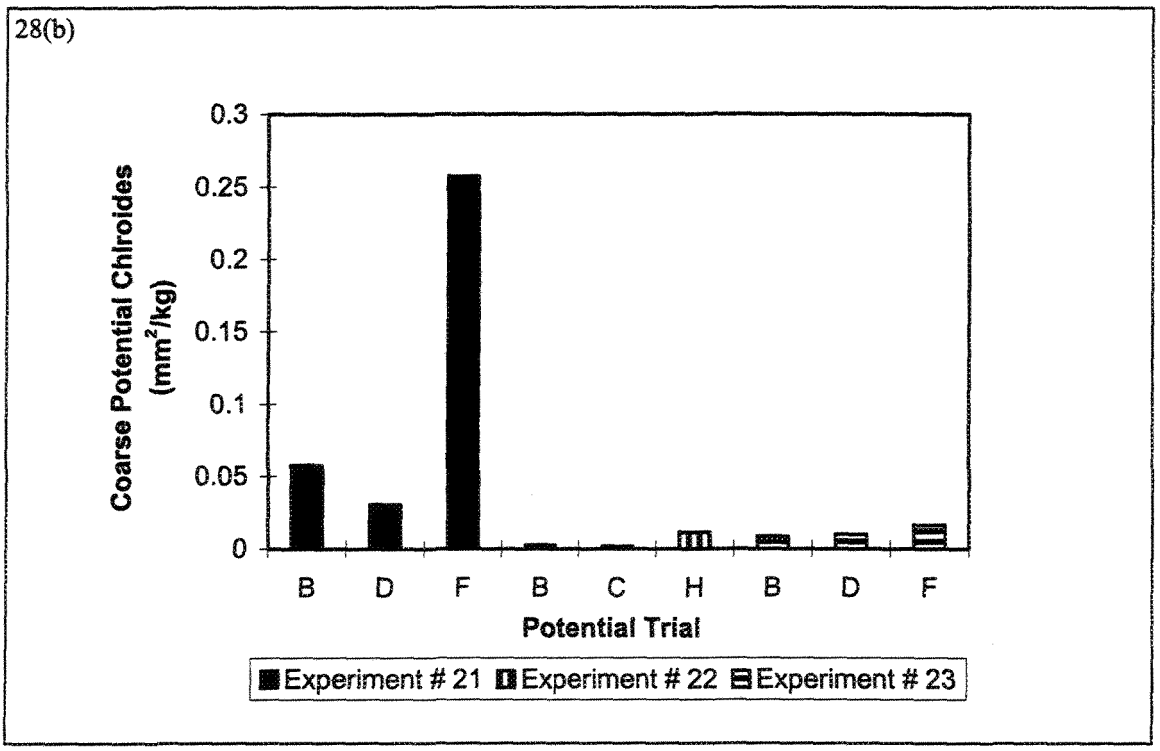

Figure 28 Experimental conditions that maximize the concentration of potential chloride inclusions: a) fine particles, b) coarse particles.

Figures 29(a) and 29(b) show the experimental conditions corresponding to maximum concentration of fine Al_4C_3 ($\leq$ 3μm) inclusions. It is evident that stirring coupled with long holding periods leads to the formation of this type of inclusion. When degassing is applied, a large part of the fine Al_4C_3 particles is removed (Figure 29(b)). Since these inclusions are very small, filtration using 10 ppi ceramic foam filter discs may not be sufficient to hinder their motion and consequent transfer into the PoDFA crucible. Figure 29(c) demonstrates the beneficial effect of degassing and settling time in minimizing the concentration of these fine Al_4C_3 inclusion particles.

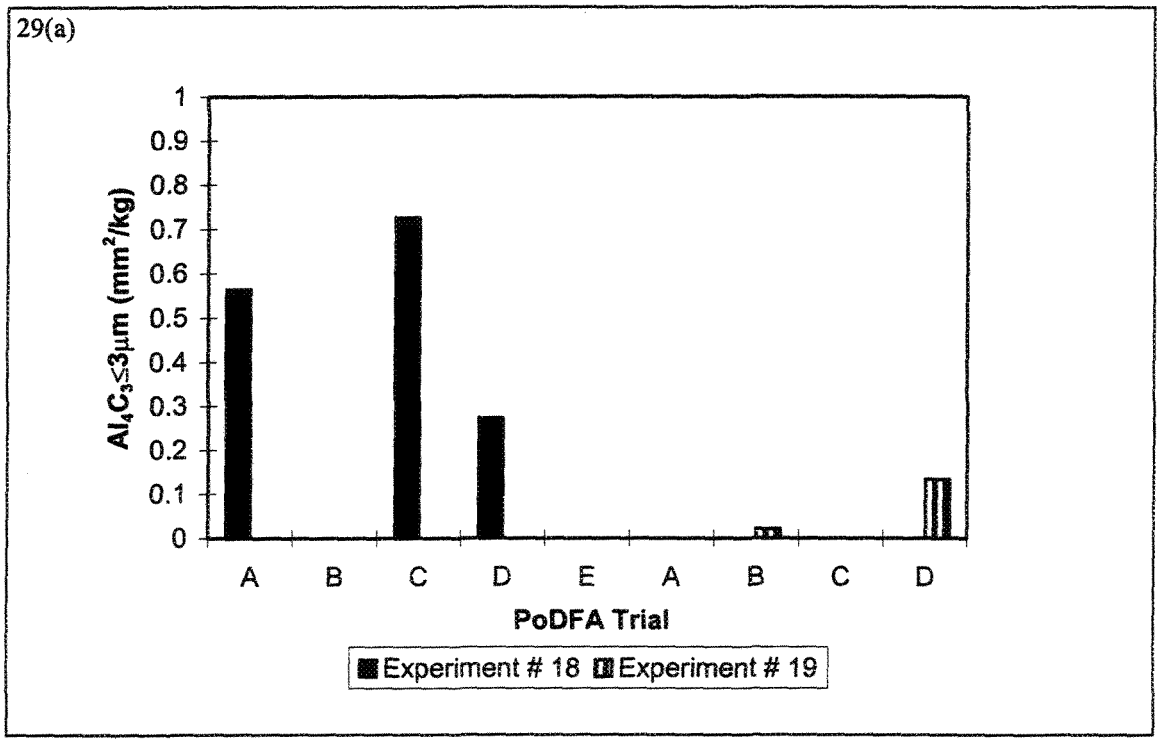

Figure 29 Experimental conditions that maximize the concentration of fine Al_4C_3 (≤3μm) inclusions: a) effect of mechanical stirring, b) effect of filtration without and with degassing, c) effect of the type of initial charge.

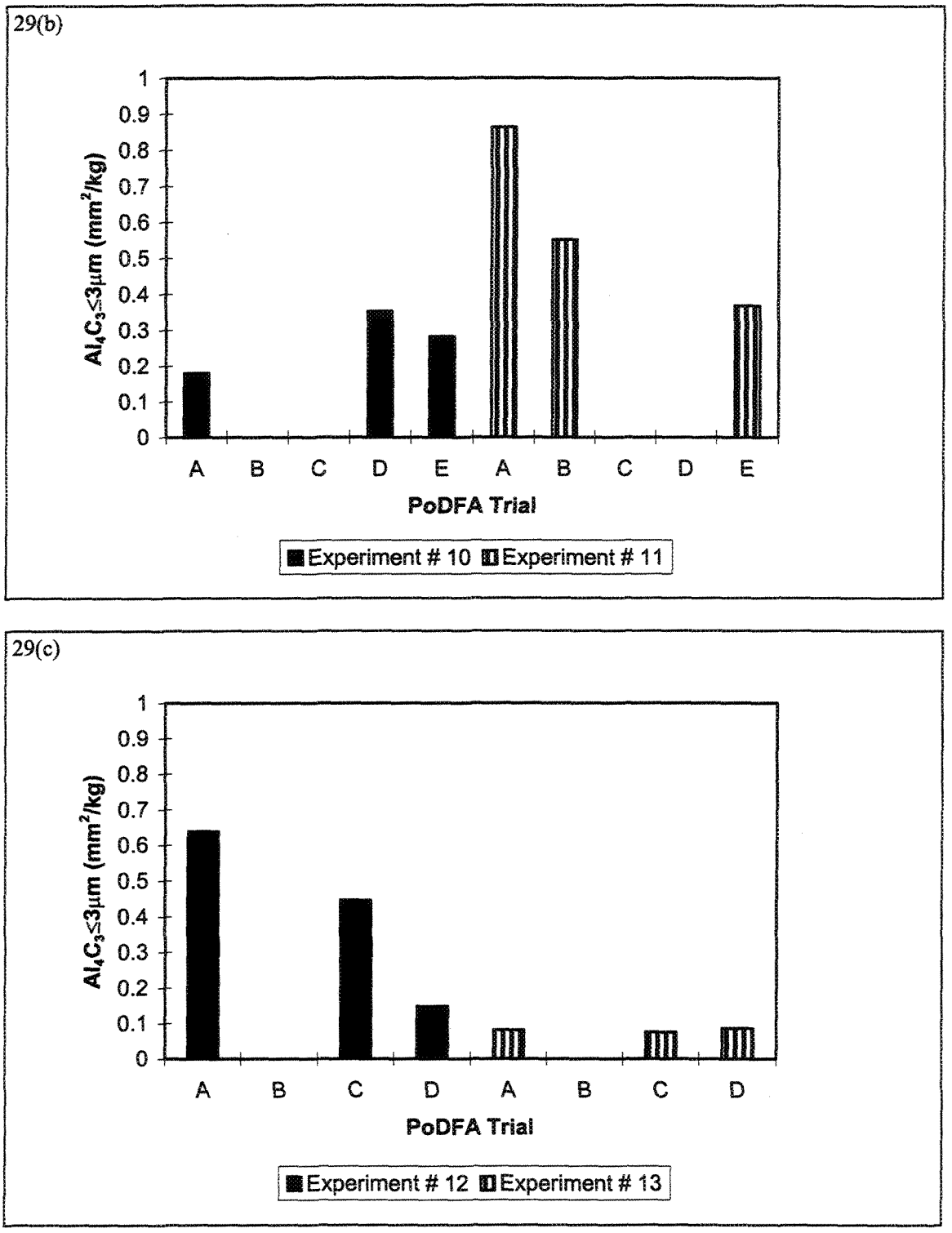

Figure 29 Experimental conditions that maximize the concentration of fine Al_4C_3 ($\leq 3\mu m$) inclusions: a) effect of mechanical stirring, b) effect of filtration without and with degassing, c) effect of the type of initial charge.

It is evident from Figure 30 that holding the liquid metal for periods as long as 72 h enhances the formation of thick Al_4C_3 inclusion particles (> 3 μm). This observation may be interpreted, at least partly, as resulting from the reaction between the molten metal and the wall of the melting crucible. It should be borne in mind that this experiment was the twentieth in the series, without changing the crucible or the coating material. It is interesting to note that filtration with 10 ppi ceramic foam filters resulted in a significant reduction in the concentration of the coarse Al_4C_3 inclusion particles. Degassing however, proved to be the most effective method in removing these inclusions.

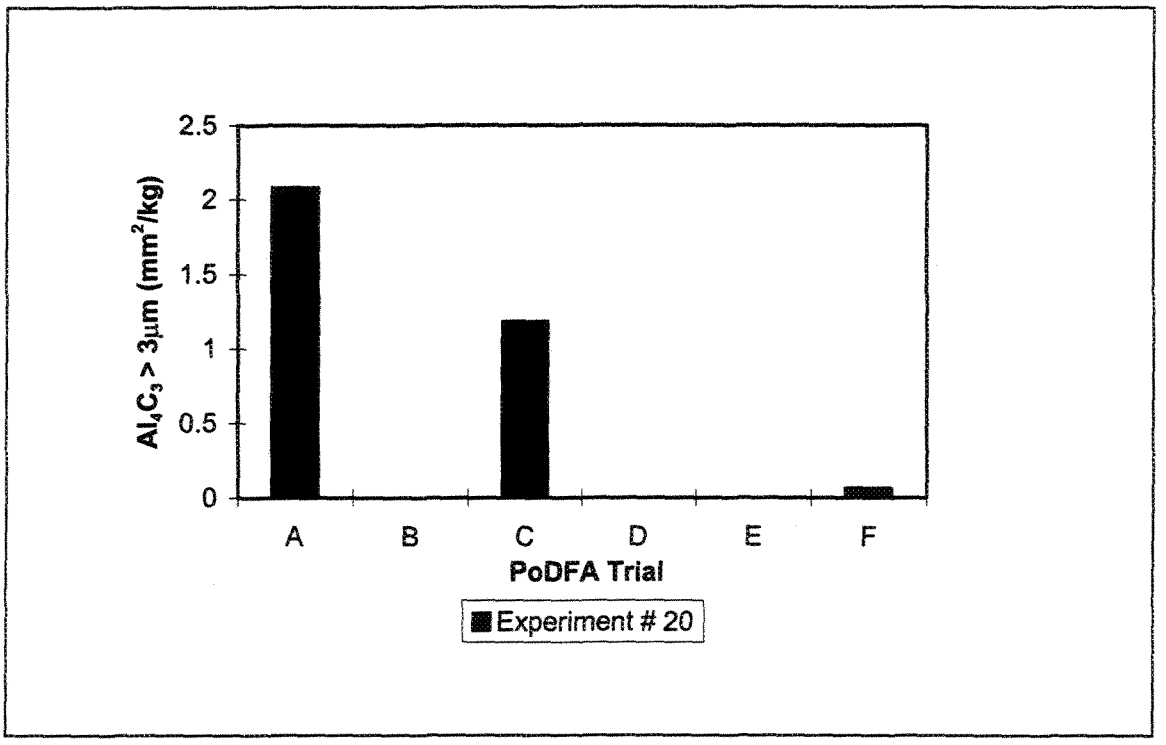

Figure 30 Experimental conditions that maximize the concentration of coarse Al_4C_3 (> 3μm) inclusions.

Magnesium oxide (MgO) is the first oxide to form in the magnesium oxide - type series. It then transforms into MgO cuboides and later on to spinel, i.e., $MgAl_2O_4$. It is obvious that long holding times (i.e., 72 h) would certainly increase the possibility of its formation. The findings of Doutre et al. [20] reveal that MgO and spinel tend to settle to the bottom of the melting crucible with time. Similar observations were made in the present study, as can be seen in Figure 31(a) for A356.2 alloy. Increasing the holding time to 4 h led to a noticeable increase in the concentration of MgO (from 0.005 to ~ 0.15 mm^2/kg). Prolonged holding times (i.e., 72 h), Figure 31(b), significantly increased the concentration of MgO to 0.9 mm^2/kg, that precipitated to the bottom of the melting crucible. Degassing, however, led to the floatation of MgO to the upper portion of the remaining liquid metal. Figure 31(c) shows the effect of the type of initial charge, i.e.,

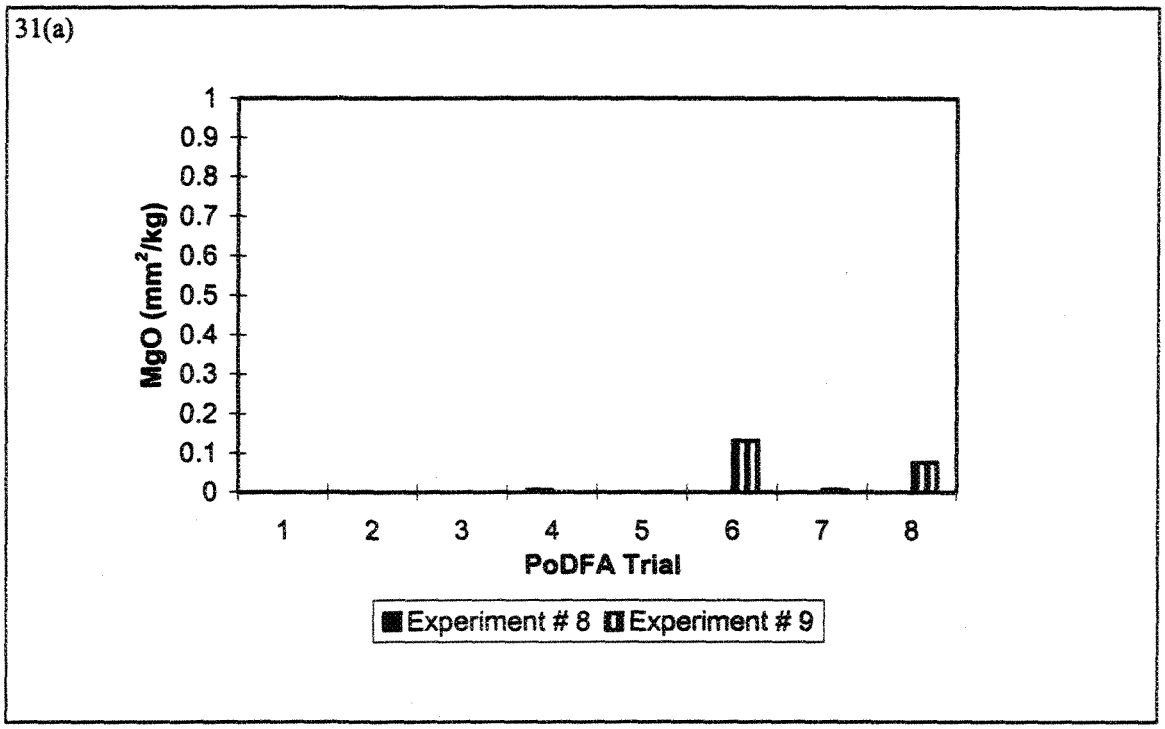

Figure 31 Experimental conditions that maximize the concentration of MgO inclusions in A356.2 alloy : a) mechanical stirring & settling time.

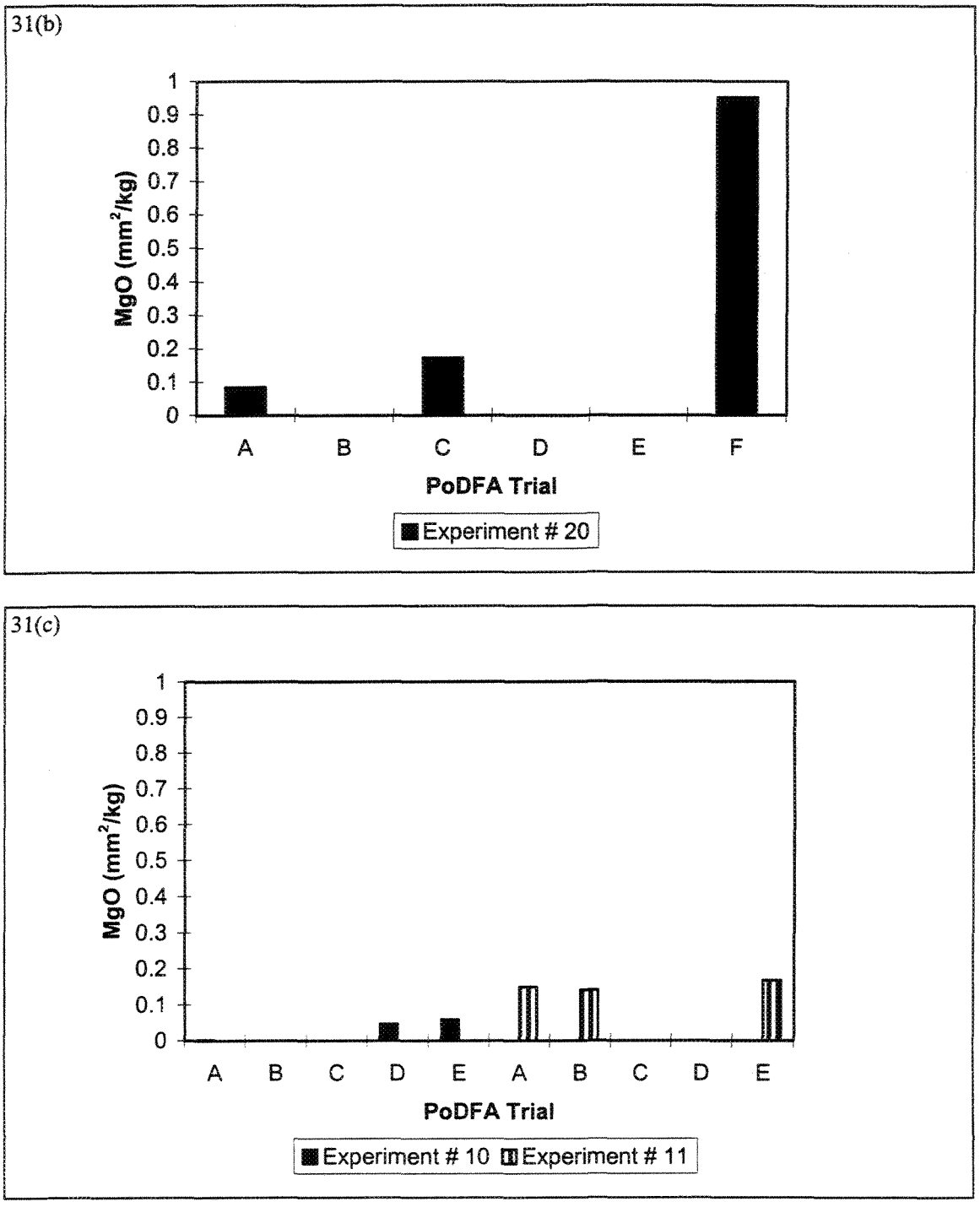

Figure 31 Experimental conditions that maximize the concentration of MgO inclusions in A356.2 alloy: a) effect of mechanical stirring and settling time, b) effect of prolonged holding time (72 h), c) effect of the type of initial charge (scrap).

scrap, on the concentration of MgO inclusions obtained.

Increasing the Mg content to 0.56 wt%, i.e., C357 alloy, resulted in a marginal increase in the concentration of MgO inclusions when the molten melt was held still, even for a period of 72 h (Figure 32(a)). In fact, sedimentation or filtration (using 10 and 20 ppi filters) significantly reduced the MgO concentration, as shown in Figure 32(b).

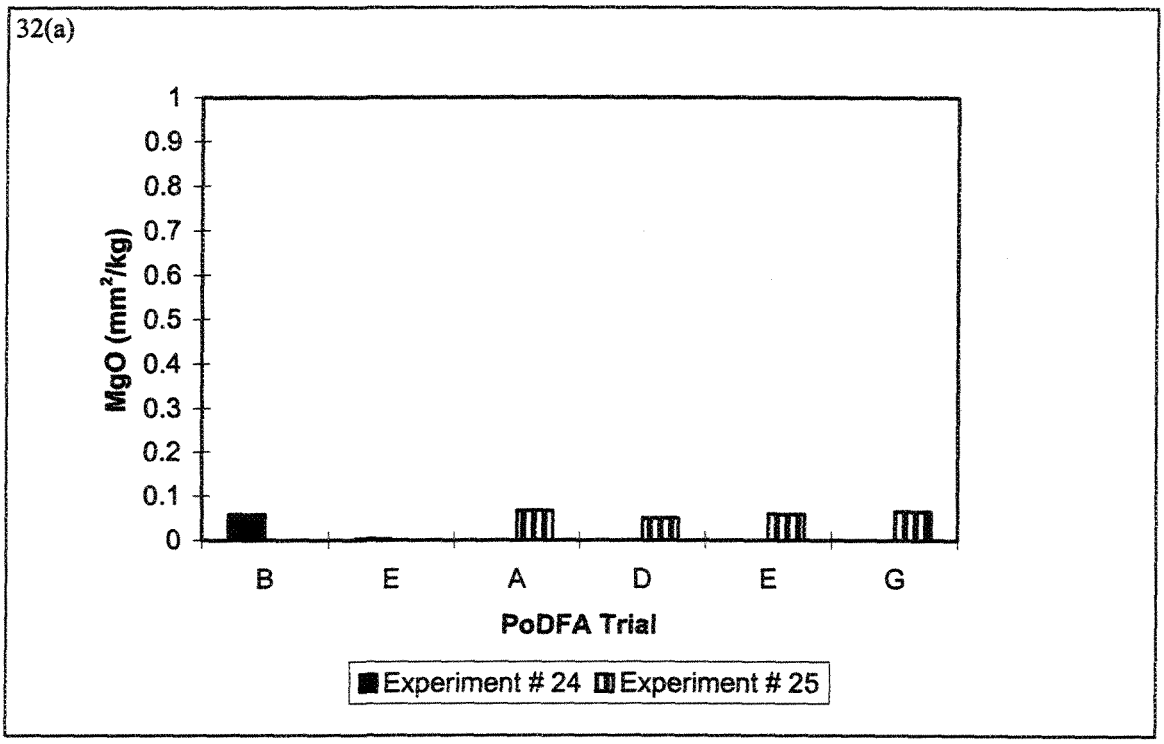

Figure 32 Experimental conditions that maximize the concentration of MgO inclusions in C357 alloy: a) effect of settling time, b) effect of mechanical stirring.

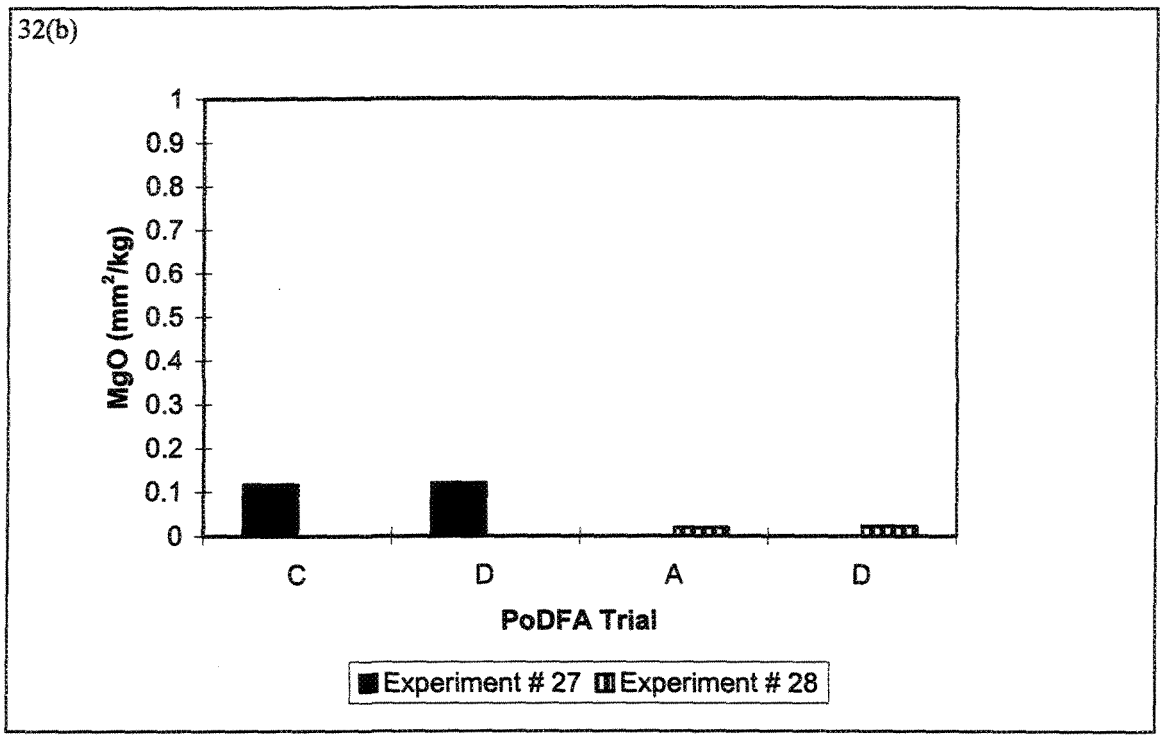

Figure 32 Experimental conditions that maximize the concentration of MgO inclusions in C357 alloy: a) effect of settling time, b) effect of mechanical stirring.

The maximum concentration of the MgO cuboides (i.e., 1.4 mm^2/kg) in A356.2 alloy was first seen when scrap alloy was remelted and held for 4 h, as shown in Figure 33(a). Evidently, most of the cuboide inclusions either floated to, or formed in the upper portion of the liquid metal, rather than settling to the bottom of the melt crucible. After this PoDFA trial, the concentration of the cuboide inclusions was seen to drop to ~ 0.07 mm^2/kg for the next trial, and further to 0.025 mm^2/kg for the following PoDFA trial. As expected, holding the liquid metal for 72 h resulted in increasing the concentration of cuboides to 1.3 mm^2/kg in the upper portion of the molten metal that was relatively more exposed to the surrounding atmosphere. Thus, a gradual reduction in inclusion concentration in the

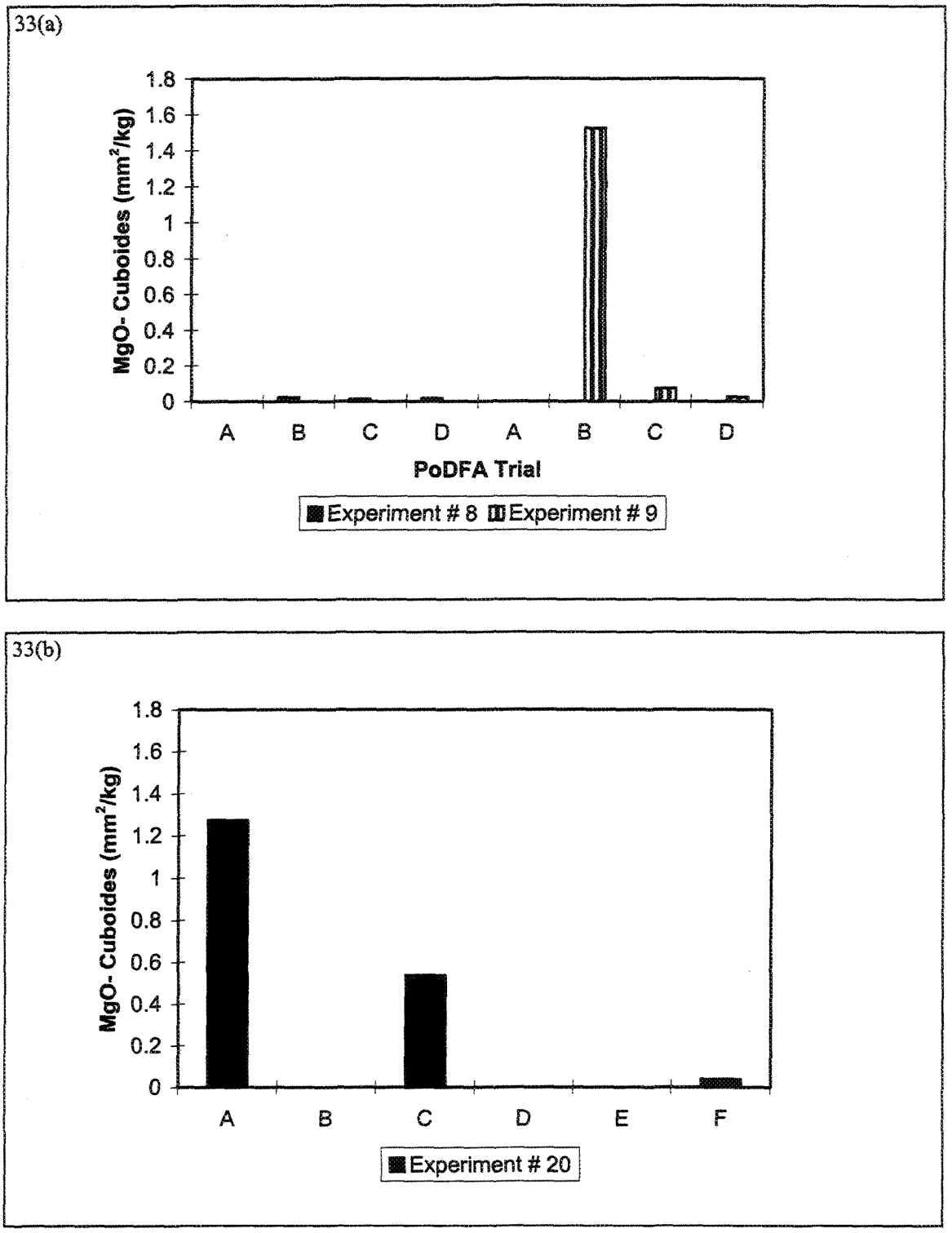

Figure 33 Experimental conditions that maximize the concentration of MgO cuboide inclusions in A356.2 alloy : a) effect of type of initial charge, b) effect of prolonged holding time (72 h).

remaining melt is noted in Figure 33(b). Filtration also appears to be effective in removing these inclusions.

Compared to A356.2 alloy, the cuboide inclusions in C357 alloy appear in much smaller quantity as seen in Figure 34(a), when the molten metal is held stagnant. Prolonged holding periods (i.e., 72 h) increased the concentration in the first PoDFA trial, representing the layer that was exposed to the surrounding atmosphere.

Mechanical agitation was more effective in distributing the inclusions that had settled to the bottom of the melting crucible. Allowing the melt to settle increased the concentration of the cuboide inclusions in the last PoDFA trials, as displayed in Figure 34(b). In all cases, the concentrations of MgO cuboide inclusions observed were much lower in the case of C357 alloy.

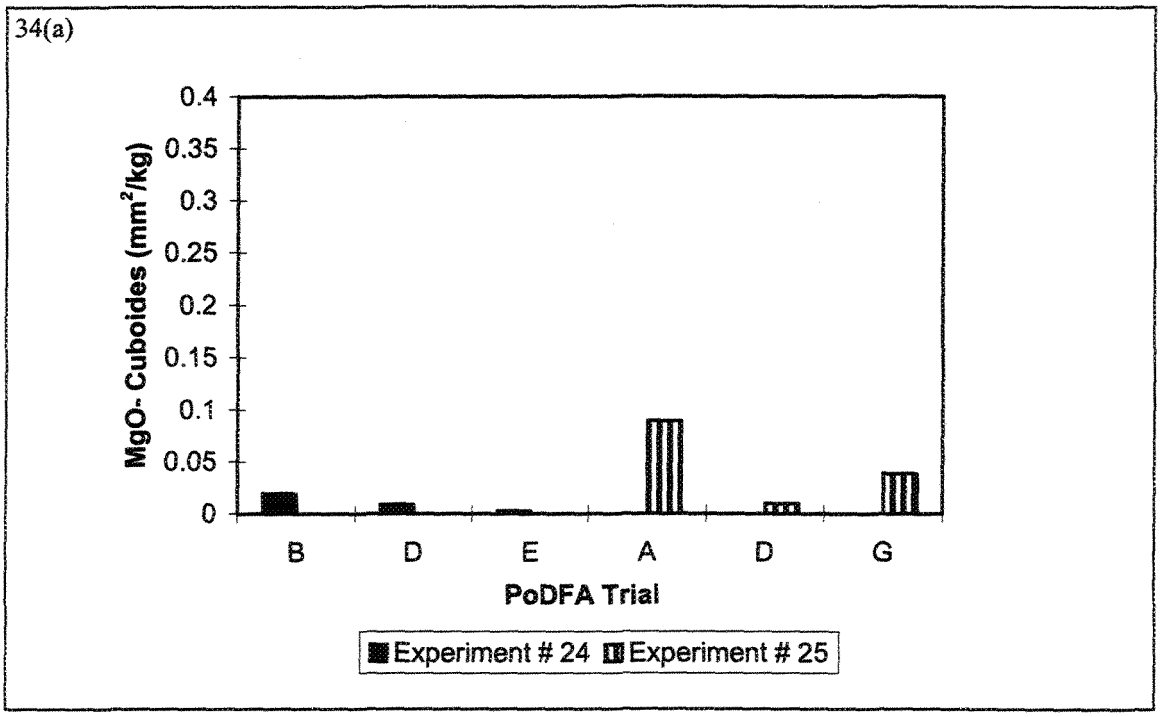

Figure 34 Experimental conditions that maximize the concentration of MgO cuboides inclusions in C357 alloy: a) effect of settling time, b) effect of mechanical stirring.

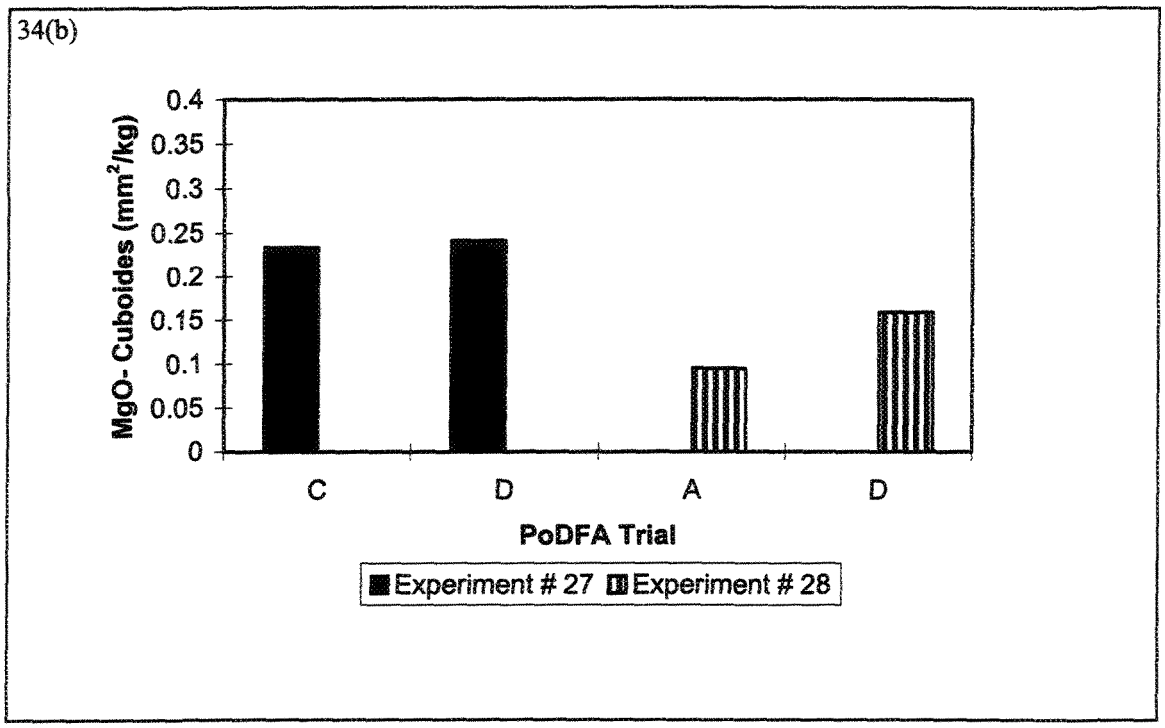

Figure 34 Experimental conditions that maximize the concentration of MgO cuboides inclusions in C357 alloy: a) effect of settling time, b) effect of mechanical stirring.

The third inclusion type in the magnesium oxides series, i.e., spinel ($MgAl_2O_4$), was also found to be more concentrated in the upper portion of the molten scrap, together with the MgO cuboides, Figure 35(a). Both types were successfully removed during the first PoDFA trial.

Degassing the molten scrap resulted in pushing most of the spinel particles upwards, whereas when the molten metal was kept stagnant, the particles tended to settle near the bottom of the melting crucible, Figure 35(b).

Another parameter that significantly contributed to the concentration of spinel inclusions in the upper layer of the molten metal was the increase in holding time (i.e.,

72h), as shown in Figure 35(c). Thus it is recommended that the first and last castings in a series of castings prepared from the same melt should be rejected.

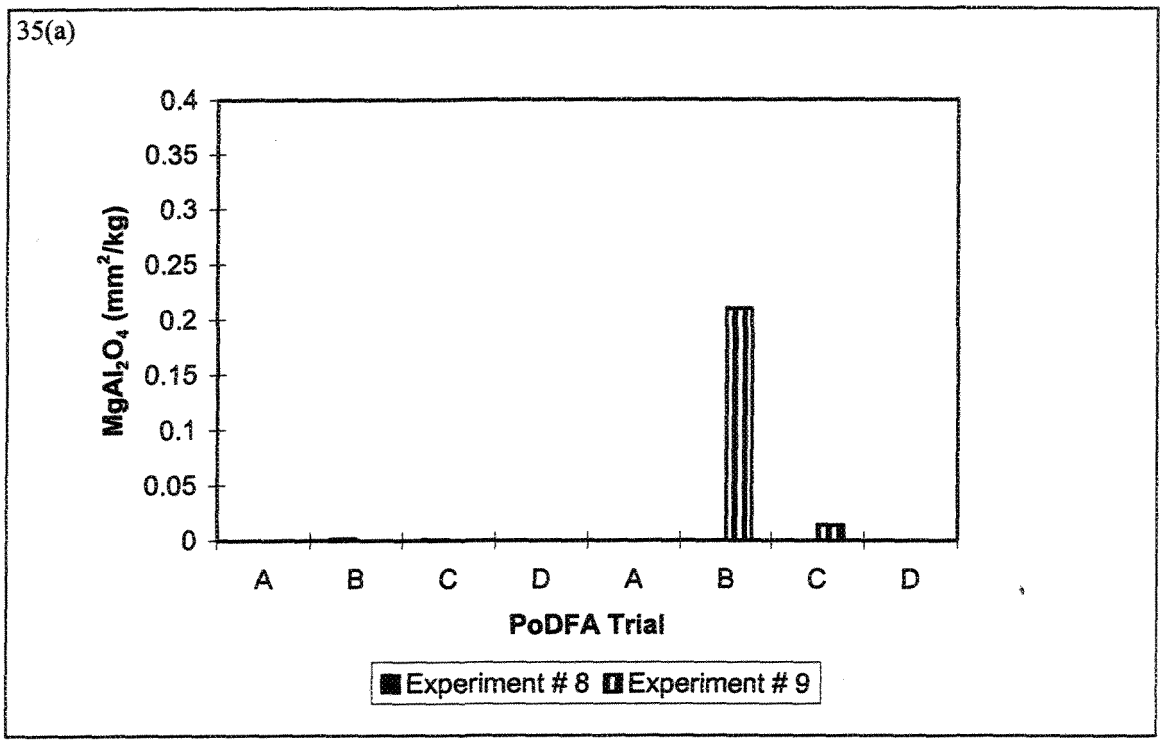

Figure 35 Experimental conditions that maximize the concentration of $MgAl_2O_4$ inclusions in A356.2 alloy: a) effect of type of initial charge, b) effect of filtration conditions, c) effect of prolonged holding time (72 h).

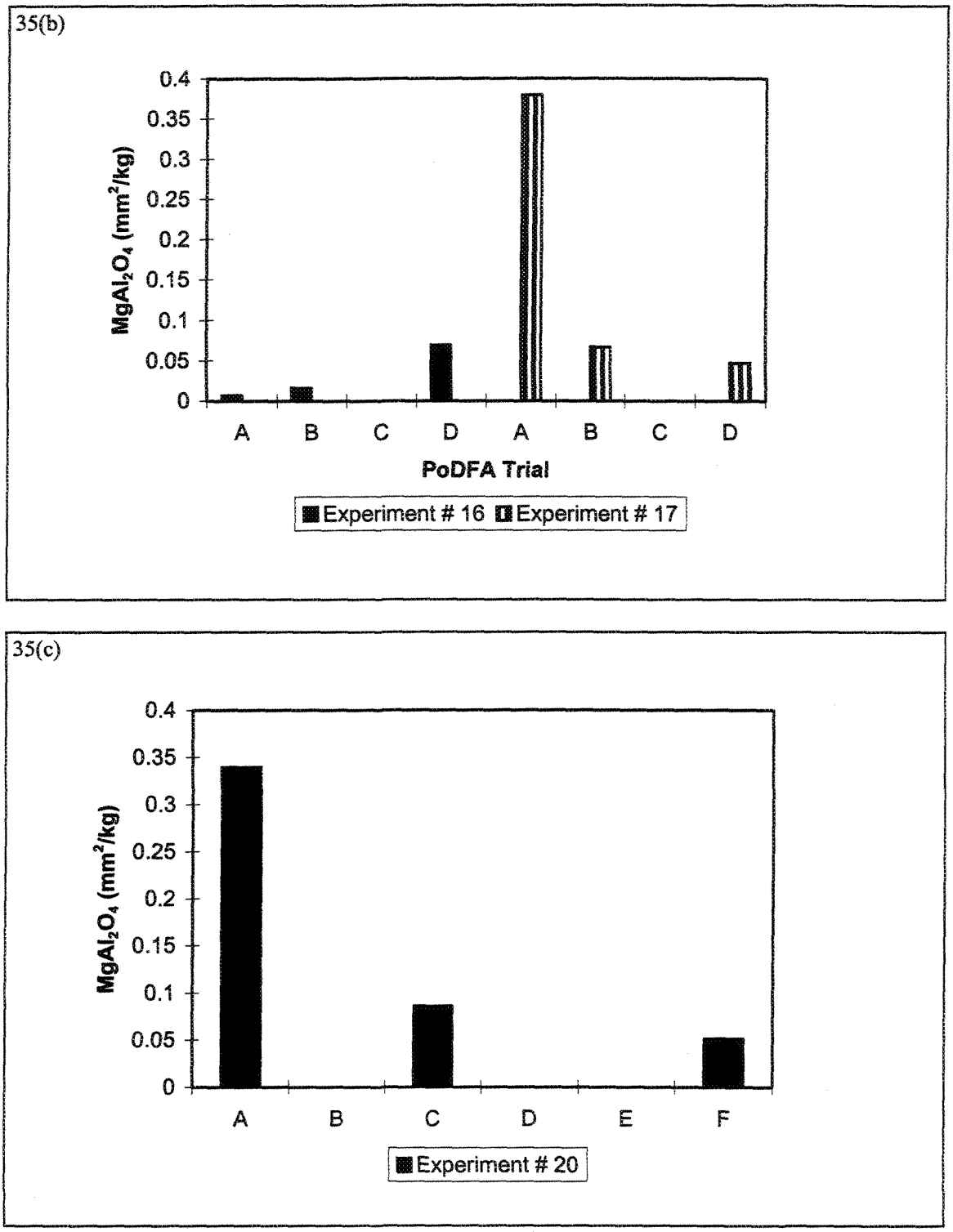

Figure 35 Experimental conditions that maximize the concentration of $MgAl_2O_4$ inclusions in A356.2 alloy: a) effect of type of initial charge, b) effect of filtration conditions, c) effect of prolonged holding time (72 h).

The rate of spinel formation was noticeably high in C357 alloy, particularly when the holding time was of the order of 72 h. A large number of the spinel inclusion particles was concentrated in the lower portion of the liquid metal as can be inferred from Figure 36(a). Mechanical stirring plus long holding times led to recontamination of the liquid metal, with a gradual increase in spinel concentration progressing towards the bottom of the melting crucible (Figure 36(b)). The effect of superheat was marginal. Apparently, most of the spinel was formed in the dross that was thoroughly skimmed before executing the PoDFA test.

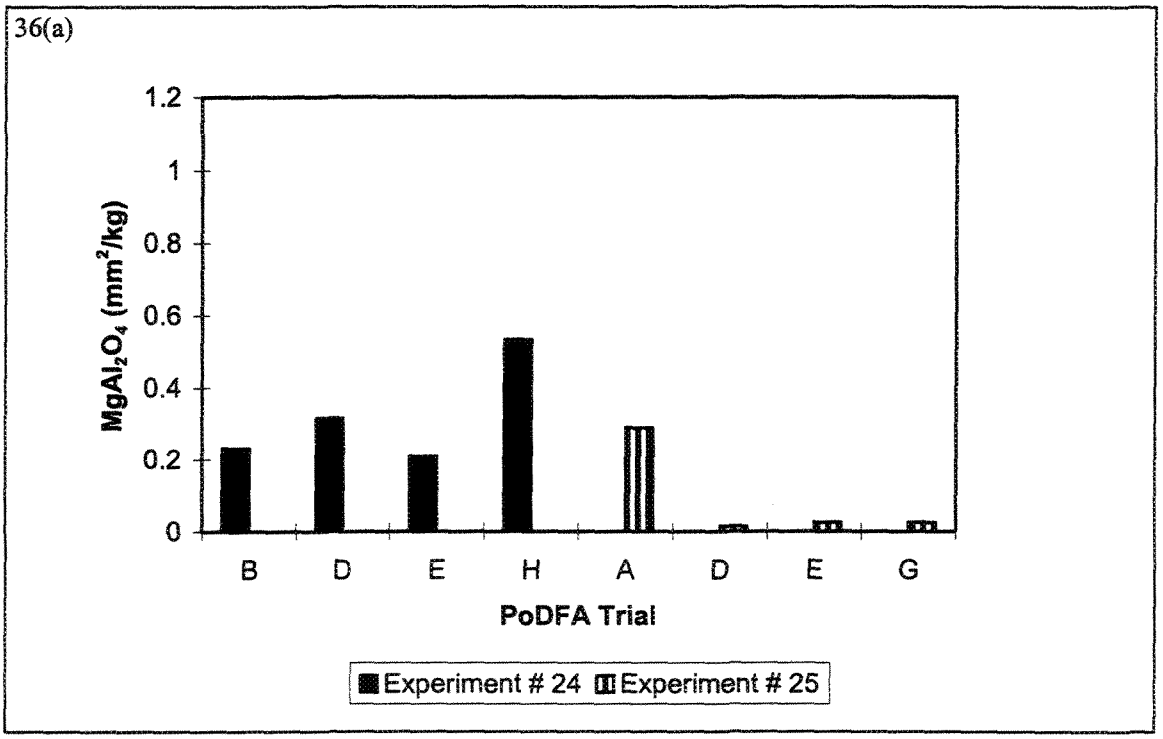

Figure 36 Experimental conditions that maximize the concentration of $MgAl_2O_4$ inclusions in C357 alloy: a) effect of settling time, b) effect of mechanical stirring.

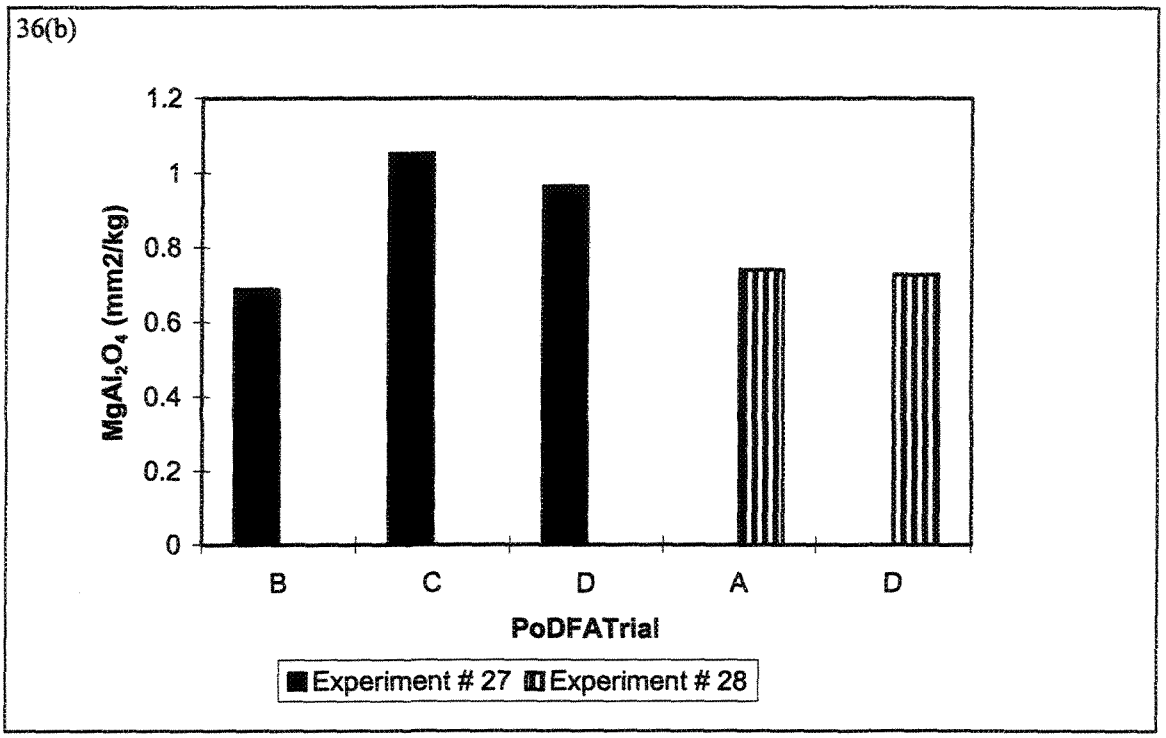

Figure 36 Experimental conditions that maximize the concentration of $MgAl_2O_4$ inclusions in C357 alloy: a) effect of settling time, b) effect of mechanical stirring.

Figure 37 shows the experimental conditions that maximize the concentration of the TiB_2 inclusions in A356.2 alloy. As seen from Figure 25, the TiB_2 particles are extremely fine. With respect to Figure 37, this explains the fact that filtration with 10 ppi ceramic foam filters could not prevent all the TiB_2 particles from entering into the liquid metal. Using finer filters (i.e., 20 ppi size filters) or degassing would be more effective in removing these inclusions. Degassing, however, would lead to floatation of these particles to the surface of the molten metal. Figure 38 demonstrates the difference in pore sizes of 10 ppi and 20 ppi ceramic foam filters, shown mounted in pouring cups.

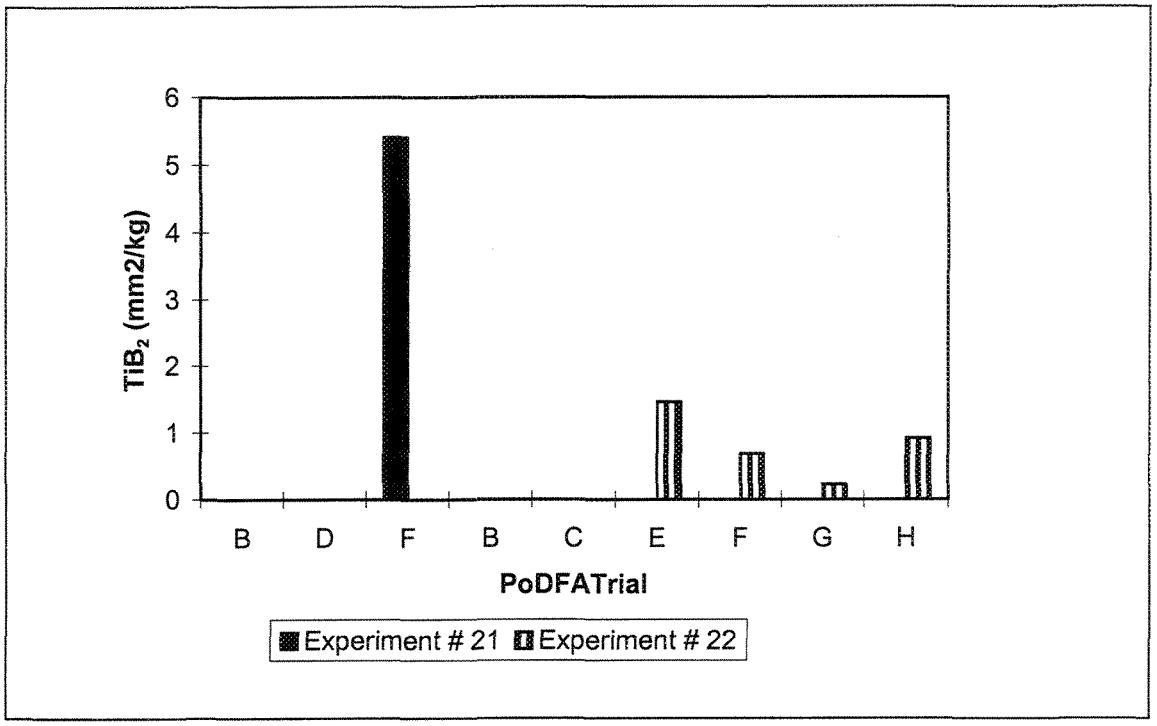

Figure 37 Experimental conditions that maximize the concentration of TiB_2 inclusions in A356.2 alloy.

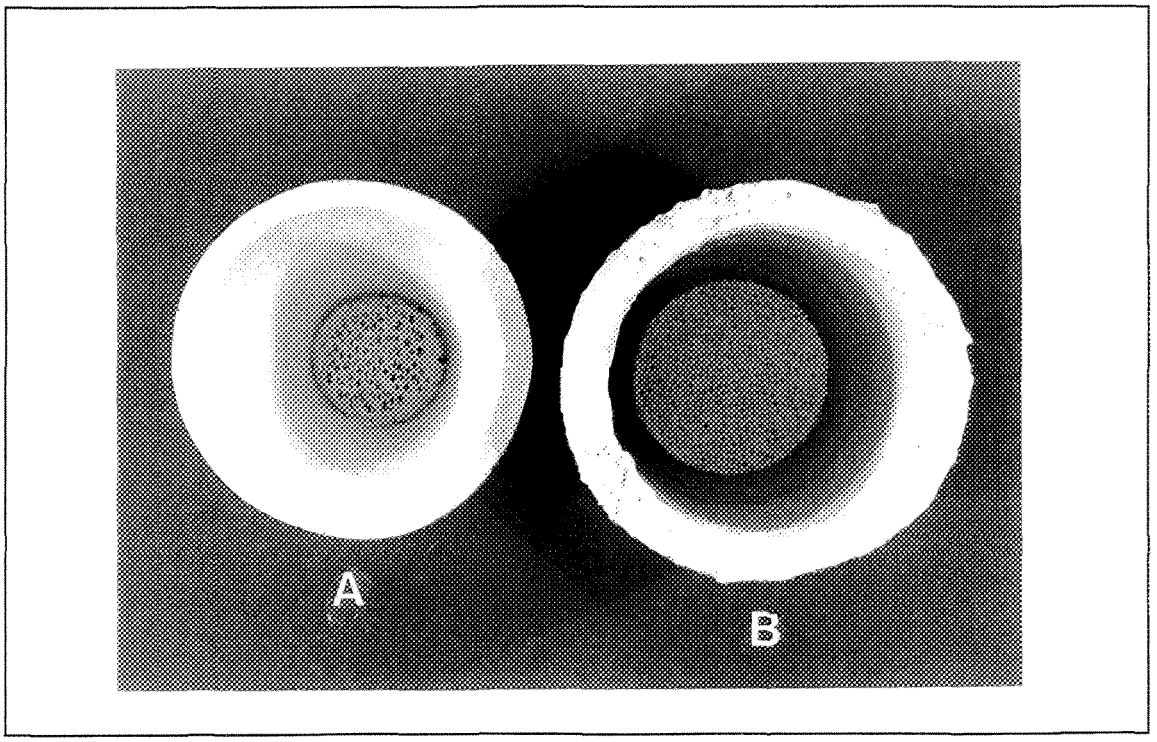

Figure 38 Pouring cups mounted with: a) 10 ppi, b) 20 ppi ceramic foam filters.

A comparison of the effects of Sr and TiB_2 addition on the PoDFA filtration behavior is exhibited in Figure 39. As can be seen, Sr addition has a marginal or almost no effect on the weight of filtered metal (i.e., 1.5 kg), compared to that obtained from the unmodified alloy. In contrast, the addition of TiB_2 produces a remarkable reduction in the weight of filtered metal, by almost 80%. Figure 40 shows clearly the masses of filtered metal obtained in the two cases.

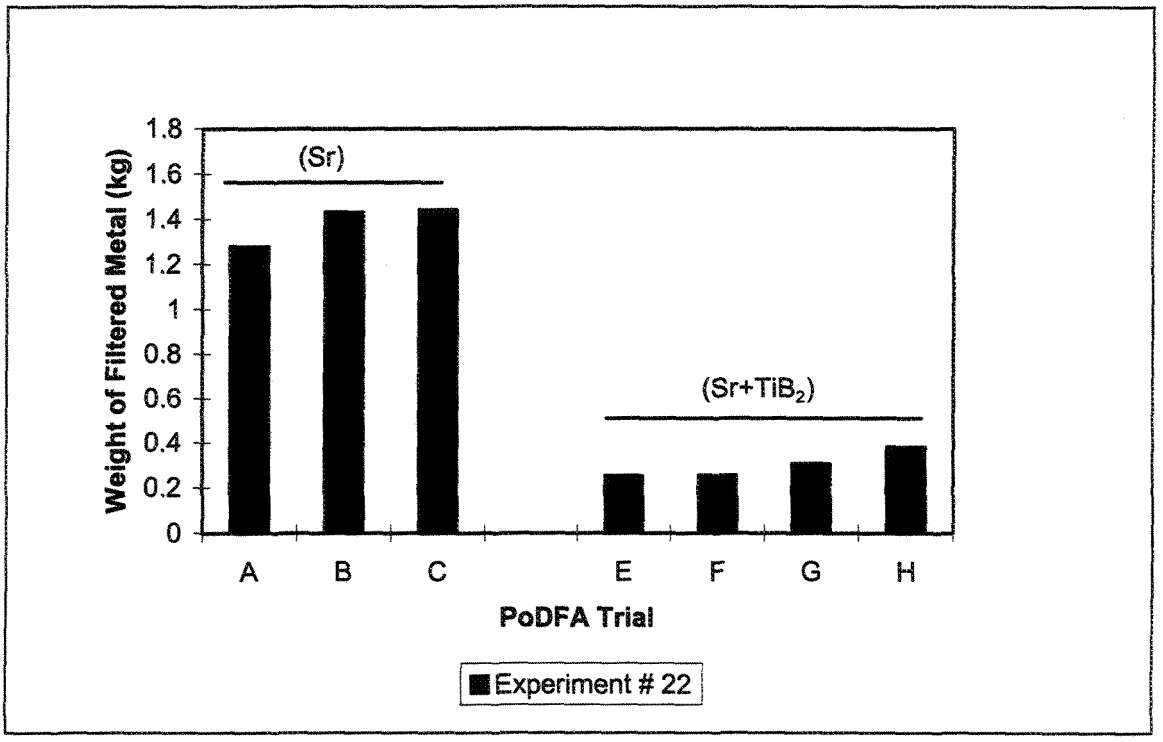

Figure 39 Effect of Sr and TiB_2 additions on the weight of filtered metal.

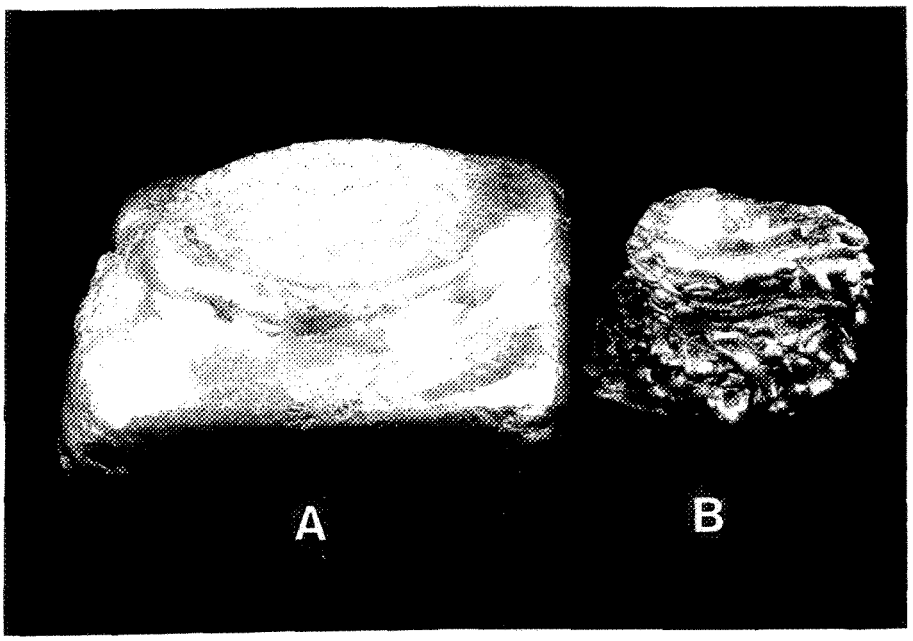

Figure 40 Effect of TiB_2 additions on the weight of filtered metal obtained in: a) Experiment 22A, b) Experiment 22E. Compare the droplet-like surface in 22E with the smooth surface in 22A.

Another interesting parameter to be considered in relation to these additions is the lengthy time needed to collect such a small amount (300 g) of filtered metal, as displayed in Figure 41(a). Figure 41(b) shows the relationship between the concentrations of SrO and TiB_2 and the filtration time. It is evident that the occurrence of a high density of fine TiB_2 particles would seal the pores of the PoDFA filters (as observed in Figure 25), leading to the results shown in Figures 37 through 40.

Figure 41(c) shows the effect of grain refining agent type viz., Al_3Ti or TiB_2 on the weight of filtered metal obtained (Experiment 29). Evidently, the presence of boron is very effective in increasing the number of TiB_2 particles that act as sites for grain nucleation as

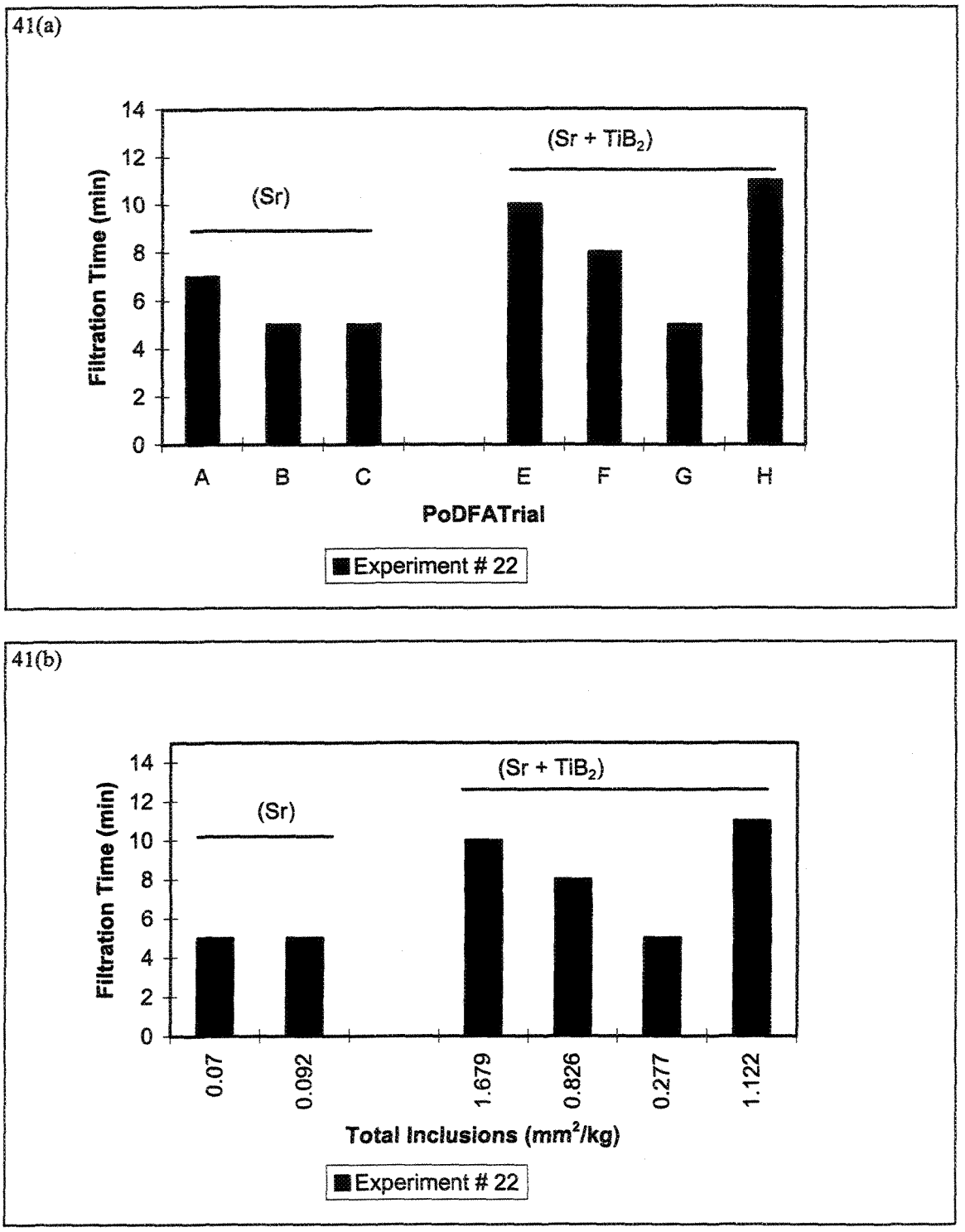

Figure 41 Effect of TiB_2 additions on: a) filtration time, b) total inclusions, c) weight of filtered metal.

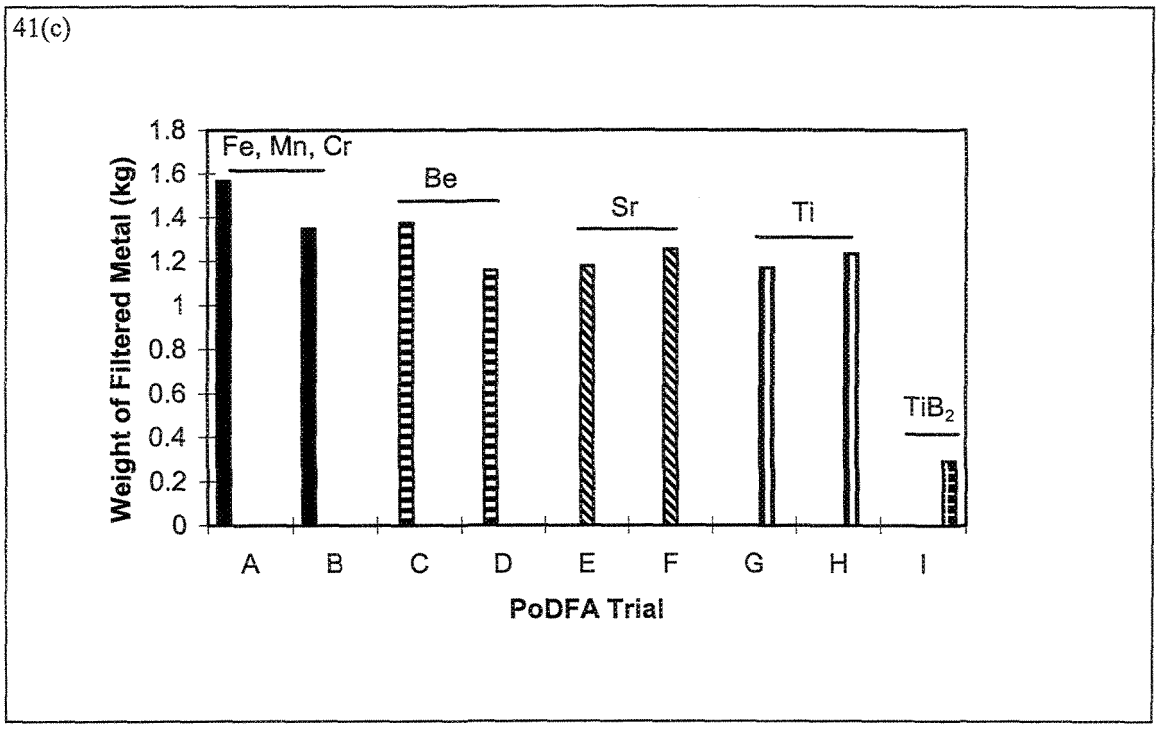

Figure 41 Effect of TiB_2 additions on : c) weight of filtered metal (Experiment 29).

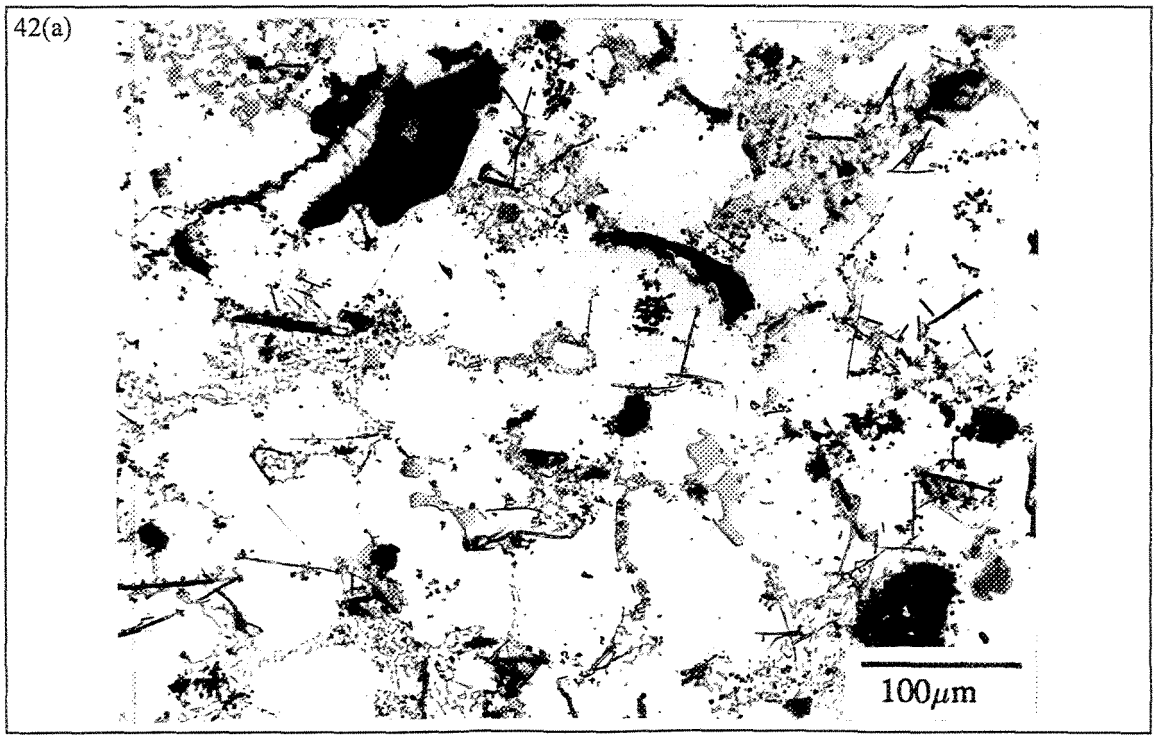

Figure 42 Effect of grain refining agent type on the number of inclusion particles: a) Al_3Ti, b) TiB_2.

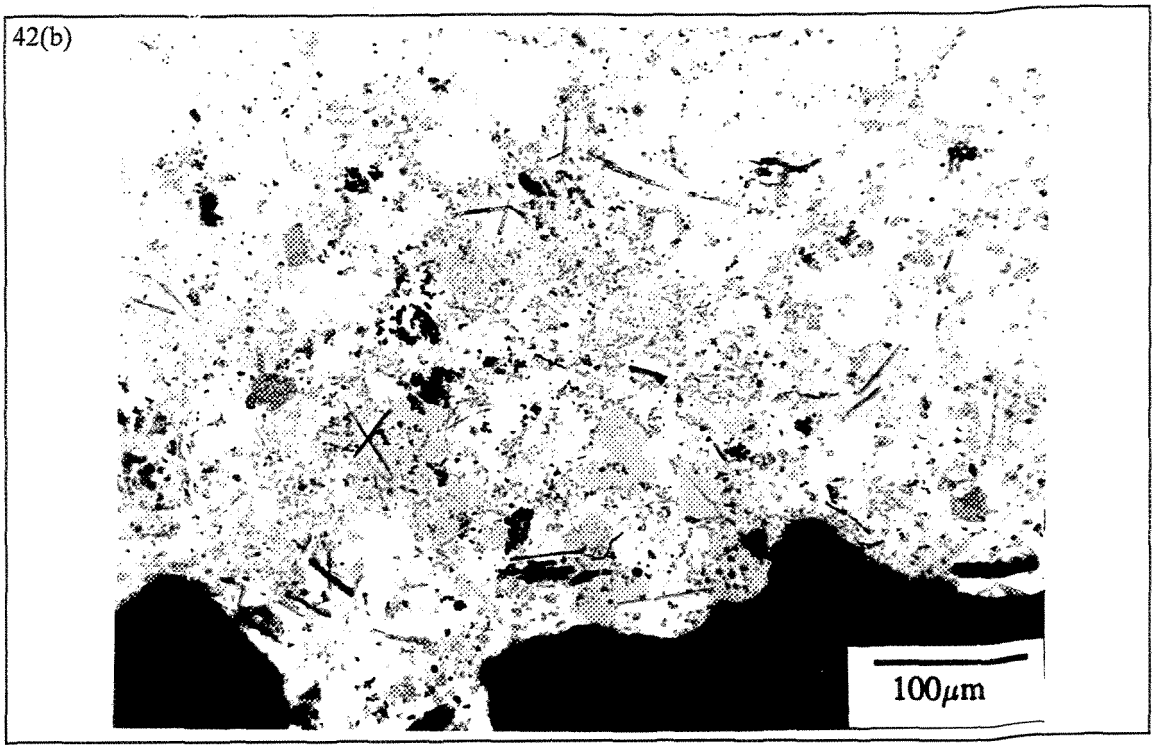

Figure 42 Effect of grain refining agent type on the number of inclusion particles: a) Al_3Ti, b) TiB_2.

exemplified in the microstructure of Figure 42, where the TiB_2 particles are observed abundantly over the entire sample surface.

The main inclusion type that occurs when the alloy is modified with Sr is SrO. The variation in SrO particle concentration depends on the total amount of Sr added to the molten alloy. In the present study, the Sr content prior to executing the PoDFA trials was in the range of 250-300 ppm. Figure 43 reveals the tendency of the SrO particles to precipitate towards the bottom of the crucible. When TiB_2 is added to the Sr-modified melt, the SrO particles show a more pronounced tendency to settle down, along with the TiB_2 particles.

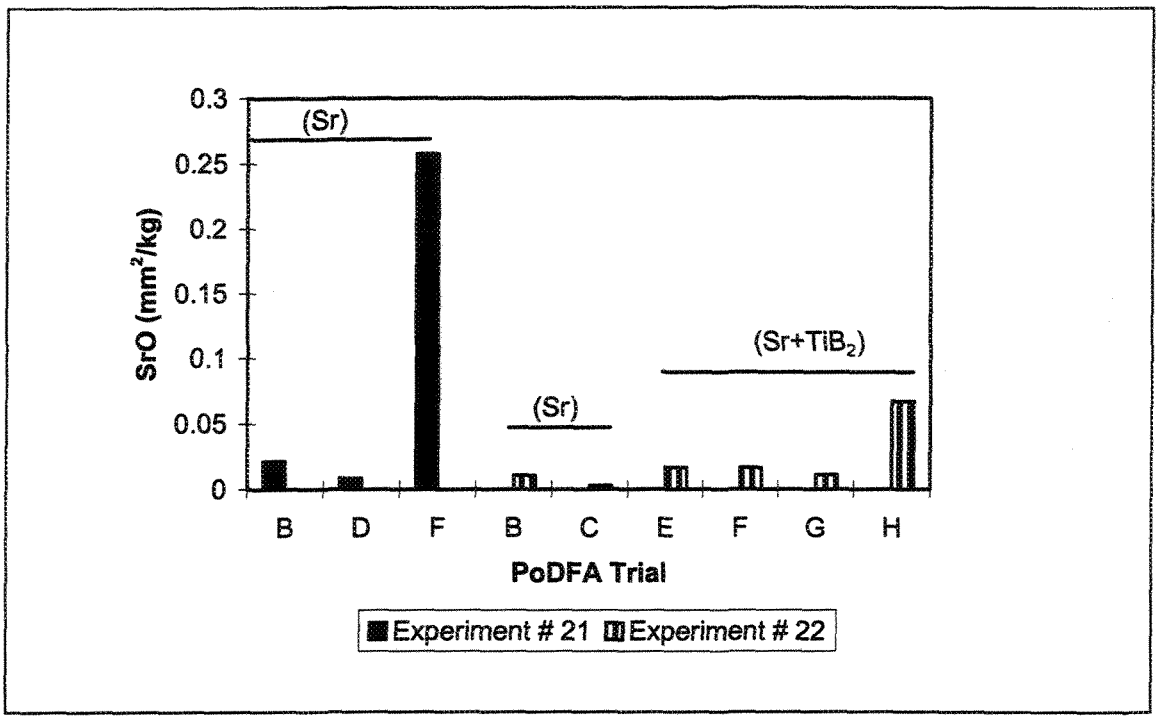

Figure 43 Experimental conditions that maximize the concentration of SrO inclusions in A356.2 alloy (Experiment 22H- degassing applied).

CHAPTER 4

INCLUSION ANALYSIS

CHAPTER 4

INCLUSION ANALYSIS

4.1 INTRODUCTION

It is well established that a large variety of inclusions are present in small quantities in commercial aluminum and aluminum alloys [4, 59, 60, 61]. The results of Simensen and Berg [4] show that commercial aluminum contains mainly the following types of inclusions: 6 to 12 ppm oxides, 3 to 12 ppm nitrides (AlN), 2 to 12 ppm carbides (Al_4C_3), and less than 1 ppm of cryolites and borides. Grain refined material contains normally 10 to 100 ppm TiB_2 and VB_2. Intermetallic phases like Al_3Zr, AlB_2, and Al_3Ti are formed in highly alloyed melts. Simensen and Hartvedt [48] could analyze the inclusions in Al-Fe-Si and Al-Mg commercial ingots with the use of 50 μm pore size filters. These ingots contained 0.1 to 2.2 ppm oxides (thin films and clusters of oxide particles of Al_2O_3, Al_2MgO_4 and MgO).

The work of Apelian and Mutharasan [62] shows that the production of quality castings necessitates that inclusion contents are of the order of several volume parts per billion and that the particle size of the population is less than 50 μm. Techniques such as sedimentation, floatation and filtration may be used to minimize the incidence of inclusions

in the casting. Gravity sedimentation may be effective for inclusions larger than 90 μm. Floatation, i.e., degassing with inert or active gas using rotating impellers, may be effective up to about 30-40 μm, whereas filtration using ceramic foam filters is generally used to remove inclusions less than 30 μm. The use of open pore ceramic foam filters would result in improved cleanliness and scrap reduction, increased yield and energy savings, reduced machining allowances, improved properties and greater assurance of quality [63, 64, 65].

The process dynamics of liquid metal filtration using reticulate ceramic filters has been analyzed by Tian [66], and Tian and Guthrie [67, 68], where the distribution of particles captured within a filter, its evolution both as a function of filtration time and melt cleanliness, together with its consequent effects on filtration efficiency and pressure drop has been simulated.

Higher aluminum quality can be expected if furnace treatment is optimized since in-line treatment units essentially remove impurities in a proportional manner. The most widely accepted methods used for furnace fluxing consist of injecting a gaseous mixture of nitrogen and chlorine (N_2/Cl_2) through stationary lances [69]. Celik and Doutre [70] showed that the volume of chlorine gas in excess of stoichiometric requirements is responsible for acid gas emissions (HCl, Cl_2). The total gas flow during fluxing controls particle/inclusion emission. Two approaches can be selected to reduce emissions associated with fluxing: abatement of emissions after they have been generated or reduction at the process source. The use of chlorine gas furnaces is mostly banned due to environmental problems, and the replacement of chlorine gas by more environmental-friendly fluxes is thus foreseeable in the near future [71].

Recently, it has been suggested that chlorine-free gas mixtures composed of sulphur hexafluoride (SF_6) and an inert carrier gas can be employed for both in-line and furnace fluxing [72, 73]. Emission levels measured during furnace fluxing with SF_6/N_2 mixtures were very low compared to those measured during furnace fluxing using Cl_2/N_2 mixtures. Severe oxidation which commonly occurs at the liquid metal surface of high magnesium alloys can be effectively inhibited by use of a cover gas composed of SF_6 and N_2.

Martin and Painchaud [12] reported on the techniques required for monitoring and minimizing the presence of non-metallic inclusions of the order of parts per billion (ppb). Such low concentrations are not accessible by direct chemical analysis methods. These techniques, based on a pre-concentration/filtration step, followed by metallographic analysis, have been variously developed as Alcan's PoDFA [17] and the Union Carbide's LAIS [74]. Obtaining results of inclusion testing by these methods, however, is time-consuming, and by the time the results are received, the metal produced may have already left the cast house.

In Chapter 3 of the present study, we reported on the effect of foundry parameters and minor alloying element additions on inclusion formation in A356.2 and C357 alloys, measured by the PoDFA technique. The obtained data were analyzed in detail and are reported in this Chapter, which complements the inclusion measurements described in Chapter 3.

4.2 RESULTS AND DISCUSSION

4.2.1 Dross Formation

Dross, the oxide layer that covers the surface of molten metal, was carefully skimmed without folding, and weighed in all of the experiments. Table 25 lists the dross weights obtained in a number of these experiments. As can be seen, the weight of dross varies from ~60-75 g after melting either a fresh or scrap charge of A356.2 alloy, to ~500 g after degassing for a short period of time (45 min). Prolonged holding times of liquid metal at temperatures of the order of 730-740 C, also have a very significant effect on increasing the weight of the dross formed i.e., from ~80 g to ~525 g. This observation is independent of alloy type, i. e., A356.2 or C357.

The surfaces of dross fragments thus obtained were examined macroscopically. Figure 44(a) shows the air-exposed surface of dross taken from an A356.2 alloy melt (Experiment 20A) that was held for 72 h at 735 C. It is seen that the surface is noticeably rough compared to the freshly formed dross (Experiment 18A) taken immediately after melting. Examination of the opposite surface of the dross sample obtained from Experiment 20A (Figure 44(b)) revealed a thick layer of aluminum that was removed with the dross, i.e., wet dross.

Increasing the Mg content (i.e., C357 alloy) does not change the melting behaviour of Al-Si-Mg alloys, as exhibited in Figure 45(a). Some black spots are, however, seen on the air-exposed surface of the dross. These spots are believed to be spinel, $MgAl_2O_4$. Holding the liquid metal for periods as long as 72 h resulted in the formation of "ashy-

layers" of what looked like burnt metal. These layers were very fragile and easy to break (Figure 45(b), corresponding to Experiment 25A). As in the case of A356.2 alloy, a fairly thick layer of molten alloy was observed, adhered to the dross (Figure 45(c)).

Table 25 Weight of dross

Experiment #	Alloy	Weight of Dross (g)
12	A356.2 - Scrap	242
13	A356.2 - Scrap	322
14	A356.2 - Fresh	480
15	A356.2 - Fresh	522
16	A356.2 - Scrap	59
17	A356.2 - Scrap	288
18	A356.2 - Fresh	74
19	A356.2 - Fresh	466
20A	A356.2 - Fresh	187
20B	A356.2 - Fresh	177
21A	A356.2 - Fresh	299
21B	A356.2 - Fresh	143
22A	A356.2 - Fresh	221
22B	A356.2 - Fresh	116
24	C357 - Fresh	84
25A	C357 - Fresh	522
25B	C357 - Fresh	73
25C	C357 - Fresh	65
26A	C357 - Fresh	428

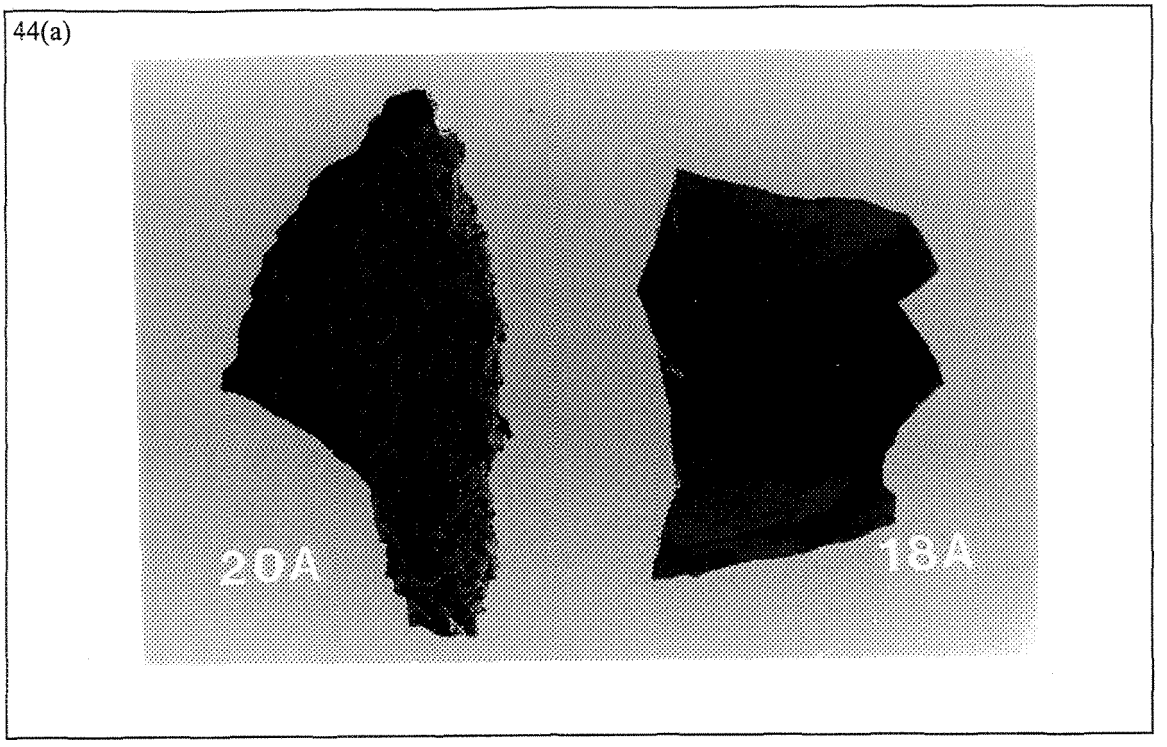

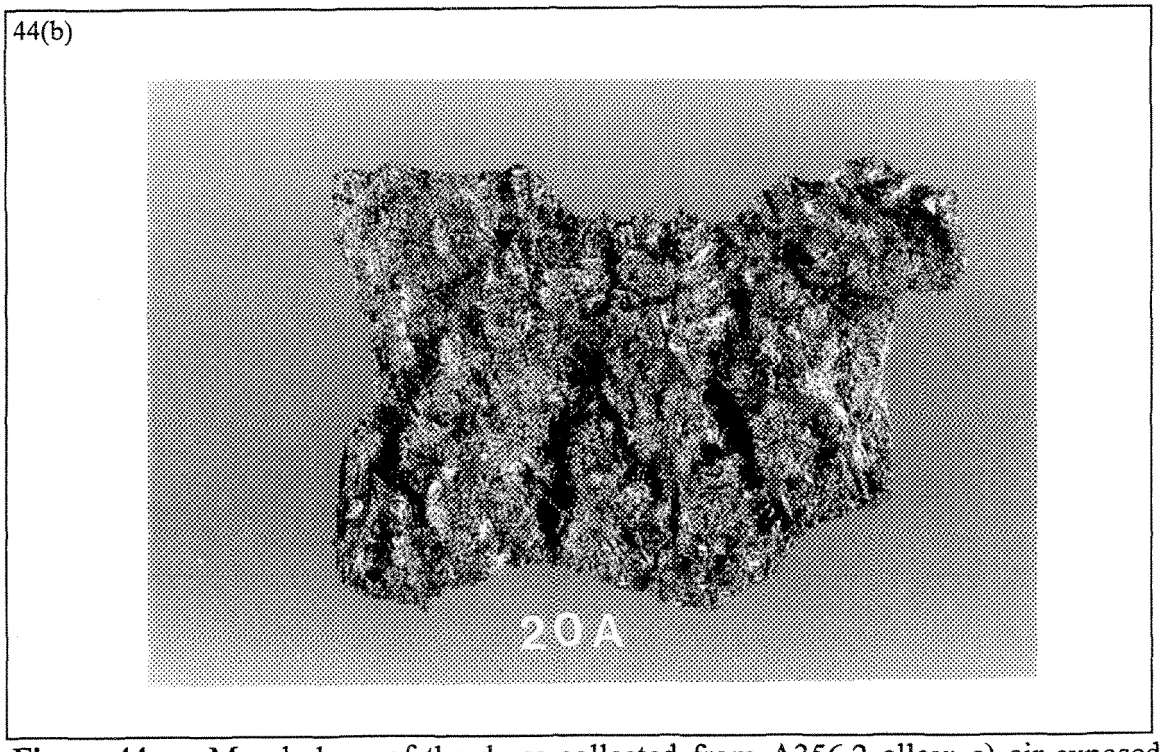

Figure 44 Morphology of the dross collected from A356.2 alloy: a) air-exposed surface, b) melt-exposed surface. Note the roughness of the surface when holding time is increased to 72 h.

45(a)

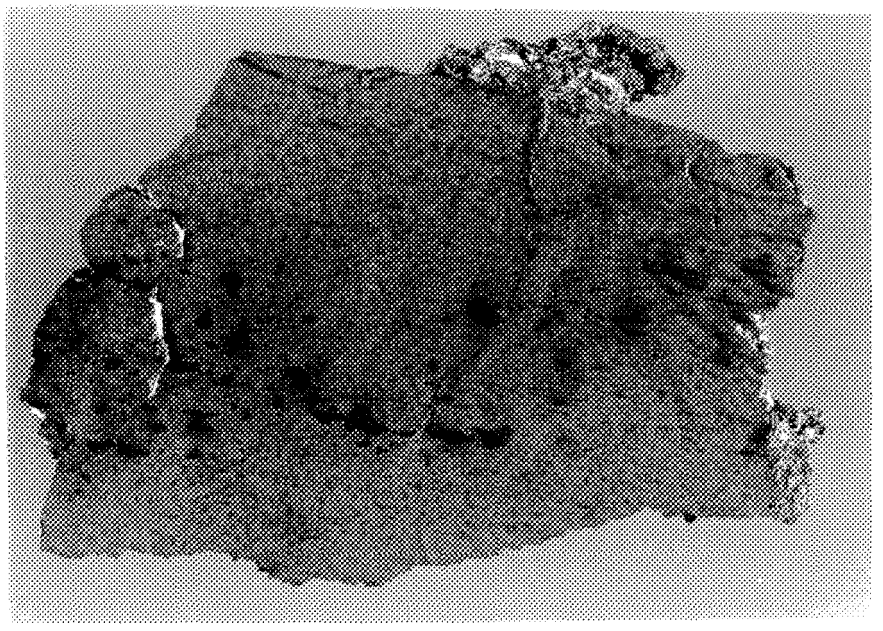

45(b)

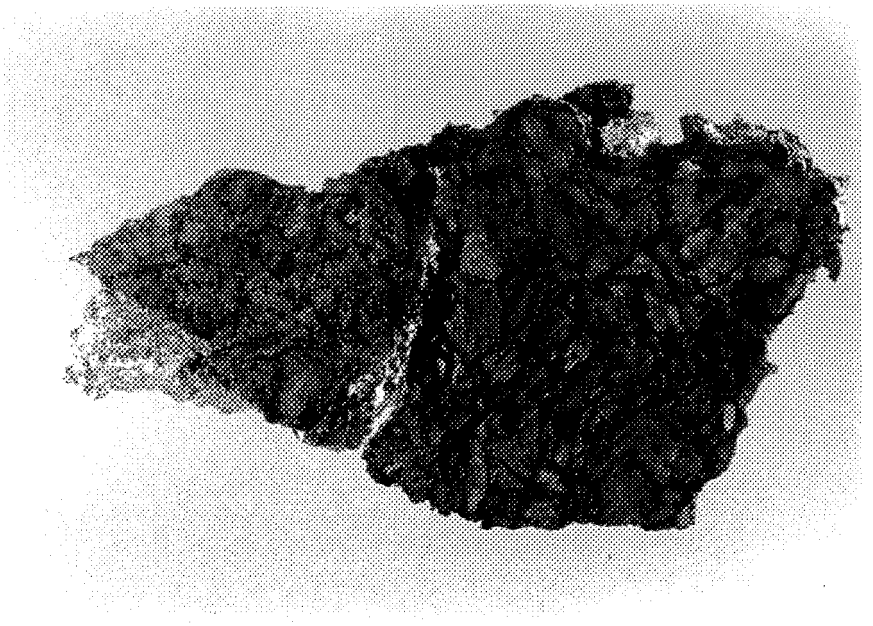

Figure 45 Morphology of the dross collected from C357 alloy: a) Experiment 24A - air-exposed surface, b) Experiment 25A - air-exposed surface, c) Experiment 25A - melt-exposed surface.

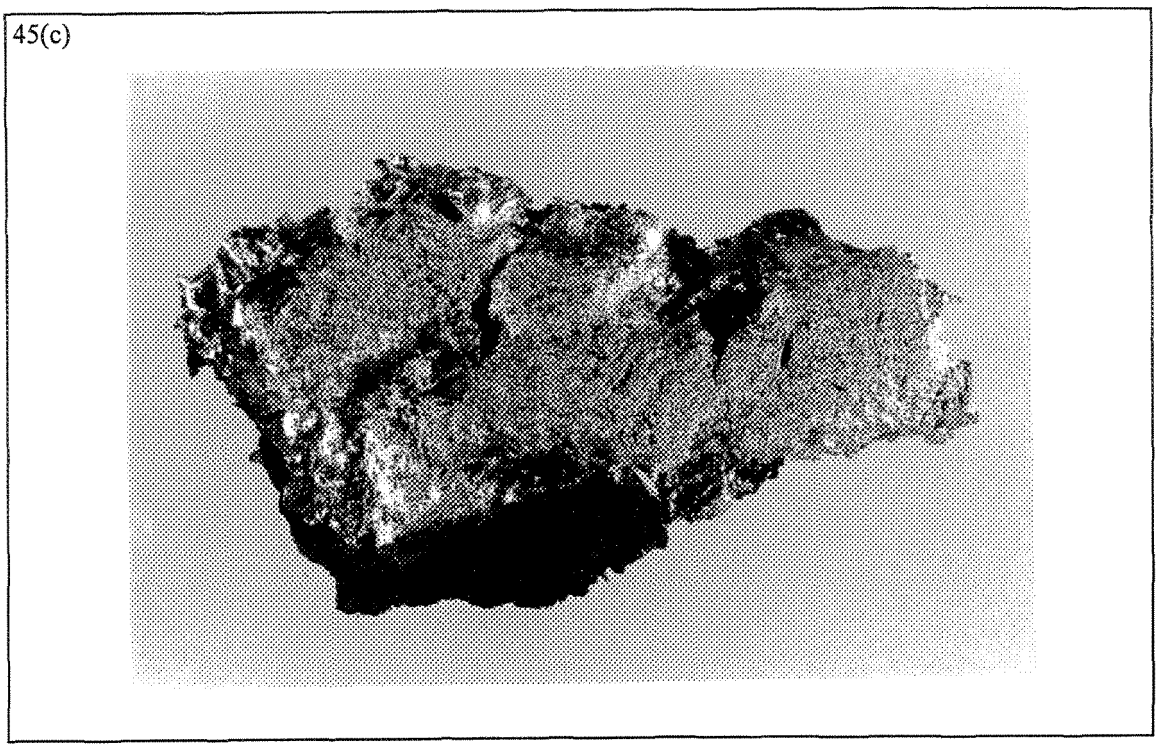

Figure 45 Morphology of the dross collected from C357 alloy: a) Experiment 24A - air-exposed surface, b) Experiment 25A - air-exposed surface, c) Experiment 25A - melt-exposed surface.

The same pieces of dross were examined in a scanning electron microscope (SEM) equipped with an energy dispersive X-ray (EDX) system. In each case, about six areas (each 400μm × 600μm) were analyzed. Figure 46(a) is an SEM micrograph obtained from the dross sample, shown in Figure 44, taken from the air-exposed surface of the melt (Experiment 18, A356.2 alloy). It is observed that the surface is not truly smooth, as appears in Figure 44(a). In fact, a large number of oxide/inclusion particles appearing to grow in a columnar fashion can be seen.

The corresponding EDX spectrum is given in Fig. 47(a), and comprises strong reflections of Al, Si, Mg and O elements. It is interesting to note the presence of a carbon

reflection also. The average elemental analysis obtained over the six areas tested for each dross sample is reported in Table 26.

Figure 46(b) shows that increasing the holding time of molten metal to 72 h (Experiment 20 - air-exposed surface) resulted in a granular surface, similar in nature to that presented in Figure 44(a). The EDX spectrum obtained from this sample is displayed in Figure 47(b), and reveals lines similar to those obtained in Figure 47(a) for Experiment 18. The difference between the two experiments lies in the amount of dross collected (Table 25). Figure 46(c) exhibits the microstructure of the other side of the dross, (i.e., the surface that was in contact with the molten metal), showing several dendrites. The corresponding EDX spectrum, Figure 47(c), shows very low concentrations of Mg and O (0.46% and 0.23%, respectively - see Table 26) compared to those obtained from the air-exposed surface (20.25% and 4.48%, respectively). It can thus be concluded that the air-exposed surface contains a large proportion of Al_2O_3, MgO, $MgAl_2O_4$, as well as Al_4C_3, whereas the melt-exposed surface is made up of mainly Al-7% Si-0.35% Mg base alloy.

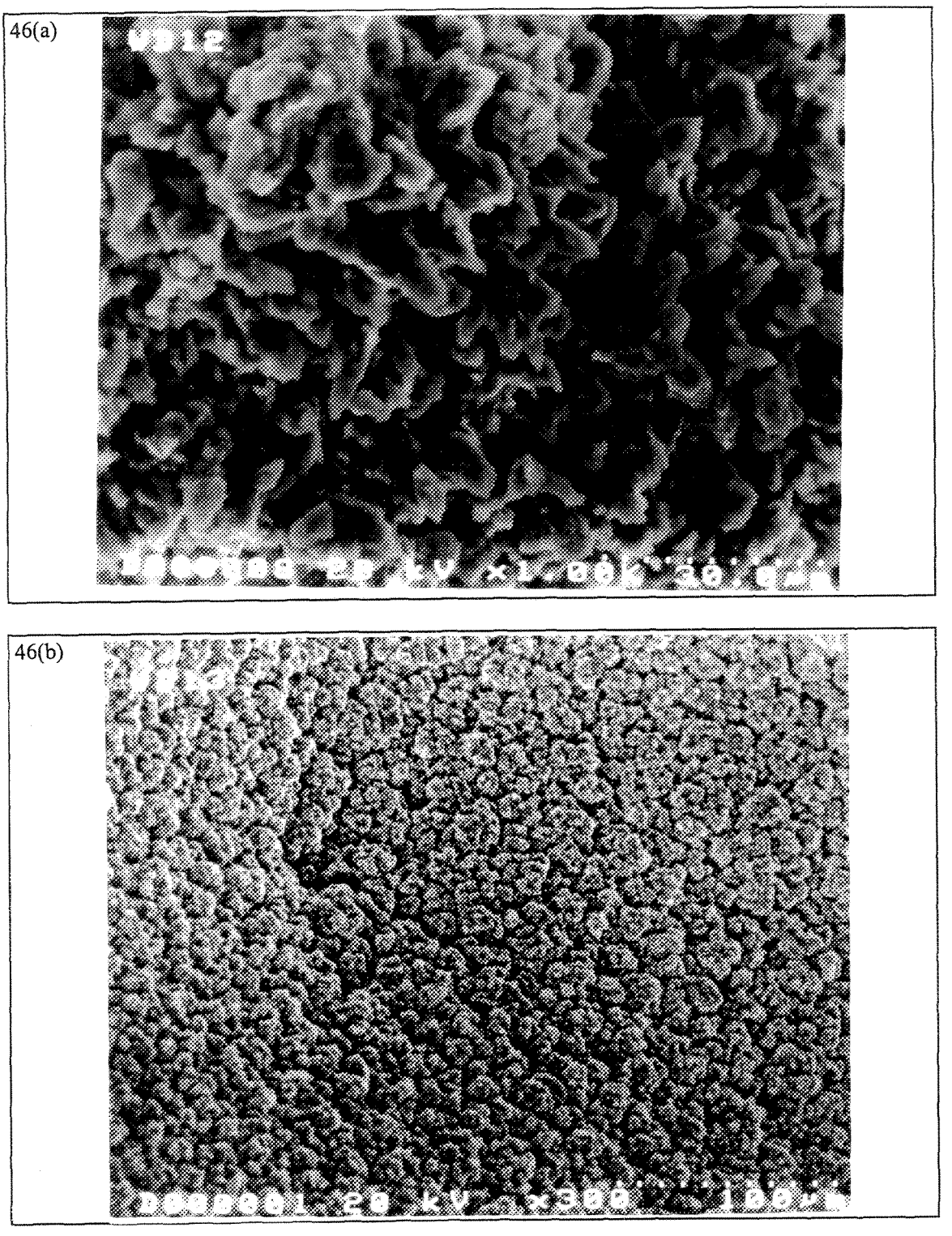

Figure 46 SEM micrographs of dross specimens collected from A356.2 alloy: a) Experiment 18A - air-exposed surface, b) Experiment 20A - air-exposed surface, c) Experiment 20A - melt-exposed surface.

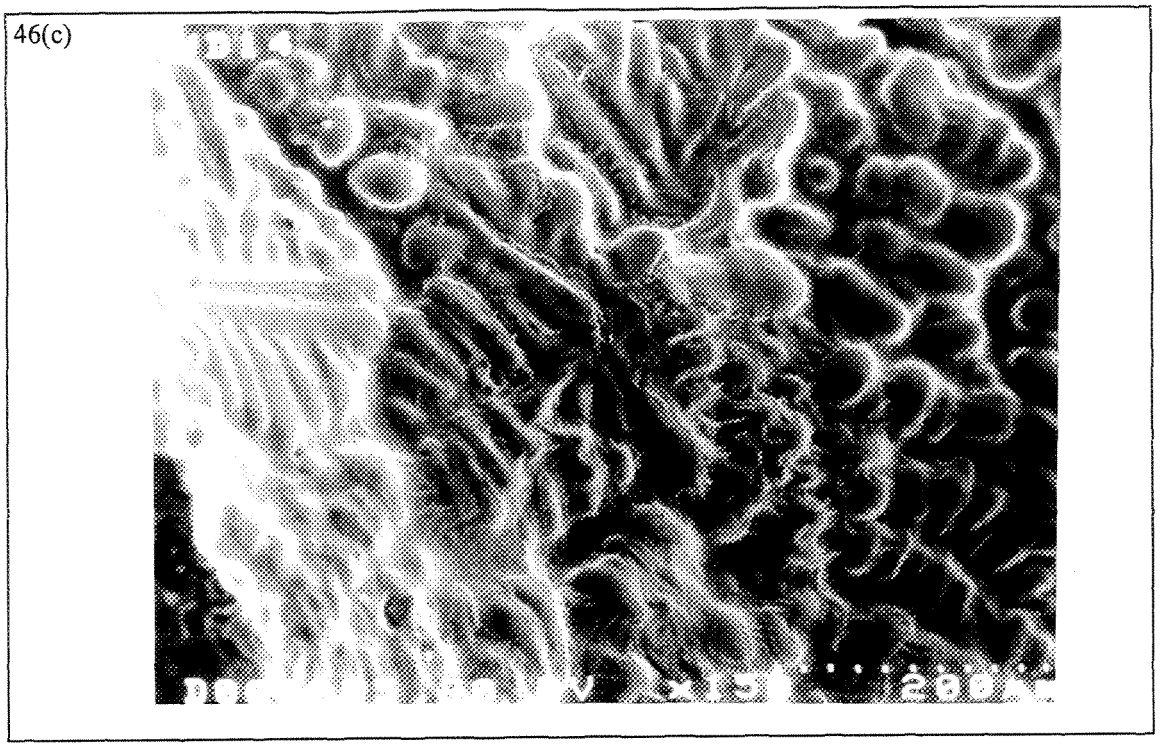

Figure 46 SEM micrographs of dross specimens collected from A356.2 alloy: a) Experiment 18A - air-exposed surface, b) Experiment 20A - air-exposed surface, c) Experiment 20A - melt-exposed surface.

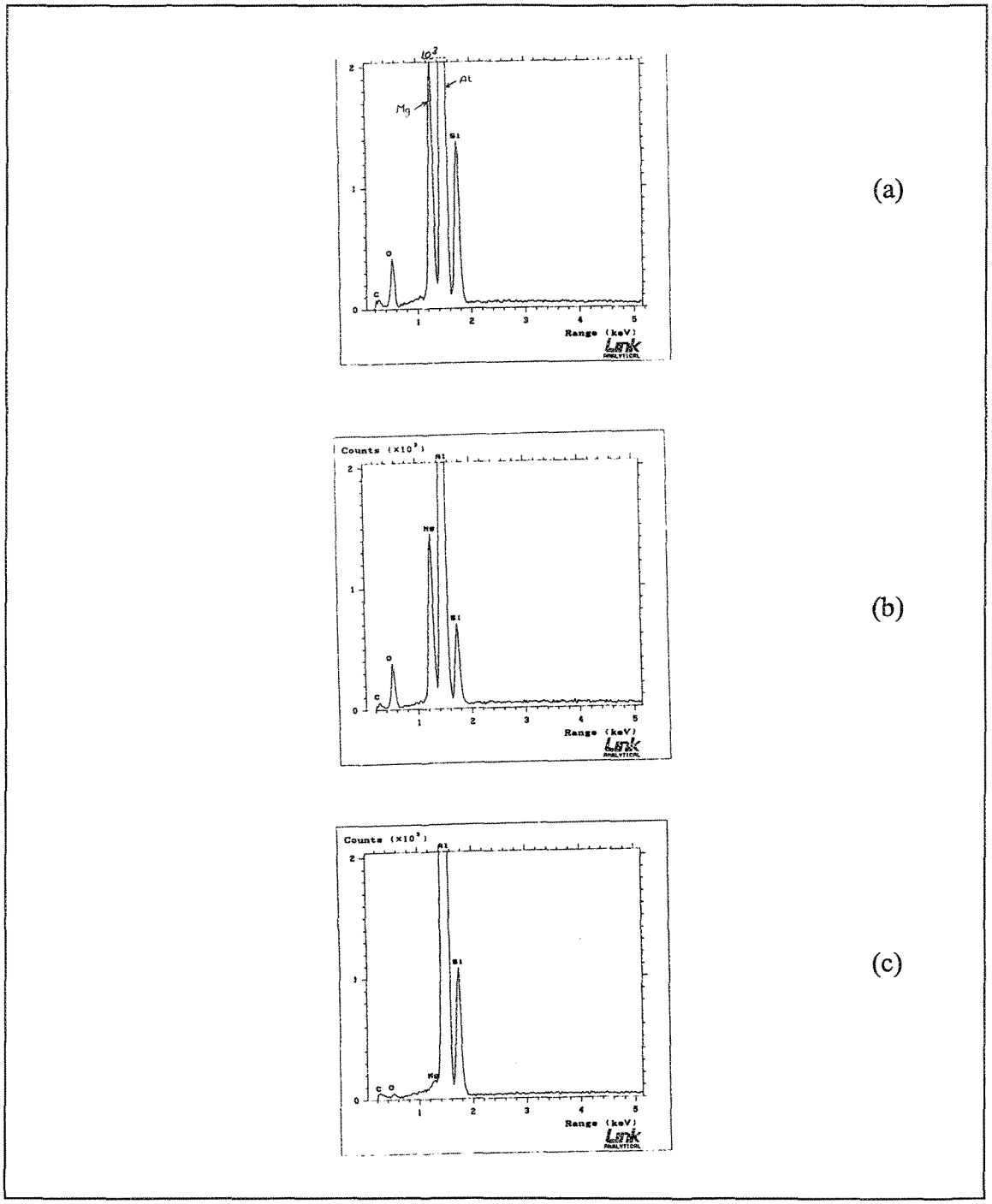

Figure 47 DX spectrums corresponding to the dross specimens of A356.2 alloys shown in Figure 46: a) Experiment 18A - air-exposed surface, b) Experiment 20A - air-exposed surface, c) Experiment 20A - melt-exposed surface.

Table 26 EDX analysis (at %) of dross samples obtained from various alloy melts.

Alloy	Experiment #	Surface Examined	Settling Time (hr)	C (at%)	O (at%)	Mg (at%)	Al (at%)	Si (at%)
A356.2	18	Air-Exposed	0	0.64	3.87	22.17	64.3	9.03
A356.2	18	Melt-Exposed	0	0.11	4.89	1.5	73.01	20.49
A356.2	20	Air-Exposed	72	0.75	4.48	20.25	68.39	6.13
A356.2	20	Melt-Exposed	72	0.15	0.23	0.46	92.77	6.4
C357	24	Air-Exposed	0	0.62	36.56	8.06	51.22	3.54
C357	24	Melt-Exposed	0	0.08	0.22	0.61	91.56	7.58
C357	25A	Air-Exposed	72	0.2	15.98	35.07	47.46	1.29
C357	25B	Air-Exposed	72	0.15	7.16	24.25	64.11	4.34
C357	25C	Air-Exposed	72	0.14	5.2	12.03	76.35	6.53

Note: Window Size: 400μm × 600μm

Average elemental analysis taken over the six areas examined in each case.

Figure 48(a) shows the roughness of the air-exposed surface of dross collected from Experiment 24A (C357 alloy). It is clear from the corresponding EDX spectrum, Figure 49(a), that the concentration of oxygen in this sample is higher than the magnesium concentration (see Table 26). This observation may indicate the progress of spinel formation. Prolonged holding periods of the molten metal, i.e., 72 h (Experiment 25A) resulted in vigorous reactions that appeared in the form of large foam bubbles, Figure 48(b). The corresponding EDX spectrum is shown in Figure 49(b), where strong oxygen, magnesium, and aluminum reflections can be seen. The reflection from silicon is relatively negligible. Another morphology of spinel phase particles is displayed in Figure 48(c). In this case the spinel occurred in the form of a bundle of sticks covered with fine particles. The associated EDX spectrum, Figure 49(c), did not reveal any special features apart from those reported earlier, while the EDX spectrum produced from the melt-exposed surface displayed reflections corresponding to the base alloy, Figure 49(d).

The morphology of freshly formed spinel (i.e., immediately after skimming) is shown in Figure 48(d), when the remaining melt was degassed with inert gas for about 45 min. The spinel seems to form some sort of a cellular structure in this case, with fine particles decorating the cell boundaries. It is of interest to observe the noticeable increase in the intensity of the silicon reflection from the associated EDX spectrum, Figure 49(e), indicating the ability of the X-ray beams to penetrate the entire oxide layer and reach the molten metal layer underneath. In other words, the oxide layer is relatively thin compared to that obtained from Experiment 25A (see Table 25). The concentration of silicon is seen

to increase progressively in Table 26, resulting from a continuing decrease in the thickness of the oxide layer.

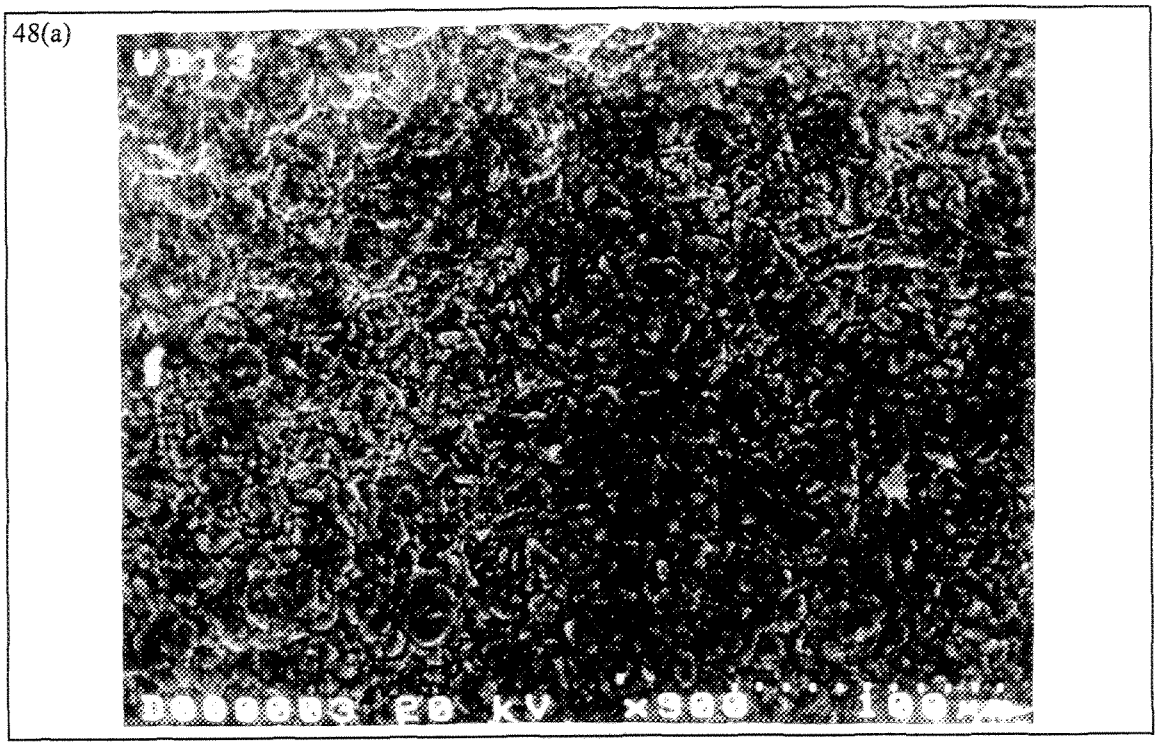

Figure 48 SEM micrographs of dross collected from C357 alloys: a) Experiment 24A - air-exposed surface, b) Experiment 25A - air-exposed surface, c) Experiment 25A - air-exposed surface, d) Experiment 25C - air-exposed surface.

48(b)

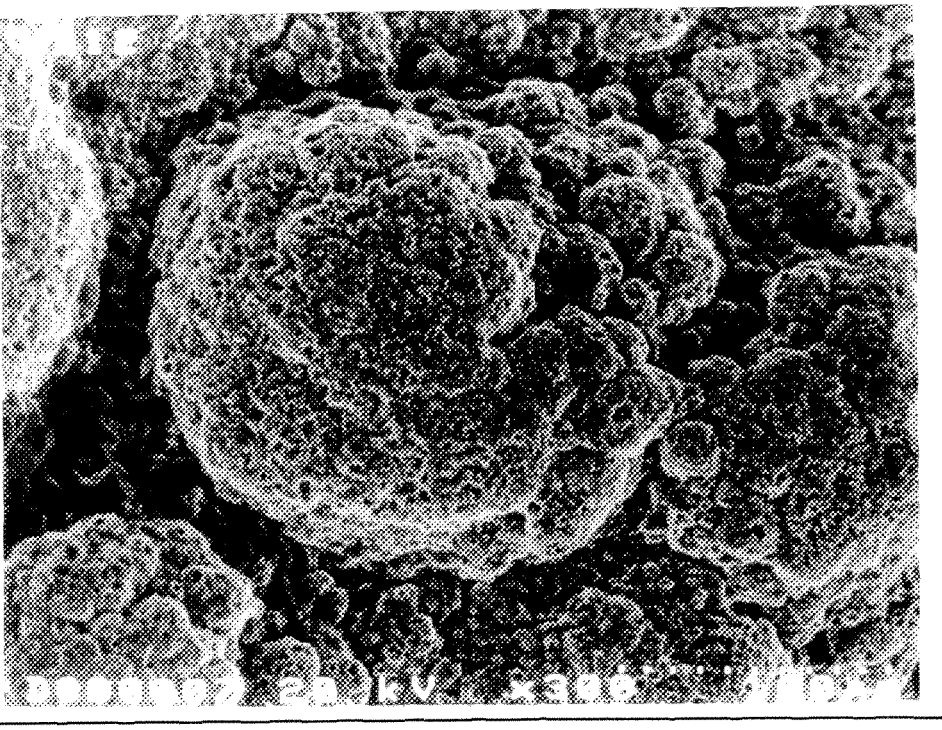

48(c)

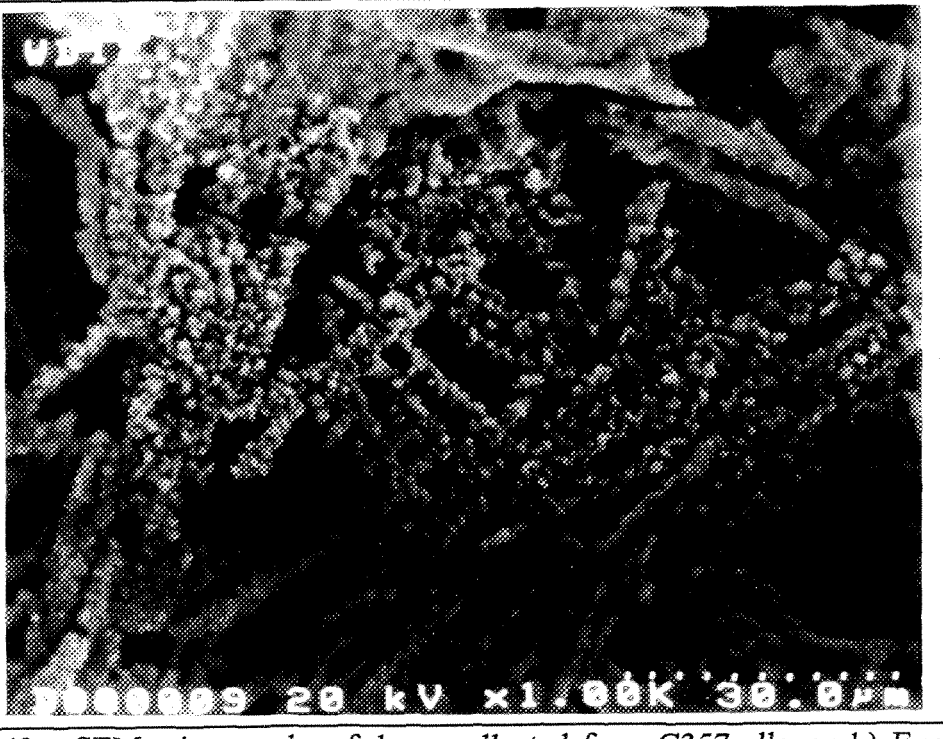

Figure 48 SEM micrographs of dross collected from C357 alloys : b) Experiment 25A - air-exposed surface, c) Experiment 25A - air-exposed surface,

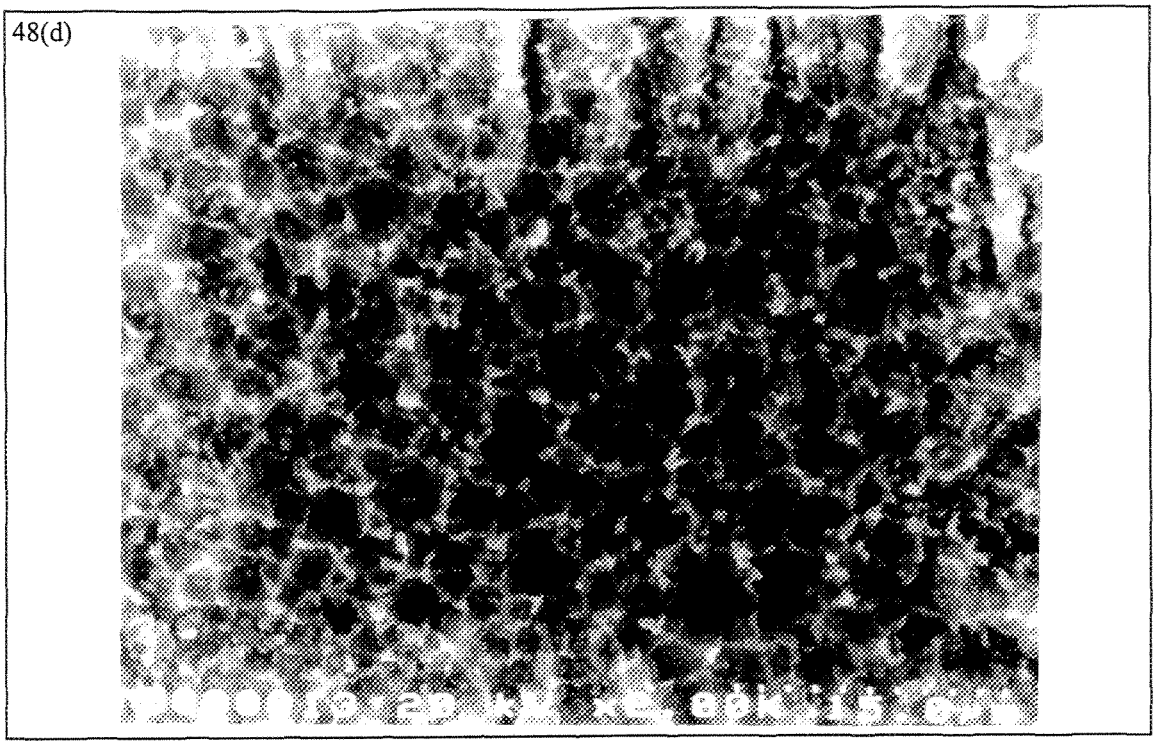

Figure 48 d) Experiment 25C - air-exposed surface.

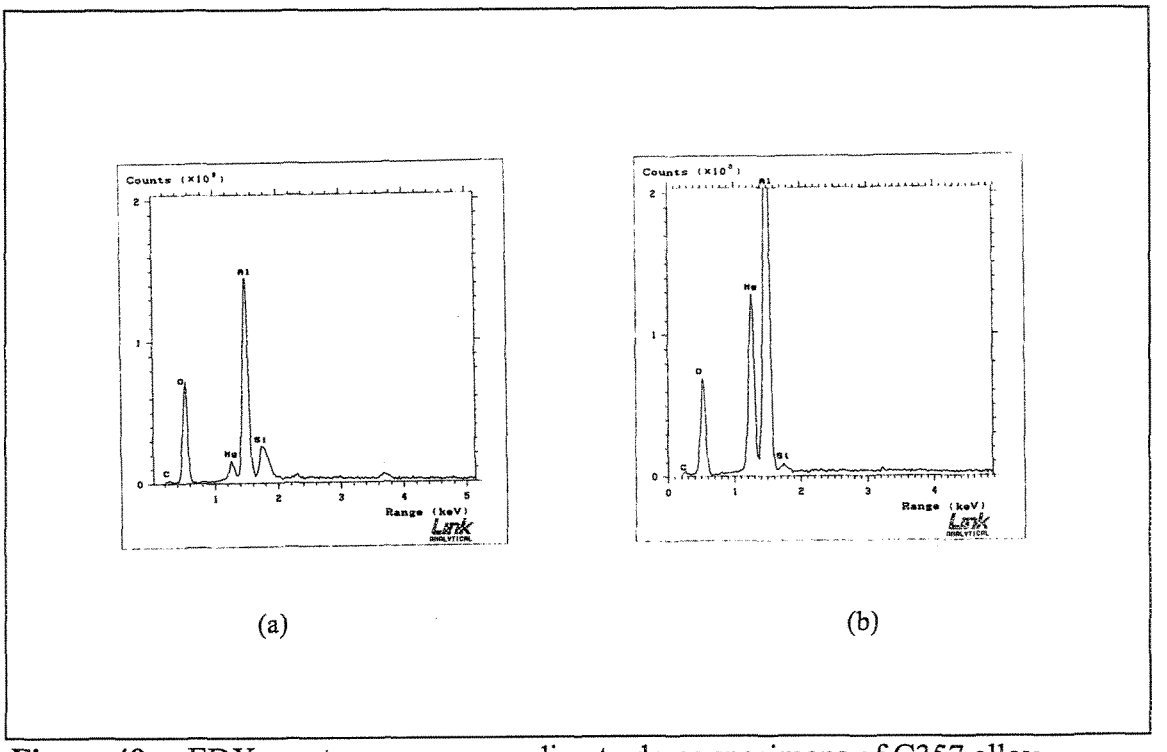

Figure 49 EDX spectrums corresponding to dross specimens of C357 alloy.

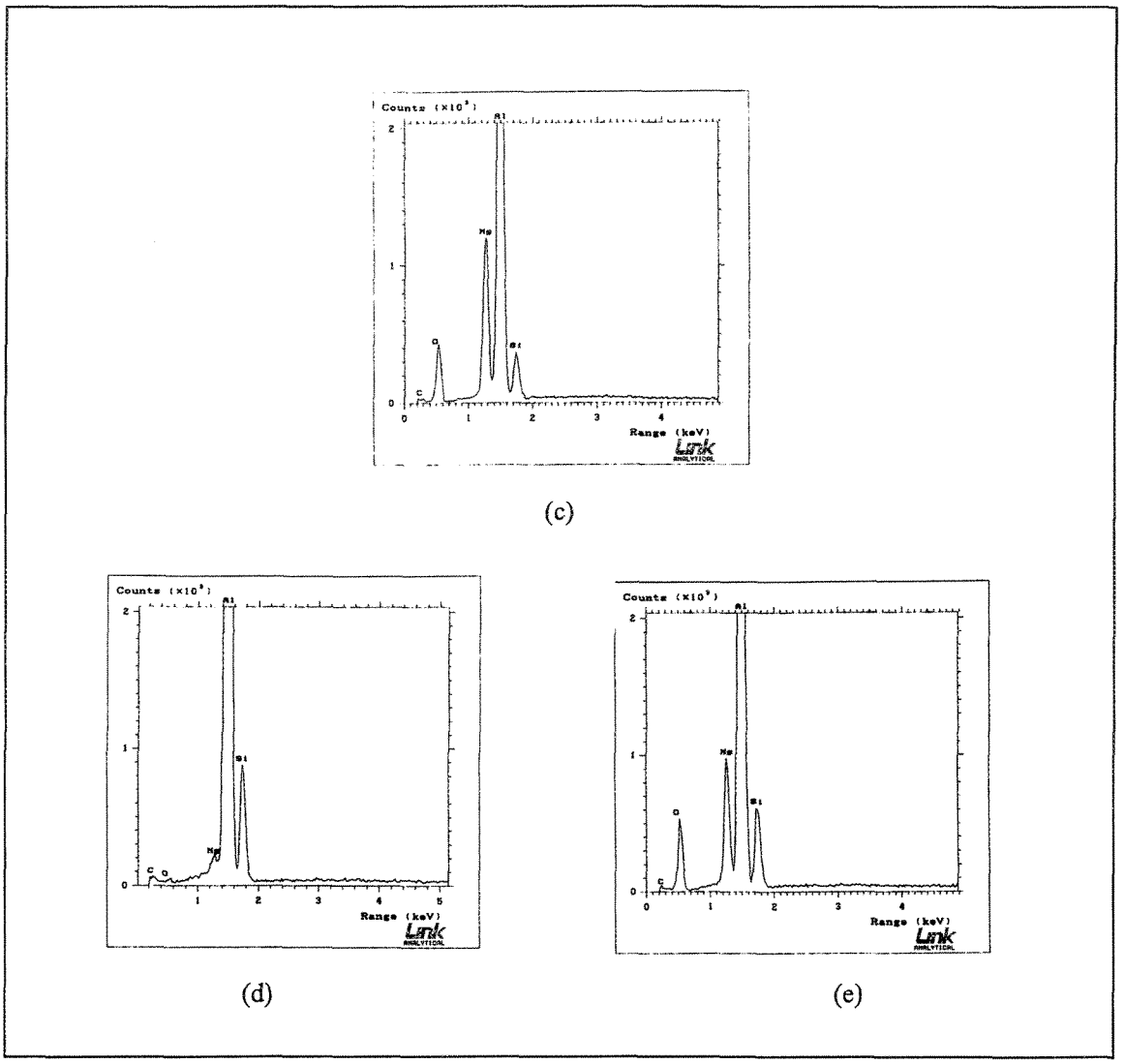

Figure 49 EDX spectrums corresponding to dross specimens of C357 alloy: a) Experiment 24A - air-exposed surface, b) Experiment 25A - air-exposed surface, c) Experiment 25A - air-exposed surface, d) Experiment 25A - melt-exposed surface, e) Experiment 25C - air-exposed surface.

4.2.2 Inclusion - Filtration Time Relationships

From the inclusion analysis of the various PoDFA samples examined in the present study, the inclusion concentrations were classified arbitrarily into five categories as listed in Table 27. The oxide film classification was done following Alcan's procedure, where the films were divided into seven classes, as shown in Table 28.

Table 27 Arbitrary codes used for inclusion classification.

Class	Inclusion Concentration (mm^2/kg)
Very Light - (1)	0 - 0.05
Light - (2)	0.5 - 0.1
Moderate - (3)	0.1 - 0.4
Heavy - (4)	0.4 - 1.2
Excessive - (5)	≥1.2

Table 28 Codes used for oxide film classification (Alcan's procedure).

Class	Oxide Film Type / Density
0	None
1	Thin / Slight
2	Thin / Moderate
3	Thin / Heavy
4	Thick / Slight
5	Thick / Moderate
6	Thick / Heavy

4.2.2.1 Cold Chamber

If the pressure chamber containing the PoDFA apparatus is not preheated before conducting the PoDFA experiments, the experiments are said to be run under cold chamber conditions.

As expected, under such conditons, the minimum time required to filter ~1.5 kg of molten metal is about 5 min [75]. The maximum inclusion concentration is of the order of 0.06 mm^2/kg, an amount considered very low to cause such an extended filtration time. It is evident that a cold chamber would result in shorter solidification times and lower fluidities, parameters for lengthy filtration periods.

From the total harmful inclusions (i.e., after subtracting fine Al_4C_3 ($\leq 3\mu m$), TiB_2, and potential chloride particles) a very low concentration of the order of 0.01 mm^2/kg could increase the filtration time to approximately 10 min. As could be seen from Tables 10-15 (Chapter 3), under these filtration conditions, oxide films of class (2), i.e., "thin/moderate" could cause considerable filtration delay.

According to the classification shown in Table 27, all inclusions are falling in the category "very light". Thus, solidification time plays a more influential role than inclusions in determining the filtration time. It should be noted, however, that the presence of very small quantities of TiB_2 (~ 0.007 - 0.01 mm^2/kg) could as well contribute to the long filtration times observed.

4.2.2.2 Hot Chamber

Here, before the PoDFA experiments are run, the pressure chamber of the PoDFA apparatus is preheated, to obtain hot chamber conditions.

4.2.2.2.1 Effect of foundry parameters

The variation in filtration time as a function of total inclusion content, when the pressure chamber was preheated using two empty PoDFA crucibles heated at 850°C, is displayed in Figure 50(a). When the inclusion concentration falls within the range classified as "very light" (Table 27), the filtration time is about 3 min. Increasing the total inclusion concentration to 0.1 mm^2/kg or more would obviously lead to filtration times varying between 5 and 10 min, depending on the concentration of harmful inclusions (Figure 50(b)), and, more importantly, on the type of oxide films (Figure 50(c)). Based on the data presented in Figure 50(c), it may be concluded that under appropriate filtration conditions, and for low concentrations of inclusions (around 0.1 mm^2/kg) or less), larger amounts of oxides (class 6 level) could be tolerated for a specified filtration time (e.g., 5 min).

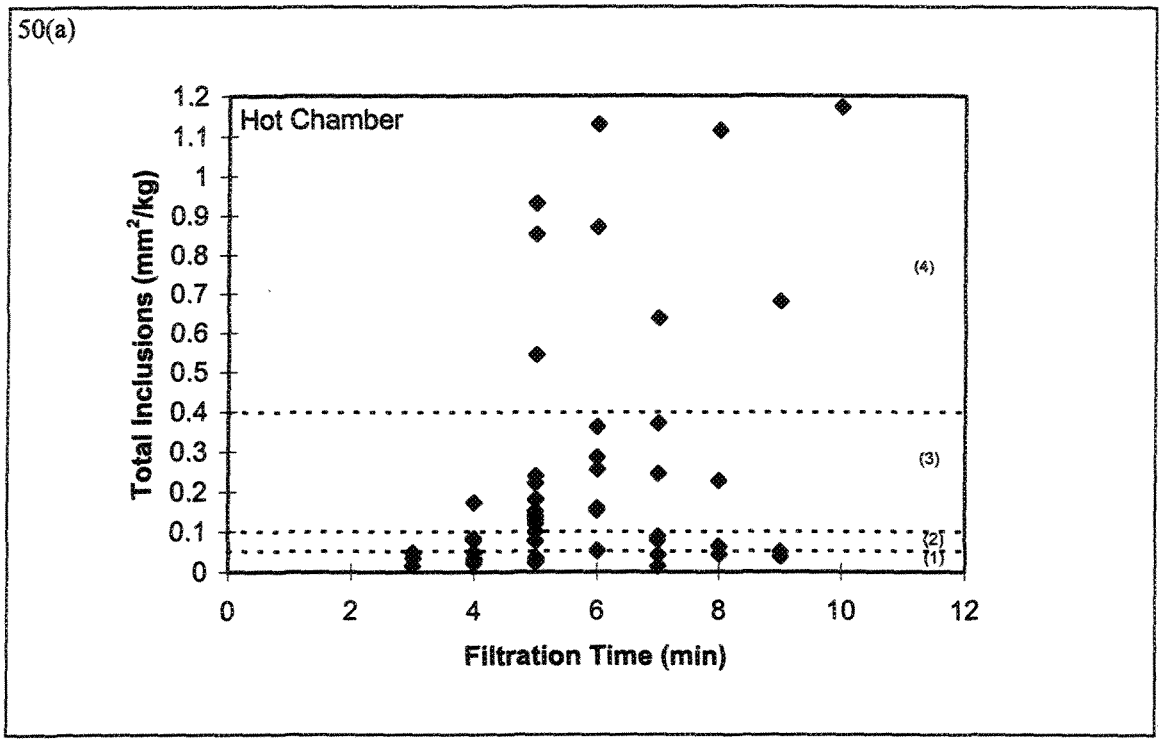

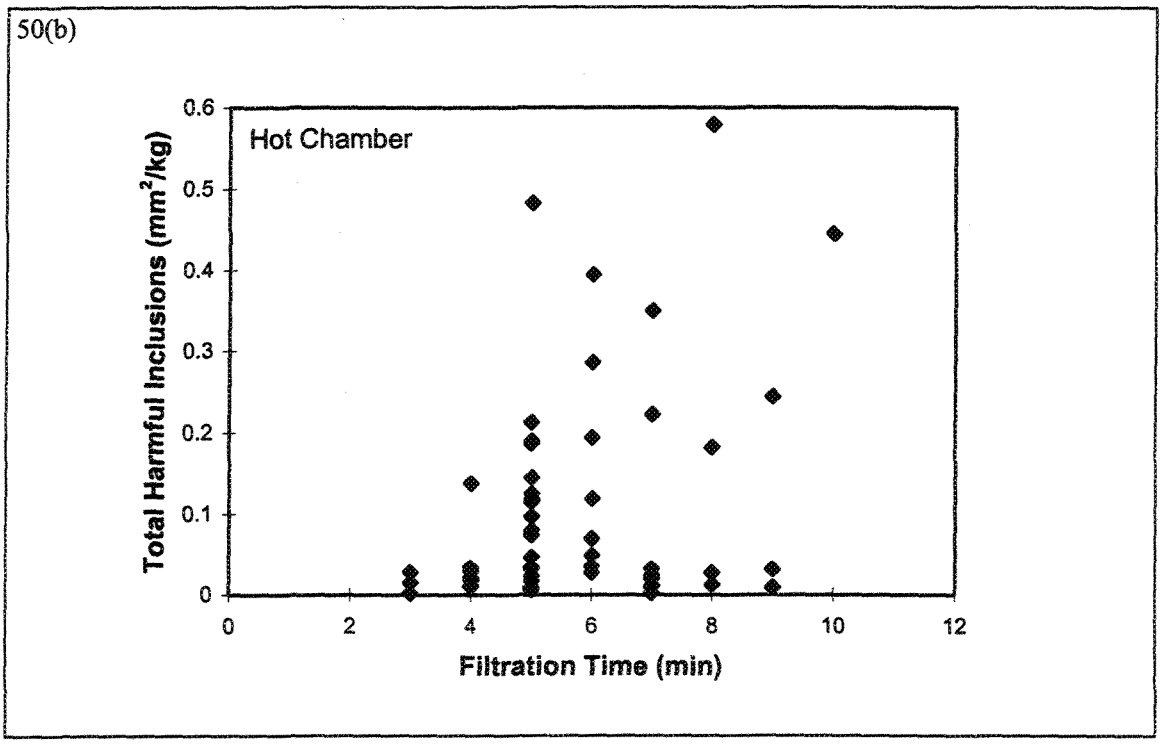

Figure 50 Dependence of filtration time on inclusion concentrations and oxide films for hot chamber: a) total inclusions, b) total harmful inclusions, c) oxide film rating.

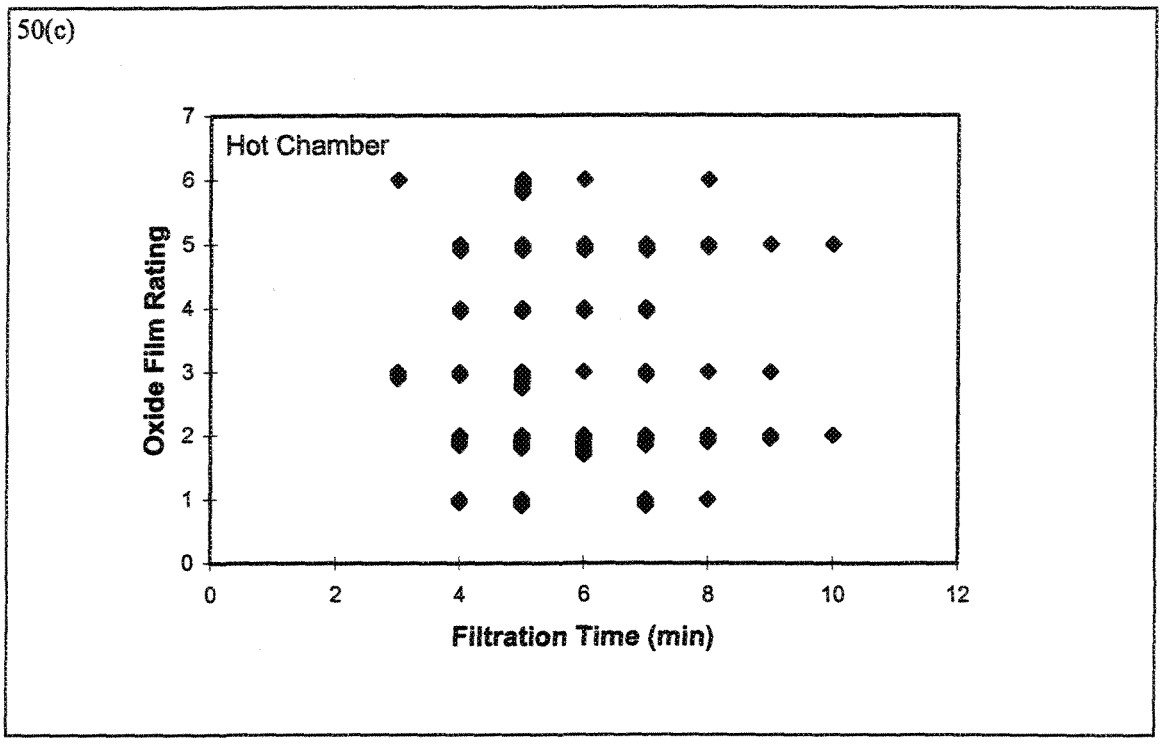

Figure 50 Dependence of filtration time on inclusion concentrations and oxide films for hot chamber: a) total inclusions, b) total harmful inclusions, c) oxide film rating.

It should be borne in mind that oxide films can be trapped easily in the unfiltered metal during sampling if the necessary precautions are not strictly followed. Turbulence of the molten metal, however, cannot be totally avoided either during filling of the ladle or pouring of the liquid metal into the PoDFA crucible. Also, using red hot (~ 850°C) PoDFA crucibles could certainly introduce, to some extent, oxide layers that may cause filtration problems in later stages. Another parameter to be considered is the distance between the melting furnace and the PoDFA apparatus. The shortest distance possible is recommended.

The dependence of filtration time on inclusion content has been divided into four major classes (according to their industrial importance) following the arbitrary classification shown in Table 27. The variation in filtration time as a function of inclusion

concentration in the range 0 - 0.05 mm^2/kg i.e., "very light" is shown in Figure 50. The data in Figure 50(a) can be divided into two sets: 3 - 5 min which represents the major number of samples, and 7 - 9 min which includes only a few samples. This separation is mainly based on the type(s) of oxide films found in each sample. As described in the previous chapter, each sample contained certain amounts of both types of oxide films, i.e., thin and thick. Based on this information, it would seem that the type of oxide films in the sample is the deciding parameter that controls the filtration time.

The effect of inclusion concentrations in the range 0.05 - 0.1 mm^2/kg on filtration time is shown in Tables 10-15 (Chapter 3). Two main observations could be drawn from these tables: a) in the presence of "thin/light" oxide films, inclusions of the order of 0.08 mm^2/kg could lead to filtration times as high as 7 min; b) for a relatively low inclusion concentration ~0.05 mm^2/kg, the presence of "thin/moderate" or "thick/heavy" type oxide films is detrimental. It is evident that without metallographic examination, it is very difficult to evaluate the effect of each parameter.

The dependence of filtration time on inclusion content in the range 0.1 - 0.4 mm^2/kg (termed "moderate" in Table 28) is displayed in Tables 10, 11, 12, and 14 (Chapter 3). Most of the experiments are clustered in the range of 5 - 7 min. It should be noted that the total harmful inclusions could be as low as 0.02 mm^2/kg, i.e., a large proportion of inclusions is fine Al_4C_3 particles $\leq 3\mu m$. Oxide films, on the other hand, are fairly thick ("moderate" and "heavy") which result in significantly longer filtration times.

When the inclusion contents are higher than 0.4 mm^2/kg, filtration times can easily be as long as 10 min, though only about half of this concentration is considered harmful to

the mechanical properties. This series of samples is characterized by a higher volume fraction of oxide films that results from the mechanical stirring of the molten melt prior to executing the PoDFA trials.

4.2.2.2.2 Effect of minor additions

Due to the fact that mechanical stirring is used to insure complete dissolution of the alloying elements added, the inclusions and oxides that settle at the bottom of the melting crucible are disturbed. Thus, it is expected that the concentration of inclusions should be relatively higher in this case than that reported earlier, for similar experimental conditions. Figure 51(a) indicates that the inclusions are possibly having concentrations greater than 0.4 mm^2/kg. Most of these inclusions are considered harmful from the mechanical properties standpoint, Figure 51(b). Another important point to note is that the oxide films are mainly "thick/heavy" as shown in Figure 51(c).

51(a)

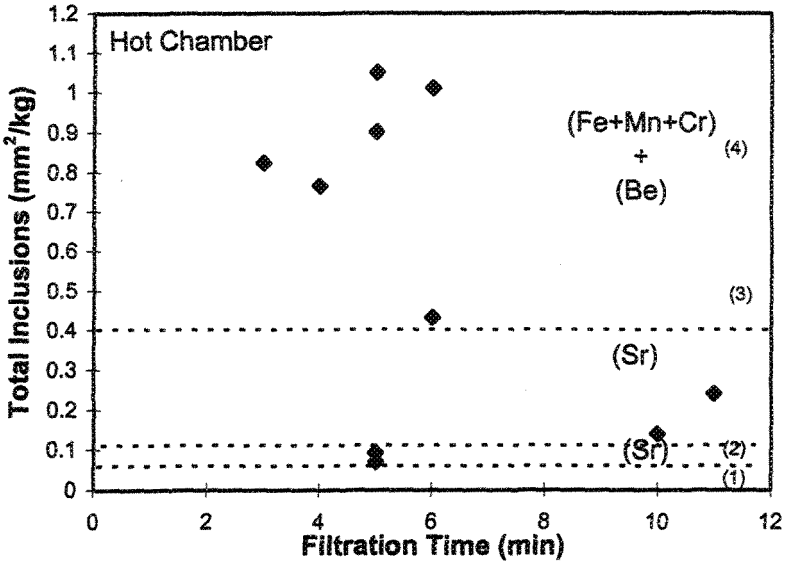

51(b)

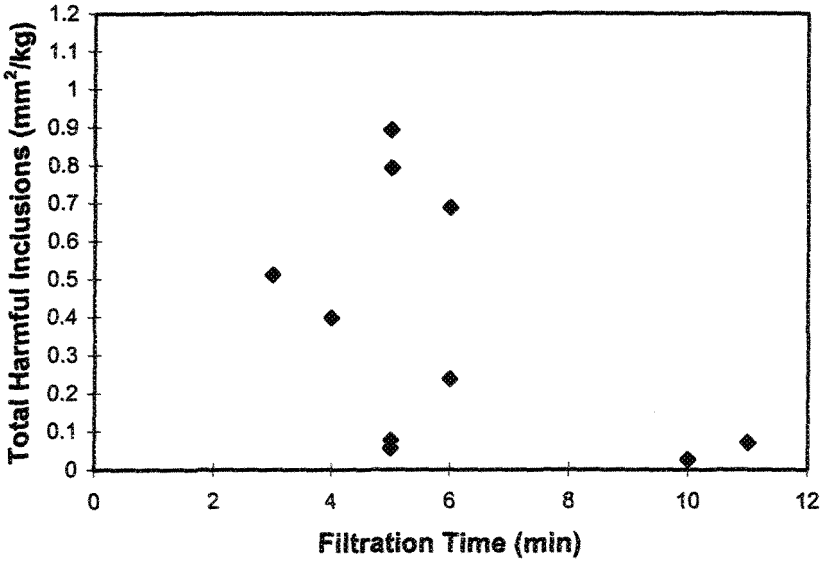

Figure 51 Dependence of filtration time on inclusions caused by minor element additions: a) total inclusions, b) total harmful inclusions, c) oxide film rating.

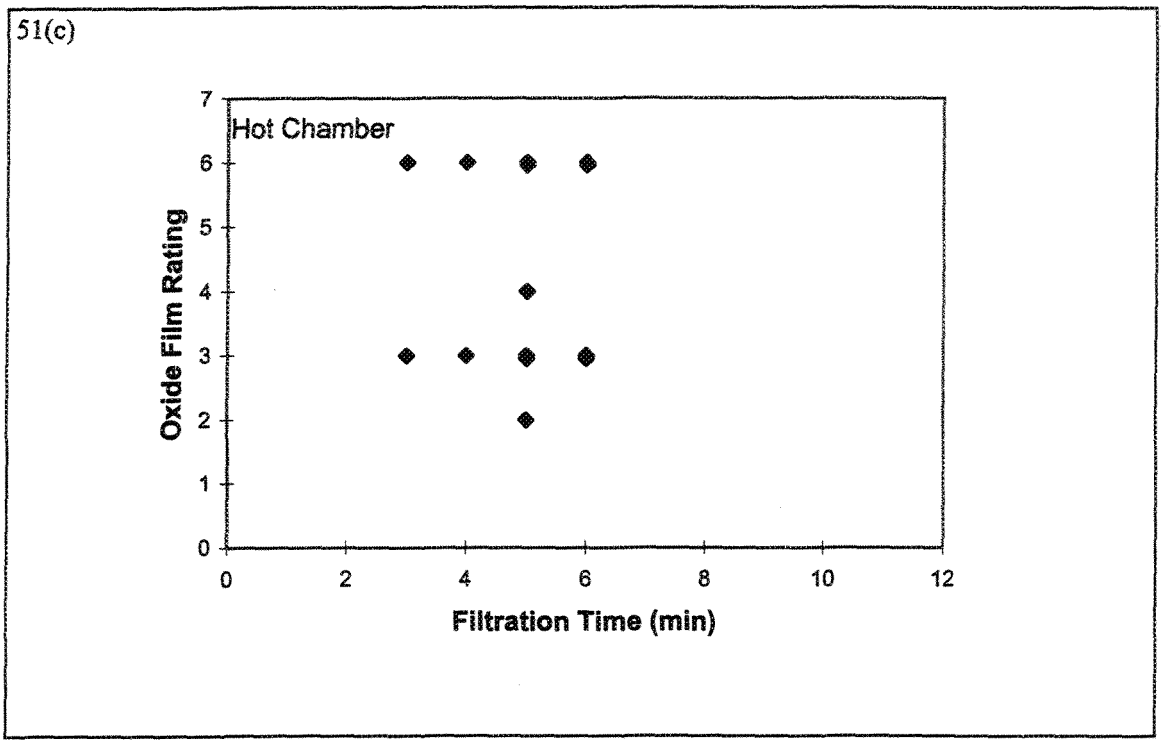

Figure 51 Dependence of filtration time on inclusions caused by minor element additions: a) total inclusions, b) total harmful inclusions, c) oxide film rating.

4.2.3 Inclusion - Fluidity Relationship

Various types of test devices have been used by different investigators to study the factors affecting fluidity of metal and alloys. Among these is the vacuum fluidity test developed by Ragone *et al.* [76]. It has been reported that this technique is considered to be a very reliable and sensitive method for studying the effects of melt composition, metal temperature and trace elements [77, 78]. The work of Venkateswaran *et al.*[79] shows that the fluidity of eutectic Al-Si alloys decreases with the addition of Na, (Na + Sr), Ti, (Na + Ti), or (Na + Sr + Ti), whereas the addition of Sb, S, (Sb + Ti), or (P + Ti), or (P + Ti) increases the fluidity of these alloys.

The dependence of fluidity (measured by the length of solidified metal in the quartz tube of the Ragone fluidity tester) on the inclusion content is explained in Figure 52(a). The average length of solidified metal in about 36 ± 2 cm, regardless of the concentration of total inclusions in the range 0 - 1.2 mm^2/kg. Considering the total harmful inclusions, Figure 52(b), they do not result in a noticeable change in the general distribution. It should be noted, however, that the inclusions for the majority of the measured samples fall in the range 0 - 0.2 mm^2/kg. The observed discrepancy in Figure 52(a) and 52(b) may be explicable in terms of the distribution of oxide films shown in Figure 52(c). It is rather difficult to separate the individual effect of each of the two main parameters, i.e., inclusion and oxide film concentrations, on the alloy fluidity.

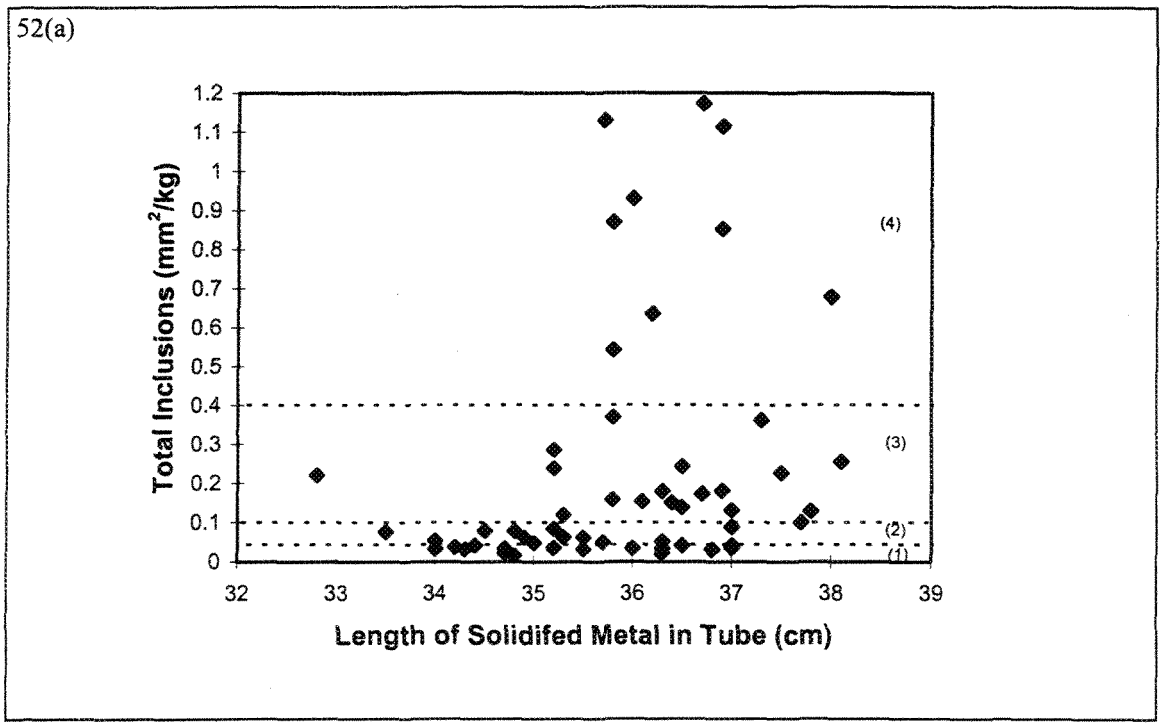

Figure 52 Dependence of the length of solidified metal obtained in the Ragone fluidity test on inclusions caused by variations in the foundry parameters: a) total inclusions, b) total harmful inclusions, c) oxide film rating.

52(b)

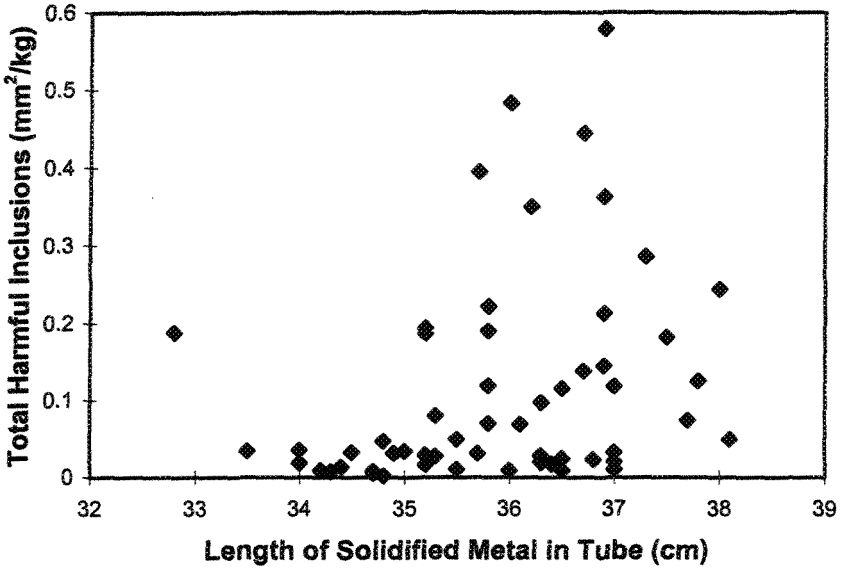

52(c)

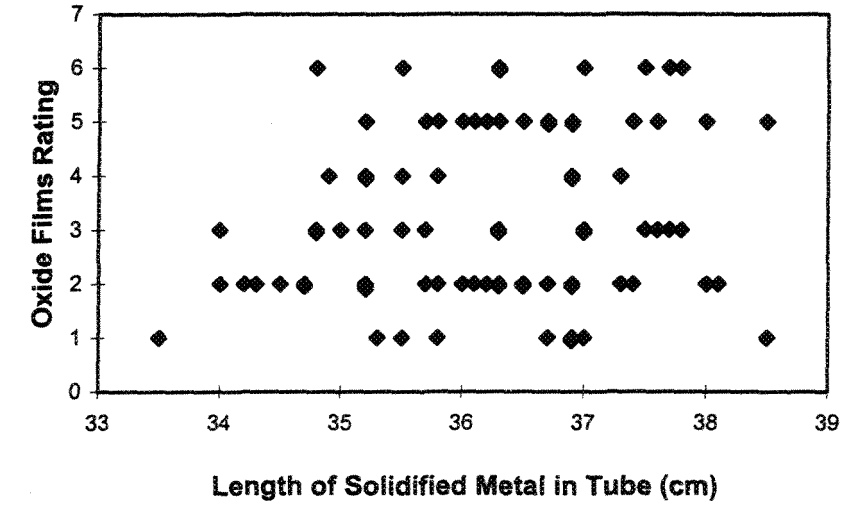

Figure 52 Dependence of the length of solidified metal obtained in the Ragone fluidity test on inclusions caused by variations in the foundry parameters: a) total inclusions, b) total harmful inclusions, c) oxide film rating.

The data on the role of minor additions is relatively limited, Figure 53(a). Modification with Sr appears to noticeably improve the alloy fluidity, Figure 53(b), whereas oxide films associated with the addition of (Fe + Mn + Cr) decrease the length of solidified metal obtained, Figure 53(c). The three elements were added in the form of Al-(~25%X) master alloys (X = Fe, Mn, Cr). Therefore, the actual quantities of added material were almost four times that needed to achieve the required element composition. This operation would certainly create more oxide films than what would be expected if pure elements were used. However, since the dissolution of pure elements is relatively very sluggish at 735°C, the technique of using master alloys is preferred instead.

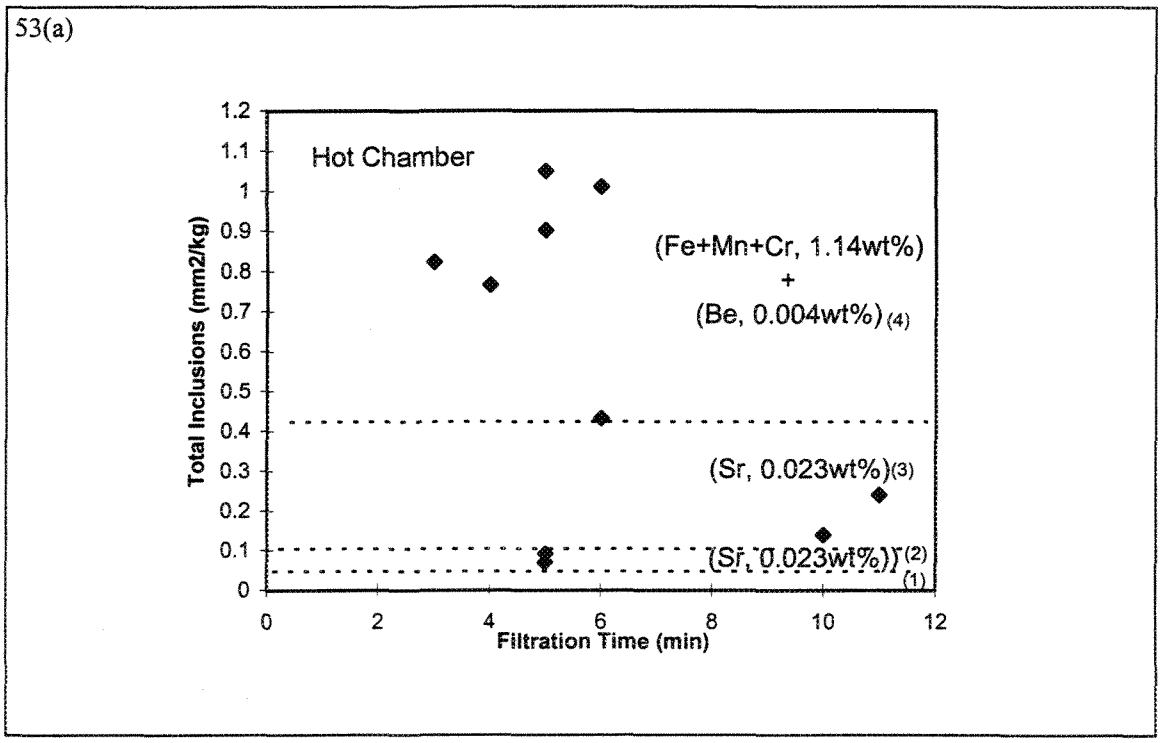

Figure 53 Dependence of the length of solidified metal obtained in the Ragone fluidity test on minor element additions (Sr, Be, Fe+Mn+Cr): a) total inclusions, b) total harmful inclusions, c) oxide film rating.

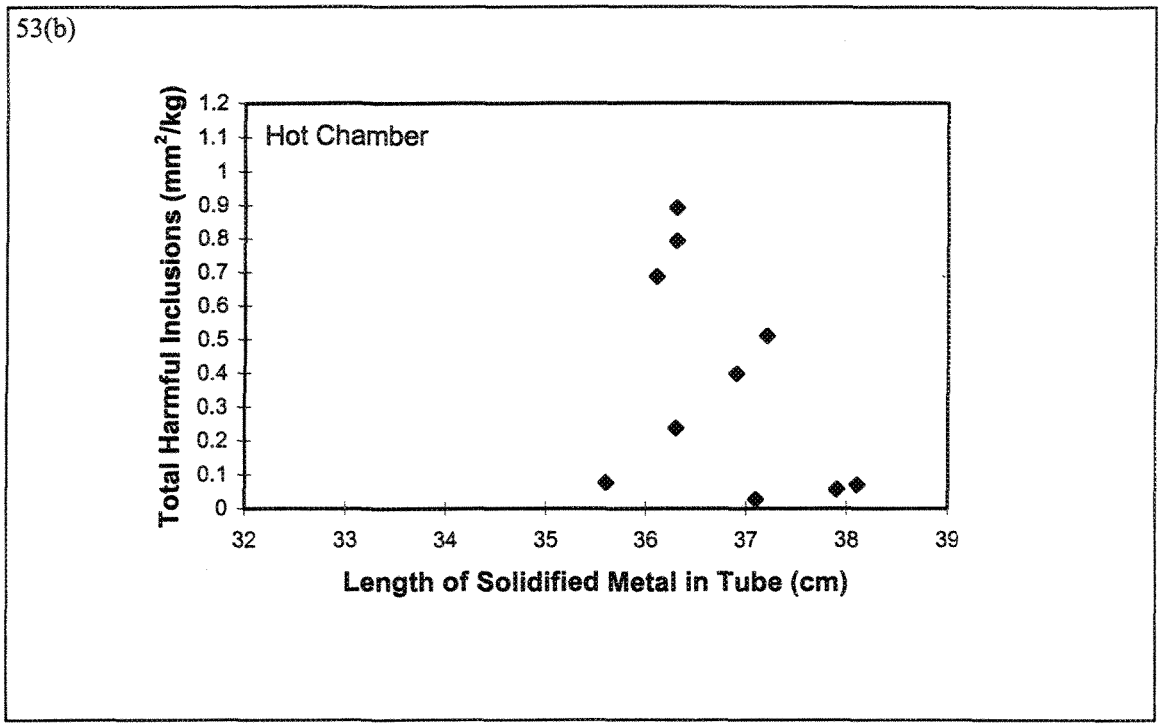

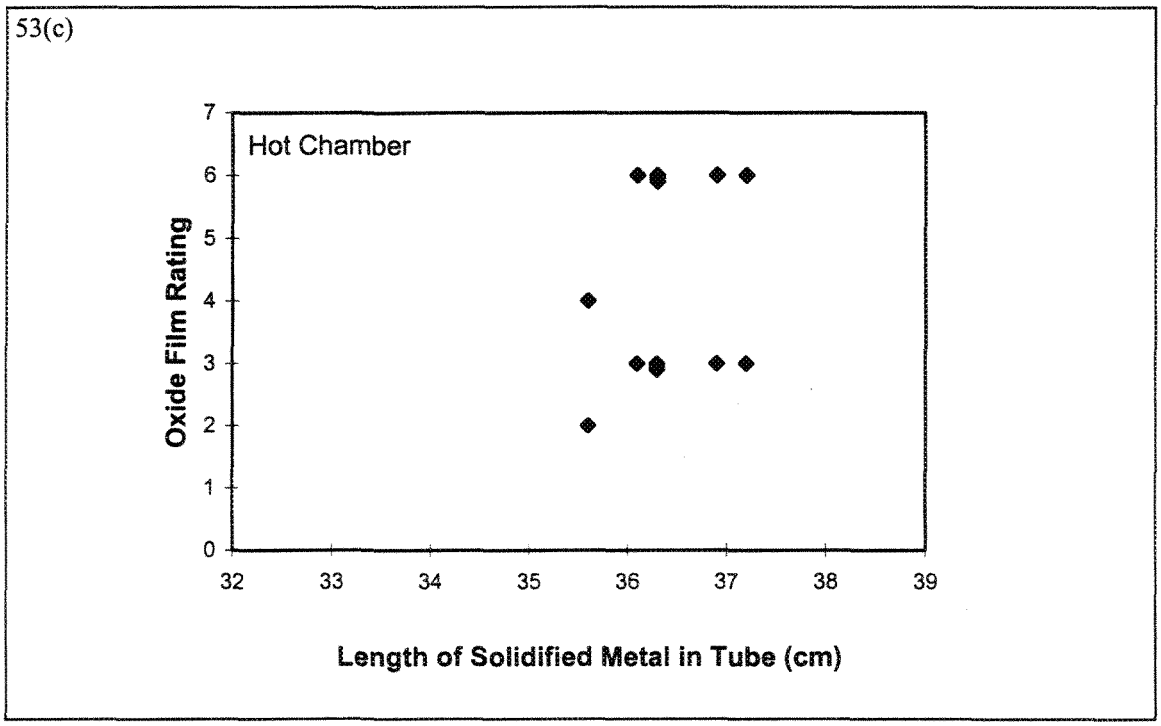

Figure 53 Dependence of the length of solidified metal obtained in the Ragone fluidity test on minor element additions (Sr, Be, Fe+Mn+Cr): a) total inclusions, b) total harmful inclusions, c) oxide film rating.

4.2.4 Examples of Inclusion Concentrations

Figure 54 shows the microstructure of the base alloy away from the inclusion cake (i.e., taken from an area above the PoDFA sample). No traces of inclusions of oxides can be seen. A typical example of what is termed as a "very light" inclusion level (i.e., 0 - 0.05 mm^2/kg) is displayed in Figure 55(a), consisting mainly of fine Al_4C_3 particles ($\leq 3\mu m$). Inclusions in the range of 0.05 - 0.1 mm^2/kg (termed "light") are presented in Figure 55(b). Though the inclusions are mainly fine Al_4C_3, some long needles of Al_4C_3 ($> 3\mu m$) can be observed. Inclusions classified as "moderate" are exemplified in Figure 55(c). They are a mixture of fine Al_4C_3 ($\leq 3\mu m$), coarse Al_4C_3 ($> 3\mu m$) and MgO. Note how the inclusions are clogging the filter pores (leading to a lengthy filtration time). An example of "heavy" inclusion concentration is shown in Figure 55(d). In this case, almost all types of inclusions are present ($Al_4C_3 \leq 3\mu m$, $Al_4C_3 \geq 3\mu m$, MgO, $MgAl_2O_4$).

When the inclusion concentration exceeds 1.2 mm^2/kg, i.e., the "excessive" level, it is rather difficult to count the concentration accurately. It should be borne in mind that the accuracy of measurements using the point count method ranges from ± 15% (light - moderate) to ± 25% (heavy -excessive). Figures 55(e) and 55(f) show two examples of such high inclusion densities. The sedimentation of the sludge crystals (gray color) contributes to the accumulation of TiB_2 inclusions, leading to the blocking of their passage in the filter pores as seen in Figure 55(f). Details of these inclusions are listed in Tables 21-23 (Chapter 3).

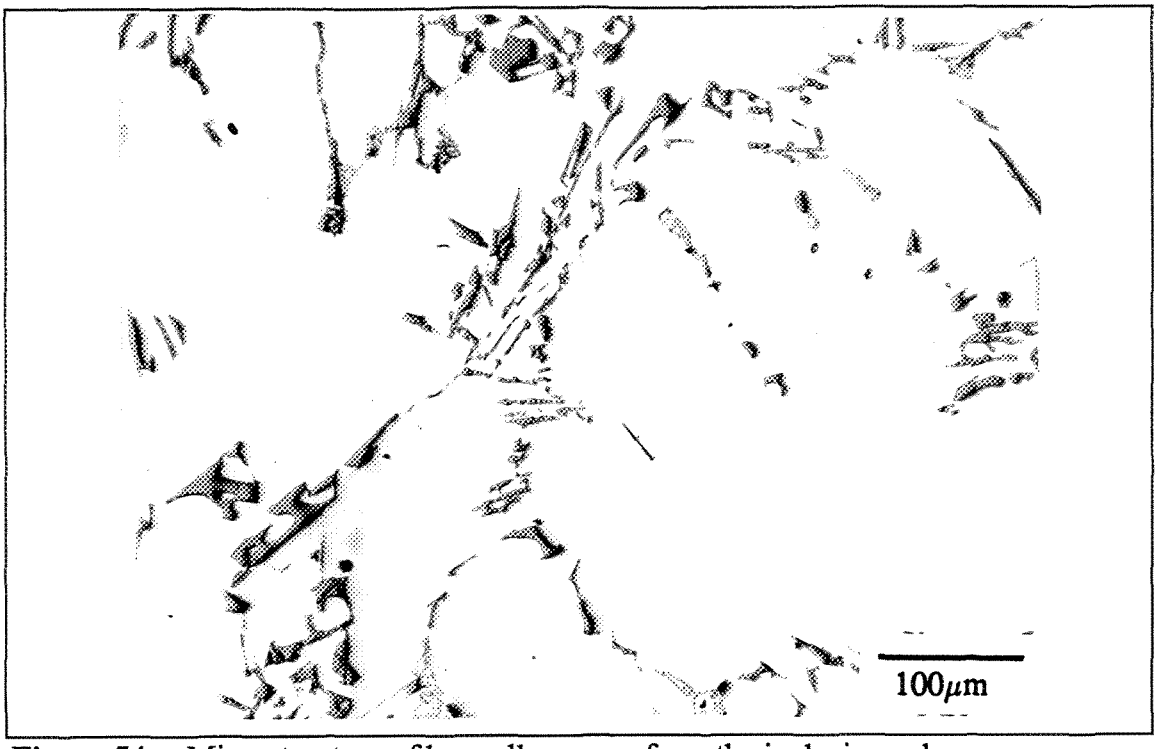

Figure 54 Microstructure of base alloy away from the inclusion cake.

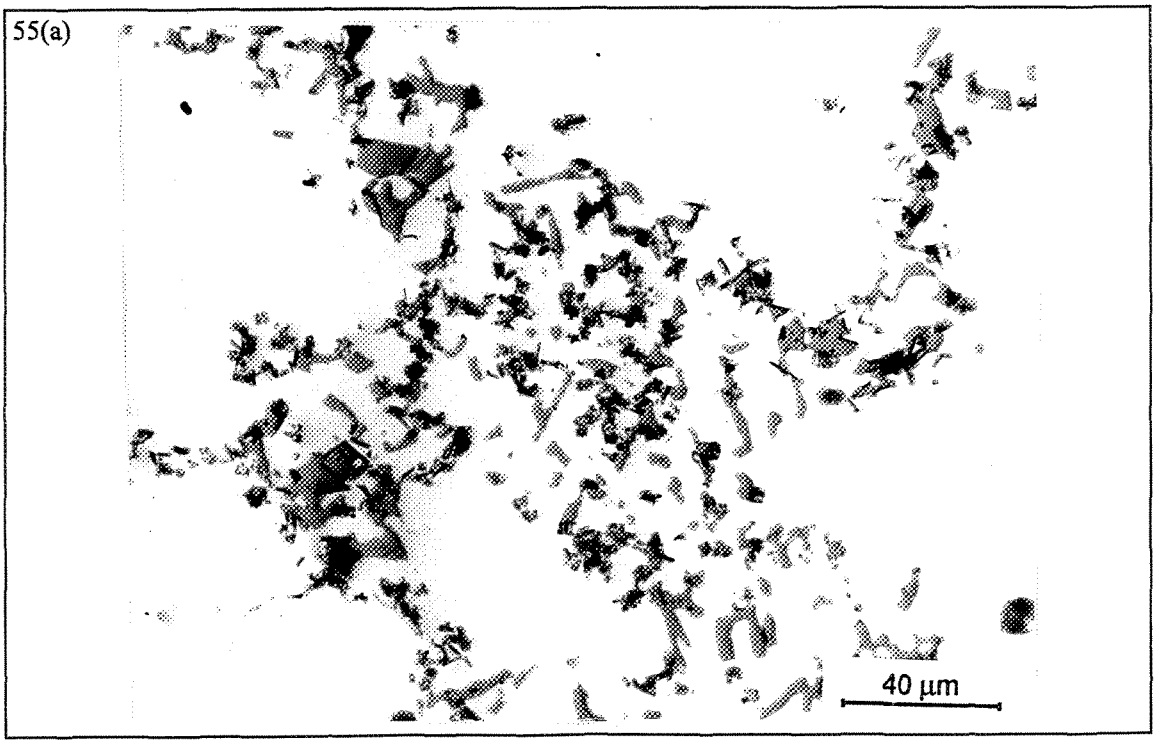

Figure 55 Examples of inclusion concentrations: a) very light - Experiment 4A.

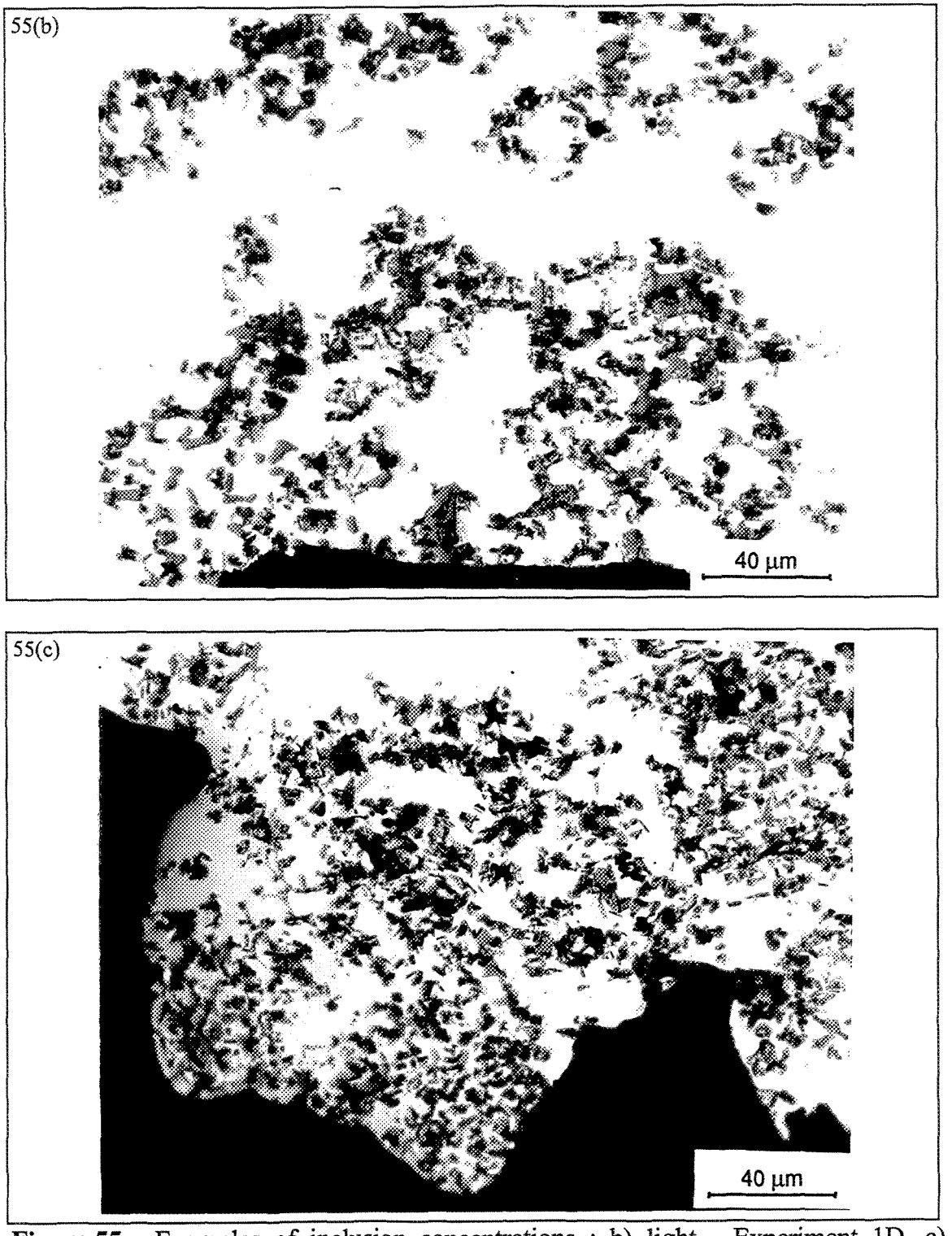

Figure 55 Examples of inclusion concentrations : b) light - Experiment 1D, c) moderate-Experiment 15E.

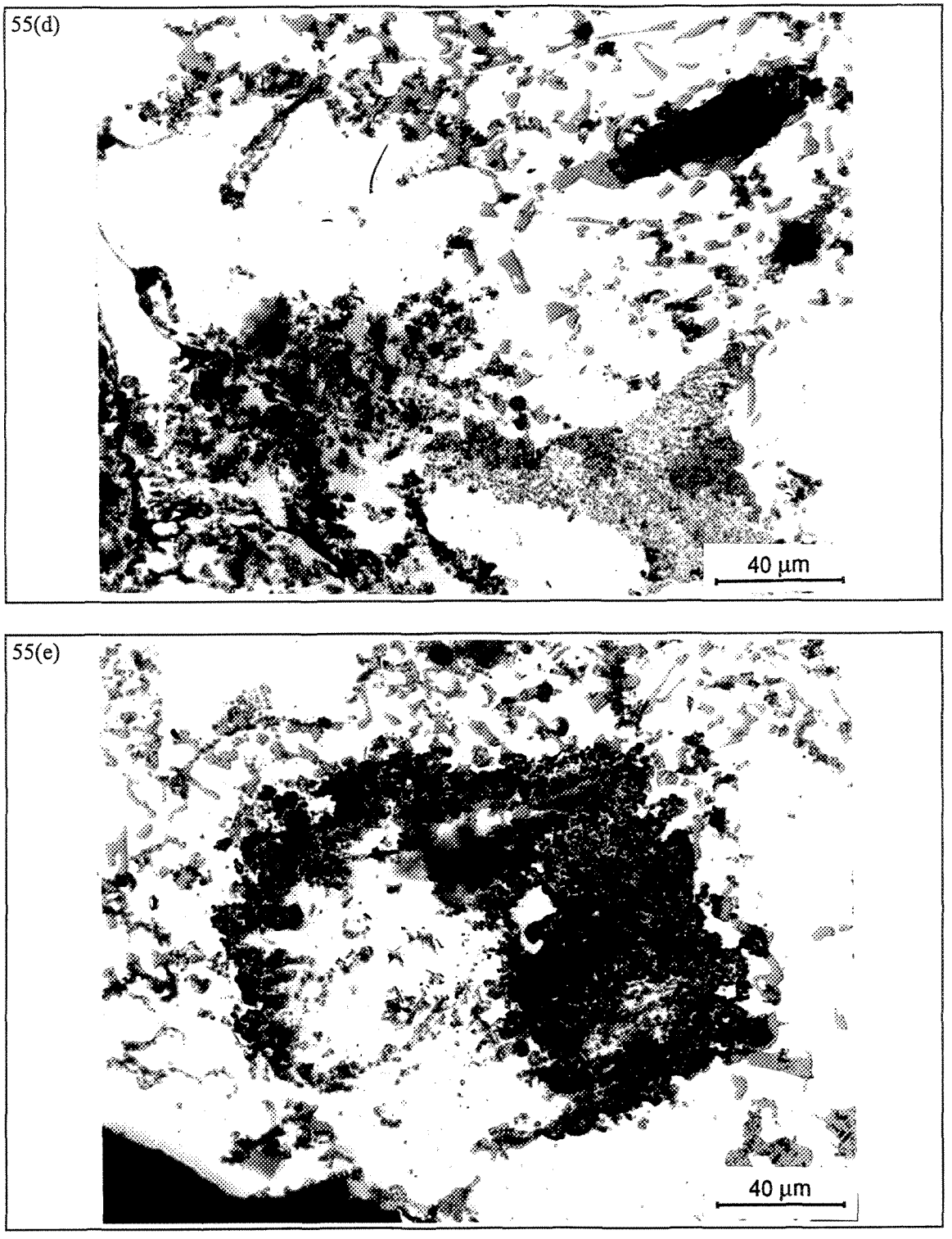

Figure 55 Examples of inclusion concentrations : d) heavy - Experiment 12C, e) excessive - Experiment 29H.

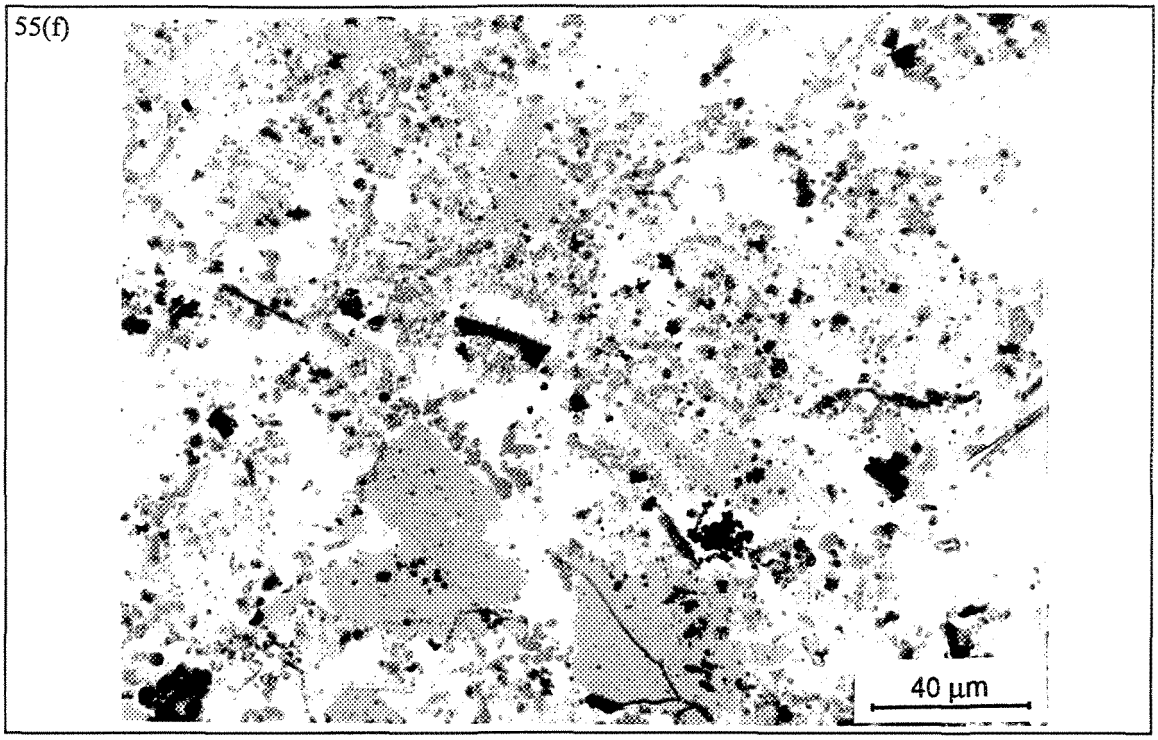

Figure 55 Examples of inclusion concentrations: a) very light - Experiment 4A, b) light - Experiment 1D, c) moderate-Experiment 15E, d) heavy - Experiment 12C, e) excessive - Experiment 29H, f) excessive - Experiment 29I.

4.2.5 Examples of Oxide Films

Figures 56(a) through 56(g) show different types of aluminum oxide (Al_2O_3), either in the form of films (thin or thick) or as dark (black) patches with irregular shapes. The ratings reported in the present study are based on the classification procedure defined by the R & D Centres of Alcan International Limited. Note that in most of the cases, the oxide films tend to precipitate towards the metal/filter interface as seen in Figure 56(g).

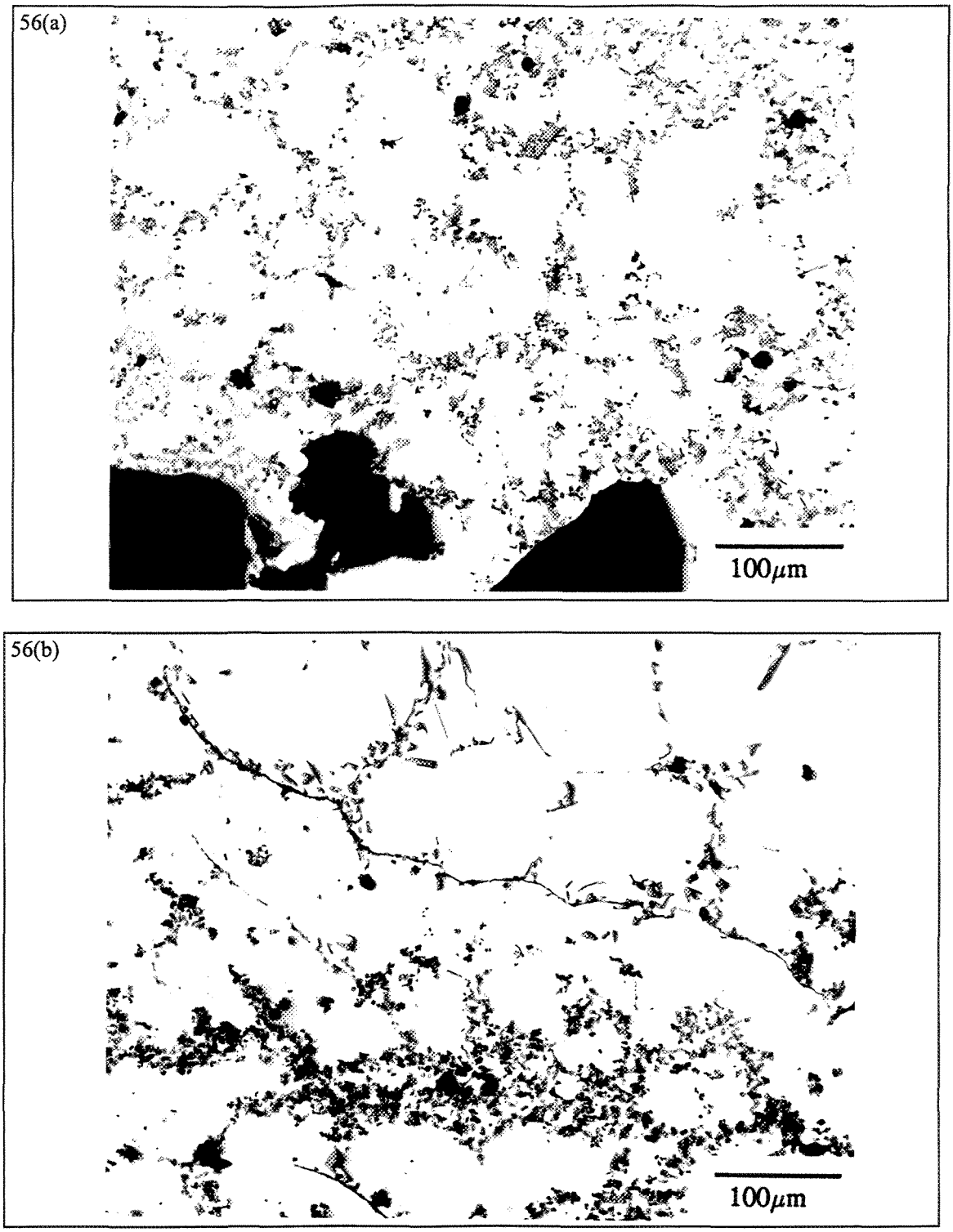

Figure 56 Examples of Al_2O_3 oxide films/particles : a) none-Experiment 3E, b) thin/light - Experiment 1D.

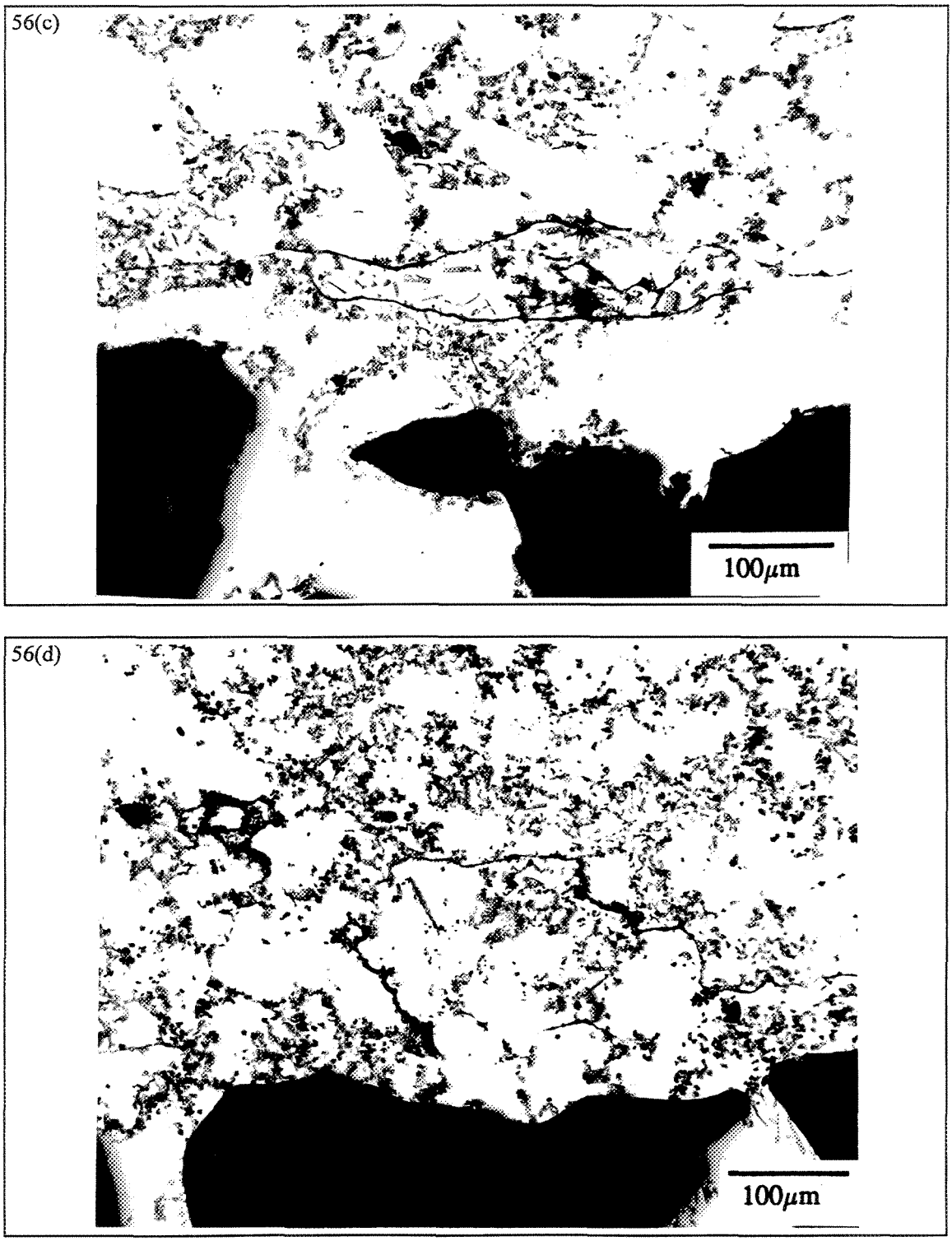

Figure 56 Examples of Al_2O_3 oxide films/particles: c) thin/moderate - Experiment 1A, d) thin/heavy - Experiment 1B.

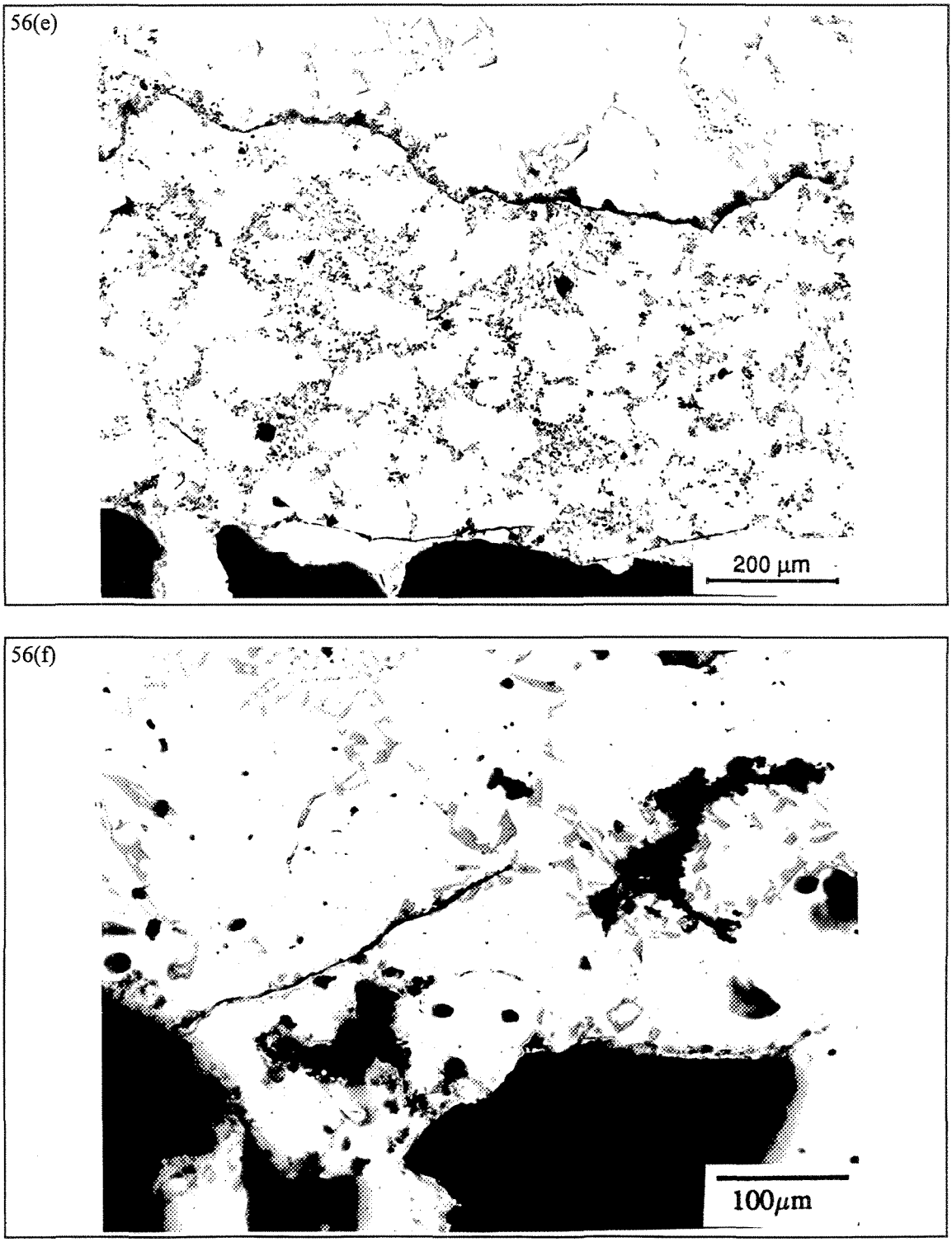

Figure 56 Examples of Al_2O_3 oxide films/particles: e) thick/light - Experiment 15E, f) thick/moderate - Experiment 14E.

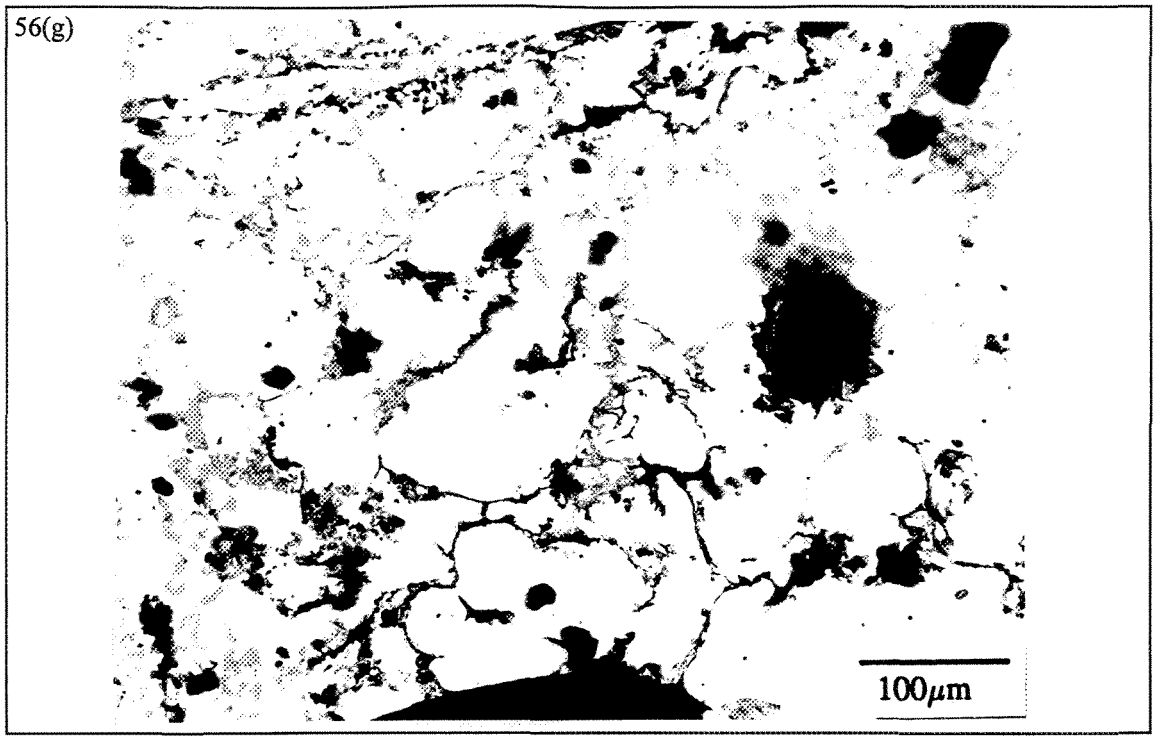

Figure 56 Examples of Al_2O_3 oxide films/particles: a) none-Experiment 3E, b) thin/light - Experiment 1D, c) thin/moderate - Experiment 1A, d) thin/heavy - Experiment 1B, e) thick/light - Experiment 15E, f) thick/moderate - Experiment 14E, g) thick/heavy - Experiment 7E.

The effect of oxide density on filtration time is well demonstrated in Figure 57. When the Al_2O_3 oxides occur in the form of pencil-like lines (Figure 57(a)-arrowed), filtration takes about 3 min or less (total inclusions ~0.015 mm^2/kg). The presence of thick/heavy oxide films, as well as oxide particles in Figure 57(b) increases the filtration time to 5 min (total inclusions ~0.044 mm^2/kg). Such a delay was commonly observed when the molten metal was disturbed during sampling or if skimming (i.e., removal of the oxide layer prior to sampling) was not properly carried out.

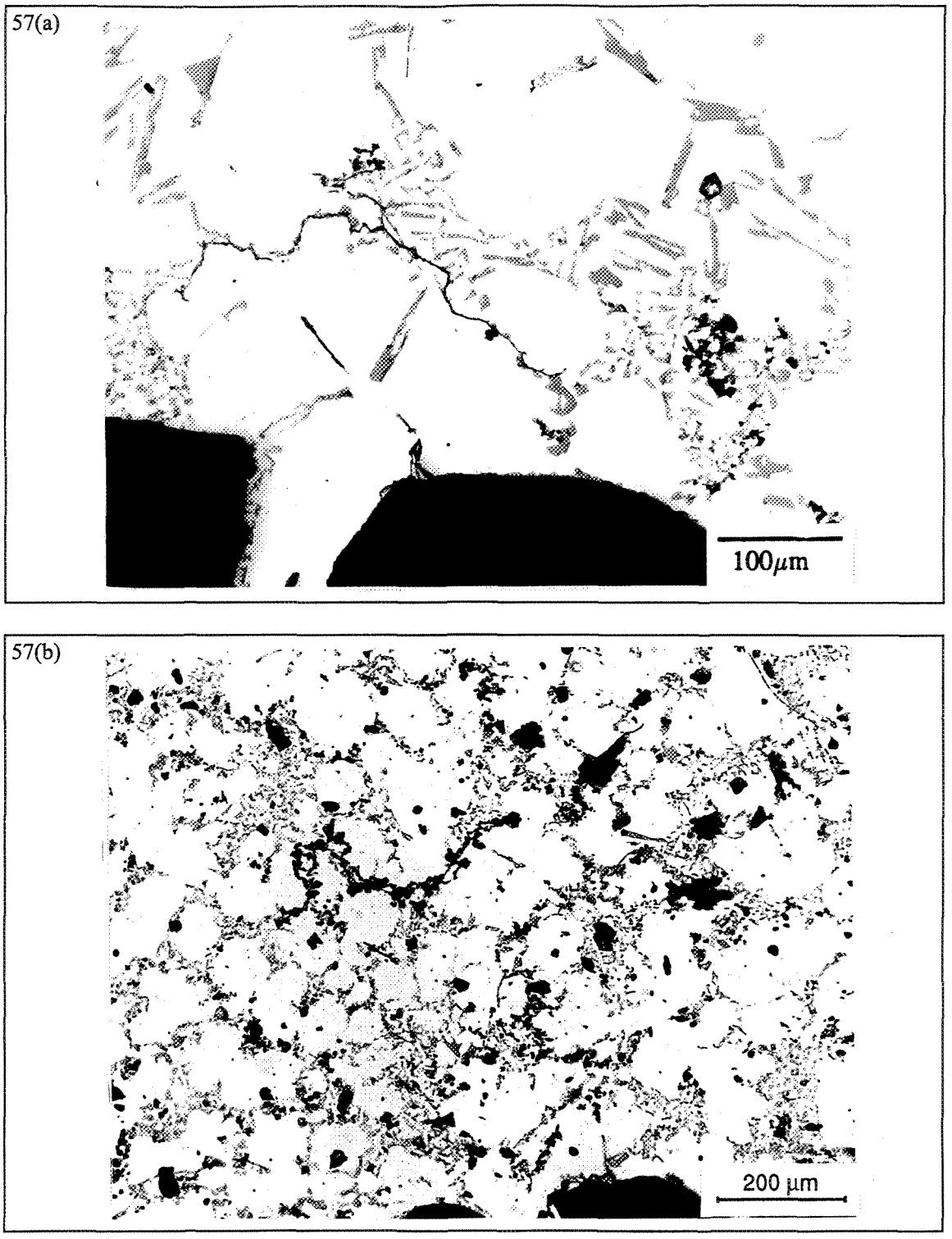

Figure 57 Effect of Al_2O_3 oxide density on filtration time : a) Experiment 2E - 3 min, b) Experiment 7A - 5 min.

CHAPTER 5

EFFECT OF INCLUSIONS ON MECHANICAL PROPERTIES

CHAPTER 5

EFFECT OF INCLUSIONS ON MECHANICAL PROPERTIES

5.1 INTRODUCTION

The detrimental effects of the presence of inclusions in aluminum are well documented [4, 43, 44, 45, 46, 47, 49, 59]. Although much work has been reported on the study of inclusions, the problem of measuring metal cleanliness through a sensitive quantitative method still exists. The difficulty is further compounded by the fact that the inclusions to be measured are usually very small, about 10-20 μm in diameter, and present in trace amounts (about 10 ppm). The main inclusions that occur during the melting of aluminum alloys or holding periods prior to casting are aluminum oxide (Al_2O_3) as dispersed particles or oxide films, aluminum carbide (Al_4C_3), magnesium oxide (MgO), spinel ($MgAl_2O_4$), titanium diboride (TiB_2), aluminum boride (AlB), and titanium aluminide ($TiAl_3$) [4, 43, 44, 45, 46, 47, 49, 59].

Many studies have been conducted on the role of non-metallic inclusions and oxide films in determining the alloy mechanical properties. The presence of oxide films can lead to a significant scatter in the tensile properties of the cast alloy due to early initiation of

fracture. Removal of such inclusions/oxides is expected to result in more consistent and reproducible mechanical properties.

Samuel *et al.* [32] have studied the effect of melt cleanliness on the mechanical properties of a 359 aluminum alloy reinforced with 20% SiC particles (average particle size ~20 μm). Their work shows that the percentage elongation varies linearly with the volume fraction of inclusions/oxides, and can be expressed by the relationship,

$$\% \text{ Elongation} = 1.06 - 0.66X$$

where X represents the volume fraction of inclusions.

Campbell [80] has reported that the oxide films that remain in the cast product will cause mechanical weakness and form leak paths that emerge thorough the wall of the casting. In some cases, the large amount of porosity associated with the oxide films can further enhance the weakness. Fractographic observations reveal that crack initiation is related to the presence of these inclusions. Spinel inclusions are often seen to be surrounded by partial or complete voids, indicating debonding between the inclusions and the matrix during fracture.

Hedjazi *et al.* [29] examined the effect of non-metallic inclusions on the tensile properties of an Al-4.5 % Cu-1.5% Mg alloy. Their study showed that inclusions which result from various physical and chemical phenomena that occur during the melting and casting process are found to be non-uniformly distributed within the cast product. Categorizing the inclusion/oxides as two types, viz., film and non-film, and further

classifying the latter type according to their size as macro-inclusions (>50 μm) and micro-inclusions (<50 μm), the authors concluded that both film and non-film inclusions lower the ductility, i.e., percentage elongation, to a greater extent than the strength of the alloy. In their opinion, filtration improves with bed depth as do the tensile properties [81].

Aria et al. [30] have observed that molten metal filtration increases the strengths of 2014, 2017 and 7075 extrusions. The reason is a decrease in the non-metallic inclusions which disturb homogeneous precipitation. Ductilities of extrusions also increase by molten metal filtration. The non-metallic inclusions act as nucleation sites for dimple cleavages [30]. Rios *et al.* [33] attribute the lower ductility and strength in the transverse direction (deformation axis normal to extrusion axis and tube radius) in hot extruded AA2014 aluminum tube specimens to the influence of coarse inclusions that fracture early during tensile deformation. The resultant cracks induce void formation around the small inclusions in the matrix.

The role of inclusions in initiating fatigue cracks under dynamic loading is well documented. Chien *et al.* [82] report that $TiAl_3$ particles nucleate cracks in A201 alloys. It is expected that other types of inclusions may act in the same way, particularly if their size is large. Gerold [83] also found that intermetallic inclusions are additional sources for crack initiation in commercial alloys. Thus, filtered metal should produce castings having an increased fatigue resistance.

In the present study, the A356.2 alloy was selected for investigating the effect of inclusions on the tensile properties. A sum of thirteen operations, typical of those customarily used in the aluminum industry, were applied to the A356.2 alloy melts, to

investigate the type and amount of inclusions that could occur as a result of these operations, and their influence on the tensile properties, in particular, the alloy ductility. The results are reported in this chapter.

5.2 EXPERIMENTAL PROCEDURE

As mentioned previously in Chapter 3, the A356.2 alloy was supplied in the form of 12.5 kg ingots. (The chemical composition of the alloy is shown again in Table 29 for convenience.) The ingots were cut, cleaned, and melted in a silicon carbide crucible of 28 kg capacity, using an electrical resistance furnace. The melting temperature was held at 735 ± 5 °C. The maximum humidity was about 15%. No degassing was applied. The hydrogen level was ≤0.1 ml/100g Al as measured by an Alscan™ apparatus. Prior to casting, melt treatment agents such as strontium (400 ppm Sr, added as Al-10% Sr master alloy) or TiB_2 (in the form of Al-5%Ti-1%B, measured in terms of a 0.02 wt% Ti addition) were added to the melt.

Table 29 Chemical composition (wt%) of A356.2 alloy.

Si	Mg	Fe	Mn	Cu	Be	Sr	Al
6.78	0.33	0.11	0.04	0.02	—	—	Bal.

Casting was done in a Stahl permanent mold (type ASTM B-108) heated at 425°C. The test bars obtained from the Stahl mold castings were solution heat treated for 8 h at 540°C, in a forced-air furnace, followed by quenching in hot water (60°C). The quenched test bars were stabilized at room temperature for 24 h prior to hardening at 150°C for 5 h.

The solutionized test bars were pulled to fracture at room temperature in an Instron Universal testing machine at a strain rate of 4×10^{-4} s^{-1}. A strain gauge extensometer (50 mm range) was attached to the test specimen for measuring the alloy ductility. The data was analyzed using a special software designed for this work. Tensile properties, namely yield stress (YS) at 0.2% offset strain, ultimate tensile strength (UTS), and fracture elongation (EL%) were derived from the data aquisition system. The volume fraction of non-metallic inclusions were measured from macrophotographs of the specimen fracture surfaces, using the point count method [84].

5.3 RESULTS AND DISCUSSION

5.3.1 Fresh Alloy

The experimental and melt conditions applied for the preparation of the tensile test bars are summarized in Table 30, while the tensile test data is listed in Tables 31through 38 for castings prepared from fresh alloy melts.

Table 30 Melt conditions for preparation of tensile test bars.

Experiment #	Type of Charge	Charge Weight (kg)	Melt Temperature (°C)	Mold Temperature (°C)	Additive	Settling Time (hr)	Stirring Speed (rpm)	Stirring Time (min)	Degassing Time (min)	Filter Size (ppi)	Humidity (%)
3	Fresh	18	735 ± 5	435 ± 3	—	72	—	—	—	—	18
4	Fresh	18	735 ± 5	435 ± 3	—	0	125 -	20	—	—	15
5	Fresh	18	735 ± 5	435 ± 3	—	0	125 -	—	45	—	17
15	Fresh	18	735 ± 5	435 ± 3	—	4[a]	125 -	—	45	—	13
6A - 6G	Fresh	25	735 ± 5	435 ± 3	—	0	—	—	—	10	17
6H - 6N	Fresh	25	735 ± 5	435 ± 3	—	0	125 -	—	45	10	17
7A - 7H	Fresh	25	735 ± 5	435 ± 3	Al - Sr	0	125 -	15	—	—	21
7I - 7P	Fresh	25	735 ± 5	435 ± 3	—	0	125 -	—	45	—	21
8A - 8E	Fresh	25	735 ± 5	435 ± 3	—	72[a]	125 -	15	—	—	16
8F - 8J	Fresh	25	735 ± 5	435 ± 3	—	0	—	—	—	10	16
8K - 8O	Fresh	25	735 ± 5	435 ± 3	—	0	125 -	—	45	—	20
9A - 9F	Fresh	20	735 ± 5	435 ± 3	Al - Ti - B	1[a]	125 -	15	—	—	17
9G - 9L	Fresh	20	735 ± 5	435 ± 3	—	0	125 -	—	45	—	17
11	Scrap	20	735 ± 5	435 ± 3	—	0	—	—	—	—	19
10	Scrap	20	735 ± 5	435 ± 3	—	72	—	—	—	—	15
12A - 12F	Scrap	20	735 ± 5	435 ± 3	—	0	125 -	20	—	—	15
12G - 12L	Scrap	20	735 ± 5	435 ± 3	—	0	125 -	—	45	—	15
14A - 14F	Scrap	20	735 ± 5	435 ± 3	—	72[a]	125 -	15	—	—	17
14G - 14K	Scrap	20	735 ± 5	435 ± 3	—	0	125 -	—	45	—	17
13A - 13G	Scrap	20	735 ± 5	435 ± 3	—	0	—	—	—	10	20
13H - 13N	Scrap	20	735 ± 5	435 ± 3	—	0	125 -	—	45	10	20

Note: a: stirring/degassing before settling.

It can be seen from Tables 30 and 31 that a settling time of 72 h enhanced the alloy properties, in particular, percentage elongation, which reached ~18-19%. It is important to note the uniformity of the tensile properties of all castings regardless of the casting sequence. Vigorous stirring appears to push the inclusions that settle close to the bottom of the crucible towards the upper surface of the molten metal. Depending upon the stirring speed and time, the thickness of the contaminated portion near the melt surface increases, and as shown in Table 32, the first six castings (4A1 through 4C2) exhibit low ductilities.

Table 31 Tensile test results of Experiment #3 (fresh alloy).

Experiment #	Y.S. (MPa)	U.T.S. (MPa)	% Elongation
3A1	108.5	271.1	12.6
3A2	106.0	264.9	11.7
3B1	101.3	253.0	12.6
3B2	101.6	253.7	9.3
3C1	98.8	247.1	11.5
3C2	106.3	263.9	13.5
3D1	103.8	259.4	9.2
3D2	106.1	264.9	10.0
3E1	103.8	259.4	14.6
3E2	103.3	257.3	13.8
3F1	106.9	265.4	15.8
3F2	103.1	257.6	10.9
3H1	107.6	268.8	16.8
3H2	109.0	272.5	12.5
3I1	109.6	273.7	15.5
3I2	107.5	268.5	11.5
3J1	121.6	277.8	19.2
3J2	106.5	265.3	11.2
3K1	112.2	277.6	17.9
3K2	107.5	268.6	14.1

Table 32 Tensile test results of Experiment #4 (fresh alloy).

Experiment #	Y.S. (MPa)	U.T.S. (MPa)	% Elongation
4A1	102.2	254.9	5.7
4A2	109.1	272.7	7.9
4B1	113.4	281.8	7.4
4B2	112.3	280.6	6.8
4C1	111.7	279.2	7.4
4C2	102.0	254.7	4.9
4D1	116.8	291.9	11.1
4D2	114.0	284.8	8.2
4E1	110.9	277.2	10.1
4E2	111.3	278.1	8.3
4F1	108.7	271.7	14.4
4F2	112.3	280.6	10.8
4G1	112.4	281.0	14.6
4G2	109.3	273.2	12.7
4H1	112.5	281.0	12.5
4H2	115.9	289.4	13.8
4I1	108.4	270.8	14.8
4I2	117.8	294.1	13.7
4J1	117.1	291.8	13.6
4J2	114.6	282.1	10.5
4K1	107.1	267.8	15.1
4K2	115.9	289.5	12.7
4L2	117.1	292.5	16.9

Degassing, on the other hand, is very effective in removing most of the inclusions and results in markedly improving the tensile properties (12-20% EL) for most of the castings, Table 33. However, if the inclusions in the upper portion of the liquid metal following the degassing are not skimmed immediately, these inclusions (with heavier densities compared to that of liquid aluminum) tend to settle down towards the bottom of

the crucible. Depending upon the settling time, the molten metal will become contaminated again, leading to unpredictable results. Table 34 shows that in some cases, when the settling time after degassing is large, e.g., 4 h (see Table 30), two test bars produced simultaneously from the same casting can possess completely different ductilities (e.g., 15D and 15G), the latter being controlled by the motion of inclusions during filling of the mold. This is explained schematically in Figure 58.

Table 33 Tensile test results of Experiment #5 (fresh alloy).

Experiment #	Y.S. (MPa)	U.T.S (MPa)	% Elongation
5A1	125.4	299.9	12.0
5A2	115.1	287.6	17.0
5B1	117.3	293.1	6.3
5B2	118.7	296.3	10.8
5C1	111.4	278.3	12.2
5D1	115.7	287.6	14.0
5D2	111.7	278.9	8.2
5E1	130.0	295.2	11.1
5E2	105.0	262.1	9.3
5F1	101.2	252.8	13.1
5F2	116.6	291.2	16.7
5G1	116.5	291.1	10.6
5G2	117.6	293.2	14.2
5H1	119.1	297.5	12.9
5H2	119.0	296.6	13.0
5I1	120.6	297.2	12.1
5J1	119.4	297.5	15.5
5J2	115.7	288.6	16.9
5K1	115.9	289.5	19.1
5K2	121.4	300.2	16.5

Table 34 Tensile test results of Experiment #15 (fresh alloy).

Experiment #	Y.S. (MPa)	U.T.S. (MPa)	% Elongation
15A1	114.0	284.5	9.7
15A2	112.6	281.2	10.0
15B1	115.1	287.4	16.0
15B2	115.1	287.6	10.2
15C1	114.6	286.4	14.1
15C2	114.2	284.9	10.4
15D1	113.8	284.3	16.5
15D2	103.2	257.6	5.4
15E1	114.4	285.5	14.2
15E2	115.9	289.7	10.3
15F1	112.7	281.2	16.9
15G1	115.9	289.5	15.0
15G2	104.0	259.4	4.2
15H1	107.9	268.1	13.2
15H2	106.4	265.7	5.3
15I1	116.2	290.0	14.7
15I2	104.6	261.0	7.8
15J1	103.3	257.9	16.7
15J2	110.4	275.6	13.5
15K1	111.2	277.4	11.7
15K2	114.9	287.1	12.8
15L1	115.8	288.9	12.4
15L2	113.6	283.9	10.0

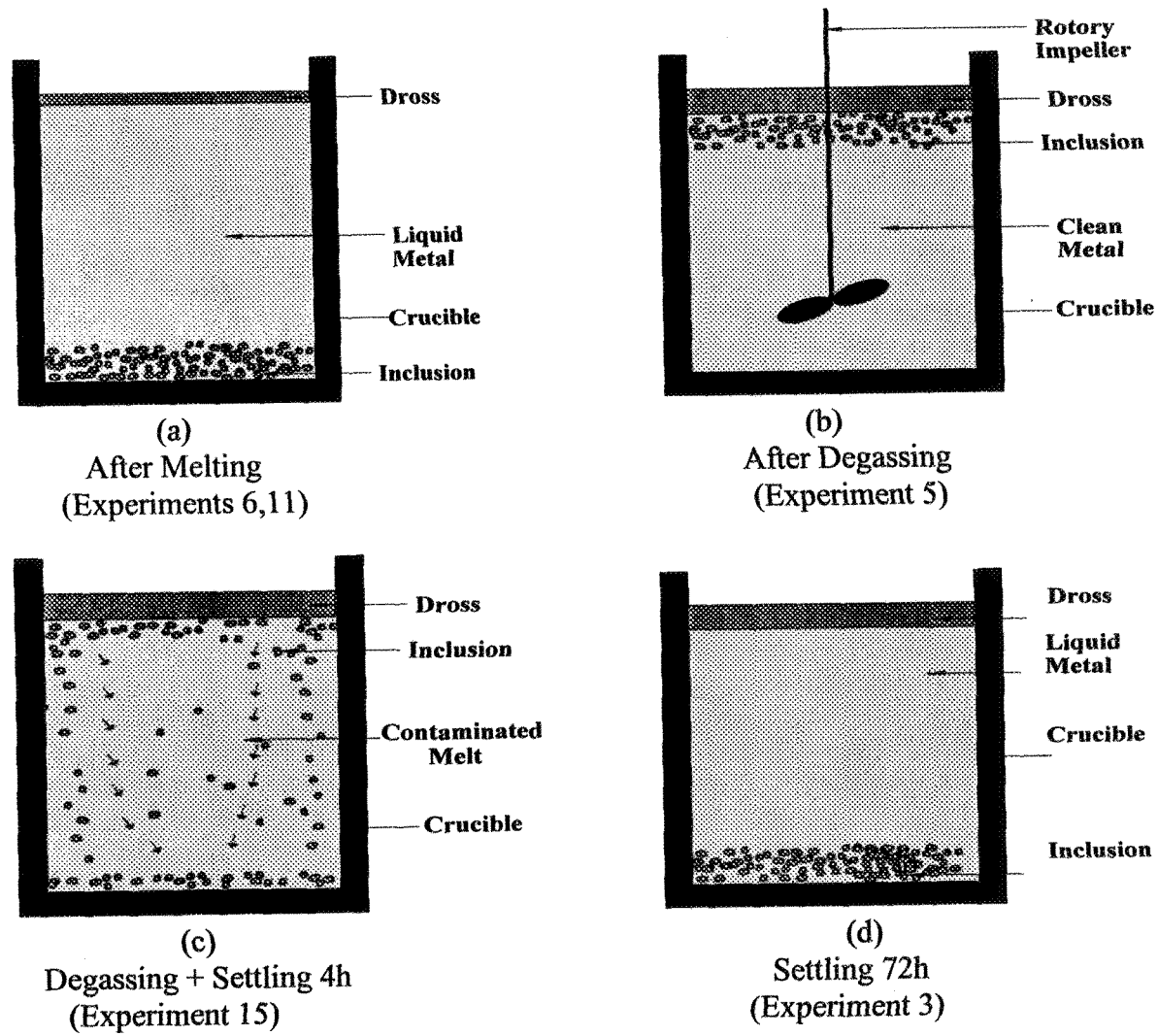

Figure 58 Schematic diagram showing the motion of inclusions under different conditions.

Filtration using ceramic foam filters is one of the most effective methods for inclusion removal. This technique is now being applied in most aluminum foundries [47, 48, 62, 85, 86, 87]. In the present work, round filter discs (50 mm diameter, 15 mm thickness) were mounted at the bottom of cylindrical stainless steel tubes. Both the tube(s) and filter(s) were preheated at 450°C, and placed firmly at the top of the sprue of the Stahl mold prior to casting. The molten metal was then poured through such tubes. Table 35 shows the consistency in tensile properties for castings marked 6A to 6G, which were obtained following such a procedure. The combined effect of degassing and filtering resulted in ductilities as high as 16%, especially for the last castings in the sequence, i.e., those taken from the melt towards the bottom of the melting crucible.

Table 35 Tensile test results of Experiment #6 (fresh alloy).

Experiment #	Y.S. (MPa)	U.T.S. (MPa)	% Elongation
6A1	111.0	277.3	11.1
6A2	117.5	293.5	11.1
6B1	117.0	288.8	8.6
6B2	119.3	291.7	12.1
6C1	112.1	279.8	12.8
6D2	125.7	283.0	9.3
6E1	117.0	292.0	8.0
6E2	112.0	278.6	10.1
6F1	111.3	277.4	7.5
6F2	119.4	298.3	13.9
6G1	116.5	290.2	8.9
6G2	114.7	285.4	11.1
6H1	108.9	271.6	6.9
6H2	118.2	289.1	13.8
6I1	122.0	288.8	12.7
6I2	114.2	284.8	14.6
6J1	117.8	293.2	11.5
6J2	115.5	287.5	11.1
6K1	120.9	301.7	12.7
6K2	115.3	287.6	9.9
6L1	116.3	288.9	17.2
6L2	123.3	304.5	14.7
6M1	116.2	286.6	9.4
6M2	115.6	288.9	7.8
6N1	116.5	289.6	14.9
6N2	113.9	284.1	17.2

Grain refining of an Al-Si casting is normally done through the addition of small amounts of TiB_2 to the melt in the form of Al-Ti-B master alloys [54, 55, 88, 89]. Various types of master alloys can be used, such as Al-10% Ti-1% B, Al-5% Ti-1% B, and Al-7.5% Ti-7.5% B. In the present work, Al-5% Ti-1% B was chosen, being commonly used in aluminum foundries. The amount needed to be added was calculated on the basis of a 0.02 wt% Ti addition. As was earlier observed, such a small amount of Al-Ti-B master alloy is enough to introduce an extremely large number of TiB_2 particles into the melt. These particles act as nucleants for the crystallization of the liquid metal during solidification. Table 36 depicts the maximum properties (castings 9A-9C) and minimum properties (castings 9D-9F), with respect to percentage elongation. It can be seen that although the alloy strength is high, the associated ductilities do not necessarily follow the same trend. Degassing the second half of the liquid metal (i.e., that in the lower portion of the crucible) did not necessarily reduce the difference in percentage elongation obtained from the two test bars produced simultaneously from the same casting. This observation has been explained schematically in Figure 59, where the amount of clean metal (or rather, its depth with respect to the crucible diameter) after degassing is much less than what would be expected from the thickness of the dross and inclusion-rich layers.

Table 36 Tensile test results of Experiment #9 (fresh alloy).

Experiment #	Y.S. (MPa)	U.T.S. (MPa)	% Elongation
9A1	117.3	292.9	9.9
9A2	114.3	285.5	7.8
9B1	108.3	270.6	6.1
9B2	114.5	286.1	6.7
9C2	116.1	290.1	9.2
9D1	116.1	289.9	8.0
9D2	112.1	279.3	8.1
9E1	115.4	288.4	9.3
9E2	116.8	291.9	12.3
9F2	118.3	294.0	11.5
9G1	116.0	289.7	9.6
9G2	113.5	283.5	9.3
9H1	112.9	281.1	7.0
9H2	107.4	268.5	5.5
9I1	119.3	295.8	11.5
9I2	111.3	278.1	7.2
9J1	116.2	290.3	9.4
9J2	154.9	386.8	11.3
9K1	113.4	283.2	14.0
9K2	116.4	290.9	15.8
9L1	117.2	293.0	9.9
9L2	116.1	289.8	13.6

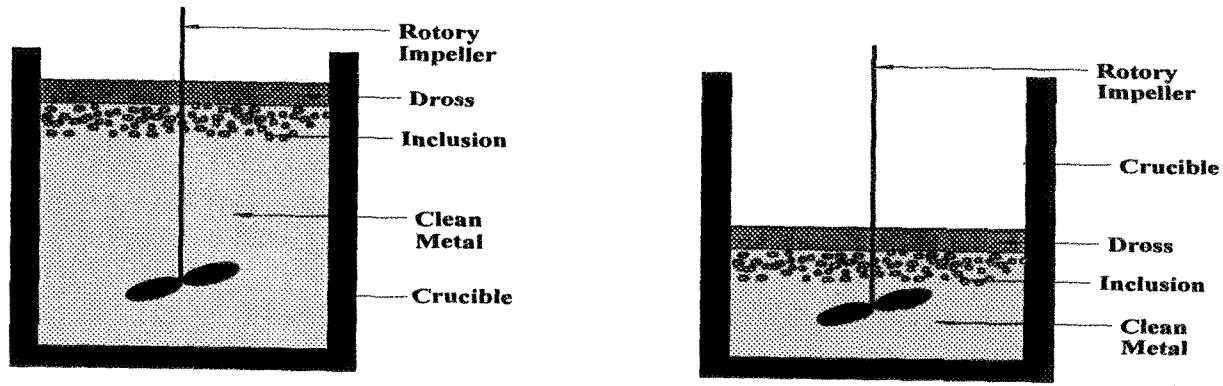

(a)

Full Crucible

(Experiment 5)

(b)

Partially Filled Crucible

(Experiments 6,7,9)

Figure 59 Schematic diagram showing the effectiveness of degassing with respect to amount of liquid metal.

Modification of A356.2 alloy with Sr in the range of 250-300 ppm is recommended in order to change the eutectic Si morphology from acicular to fibrous and enhance the alloy properties [51, 52, 53, 90, 91]. This type of melt treatment is expected to shorten the solution heat treatment time required to achieve more or less complete spheroidization of the eutectic Si partilces. However, the addition of Sr causes a significant increase in the porosity volume fraction which, in turn, affects the alloy strength. Table 37 depicts the tensile properties of Sr-modified alloy obtained in the present study. Apparently, degassing leads to contamination of the liquid metal due to the reason mentioned above. It is expected the porosity associated with the addition -Sr would lower further mechanical properties.

When the liquid metal is held at a sufficiently high temperature, e.g., 735°C, for a lengthy period of time (~72 h), most of the inclusions will settle to the bottom of the crucible. Thus, it is expected that the upper portion of the liquid metal (i.e., that in the upper one-third of the crucible) is reasonably clean, Table 38. Using ceramic foam filters for the next one-third portion of the melt proved to be effective in removing the settled inclusions. As the amount of liquid metal remaining thereafter was not much, degassing resulted in disturbing the settled inclusions at the bottom of the crucible, and, hence, random ductilities.

Table 37 Tensile test results of Experiment #7 (fresh alloy).

Experiment #	Y.S. (MPa)	U.T.S. (MPa)	% Elongation
7A1	113.1	282.7	9.2
7A2	112.7	281.5	10.7
7B1	116.6	291.0	11.7
7B2	111.5	278.7	11.5
7C1	106.7	266.3	7.5
7C2	115.5	288.3	9.4
7D1	107.2	267.7	7.8
7D2	112.8	281.7	11.3
7E1	110.2	275.5	7.2
7E2	114.0	284.7	10.5
7F1	113.7	284.0	9.0
7F2	115.2	287.6	13.5
7G1	106.5	266.1	6.5
7G2	113.7	283.8	8.8
7H1	110.8	276.5	8.5
7H2	116.6	291.0	13.4
7I1	109.4	273.1	13.4
7J1	106.7	266.5	7.4
7J2	113.2	282.9	10.4
7K1	98.2	245.2	5.5
7K2	110.1	274.9	9.2
7L1	99.5	248.6	5.9
7L2	104.7	261.6	7.8
7M1	99.0	247.5	3.7
7M2	115.0	287.3	12.5
7N2	117.6	293.5	12.0
7O1	96.9	242.1	4.4
7O2	111.1	277.4	10.7
7P1	99.5	248.4	4.2
7P2	104.0	259.7	11.3

Table 38 Tensile test results of Experiment #8 (fresh alloy).

Experiment #	Y.S. (MPa)	U.T.S. (MPa)	% Elongation
8A1	112.9	282.1	8.0
8A2	107.5	268.5	6.4
8B1	115.7	288.9	14.5
8B2	114.4	286.0	9.8
8C1	103.4	258.2	4.2
8C2	110.5	275.8	9.2
8D1	112.2	280.3	9.7
8D2	111.4	278.3	6.2
8E1	111.5	278.5	9.3
8E2	110.7	276.8	10.9
8F2	113.8	284.1	8.3
8G1	110.6	276.4	10.5
8G2	113.3	282.9	9.0
8H1	114.4	283.6	12.0
8H2	109.3	273.1	6.9
8I1	115.1	287.6	8.4
8I2	110.1	275.2	6.8
8J1	116.0	289.3	10.8
8J2	111.5	278.4	7.0
8K1	96.3	240.2	2.7
8K2	113.7	284.0	11.0
8L1	91.6	228.1	2.2
8L2	111.4	278.4	7.0
8M1	89.4	223.4	1.9
8M2	112.2	280.4	7.5
8N1	108.9	272.2	7.4
8N2	112.6	281.4	10.7
8O1	95.7	238.8	2.4
8O2	113.5	283.5	6.6

5.3.2 Recycled (Scrap) Alloy

The recycled material used in the present work consisted of a mixture of gates and runners collected from the fresh alloy castings (except those containing TiB_2 and Sr), as well as any remaining metal that was not used for making the test bars. The main type of inclusions observed in the recycled (scrap) alloy was the large number of oxide films that floated to the surface during melting.

Table 39 demonstrates the effect of oxide films on the alloy strength immediately after melting. As can be seen, the ductility improved gradually along the length of the melting crucible (Compare experiment 11A with experiment 11K). Holding the liquid metal at 735°C for a period as long as 72 h led to floatation of most of the oxide films to the upper surface of the molten metal which could be removed easily, and sedimentation of heavy inclusions to the bottom of the crucible. This process resulted in elongations that ranged between 12 and 18 %, Table 40, compared to 4-14% shown in the previous case, Table 39.

One of the serious problems that could occur during melting is if the melt is vigorously stirred : such an operation would disturb a large portion of the oxide films in suspension near the upper surface of the liquid metal, and incorporate them into the bulk of the melt. Their concentration within the melt will determine the alloy properties, Table 41. These properties are found to be more or less comparable with those shown in Table 39. Thus, degassing may be the better way to remove both inclusions and oxide films. The effectiveness of the degassing process will depend directly on the amount of molten metal.

Table 39 Tensile test results of Experiment #11 (scrap alloy).

Experiment	Y.S. (MPa)	U.T.S. (MPa)	% Elongation
11A1	98.1	245.2	4.6
11A2	103.4	258.2	5.1
11B1	105.6	263.6	7.1
11B2	100.2	250.5	4.7
11C1	106.5	170.0	7.4
11C2	103.7	258.9	5.4
11D1	109.8	273.2	6.9
11D2	110.9	277.1	9.1
11E1	113.7	283.8	10.4
11E2	113.8	284.4	10.0
11F1	111.2	277.6	12.1
11F2	112.0	279.6	10.2
11G1	110.5	276.3	8.9
11G2	104.9	262.0	5.6
11H1	111.7	278.8	8.3
11H2	96.9	242.3	10.2
11I1	114.0	176.4	11.0
11I2	110.4	275.8	10.3
11J1	111.0	277.1	13.4
11J2	113.6	284.0	14.5
11K1	111.0	277.2	14.2
11K2	112.3	280.3	13.1
11L1	109.3	273.2	10.5
11L2	114.0	284.5	10.8

Table 40 Tensile test results of Experiment #10 (scrap alloy).

Experiment #	Y.S. (MPa)	U.T.S. (MPa)	% Elongation
10A1	110.8	276.5	16.5
10A2	113.1	282.7	10.0
10B1	112.8	281.7	14.5
10B2	107.7	269.1	7.3
10C1	114.5	286.3	9.5
10C2	114.9	287.1	11.9
10D1	113.7	283.5	13.4
10D2	115.6	288.6	14.8
10E1	114.1	284.7	14.5
10E2	113.9	284.6	15.9
10F1	111.5	278.2	10.5
10F2	113.7	282.0	12.4
10G1	111.3	278.2	9.4
10G2	109.2	272.1	6.3
10H1	114.6	285.5	13.6
10H2	112.3	280.4	11.2
10I1	110.0	274.4	13.0
10I2	115.1	287.5	10.8
10J1	112.5	281.1	10.6
10J2	111.9	279.6	8.2
10K1	97.1	242.5	16.0
10K2	111.2	277.6	11.6
10L1	113.1	282.4	15.8
10L2	112.5	281.2	15.8
10M1	107.7	269.1	12.9
10M2	112.6	281.3	14.8

Table 41 Tensile test results of Experiment #12 (scrap alloy).

Experiment	Y.S. (MPa)	U.T.S. (MPa)	% Elongation
12A1	110.4	275.8	7.6
12A2	110.3	275.7	6.4
12B1	108.6	271.2	7.2
12B2	106.8	266.9	7.5
12C1	106.4	265.8	10.8
12C2	111.6	279.0	8.0
12D1	112.2	280.3	9.4
12D2	111.6	279.0	9.0
12E1	113.9	284.5	11.6
12E2	114.2	181.8	10.3
12F1	114.2	285.1	13.1
12F2	112.8	281.7	12.1
12G1	115.0	287.5	12.3
12H1	114.5	286.2	11.6
12H2	112.4	280.8	8.9
12I1	114.4	285.9	9.8
12I2	120.5	298.4	12.7
12J1	116.0	289.5	17.5
12J2	115.5	288.6	15.5
12K1	112.0	279.8	11.1
12K2	114.8	287.0	12.4
12L1	110.6	276.3	11.4
12L2	113.4	277.3	14.2

The combined effect of sedimentation (72 h at 735°C) and degassing on the alloy tensile properties is shown in Table 42. It is interesting to note the role of settling time in improving the tensile properties of the castings prepared from the melt near to the upper portion of the crucible, whereas degassing tends to enhance the ductilities of castings made from metal close to the crucible bottom. Casting #14G is a good example of inclusion concentration caused by inclusion floatation.

Table 42 Tensile test results of Experiment #14 (scrap alloy).

Experiment #	Y.S. (MPa)	U.T.S. (MPa)	% Elongation
14A1	95.3	256.9	10.9
14A2	95.5	257.3	11.3
14B1	89.2	240.0	5.8
14B2	92.3	249.0	7.9
14C1	93.4	251.7	11.9
14C2	93.2	250.6	12.5
14D1	96.0	258.5	13.3
14D2	93.5	252.1	9.6
14E1	95.8	258.3	12.2
14E2	93.8	252.9	8.8
14F1	97.5	262.9	11.3
14F2	95.1	256.4	10.4
14G1	91.3	246.0	5.2
14G2	93.7	252.2	10.4
14H1	95.1	256.6	11.9
14H2	92.9	250.4	9.2
14I1	94.0	253.3	12.7
14I2	84.3	227.2	6.0
14J1	93.6	252.3	8.4
14J2	95.3	257.0	13.2
14K1	92.5	249.4	15.4
14K2	91.6	246.7	13.6

Filtration of liquid aluminum with 10 ppi ceramic foam filters is an important process of inclusion/oxide removal. Table 43 shows that due to flotation of oxide films to the upper surface of the liquid metal, filtration with 10 ppi filters might not be very effective, and a finer filter size (i.e., 20 ppi) would be more appropriate. It is also observed that the alloy elongation improves gradually with increasing casting sequence. Applying degassing reduces the tensile properties of the first casting (i.e., 13H), as explained schematically in Figure 59. Beyond that, the alloy exhibits consistent improvement (13L).

Table 43 Tensile test results of Experiment #13 (scrap alloy).

Experiment #	Y.S. (MPa)	U.T.S. (MPa)	% Elongation
13A1	107.6	268.9	5.4
13A2	108.0	269.7	5.6
13B1	107.2	268.0	9.0
13B2	70.8	176.9	8.7
13C1	115.2	287.9	10.9
13C2	110.3	275.4	5.9
13D1	118.4	295.8	9.3
13D2	115.4	288.3	10.3
13E1	117.7	293.9	10.9
13E2	109.1	272.5	11.4
13F1	115.3	287.6	11.3
13F2	113.1	282.6	10.0
13G1	117.3	293.2	14.3
13G2	114.0	285.1	10.9
13H1	111.3	278.0	9.2
13H2	102.8	256.8	8.0
13I1	116.7	291.5	7.9
13I2	115.2	288.0	13.7
13J1	103.5	258.4	12.3
13K2	115.1	287.5	9.6
13L1	115.2	287.8	9.5
13L2	116.2	290.1	13.3

Tables 44 and 45 summarize the average tensile properties of the A356.2 alloy studied for the different experimental conditions listed in Table 30.

Table 44 Average tensile properties of A356.2 alloy (fresh alloy).

Experiment #	Y.S. (MPa)	U.T.S. (MPa)	% Elongation
3	106.5 ± 4.8	264.5 ± 8.3	13.2 ± 2.8
4	111.9 ± 4.3	279.2 ± 10.7	11.0 ± 3.4
5	116.7 ± 6.3	288.7 ± 12.4	17.6 ± 19.7
15	111.2 ± 5.1	277.6 ± 12.8	11.4 ± 4.
6A - 6G	116.1 ± 4.3	286.3 ± 7.1	10.4 ± 2.0
6H - 6N	116.8 ± 3.6	289.1 ± 7.7	12.4 ± 3.2
9A - 9F	114.9 ± 2.9	286.9 ± 7.2	8.9 ± 2.0
9G - 9L	117.9 ± 12.1	294.2 ± 30.1	10.3 ± 3.1
7A - 7H	112.3 ± 3.3	280.4 ± 8.2	9.8 ± 2.1
7I - 7P	106.1 ± 6.8	264.9 ± 17.0	8.5 ± 3.3
8F - 8J	112.7 ± 2.4	281.2 ± 5.7	8.9 ± 1.9
8K - 8O	104.5 ± 10.0	261.0 ± 25.1	5.9 ± 3.5

Table 45 Average tensile properties of A356.2 alloy (scrap alloy).

Experiment #	Y.S. (MPa)	U.T.S. (MPa)	% Elongation
11	108.7 ± 5.1	262.9 ± 30.3	9.3 ± 3.0
10	111.8 ± 3.7	279.2 ± 9.1	12.4 ± 2.9
14A - 14F	94.2 ± 2.2	253.9 ± 5.9	10.5 ± 2.2
14G - 14K	92.4 ± 3.2	249.1 ± 8.5	10.6 ± 3.4
12A - 12F	111.1 ± 2.7	268.9 ± 28.1	9.4 ± 2.2
12G - 12L	114.5 ± 2.6	285.2 ± 6.4	12.5 ± 2.5
13A - 13G	109.9 ± 11.9	274.7 ± 29.8	9.6 ± 2.5
13H - 13N	112.0 ± 5.7	279.8 ± 14.3	10.4 ± 2.3

For castings made from fresh ingots, degassing of a large quantity of liquid metal (viz., a full crucible in the present case) seems to be the best method for inclusion removal and, hence, for achieving the highest percentage elongation. However, when applied to a very limited amount of liquid metal, degassing causes liquid contamination instead, leading to the lowest values of elongation observed. When the castings are made from recycled material, the obtained ducilities are more or less the same, regardless of the type of melt treatment. This observation may be explicable in terms of the large amount of oxide films present in the recycled alloy melts.

5.3.3 Ductility - Percentage Inclusion Relationship

Figures 60(a) through 60(g) show the size and distribution of non-metallic inclusions/oxide films found on the fracture surfaces of test bars obtained from fresh alloy. Similarly, the inclusions observed on the fracture surfaces of test bars obtained from scrap are shown in Figure 61. The volume fractions of inclusions/oxides were measured from photographs similar to those shown in Figures 60 and 61, using the point count method. A linear relationship between percentage elongation and log percentage inclusions was obtained, and is presented in Figure 62. This relationship, expressed as,

$$\text{Percentage Elongation} = 9.5 - 2.98 \log \text{Percentage Inclusions/Oxide Films}$$

had a fitness coefficient $R^2 \sim 0.9$, indicating the good relation between the two parameters.

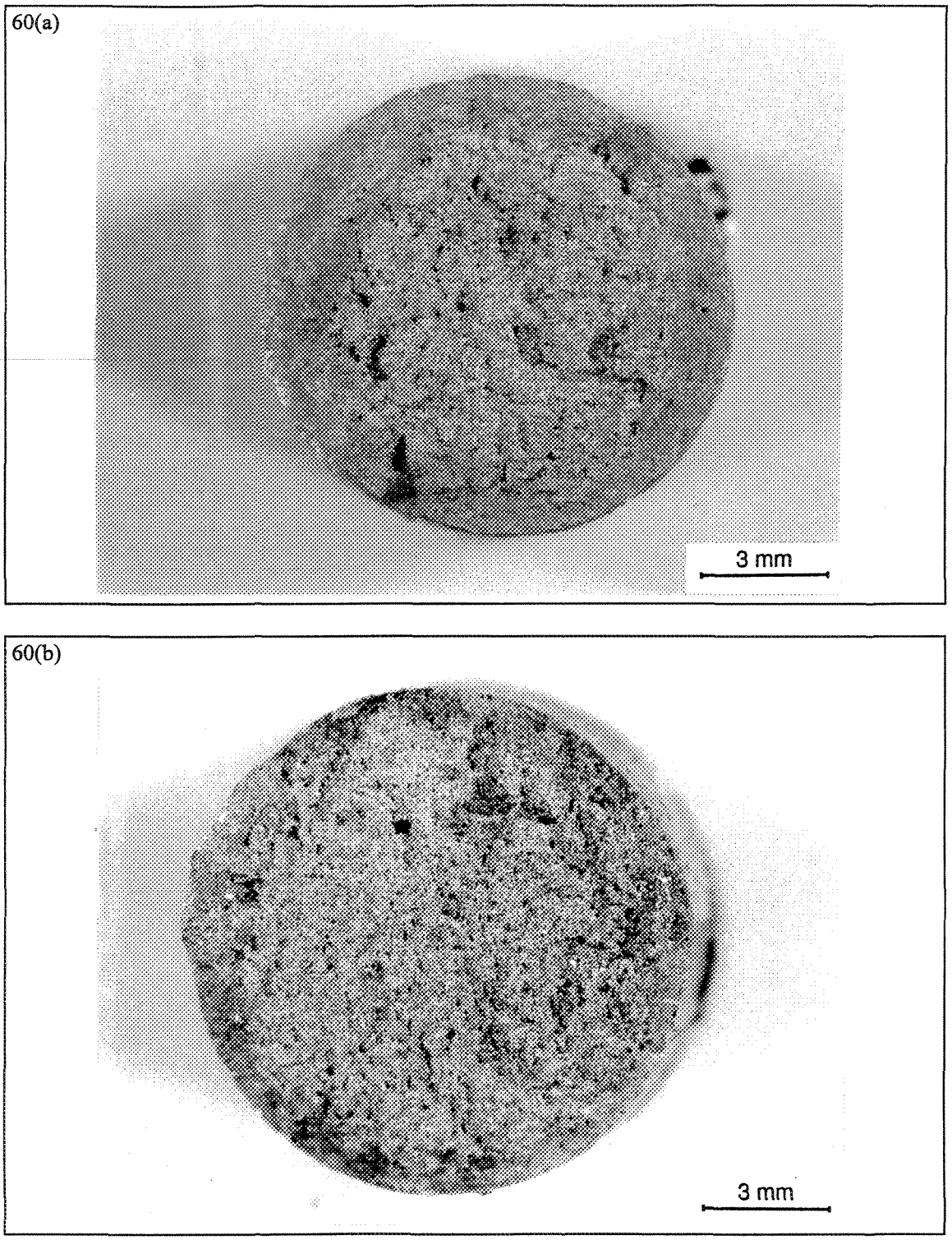

Figure 60 Optical macrographs showing the size and distribution of non-metallic inclusions/oxide films in tensile-tested bars obtained from fresh alloy, and corresponding to elongations of: a) 19%, b) 16%.

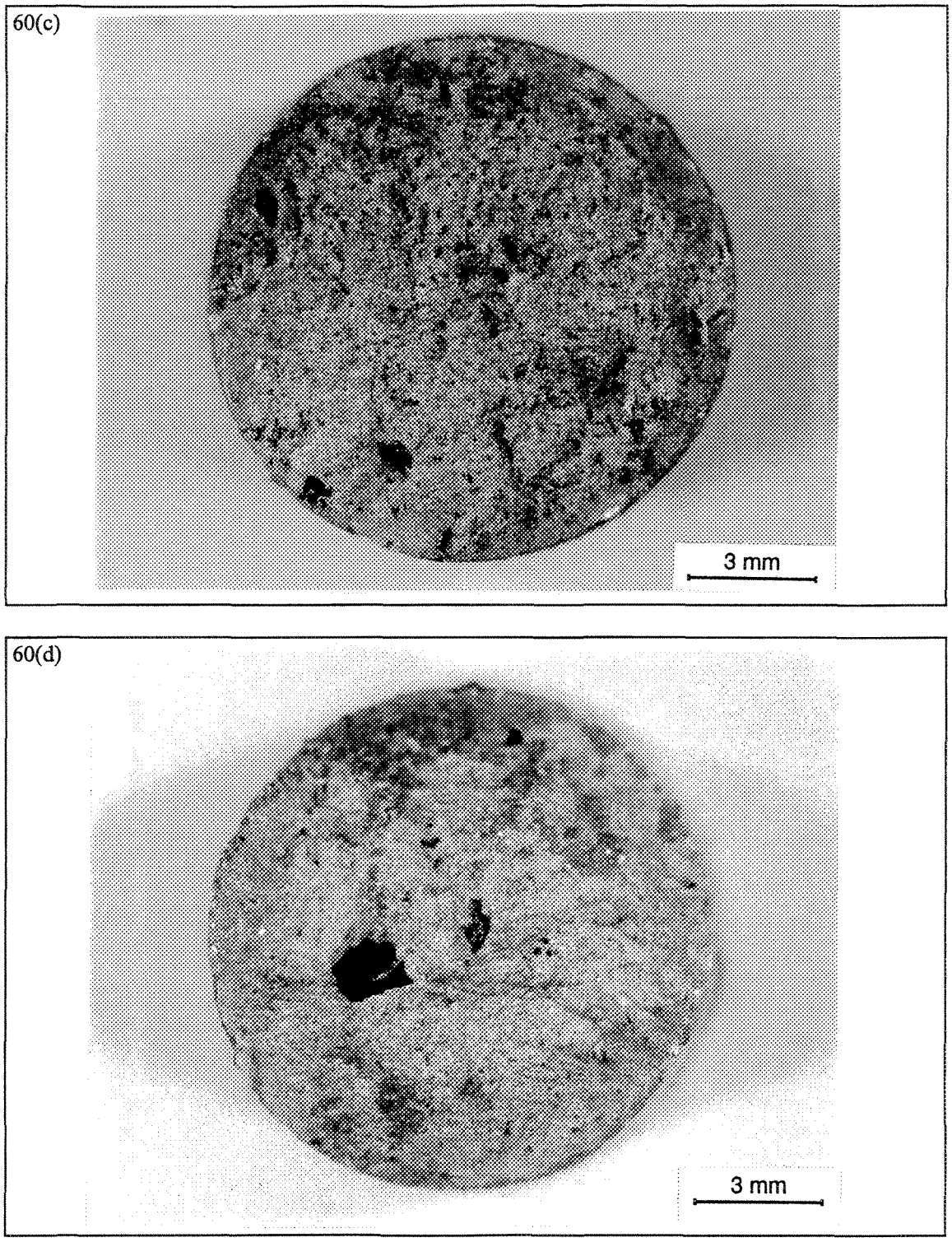

Figure 60 Optical macrographs showing the size and distribution of non-metallic inclusions/oxide films in tensile-tested bars obtained from fresh alloy, and corresponding to elongations of: c) 10%, d) 8%.

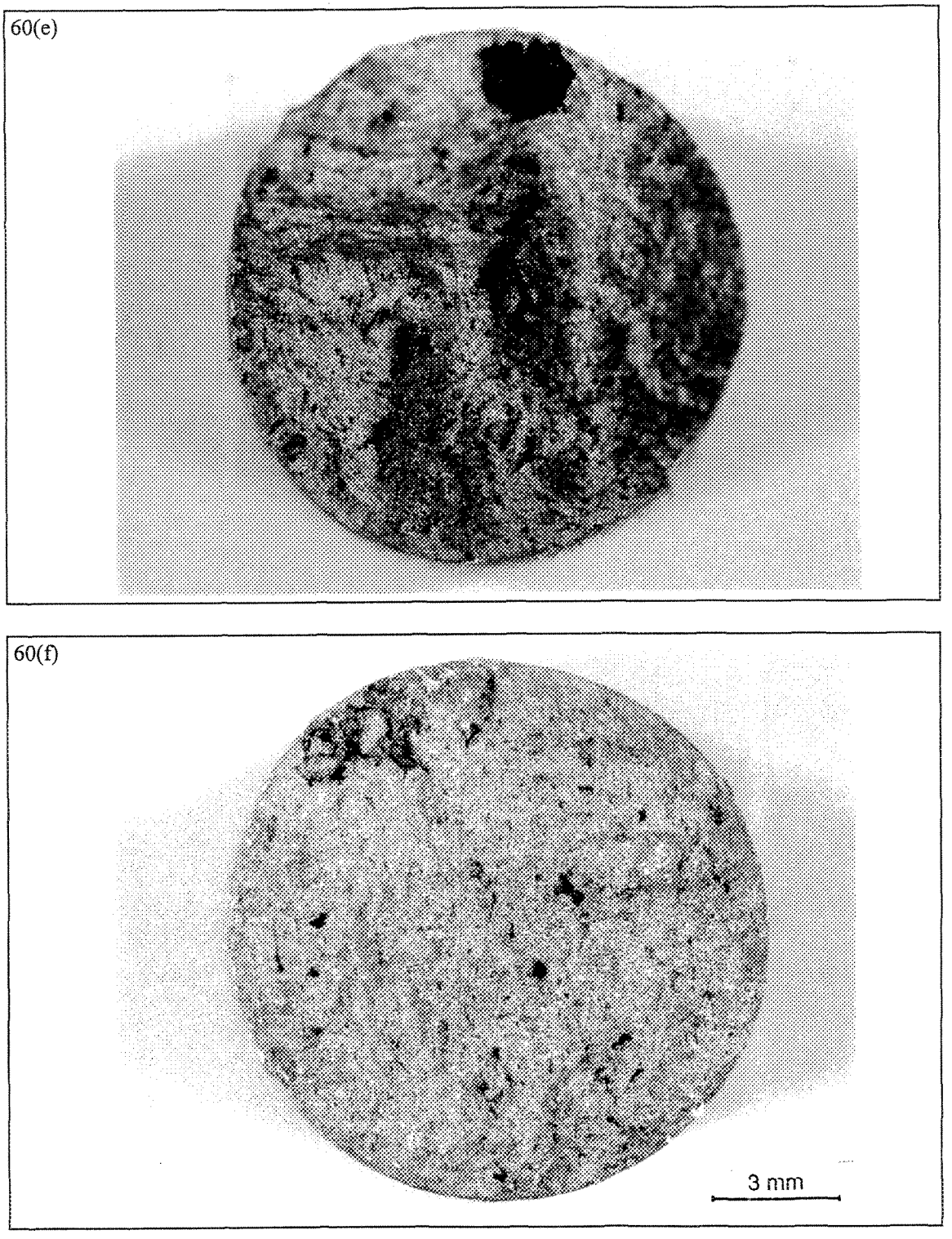

Figure 60 Optical macrographs showing the size and distribution of non-metallic inclusions/oxide films in tensile-tested bars obtained from fresh alloy, and corresponding to elongations of: e) 5%, f) 3.5%.

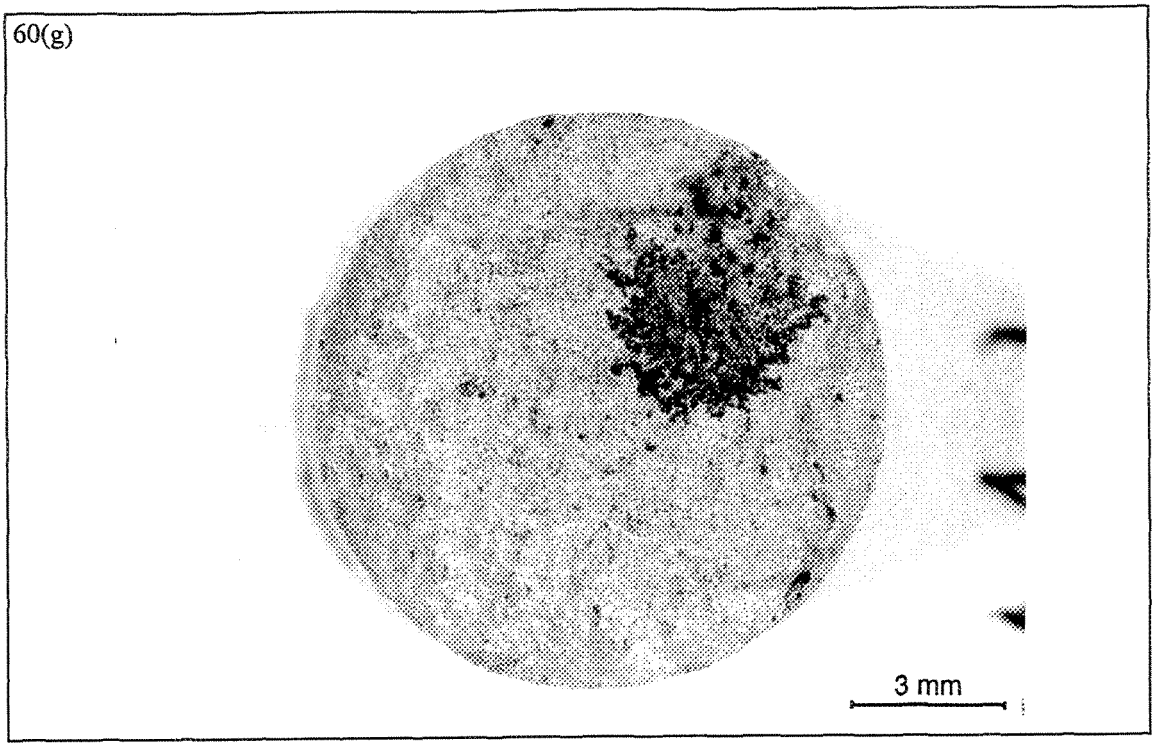

Figure 60 Optical macrographs showing the size and distribution of non-metallic inclusions/oxide films in tensile-tested bars obtained from fresh alloy, and corresponding to elongations of: a) 19%, b) 16%, c) 10%, d) 8%, e) 5%, f) 3.5%, g) 1.5%.

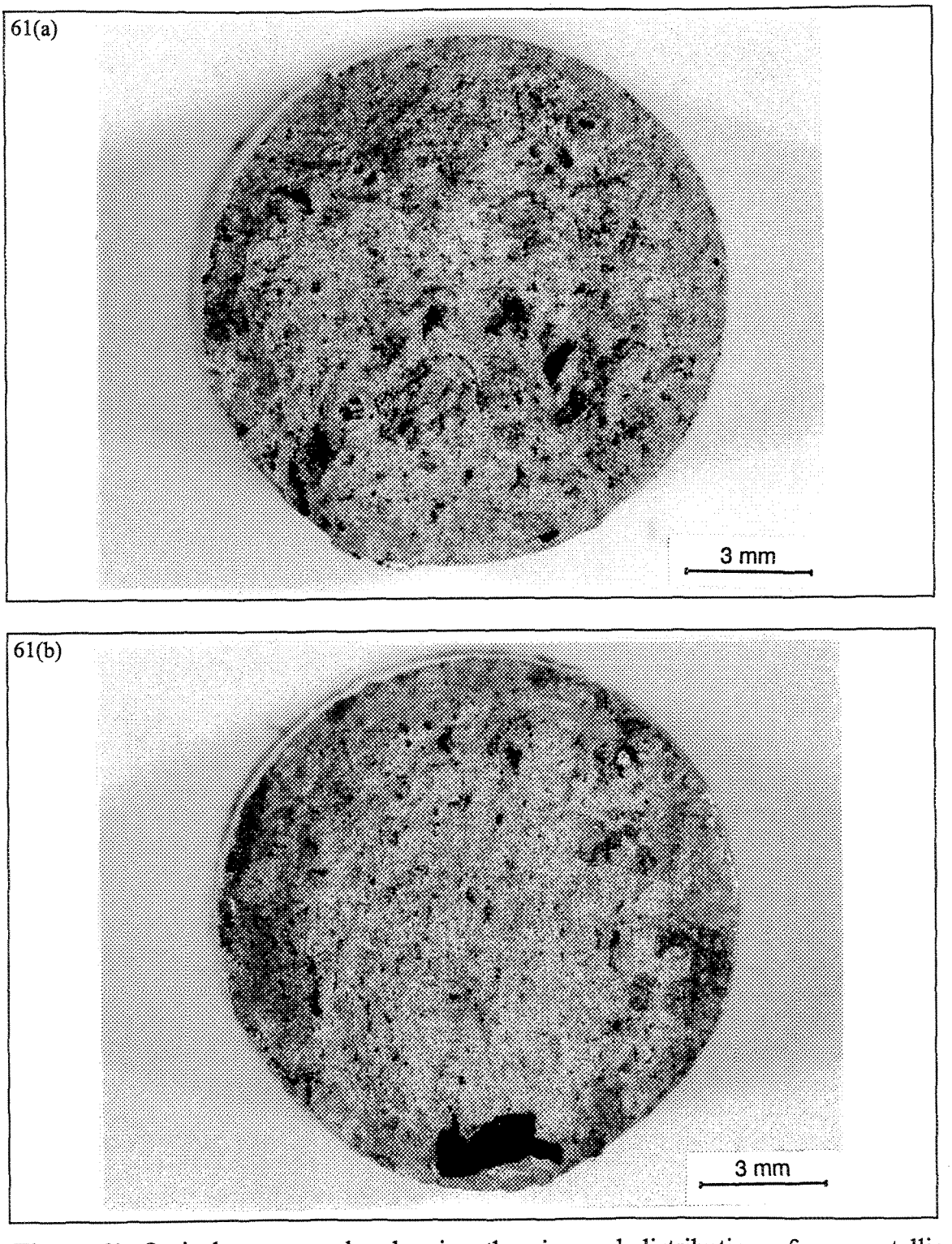

Figure 61 Optical macrographs showing the size and distribution of non-metallic inclusions/oxide films in tensile-tested bars obtained from recycled (scrap) alloy, and corresponding to elongations of a) 7.5%, b) 5%, c) 3.5%.

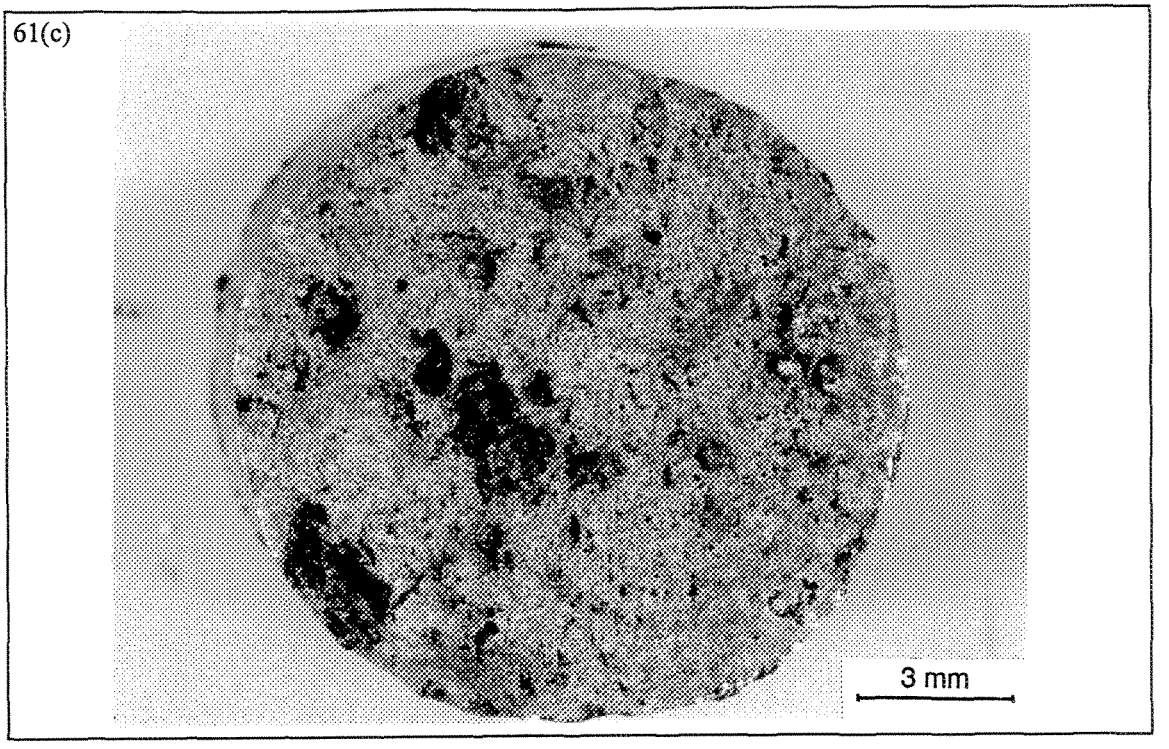

Figure 61 c) 3.5%.

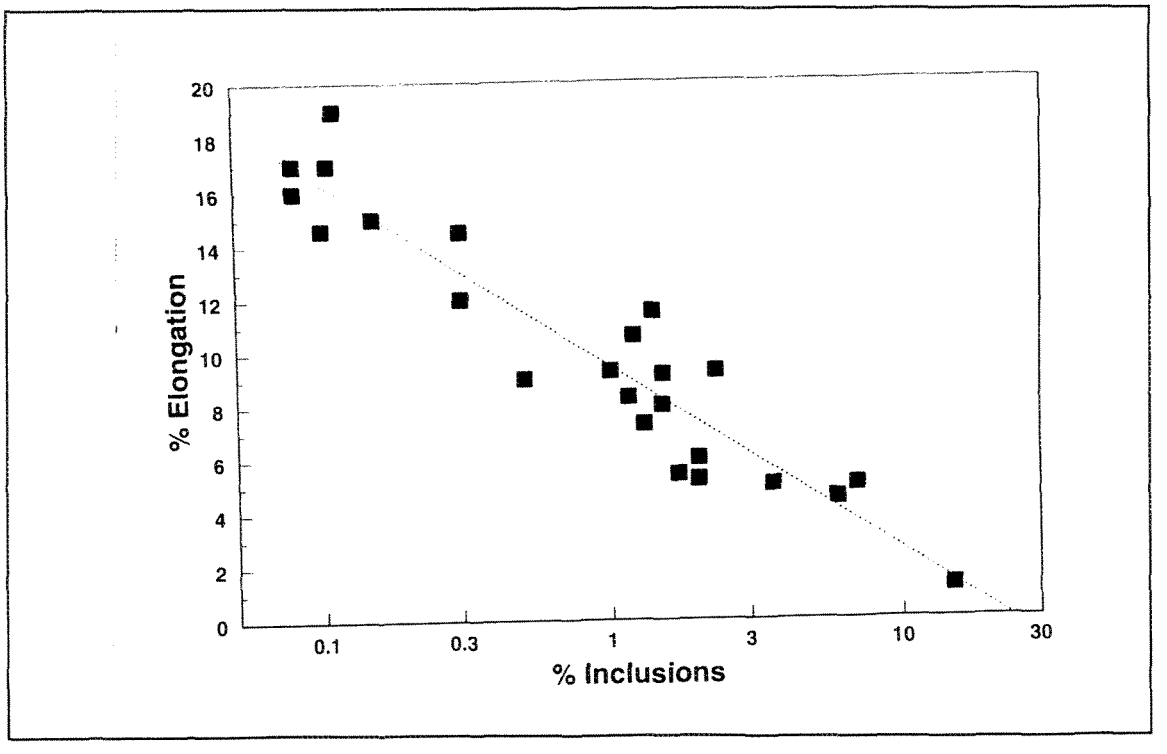

Figure 62 Percentage Elongation-log Percentage Inclusions/Oxide Films relationship.

Table 46 lists the total inclusion, harmful inclusion and oxide film concentrations as measured by the PoDFA technique [75, 92], and the corresponding tensile properties measured for similar melt experimental conditions. It is evident from this table that the oxide films have a far more deleterious effect on the mechanical properties. This observation matches well with the oxides observed in Figures 60 and 61.

5.3.4 Fractography

As shown in the previous chapters, the main oxide inclusions in A356.2 alloy melts held for a long period i.e. 72 h at 735°C are aluminum oxide (Al_2O_3) and spinel ($MgAl_2O_4$). Due to plastic deformation during tensile loading, these oxides tend to break into small fragments that are segregated in certain locations, as shown in the optical macrograph of Figure 60(g). The corresponding SEM micrograph, Figure 63(a), reveals the presence of small particles (arrowed) on the fracture surface. A high magnification fractograph, Figure 63(b), shows how the flow of liquid aluminum (shiny phase) is trapped within some of these oxide particles.

An interesting feature is exhibited in Figure 63(c), where a large particle of spinel (as confirmed by the associated EDX spectrum, shown in Figure 64) is seen debonded from the surrounding matrix (arrowed). Such type of decoherence would weaken the alloy, leading to premature failure. Another example of decohesion between oxide particles and the matrix is shown in Figure 63(d), where a lump of wrinkled layers of oxide films is seen. The arrow in Figure 63(d) indicates the passage of a crack through the oxide film.

Table 46 Inclusion/oxide - tensile properties relationships for A356.2 alloy.

S.No.	Total Inclusions (mm^2/kg)	Harmful Inclusions (mm^2/kg)	Oxide Film Classification		Y.S. (MPa)	U.T.S. (MPa)	EL%
			Thin	Thick			
1	0.06	0.02	None	None	123.40	310.10	19.20
2	0.02	0.02	Moderate	Moderate	118.54	294.43	14.82
3	0.24	0.02	Moderate	Moderate	116.60	290.61	13.88
4	0.68	0.24	Moderate	Moderate	112.52	281.16	13.38
5	0.17	0.14	Light	Moderate	108.61	271.13	13.16
6	0.54	0.19	Moderate	Moderate	114.45	284.68	13.15
7	0.18	0.15	Light	Light	118.03	294.58	12.66
8	0.03	0.01	Moderate	–*	112.25	253.31	12.29
9	0.37	0.22	Light	Light	112.70	280.06	12.26
10	4.24	3.78	None	None	104.35	260.70	11.54
11	0.24	0.19	Heavy	Moderate	111.81	279.28	11.31
12	0.85	0.21	Light	Light	114.00	284.83	10.93
13	0.36	0.29	Moderate	Light	115.47	288.44	10.78
14	0.01	0.00	Heavy	–*	112.65	281.34	10.67
15	1.41	1.12	Heavy	Moderate	111.36	278.27	10.60
16	0.64	0.35	Moderate	Moderate	115.59	287.79	10.03
17	1.25	0.36	Moderate	Moderate	114.92	286.61	9.85
18	0.05	0.03	Moderate	Heavy	110.46	276.02	9.32
19	0.03	0.03	Heavy	Heavy	114.80	286.83	9.11
20	0.04	0.01	Moderate	–*	106.01	264.83	8.24
21	1.68	0.08	Light	–*	113.61	283.79	7.63
22	0.03	0.01	Moderate	–*	107.73	244.76	7.21
23	0.10	0.07	Heavy	Heavy	98.39	245.87	7.18
24	0.93	0.48	Moderate	Moderate	109.25	272.51	6.95
25	0.04	0.02	Moderate	Heavy	101.82	254.35	5.36
26	1.40	1.12	Heavy	Heavy	89.40	223.40	1.94

Note: * Classification indeterminable

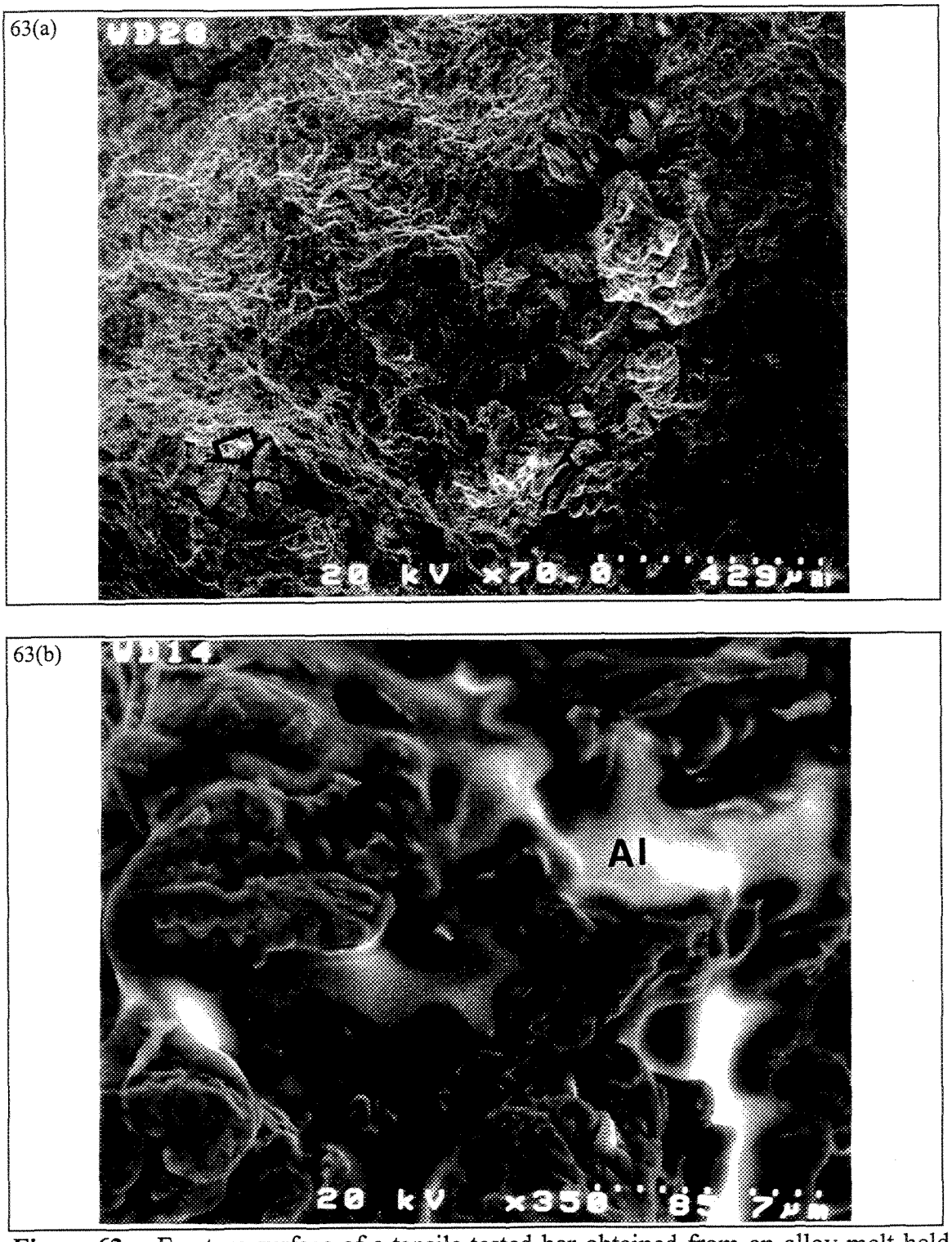

Figure 63 Fracture surface of a tensile tested bar obtained from an alloy melt held for 72 h at 735°C, showing: a) fragmentation of oxides particles (corresponding to Fig. 60(g)), b) presence of liquid aluminum entrapped within oxide film particles.

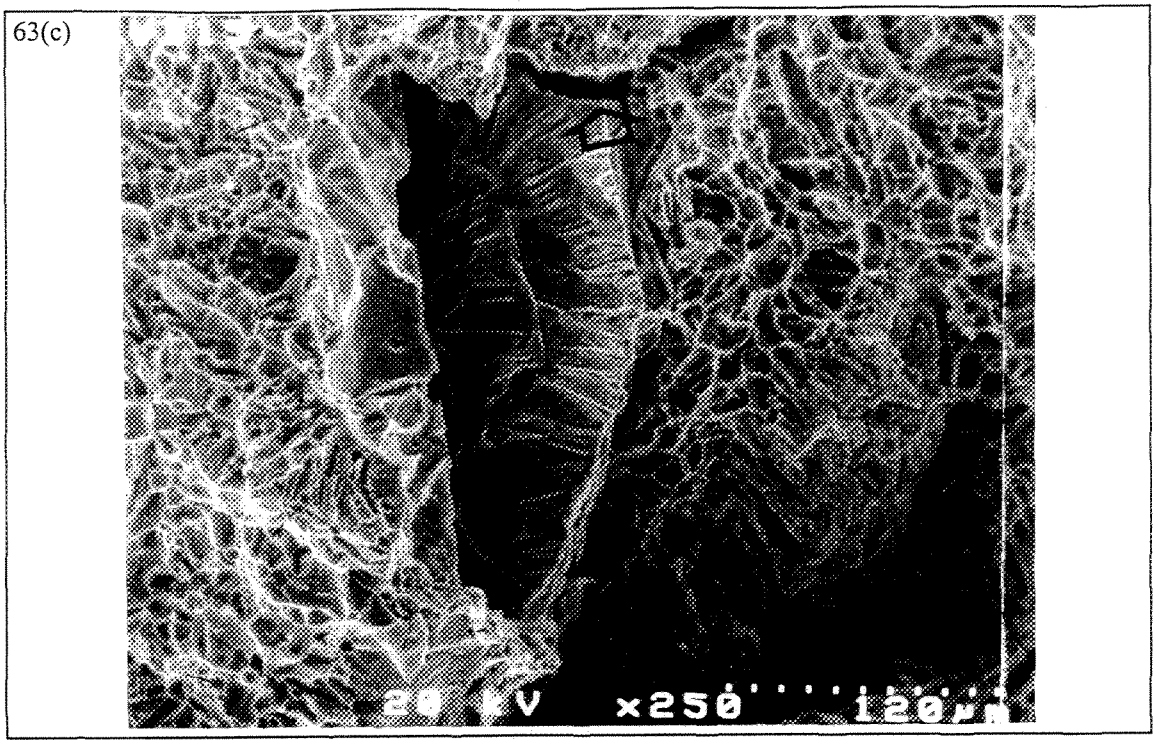

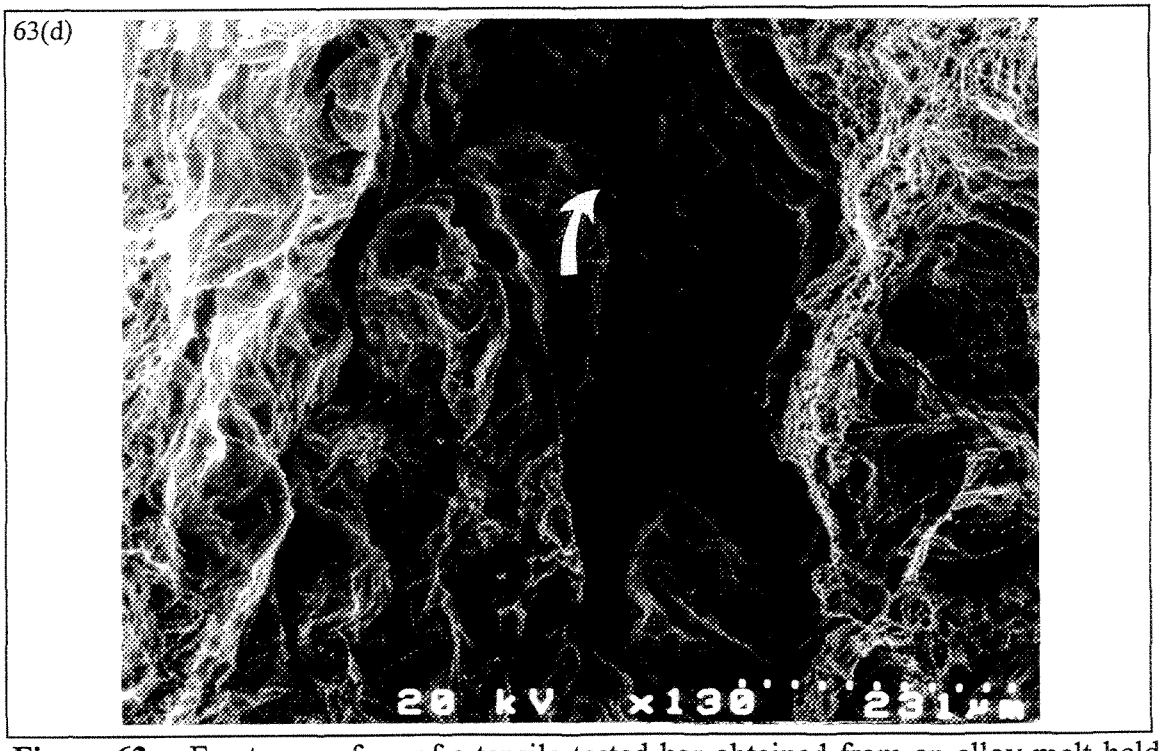

Figure 63 Fracture surface of a tensile tested bar obtained from an alloy melt held for 72 h at 735°C, showing: c) debonding of a large spinel particle from the surrounding matrix, d) a crumpled mass of oxide films (the arrow denotes the crack path).

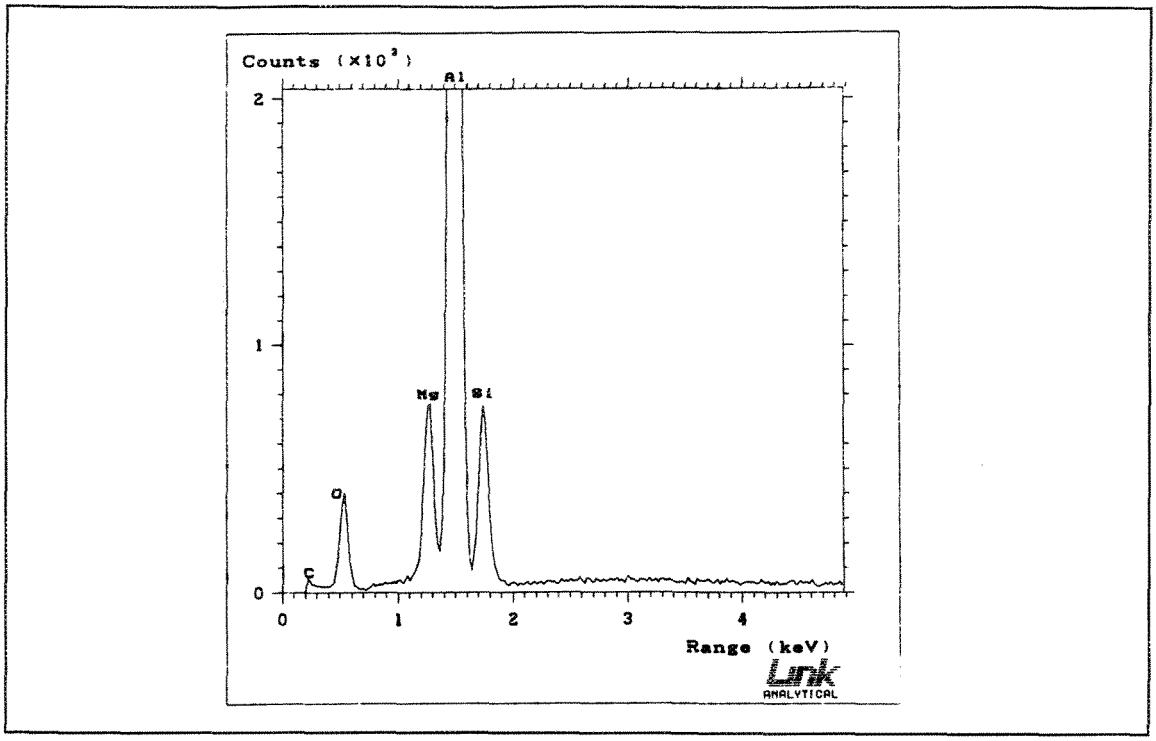

Figure 64 The energy dispersive X-ray (EDX) spectrum corresponding to the arrowed particle in Fig. 63(c), showing strong reflections due to O, Mg and Al.

Besides the spinel particles, the other main type of defect observed on the fracture surface is the presence of large volume fractions of Al_2O_3 oxide films, in the form of crumpled layers. These films occur randomly in the melt and, hence, test bars. Figures 65(a) and 65(b) depict examples of these films near the edge and the center of the test bar, respectively. The associated EDX spectrum, Figure 66, shows strong reflections due to Al and O, and a very weak Mg reflection, indicating the presence of small amounts of MgO and spinel ($MgAl_2O_4$).

65(a)

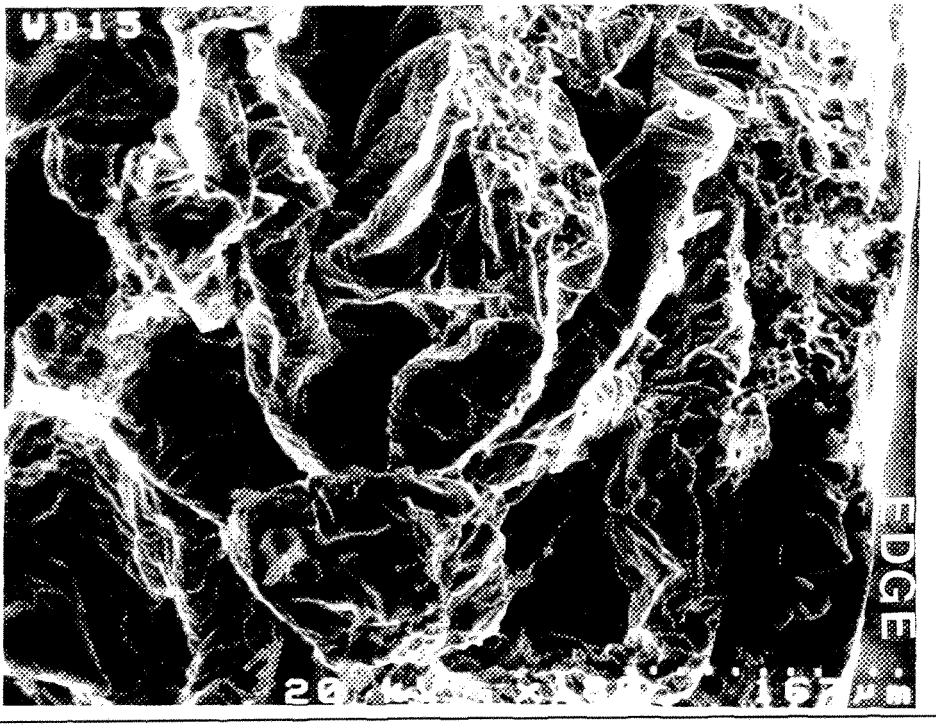

65(b)

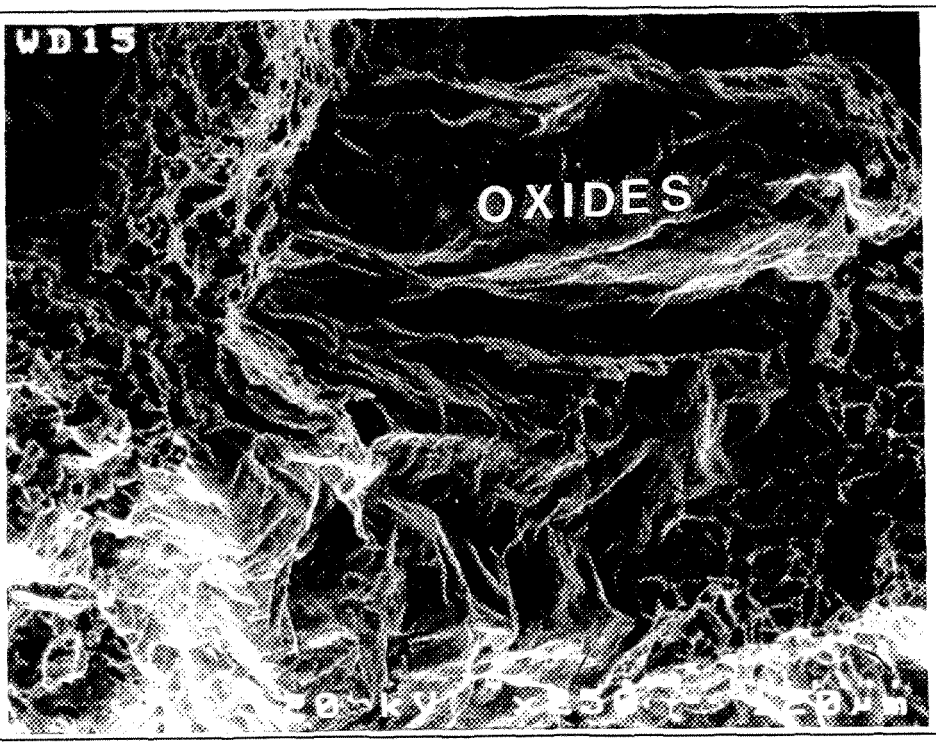

Figure 65 Fracture surface of a tensile-tested bar obtained from recycled alloy, showing a crumpled mass of oxide films: a) near the edge, and b) close to the centre of the test bar.

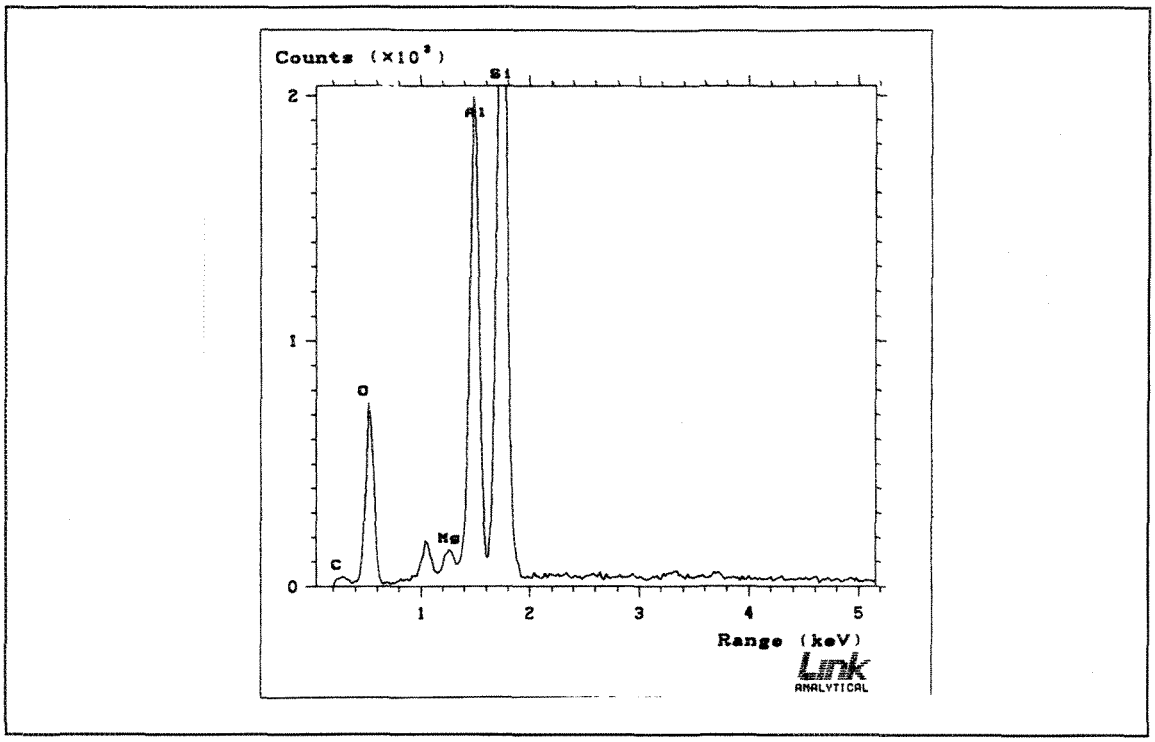

Figure 66 Typical energy dispersive X-ray (EDX) spectrum corresponding to the Al_2O_3 oxide films shown in Fig.65(a). Note the very weak Mg reflection.

The effect of oxide particles or films in weakening the alloy through the initiation of cracks at their interfaces with the matrix is best illustrated by Figure 67. It is evident from these fractographs that due to difference in the rigidity (measured by Young's modulus) of the matrix and inclusions, the crack initiates easily at particle/matrix interfaces, leading to rapid crack propagation, large crack paths, and, hence, early failure.

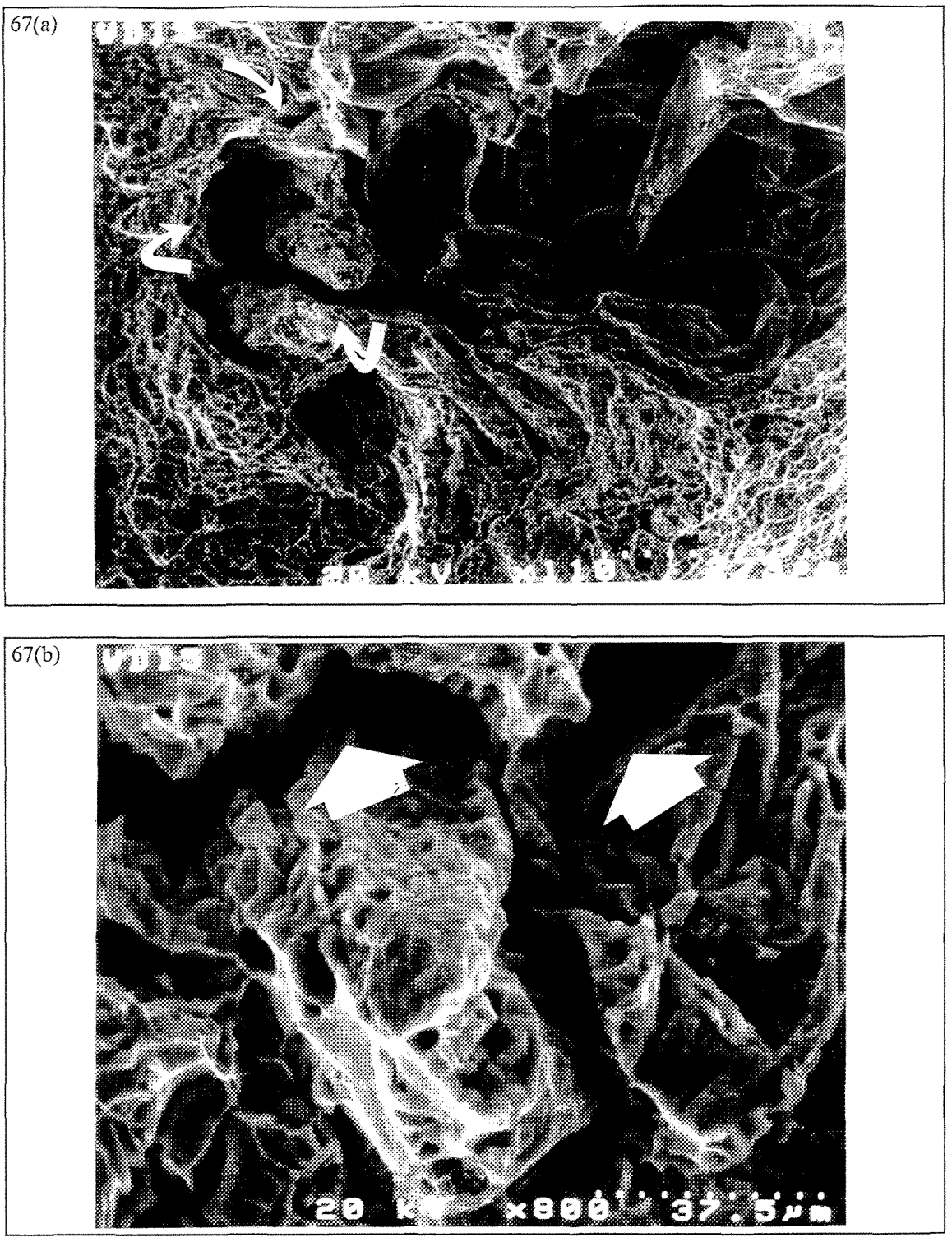

Figure 67 Fracture surfaces showing crack paths located at oxide/matrix interfaces in the samples corresponding to those shown in a) Fig.61(a), and b) Fig.61(c).

CHAPTER 6

CONCLUSIONS

CHAPTER 6

CONCLUSIONS

The present study was carried out to investigate the role of the major operating parameters applied in aluminum foundries and that of minor alloying element additions on inclusion formation in A356.2 and C357 Al-Si casting alloys, using the PoDFA technique. The types and concentrations of inclusions and oxide films that occurred in the alloy melts prior to casting were identified and measured. The tensile properties of A356.2 alloy were also studied for the same melt conditions to study the relationship between the inclusions present and the obtained properties.

From an analysis of the results obtained as reported in Chapters 3, 4 and 5, the following conclusions may be drawn.

1. Mechanical stirring is one of the major parameters that contaminates the molten metal with inclusions. Degassing, on the other hand, using a rotary impeller, is very effective in removing the inclusions through floatation into the upper portion of the crucible. The thickness of the layer rich in inclusions, however, is determined by the degassing time and the amount of inert gas purged into the molten metal. Thus, mechanical stirring normally used to ensure dissolution of grain refiners or modifiers may be replaced by degassing using a rotary impeller.

2. Addition of alloying elements such as Sr, Fe, Mn, Cr, Be does not lead to inclusion formation if mechanical stirring is avoided. Another way of adding the alloying elements is by employing degassing as mentioned in 1.

3. With respect to the preparation of the tensile test bars using a Stahl mold, the use of ceramic foam filters in the pouring cup would greatly help in removing the oxide films provided the pouring cup (containing the filter) is placed tightly at the top of the downsprue of the Stahl mold without air gaps, to avoid metal re-oxidation. Filtration using 10 or 20 ppi ceramic foam filters is highly recommended for inclusion removal in dry atmospheres.

4. A long holding time may lead to the sedimentation of several inclusions. However, in the case of Mg-containing alloys (i.e., 356 and 357), lengthy holding periods would accelerate the formation of high concentrations of cuboides and spinels near the surface.

5. The weight of dross increases with the increase in holding period of the molten metal at temperatures in the range 735 ± 5°C. The dross is always wet with the molten metal. Spinel is the main inclusion observed to form. Its amount is enhanced by the increase in either the Mg content (i.e., C357 alloy), or holding time (~72 h). Carbides, such as Al_4C_3, may also occur.

6. Oxides (films or clusters) are the most influential parameter in determining the filtration time when using the PoDFA technique. However, during sampling, it is rather difficult to separate the individual effects of inclusions and oxides on the filtration time, more so if the molten metal is disturbed or not properly skimmed.

7. Although the PoDFA technique is a powerful tool in determining both inclusion types and their densities, the process is fairly long. Thus, an in-line measuring apparatus such as the LiMCA may be recommended, especially in the preparation of critical components for aeronautical applications.

8. In the case of fresh alloy melts, and under very dry conditions (humidity ~ 10-13%), melt cleanliness by sedimentation, i.e., holding the liquid metal at 735 C for ~72 h, results in the settlement of inclusions to the bottom of the melting crucible, leading to good mechanical properties. Increase in the humidity level, however, will introduce hydrogen to the melt, and result in a large amount of porosity formation, deleterious to the mechanical properties.

9. Degassing using a rotary impeller appears to be the most effective method for removing both hydrogen and inclusions provided it is applied to a reasonably large amount of liquid metal. The first casting, however, should be rejected, since it is taken from the melt surface layer that is rich in inclusions/oxides.

10. In the case of recycled (scrap) alloy melts, holding the liquid metal for a lengthy period of time also improves the melt cleanliness, similar to that observed for fresh alloy melts. Due to the presence of excessive amounts of inclusions and oxide films in such melts, however, degassing and/or filtration may be a more appropriate procedure to follow.

11. In both fresh and recycled alloy castings, cracks are initiated at the inclusion (or oxide film) - matrix interface, followed by their relatively rapid propagation, leading to the formation of large crack paths through the matrix and, hence, premature failure.

REFERENCES

References

1 J.E. GRUZLESKI and B.M. CLOSSET, "The Treatment of Liquid Aluminum-Silicon Alloys", American Foundrymen's Society, Inc., Des Plaines, Illinois, (1990).

2 D.V. NEFF, "The Filtering and Degassing of Aluminum Die Casting Alloys", Die Casting Engineer, vol. 30 (1986), p. 18-24.

3 G. LASLAZ and P. LATY, "Gas Porosity and Metal Cleanliness in Aluminum Casting Alloys", AFS Transactions, vol. 99 (1991), p. 83-90.

4 C.J. SIMENSEN and G. BERG, "A Survey of Inclusions in Aluminum", Aluminium, vol. 56 (1980), p. 335-340.

5 D. APELIAN and S. SHIVKUMAR, "Molten Metal Filtration - Past, Present and Future Trends", Proceedings of the 2nd International Conference on Molten Aluminum Processing, Orlando, Florida, November 6-7, 1989, American Foundrymen's Society, Des Plaines, Illinois USA, (1989), p. 14.1-14.36.

6 D.K. LEWIS, "Control of Hardspot Inclusions in Aluminum Die Casting", Die Casting Engineer, vol. 35 (1991), p. 18-22.

7 M.J. LESSITER and W.M. RASMUSSEN, "To Pour or Not to Pour - The Dilemma of Assessing Your Aluminum Melt's Cleanliness", Modern Casting, vol. 86 (1996), p. 45-48.

8 C.E. ECKERT, "Inclusions in Aluminum Foundry Alloys", Modern Casting, vol. 81 (1991), p. 28-30.

9 Metals Handbook, (9th Edition), vol.15 : Casting, American Society for Metals, Metals Park, OH (1988).

10 H. HU and A. LUO, "Inclusions in Molten Magnesium and Potential Assessment Techniques", JOM, vol. 48 (1996), p. 47-51.

11 N.D.G. MOUNTFORD and R. CALVERT, "Precipitation Effects in Liquid Aluminum Alloys: Experiments with A Pulsed Ultrasonic Technique", J. Institute of Metals, vol. 88 (1959-60), p. 121-127.

12 J.P. MARTIN and F. PAINCHAUD, "On-Line Cleanliness Determination in Molten Aluminum Alloys Using the LiMCA II Analyser", Light Metals (1994), p. 915-920.

13 D.A. BATES and L.C. HUTTER, "An Evaluation of Aluminum Filtering Systems Using a Vacuum Filtration Sampling Device", Light Metals (1981), p. 707-721.

14 J.L. ROBERGE and M. RICHARD, "Qualiflash Apparatus for Testing the Inclusion Quality of Aluminum Alloy Baths", Proceedings of the 4th International Conference on Molten Aluminum Processing, Orlando, Florida, November 12-14, 1995, American Foundrymen's Society, Des Plaines, IL (1996), p. 29-42.

15 X.G. CHEN, R.I.L. GUTHRIE and J.E. GRUZLESKI, "Quantitative Measurement of Melt Cleanliness in Aluminum-Silicon Casting Alloys", Proceedings of the 4th International Conference on Molten Aluminum Processing, Orlando, Florida, November 12-14, 1995, American Foundrymen's Society, Des Plaines, IL (1996), p. 15-28.

16 S. SHIVKUMAR, D. APELIAN and H. BRUCHER, "Melt Cleanliness in Die Cast Aluminum Alloys", Transactions of the 16th International Die Casting Congress and Exposition, Detroit, Michigan, USA, 30 Sept. - 3 Oct. 1991, North American Die Casting Association, River Grove, USA (1991), p. 143-152.

17 D. DOUTRE, B. GARIÉPY, J.P. MARTIN and G. DUBÉ, "Aluminum Cleanliness Monitoring: Methods and Applications in Process Development and Quality Control", Light Metals (1985), p. 1179-1189.

18 Mechanical Metallurgy, G.E. DIETER (ed.), McGraw-Hill Book Company, Inc., New York (1961).

19 Aluminum Alloys: Structure and Properties, L.F. MONDOLFO, Butterworth & Co. Ltd., London (1976).

20 R. DASGUPTA, C.C. BROWN and S. MAREK, "Effect of Increased Magnesium Content on the Mechanical Properties of Sand-Cast 319 Aluminum Alloy", AFS Transactions, vol. 97 (1989), p. 245-253.

21 G.K. SIGWORTH, S. SHIVKUMAR and D. APELIAN, "The Influence of Molten Metal Processing on Mechanical Properties of Cast Al-Si-Mg Alloys", AFS Transactions, vol. 97 (1989), p. 811-823.

22 C. VASS, "The Effect on Grain Size and Physical Properties of Various Titanium/Boron Ratios", Proc. Conf. International Molten Metal Processing, City of Industry, CA, February, 1986, American Foundrymen's Society, Inc., Des Plaines, IL, USA, p 101-147.

23 B. CLOSSET and J.E. GRUZLESKI, "Mechanical Properties of A356.0 Alloys Modified with Pure Strontium", AFS Transactions, vol. 90 (1982), p. 453-464.

24 N. FAT-HALLA, "Deformation and Fracture of Modified and Nonmodified Al-7Si-0.3Mg Alloy", Proc. Conf. Current Advances in Mechanical Design and Production III, Cairo, Egypt, December 28-30, 1989, Pergamon Press, Oxford, UK, (1986), p. 239-246.

14 J.L. ROBERGE and M. RICHARD, "Qualiflash Apparatus for Testing the Inclusion Quality of Aluminum Alloy Baths", Proceedings of the 4th International Conference on Molten Aluminum Processing, Orlando, Florida, November 12-14, 1995, American Foundrymen's Society, Des Plaines, IL (1996), p. 29-42.

15 X.G. CHEN, R.I.L. GUTHRIE and J.E. GRUZLESKI, "Quantitative Measurement of Melt Cleanliness in Aluminum-Silicon Casting Alloys", Proceedings of the 4th International Conference on Molten Aluminum Processing, Orlando, Florida, November 12-14, 1995, American Foundrymen's Society, Des Plaines, IL (1996), p. 15-28.

16 S. SHIVKUMAR, D. APELIAN and H. BRUCHER, "Melt Cleanliness in Die Cast Aluminum Alloys", Transactions of the 16th International Die Casting Congress and Exposition, Detroit, Michigan, USA, 30 Sept. - 3 Oct. 1991, North American Die Casting Association, River Grove, USA (1991), p. 143-152.

17 D. DOUTRE, B. GARIÉPY, J.P. MARTIN and G. DUBÉ, "Aluminum Cleanliness Monitoring: Methods and Applications in Process Development and Quality Control", Light Metals (1985), p. 1179-1189.

18 Mechanical Metallurgy, G.E. DIETER (ed.), McGraw-Hill Book Company, Inc., New York (1961).

19 Aluminum Alloys: Structure and Properties, L.F. MONDOLFO, Butterworth & Co. Ltd., London (1976).

20 R. DASGUPTA, C.C. BROWN and S. MAREK, "Effect of Increased Magnesium Content on the Mechanical Properties of Sand-Cast 319 Aluminum Alloy", AFS Transactions, vol. 97 (1989), p. 245-253.

21 G.K. SIGWORTH, S. SHIVKUMAR and D. APELIAN, "The Influence of Molten Metal Processing on Mechanical Properties of Cast Al-Si-Mg Alloys", AFS Transactions, vol. 97 (1989), p. 811-823.

22 C. VASS, "The Effect on Grain Size and Physical Properties of Various Titanium/Boron Ratios", Proc. Conf. International Molten Metal Processing, City of Industry, CA, February, 1986, American Foundrymen's Society, Inc., Des Plaines, IL, USA, p 101-147.

23 B. CLOSSET and J.E. GRUZLESKI, "Mechanical Properties of A356.0 Alloys Modified with Pure Strontium", AFS Transactions, vol. 90 (1982), p. 453-464.

24 N. FAT-HALLA, "Deformation and Fracture of Modified and Nonmodified Al-7Si-0.3Mg Alloy", Proc. Conf. Current Advances in Mechanical Design and Production III, Cairo, Egypt, December 28-30, 1989, Pergamon Press, Oxford, UK, (1986), p. 239-246.

25 C.W. MEYERS, "Solution Heat Treatment Effects on Ultimate Tensile Strength and Uniform Elongation in A357 Aluminum Alloy", AFS Transactions, vol. 94 (1986), p. 511-518.

26 S. SHIVKUMAR, S. RICCI, Jr., C. KELLER and D. APELIAN, "Effect of Solution Treatment Parameters on Tensile Properties of Cast Aluminum Alloys", J. Heat Treating, vol. 8, (1990), p. 63-70.

27 F.H. SAMUEL and A.M. SAMUEL, "Effect of Heat Treatment on the Microstructure, Tensile Properties, and Fracture Behavior of Permanent Mold Al-10 wt pct Si-0.6 wt pct Mg/SiC/10_p Composite Castings", Metallurgical and Materials Transactions A, vol. 25A (1994), p. 2247-2263.

28 N.R. GREEN and J. CAMPBELL, "Influence of Oxide Film Filling Defects on the Strength of Al-7Si-Mg Alloy Castings", AFS Transactions, vol. 102 (1994), p. 341-347.

29 Dj. HEDJAZI, G.H.J. BENNETT and V. KONDIC, "Effects of Non-Metallic Inclusions on Tensile Properties of an Al-4.5Cu-1.5Mg Alloy", Metals Technology, vol. 3 (1976), p. 537-541.

30 K. ARAI, T. ONISHI, M. GOTO and R. OTSUKA, "Effects of Nonmetallic Inclusions on Strength and Ductility of Aluminum Alloys", Journal of Japan Institute of Light Metals, vol. 27 (1997), p. 319-325.

31 E. KATO, Y. UEDA and T. KOBAYASHI, "The Influence of the Inclusion on the Fracture Toughness of the High-Strength Al", Journal of Japan Institute of Light Metals, vol. 25 (1985), p. 282-325.

32 F.H. SAMUEL, H. LIU, and A.M. SAMUEL, "Effect of Melt Cleanliness on the Properties of an Al-10 wt Pct Si-10 Vol Pct SiC(p) Composite", Metallurgical Transactions A, vol. 24A (1993), p. 1631-1645.

33 P.R. RIOS, J.C. BRUNO and A.S.M. FONSECA, "Influence of Coarse Inclusions on Strength, Ductility and Fracture of a Hot Extruded AA2014 Aluminium Tube", J. Materials Science Letters, vol. 10 (1991), p. 1346-1348.

34 Metals Handbook, (9^{th} Edition), vol.8 : Mechanical Testing, American Society for Metals, Metals Park, OH (1985), p. 363-365.

35 C.Q. BOWLES and J. SCHIJVE, "Role of Inclusions in Fatigue Crack Initiation in an Aluminum Alloy", Int. J. Fracture, vol. 2 (1973), p. 171-179.

36 K. TANAKA and T. MURA, "A Theory of Fatigue Crack Initiation at Inclusions", Metallurgical Transactions A, vol. 13A (1982), p. 117-123.

37 J.F. KNOTT and J.E. KING, "Fatigue in Metallic Alloys Containing Non-Metallic Particles", Proc. Conf. Fatigue 90, Hawaii, USA, July 15-20, 1990, Materials and Component Engineering Publications, Edgbaston, Birmingham, (1990), p.2557-2569.

38 C.C. BAKER, "The Effect of Nonmetallic Inclusions and Test Temperature on the Fatigue Life of Cast C355, 354, and A206 Aluminum", International Symposium for Testing and Failure Analysis, Los Angeles, CA, October 20-24, 1986, ASM International, Metals Park, OH (1986), p. 299-307.

39 S. SHIVKUMAR, S. RICCI, Jr., B. STEENHOFF, D. APELIAN and G. SIGWORTH, "An Experimental Study to Optimize the Heat Treatment of A356 Alloy", AFS Transactions, vol. 97 (1989), p. 791-810.

40 C.W. MEYERS and N. McRAY, "Simplified Supersaturation Effects on the Tensile Properties of A357 Alloys", in Technology for Premium Quality Castings, E. DUNN and D.R. DURHAM (Eds.), The Minerals, Metals & Materials Society, Warrendale, PA, (1988), p. 107-122.

41 D. APELIAN, S. SHIVKUMAR and G. SIGWORTH, "Fundamental Aspects of Heat Treatment of Cast Al-Si-Mg Alloys", AFS Transactions, vol. 97 (1989), p. 727-742.

42 K.J. OSWALT and W.S. MISRA, "Dendrite Arm Spacing (DAS): A Non Destructive Test to Evaluate Tensile Properties of Premium Quality Aluminum Alloy (Al-Si-Mg) Castings", AFS Transactions, vol. 88 (1980), p. 845-862.

43 W. SIMMONS, "The Filtering of Molten Metal to Improve Productivity, Yield, Quality and Properties", Indian Foundry J. (1988), p. 21-28.

44 D. APELIAN, 1988 Electric Furnace Conference Proceedings, Pittsburgh, December 6-9, 1988, Iron & Steel Society, Warrendale, Pennsylvania (1989), p. 325.

45 D. APELIAN, R. MUTHARASAN and S.ALI, "Removal of Inclusions from Steel Melts by Filtration", J. Materials Science, vol. 20 (1985), p. 3501-3514.

46 H.C. CUMMINGS, F.B. STULEN and W.C. SCHULTE, Transactions of ASM, vol. 49 (19), p. 487.

47 C.E. ECKERT, R.E. MILLER, D. APELIAN and R. MUTHARASAN, "Molten Aluminum Filtration: Fundamental Models", Light Metals (1984), p. 1281-1304.

48 C.J. SIMENSEN and U. HARTVEDT, "Analysis of Oxides in Aluminum by Means of Melt Filtration", Z. Metallkunde, vol. 76 (1985), p. 409-414.

49 J. GORBRECHT, "Schwereseigerungen von Eisen, Mangan und Chrom in Aluminum-Silicium-Guβlegierungen (Teil 1)", Giesserei, vol. 62 (1975), p. 263-266.

50 S. JACOB, "Modification de l'A-S7G06 par le Sodium, l'Antimoine et le Strontium", Fonderie, no. 363 (1977), p. 13-25.

51 R. DASGUPTA, C.G. BROWN and S. MAREK, "Analysis of Overmodified 356 Aluminum Alloy", AFS Transactions, vol. 96 (1988), p. 297-310.

52 P.D. HESS and E.V. BLACKMUN, "Strontium as a Modifying Agent for Hypoeutectic Aluminum-Silicon Alloys", AFS Transactions, vol. 84 (1975), p. 87-90.

53 D. APELIAN, G.V. SIGWORTH and K.R. WHALER, "Assessment of Grain Refinement and Modification of Al-Si Foundry Alloys by Thermal Analysis", AFS Transactions, vol. 92 (1984), p. 297-307.

54 L.F. MONDOLFO, "Grain Refinement in the Casting of Non-Ferrous Alloys", Metallurgical Society of AIME (1983), p. 3-50.

55 S. KENNERKNECHT, "Metallurgical Aspects of Quality Control in the Production of Premium Quality Aluminum Investment Castings for the Aerospace Industry", Advanced Casting Technology, AGARD/NATO Conference Proceedings CP325, August 1982.

56 Aluminum - Properties and Physical Metallurgy, J. E. HATCH (ed.), American Society for Metals, Metals Park, OH, (1984).

57 J.L. JORSTAD, "Understanding Sludge", Die Casting Engineer, vol. 30 (1986), p. 30-36.

58 A. M. SAMUEL and F. H. SAMUEL, "Review: Various Aspects Involved in the Production of Low Hydrogen Aluminum Castings", J. Materials Science, vol. 27 (1992), p. 6533-6563.

59 C.J. SIMENSEN, "Sedimentation Analysis of Inclusions in Aluminum and Magnesium", Metallurgical Transactions B, vol. 12B (1981), p. 733-743.

60 C.J. SIMENSEN, "Analysis of Inclusions and Hydrogen in Aluminum and Magnesium", Ph.D. Thesis, NTH, Trondheim, (1982).

61 R.B. BLACKBURN, "Sampling Molten Aluminum for Non-Metallic Inclusions", Aluminium, vol. 56 (1980), p. 585-587.

62 D. APELIAN and R. MUTHARASAN, "Filtration: A Melt Refining Method", J. of Metals, Sept (1980), p. 14-19.

63 W. SIMMONS and J. HACK, "Filtration of Non-Ferrous Casting in the Mold", The British Foundryman, vol. 76 (1983), p. 10-11.

64 W. SIMMONS, "Foundry Experience with Ceramic Filters", Foundry Trade J., vol. 158 (1985), p. 23-27.

65 W. SIMMONS, and M.L.H. WISE, Foundry Practice, March (1986), p. 217.

66 C. TIAN, Ph.D. Thesis, McGill University, Montreal, Canada, 1994.

67 C. TIAN and R.I.L. GUTHRIE, "Fundamentals of Liquid Metal Filtration", Recent Developments in Light Metals, Proc. Int. Sympos., M. Gilbert, P. Tremblay and E. Ozberk (eds.), The Metallurgical Society of CIM, Montreal, Canada (1994), p. 415-430.

68 C. TIAN and R.I.L. GUTHRIE, "The Dynamic Process of Liquid Metal Filtration", Light Metals (1995), p. 1263-1272.

69 G. DUBÉ and V. NEWBERRY, "TAC - A Novel Process for the Removal of Lithium and Other Alkalis in Primary Aluminum", Light Metals (1983), p. 991-1003.

70 C. CELIK and D. DOUTRE, "Theoretical and Experimental Investigation of Furnace Chlorine Fluxing", Light Metals (1989), p. 793-800.

71 G. BÉLAND, C. DUPUIS and J.P. MARTIN, "Improving Fluxing of Aluminum Alloys", Light Metal (1995), p. 1189-1195.

72 G.K. SIGWORTH and T.A. ENGH, "Chemical and Kinetic Factors Related to Hydrogen Removal from Aluminum", Metallurgical Transactions A, vol. 13A (1982), p. 447-460.

73 P. WAITE and D. BERNARD, "Recent Experience with the Use of Sulphur Hexafluoride for Aluminum Fluxing", Light Metals (1990), p. 775-784.

74 S.A. LEVY, "Applications of the Union Carbide Particulate Tester", Light Metals (1981), p. 723-733.

75 L. LIU and F.H. SAMUEL, "Assessment of Melt Cleanliness in A356.2 Aluminum Casting Alloy Using the PoDFA Technique: Part I - Inclusion Measurement", J. Materials Science, vol. 33 (22) (1997), p. 5901-5925.

76 D.V. RAGONE, C.M. ADAMS and H.F. TAYLOR, AFS Transactions, vol. 64 (1953), p. 653.

77 M.C. FLEMINGS, F.R. MOLLARD, E.F. NIIYAMA and H.F. TAYLOR, AFS Transactions, vol. 70 (1962), p. 1029.

78 S.F. LIU, M.C. FLEMINGS and H.F. TAYLOR, The British. Foundryman, Sept. (1960), p. 413.

79 S. VENKATESWARAN, R.M. MALLYA and M.R. SESHADRI, "Effect of Trace Elements on the Fluidity of Eutectic Al-Si Alloy Using the Vacuum Suction Technique", AFS Transactions, vol. 94 (1986), p. 701-707.

80 J.E. CAMPBELL, Castings, Butterworth-Heinemann, Oxford, (1991).

81 D. HEDJAZI, G.H.J. BENNETT and V. KONDIC, "Removal of Non-Metallic Inclusions and Their Assessment in Al-Alloy Melts", The British. Foundryman, vol. 68 (1975), p. 305-309.

82 K.H. CHIEN, T.Z. KATTAMIS and F.R. MOLLARD, "Cast Microstructure and Fatigue Behavior of a High Strength Aluminum Alloy", Metallurgical Transactions A, vol. 4A (1973), p. 1069-1076.

83 V. GEROLD, "The Fatigue Properties of Precipitation-Hardened Aluminum Alloys", Materials Science Forum, vols. 3-14 (1987), p. 175-194.

84 Metals Handbook, (9th Edition), vol. 9 : Metallography and Microstructures, American Society for Metals, Metals Park, OH (1985), p. 123-134.

85 D. APELIAN and R. MUTHARASAN, "Modelling of Inclusion Removal of Metal Systems", 72th Annual AIChE Meeting, San Francisco, CA, November, 1979.

86 L.J. GAUCKLER, M.M. WEBER, C. CONTI and M. JACOB-DULIERE, "Industrial Applications of Open Pore Ceramic Foam for Molten Filtration", Light Metals (1985), p. 1261-1283.

87 T. CALLAIS, M. RICHARD et M. STUCKY, "Évaluation de l'appareil HYVAC pour la mesure de la propreté et du gazage des bains d'aluminium", Fonderie-Fondeur d'aujourd'hui, vol. 97 (1990), p. 22-27.

88 M.M. GOZOWSKI, G.K. SIGWORTH, and D.A. SENTER, "The Role of Boron in the Grain Refinement of Aluminum with Titanium", Metallurgical Transactions A, vol. 18A (1987), p. 603-619.

89 G. K. SIGWORTH and M.M. GOZOWSKI, "Grain Refining of Hypoeutectic Al-Si Alloys", AFS Transactions, vol. 87 (1978), p. 907-912.

90 S.Z. LU and A. HELLAWELL, "The Mechanism of Silicon Modification in Aluminum - Silicon Alloys: Impurity Induced Twinning", Metallurgical Transactions A, vol. 18A (1987), p. 1721-1733.

91 M. GARAT and R. SCALLIET, "A Review of Recent French Casting Alloy Developments", AFS Transactions, vol. 84 (1984), p. 549-562.

92 L. LIU and F.H. SAMUEL, "Assessment of Melt Cleanliness in A356.2 Aluminum Casting Alloy Using the PoDFA Technique: Part II-Inclusion Analysis", J. Materials Science., vol. 33 (22) (1997), p. 5927-5944.